Design and development of mobile channel simulators using digital signal processing techniques

Khawar Siddique Khokhar,

ABSTRACT

Design and Development of Mobile Channel Simulators using Digital Signal Processing Techniques

Khawar Siddique Khokhar

A mobile channel simulator can be constructed either in the time domain using a tapped delay line filter or in the frequency domain using the time variant transfer function of the channel. Transfer function modelling has many advantages over impulse response modelling. Although the transfer function channel model has been envisaged by several researchers as an alternative to the commonly employed tapped delay line model, so far it has not been implemented. In this work, channel simulators for single carrier and multicarrier OFDM system based on time variant transfer function of the channel have been designed and implemented using DSP techniques in SIMULINK

For a single carrier system, the simulator was based on Bello's transfer function channel model. Bello speculated that about $10B\tau_{max}$ frequency domain branches might result in a very good approximation of the channel (where B is the signal bandwidth and τ_{max} is the maximum excess delay of the multi-path channel). The simulation results showed that $10B/B_c$ branches gave close agreement with the tapped delay line model (where B_c is the coherence bandwidth). This number is π times higher than the previously speculated $10B\tau_{max}$.

For multicarrier OFDM system, the simulator was based on the physical (PHY) layer standard for IEEE 802.16-2004 Wireless Metropolitan Area Network (WirelessMAN) and employed measured channel transfer functions at the 2.5 GHz and 3.5 GHz bands in the simulations. The channel was implemented in the frequency domain by carrying out point wise multiplication of the spectrum of OFDM time domain signal with the transfer function of the channel by employing FFT convolution. The simulator was employed to study BER performance of rate 1/2 and rate 3/4 coded systems with QPSK and 16-QAM constellations under a variety of measured channel transfer functions. The performance over the frequency selective channel mainly depended upon the frequency domain fading and the channel coding rate.

Design and Development of Mobile Channel Simulators using Digital Signal Processing Techniques

By

Khawar Siddique Khokhar.

A thesis submitted to the
School of Engineering,
University of Durham, Durhan, United Kingdom.
for the degree of Ph.D
2006

TABLE OF CONTENTS

LIST OF FIGURES

Chapter 2

Chapter 3

Chapter 4

Chapter 5

Chapter 6

LIST OF TABLES

Chapter 4

Chapter 5

Chapter 6

DECLARATION

No portion of the work referred to in this thesis has been submitted in support of an application for another degree or qualification of this or any other university, or institution of learning. The copyright of this thesis rests with the author. No quotation from it should be published in any format, including electronic and the internet, without the author's prior written consent. All information derived from this thesis must be acknowledged appropriately.

CHAPTER 1

INTRODUCTION

Ever since the launch of mobile radio links by M.G. Marconi in the late 1800s between a tugboat and a stationary base station, mobile systems kept on improving due to the technological advancements. Early mobile radio systems were made of vacuum tubes and were very bulky and heavy. Invention of the transistor revolutionized the electronics technology and consequently the size of mobile radio equipment was reduced due to less occupancy of space and low power consumption. The commercial availability of integrated circuits by the middle of the 1970s not only further reduced the equipment size but also increased the reliability and manoeuvrability. The process of large scale integration (LSI) and very large scale integration (VLSI) made it possible to produce light weight and hand held mobile terminals at low cost [1].

The cellular communication concept was developed at AT&T Bell Laboratory. This idea divides the required geographical area into small regions called cells. This increases the capacity of a wireless communication network by reusing some of the channels (frequencies) over and over again in different cells. Moreover, this concept also allows subscribers to move swiftly from one location to another without experiencing any interruption and performance degradation, and to become mobile subscribers [2].

The earlier systems were analog in nature and were referred to as first generation (1G) cellular systems. One such system was first implemented in Japan in 1979. It was developed by NTT and operated at 400/800 MHz. In 1983, Advance Mobile Phone System (AMPS) was deployed in the USA. It operated in the 800 MHz band and divided the spectrum in two, using one band for transmission and the other for reception to realize a duplex mode of operation. Each band spanned 30 kHz and was meant for a single voice channel. It used frequency modulation (FM) for voice transmission. The first generation system implemented in Europe was called Total Access Communication System (TACS). It operated in the 900 MHz band and also used frequency modulation (FM) to convey voice.

The second generation systems (2G) surfaced in the early 1990's. First such system was deployed in Europe in 1990 and termed as Global System for Mobile (GSM). It is the most widely employed system in the world and considered as the world's first cellular system to incorporate digital modulation and network level architectures and services. It was initially conceived to be operated in the 900 MHz band, but now has been adapted for the 1800 MHz band, known as Digital Communication System 1800 (DCS 1800) . In GSM, a radio channel of 200 kHz bandwidth is time shared by eight users with Gaussian-filtered minimum shift keying (GMSK). This scheme permits the use of low-cost nonlinear amplifiers in handsets to reduce its weight and cost. In US, the cellular system is called Interim Standard (IS-54) United States Digital Cellular (USDC) system. It maintains backward compatibility with AMPS by keeping the duplex provision. It separates the bidirectional transmission over frequency bands separated by 45 MHz. It employs $\pi/4$ differential quadrature phase shift keying ($\pi/4$-QPSK) as a modulation scheme and TDMA to access the channel. Frequency division duplex (FDD) is used in the same format as in AMPS. Other second generation systems include European Radio Message System (ERMES), North American Digital Cellular (NADC) [1-4].

The third generation (3G) systems were designed to cope with the high rate demands for services such as, high speed data, video and e-mail. 3G was first proposed by the European Telecommunication Standards Institute (ETSI) and called Universal Mobile Telecommunication System (UMTS). Two bands centered at 1945 MHz and 2135 MHz with 60 MHz bandwidth have been allocated for UMTS FDD as the uplink and downlink bands, respectively. The UMTS systems employ RAKE receivers at the base station to combat multipath fading. W-CDMA from the Association of Radio Industry and Business (ARIB), Japan and cdma-2000 from Telecommunication Industry Association (TIA), US were proposed to the International Telecommunication Union (ITU) for third generation systems. The third generation systems are also called International Mobile Telecommunications-200 (IMT-2000) in the ITU [5-6]. 3G systems have already been deployed in some counties [7].

Research on 4G has begun [8]. Various forums and organizations for wireless research, such as Wireless World Research Forum (WWRF) and ITU have already started discussions on 4G systems [9-10]. They are likely to be deployed around 2010

[7]. The ITU assembly has already approved question ITU-R 229/8 on the future development of IMT-2000 and systems beyond IMT-2000. These systems will support data rates up to approximately 100 Mb/s for high mobility and up to approximately 1 Gb/s for low mobility [7].

Multicarrier CDMA (MC-CDMA) and frequency hopping OFDMA (FH-OFDMA) are two of the most promising technologies for 4G systems [11]. In MC-CDMA, user data are spread by different orthogonal or near orthogonal codes over the frequency domain, and more than one user occupy the same set of frequencies at the same time. The spreading helps improve immunity against intercell interference and obtain a frequency diversity effect. However, while the orthogonality of the code for different users can be preserved in the downlink, the orthogonality breaks up completely in the uplink because different user signals undergo different multi-path fading. In FH-OFDMA, users within the same cell are allocated a disjoint set of subcarriers. The hopping patterns for different users are mutually designed in such a way that they are mutually orthogonal within the same cell, and interference level from other cells is maintained below some level. Therefore, an FH-OFDMA systems does not suffer from intercell interference under ideal frequency and timing synchronization conditions. Moreover, frequency hopping offers frequency diversity and intercell interference averaging effects. The intercell interference can be reduced even further when information about the status of adjacent cells is combined with frequency hopping.

Most of the researchers are of the view that Orthogonal Frequency Division Multiplexing (OFDM) is more likely to be adopted in 4G systems due to its superior performance in multipath propagation environment and lower complexity of equalizers for high delay spread channels [12-13].

The Mobile Communications channel is characterized by multi-path propagation. This phenomena results in constant variations in the received signal envelope on account of the movement of the mobile. In digital communications, the arrival of various copies of the transmitted signal one after another results in broadening of the transmitted pulse. Such broadening of the pulse causes intersymbol interference. In the frequency domain, the spreading of the received signal is viewed as frequency selective fading. Such characteristics of channel degrade the system performance. Therefore, the process involved in the design and development of mobile communication system

requires that it is tested time and again in the field to quantify its performance. Field testing is expensive and time consuming. Simulators can perform the testing of mobile systems in a laboratory. It creates multi-path fading environment and exactly replicates the time varying characteristics of the mobile communication channel. It is considered as the channel in a box.

This work pertains to the design and development of channel simulators for single carrier and multicarrier OFDM systems based on the time variant transfer function of the channel. For a single carrier system, DQPSK modulation scheme of the U.S. Digital Cellular Standard IS-54 with two-ray power delay profile was used to simulate the channel in the frequency domain. For multicarrier OFDM system, the simulator was based on the physical (PHY) layer standards for IEEE 802.16-2004 Wireless Metropolitan Area Network (WirelessMAN) and employed measured channel transfer functions in the 2.5 GHz and 3.5 GHz bands.

The transfer function modelling has several advantages over impulse response modelling. These include: non independence of fading statistics over the bandwidth, fulfillment of central limit theorem for all frequencies and instants with respect to all domains, and consistent extension from narrowband to wideband. However, its main advantage arises for ultra wideband systems, where the number of taps in the time domain becomes very large as the bandwidth permits the resolution of more components, therefore limiting the applicability of the central limit theorem[14-16].

1.1 BRIEF DESCRIPTION OF CHAPTER CONTENTS

Chapter 2 presents a theoretical background of the mobile radio propagation channel. Multipath fading and various statistical models applicable to fading characteristics are described in detail. Clark's, Aulin's and Parson's Doppler power spectrum are also described. Channel parameters such as RMS delay spread, profile width, delay window, and frequency correlation function are introduced. Their impact on system performance are highlighted. Randomly time variant behaviour of the mobile channel is defined in the time domain and in the frequency domain using Bello's four system functions and their inter-relationships are presented. Classification of the channel as narrowband, wideband, slow fading and fast fading is given.

Chapter 3 describes the architecture of some of the popular channel simulators built over the last three decades and their operating principles are explained in detail.

Chapter 4 pertains to the transfer function channel modeling and simulation. The main aim of this chapter is to present the advantages of the time variant transfer function modeling over impulse response modeling and to demonstrate that a wide band mobile channel simulator can equivalently be constructed in the frequency domain using the time variant transfer function T(f,t) of the channel. This chapter also proposes a suitable implementation for the transfer function model using Digital Signal Processing (DSP) techniques in SIMULINK and verifies the bit error rate (BER) results with the published results from the commonly used tapped delay line model employing a two-ray power delay profile and differential quadrature phase shift keying (DQPSK) modulation. In this chapter, the design of the simulator is optimized to permit future implementation in DSP for real time ultra wideband systems

Chapter 5 describes the SIMULINK implementation of frequency domain channel simulator for OFDM based physical (PHY) layer of IEEE 802.16-2004 WirelessMAN. The simulator employs measured channel transfer functions at 2.5 GHz and 3.5 GHz to implement the channel in the frequency domain by FFT convolution. This chapter not only presents the system design in DSP but also focuses on each and every aspect of the standard. Various parameters associated with each SIMULINK block are thoroughly explained. This chapter also presents a brief introduction of OFDM technology and its advantages over single carrier systems and highlights the role of cyclic prefix in eliminating inter symbol and intercarrier interference in highly dispersive multipath channels.

Chapter 6 presents the BER performance results using a variety of measured channel transfer functions for the 2.5 GHz and 3.5 GHz bands. These transfer functions differ from one another in terms of the frequency selective fading. The design of the simulator is validated first by studying its BER performance over an additive white Gaussian noise (AWGN) channel and comparing the BER simulation results with the theoretical results and other published results. In the first phase of the simulations, the BER results for rate 1/2 coded OFDM system using QPSK and 16-QAM constellation mapping are obtained for three sets of measured transfer functions for both bands. In the second phase of the simulations, profiles from the 2.5 GHz band are employed to study

the BER performance of rate 3/4 coded OFDM system. The effects of frequency selective fading on rate 1/2 and 3/4 channel coding schemes, specified in the IEEE 802.16-2004 standards, are studied in the third phase of simulations using highly frequency selective transfer functions.

In chapter 7, conclusions are made and directions for future works are given.

1.2 Bibliography

1. M.D. Yacoub, Foundations of Mobile Radio Engineering, New York: CRC Press, 1993.
2. P.M. Shankar, Introduction to Wireless Systems, New York: John Wiley & Sons, 2002.
3. N.H. Shepherd, Mobile Radio Services, in Communications System Engineering Handbook, New York: McGraw-Hill,1967.
4. G. Calhoun, Digital Cellular Radio, New Jersey: Artech House, 1988.
5. UMTS Forum Report No.9, "The UMTS Third Generation Market – Structuring the Service Revenue Opportunities," August 2000.
6. UMTS Forum Report No.13, "The UMTS Third Generation Market – Phase II: Structuring the Service Revenue Opportunities," April 2001.
7. K Yungsoon, J.J. Byung, C.Jaehak, C. Hwang, S.R. Joon, and K.Kyan, "Beyond 3G: Vision, Requirements, and Enabling Technologies," IEEE Commun. Mag., March 2003, pp 120-124.
8. W.W. Lu, "4G Research in Asia," IEEE Commun. Mag., March 2003, pp 104-106.
9. Wireless World Research Forum:htt://www.wireless-world-research.org/
10. ITU-R PDNR WP8F, "Vision, Framework and Overall Objectives of the Future Development of IMT-2000 and Systems beyond IMT-2000," 2002.
11. S.Hara and R.Prasad, "Overview of Multicarrier CDMA," IEEE Commun. Mag., vol.35, Dec 1997, pp. 126-36.
12. D. Falconer, and S.L. Ariyavisitakul, "Frequency domain equalization for single-carrier broadband wireless systems," IEEE Commun. Mag., April 2002, pp 58- 66.

13. D. Karampatis and I. Darwazeh, "OFDM; A Possible Technology for 4th Generation Mobile Systems?," International Symposium on Telecommunications IST 2001, Tehran, Iran.
14. T. Englert and H. Fruchting,"Bandwidth dependence of the characteristics of time variant impulse response," Proceeding of 2000 European Conference on Wireless Technology (ECWT 2000), Paris, France, Oct 5-6. 2000, pp. 230-233.
15. D. Cassioli, and A.F. Molisch, "A statistical model for UWB indoor channel," IEEE Vehicular Technology Conference(VTC 2001 Spring), Rhodes, Greece, May 6-9. 2001, pp.1159-1163.
16. R. Kattenback, "Statistical modeling of small scale fading in directional radio channel," IEEE Journ. on Selected Areas in Communications, vol. 20, no.3, April 2002, pp. 584-592.

CHAPTER 2

INTRODUCTION TO MOBILE COMMUNICATION CHANNEL

2.1 INTRODUCTION

A communication link in which the transmitter and/or the receiver has the ability to move is termed as a mobile channel. The mobile radio channel is characterised by the multi-path phenomena which results in variations in the received signal strength as a function of time and frequency. Deep fades reduce the instantaneous signal to noise ratio of the channel and cause bursts of errors. These bursts are usually reduced using various channel coding and diversity schemes which take into account the channel behaviour. As the system operates in different kinds of environments, different amounts of delay spread is experienced which impact on the achievable data rate. The delay spread results in intersymbol interference (ISI) and causes irreducible bit error rate (BER). Equalizers are usually employed by the receivers to remove ISI and regenerate symbols correctly. In order to effectively mitigate the effects of delay spread, the impulse response of the mobile radio channel must be determined by channel sounding. As the mobile channel may change rapidly both in time and space, the impulse response must be frequently measured. These channel characteristics are employed to design equalizers. Moreover, in order for communication systems to absorb the time varying nature of the channel and to deliver acceptable performance, it has to be designed keeping in view the operating channel conditions.

Simulators are employed to replicate the adverse effects of multi-path propagation to assess and quantify system performance. The simulators are designed on the basis of channel characteristics in various operating environments such as, outdoor, indoor, urban, suburban, rural and mountainous. Channel sounding techniques are used to measure the channel characteristics for the purpose of developing various channel models for these operating conditions. Therefore, it is imperative to thoroughly investigate and characterize the channel so that its effects on the performance could be mitigated effectively. Section 2.3 of this chapter presents the concept of multi-path fading and various statistical models applicable to the fading characteristics. Section 2.4 deals with the Doppler power spectrum of the fading signal. In section 2.7, channel

system functions and their inter-relationships are explained. Section 2.8 is devoted to channel modelling. Classification of the channel is dealt with in section 2.9.

2.2 MULTI-PATH PROPAGATION

In mobile communications usually there exists no line of sight propagation. The signal undergoes the phenomena of reflection, refraction, diffraction and scattering from the buildings, structures, and obstructions in the path [1-4]. As a result of these phenomena, the signal reaches the receiving antenna through various paths with different time delays, phases and amplitudes. These components interact with each other vectorially. They reinforce the effects of each other if they are in-phase and cancel each other if they are out of phase. Such propagation is called multi-path propagation [5-8] and is shown in Figure 2.1.

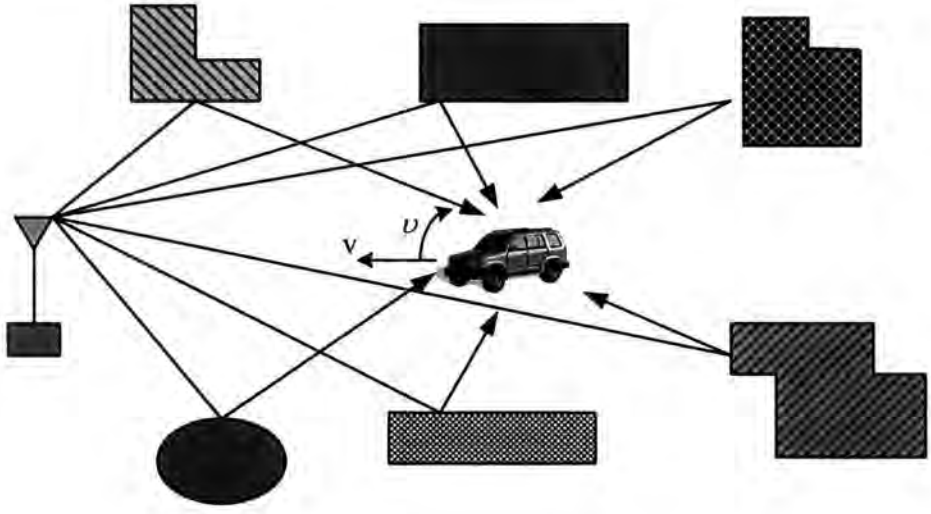

Figure 2.1 Signal strength variations due to mobile motion.

2.2.1 Fading

As a result of constructive and destructive combination of the multi-path signals, the amplitude of the received signal changes with the movement of the mobile. This phenomenon is called fading. Since at different points in space the phase relationship among the various component waves is different, their vector sum is different. Therefore, the signal strength varies spatially. If a mobile is stationary, then it receives a

signal that has a certain level of strength associated with this particular spatial point. But when a mobile moves through this spatially varying field strength, the spatial phenomena becomes temporal and the signal strength received by the mobile varies constantly. Also, variations in signal strength are observed due to movement of other vehicles i.e., temporal fading is not only due to the movement of the user but also the environment.

The signal variations experienced by the mobile due to multi-path are demonstrated in Figure 2.2. The fading has been simulated using SIMULINK. The amplitude changes significantly even if there is change in location by a short distance. There are two kinds of fading: fast fading or short term and slow fading or long-term fading [9].

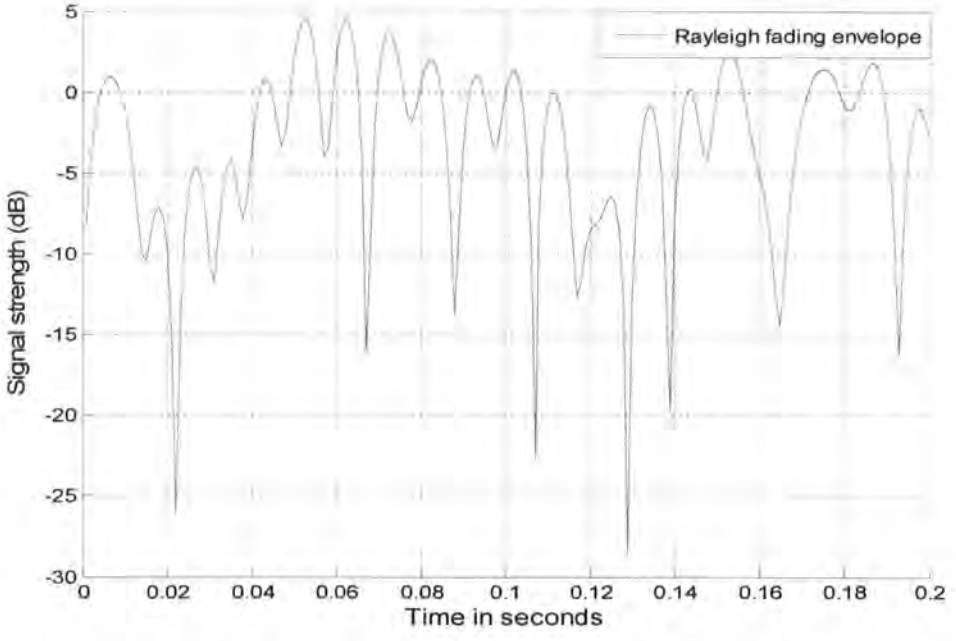

Figure 2.2 A typical simulated Rayleigh fading envelope at 60 Hz Doppler using SIMULINK.

2.2.1.1 Short-Term and Long-Term Fading

The rapid fluctuations in the received signal due to the movement of the mobile over a small area are termed as fast or short-term fading. This fading is caused by the local multi-path environment where small movement of a mobile causes a substantial change

in the phase relationship of the incoming signal. However, within this small area, the mean value of the signal remains the same. The variations in the mean signal level observed over a large area is referred to as long-term fading. The phenomena of short-term and long-term fadings are depicted in Figure 2.3.

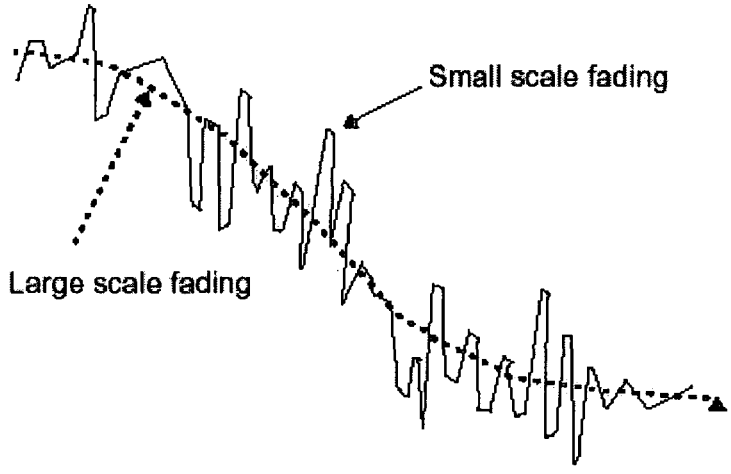

Figure 2.3 Short-term and long-term fading.

2.3 STATISTICAL PROPERTIES OF RECEIVED SIGNAL ENVELOPE

As the envelope of the received signal is a vector sum of a large number of random phase waves, it is also a random quantity. Hence statistical theory has to be applied to study its properties. It has been observed that the received signal envelope obeys various distributions depending upon the existence of a direct line-of-sight component, the area surrounding the mobile and closeness of scattering objects. Different models exist to study the statistical behavior and to calculate the probability density function (PDF) of the received signal envelope for short term fading. These models vary from each other depending on the assumption made for calculating the PDF. The widely employed statistical distributions are the Rayleigh, the Rician, the Nakagami, the Weibull, the Log-Normal and the Suzuki [6, 10-14].

2.3.1 Rayleigh Model

It is the most commonly employed model to study the statistical behavior of multi-path short-term fading. It is based on the assumption that the received multi-path signal has

no direct line of sight component and each scattered component has the same magnitude. It further assumes that the received signal consists of a large (theoretically infinite) number of independently reflected and scattered components each with a random phase with uniform distribution in the range (0-2π) [15-17]. If the received signal is expressed in terms of the in-phase and quadrature components, then each component is the resultant of a large number of waves and by virtue of the central limit theorem, becomes a Gaussian random variable and the resultant envelope of the in-phase and quadrature components will be Rayleigh distributed.

At any instant of time, the pdf of the phase $\theta(t)$, denoted by $P_\theta(\theta)$ and the pdf of the envelope $r_f(t)$, denoted by $P_{rf}(r)$ are given by the following relationships.

$$P_\theta(\theta) = \frac{1}{2\pi} \qquad 0 \le \theta \le 2\pi \tag{2.1}$$

$$P_{rf}(r) = \frac{r}{\sigma^2}\exp\left(\frac{-r^2}{2\sigma^2}\right) \qquad 0 \le r \tag{2.2}$$

where r = magnitude of envelope, σ^2 is variance which represents the total received power P, and σ is the standard deviation and is equal to $\sqrt{4-\pi}/2\left(\sqrt{r^2}\right)$.

The Rayleigh distribution is also unique in terms of its ratio of mean to standard deviation. This ratio is 1.91. While the envelope is Rayleigh distributed, the power P follows an exponential distribution and is given by the following relationship.

$$f_p = \frac{1}{2\sigma^2}\exp\left(\frac{-P}{2\sigma^2}\right) \tag{2.3}$$

where $2\sigma^2$ = average power = P

The probability that the random variable has a value $r_f(t) \le R$ is called Cumulative Distribution Function (CDF) and is given by the following relationship.

$$CDF = P_{ff}\left[r_f \le R\right] = \int_0^R P_{rf}(r)dr = 1\text{-}\exp\left(\frac{-R^2}{2\sigma^2}\right) \tag{2.4}$$

2.3.2 Rician Model

If the received signal is a combination of a number of indirect paths and a direct line-of-sight path then the received signal envelope will follow the Rician distribution [18-19]. Consequently, the mean of two random variables, representing the I and Q components, does not remain zero. But when the dominant path becomes weaker, the distribution approaches to Rayleigh. The power of the direct component will have to be greater than the total multipath power before it can affects the Rayleigh distribution. It is worth mentioning that the Rice distribution also applies whenever one path is much stronger than the other multi-path. The PDF is given by the following relationship [15, 20].

$$P(r) = \frac{r}{\sigma^2} e^{-\frac{r^2+A^2}{2\sigma^2}} I_0\left(RA/\sigma^2\right) \tag{2.5}$$

A is the amplitude of the dominant signal and $I_0(\bullet)$ is the modified zero-order Bessel function of first kind and σ^2 is the variance of either the real or imaginary component of the multi-path part alone. The distribution becomes Rayleigh when $A^2 = 0$.

The CDF is given as

$$\text{Prob}(r \le R) = \frac{1}{2} + \frac{1}{2}\text{erf}\left(\frac{R-A}{\sqrt{2}}\right) - \frac{1}{\sqrt{8\pi A}}\left[1 - \frac{R-A}{4A} + \frac{1+(R-A)^2}{8A^2}\right] e^{\frac{(R-A)^2}{2}} \tag{2.6}$$

and the error function is defined by

$$\text{erf}(y) = \frac{2}{\pi}\int_0^y e^{-t^2} dt \tag{2.7}$$

The Rice PDF can be expressed in terms of another parameter, K, called Rice factor and is defined as

$$K = \frac{\text{Power in constant part}}{\text{Power in random part}}$$

$$= \frac{A^2}{2\sigma^2}$$

K factor is usually expressed in dB. It has a great impact on the bit error rate performance of a communication system. As the K factor increases, the probability of encountering a deep fade reduces, and consequently the mean error rate decreases. The Rice channel is considered more friendly as compared to Rayleigh, which is regarded as the worst case mobile channel.

2.3.3 Nakagami Model

Unlike Rayleigh and Rician where it is assumed that the amplitude of scattered components is the same, the Nakagami model incorporates the provision of different amplitudes of scattered waves. It also incorporates the possibility of partial correlation that exists between scattering elements. It usually models the channel conditions that are either more or less severe than the Rayleigh distribution [13, 21-22]. The probability density function is given by

$$P(r) = \frac{2}{\Gamma(m)}\left(\frac{m}{\Omega}\right)^m r^{2m-1} e^{-\frac{mr^2}{\Omega}} \qquad (2.8)$$

where $m = \frac{\left(\overline{r^2}\right)^2}{\left(r - \overline{r^2}\right)} \geq \frac{1}{2}$, $\Gamma(m)$ is Gamma function and $\Omega = \overline{r^2}$

It contains two parameters m and Ω, due to which it provides more accurate fitting for observed data statistics. This model is a general model. The Rayleigh and Rician

distributions can be derived out of the above relationship by assigning appropriate values to m. If m=1, the Rayleigh distribution is obtained with exponentially distributed instantaneous power. The Rician distribution is derived by assigning $m \geq 1$. However, for the Nakagami distribution, the value of m is restricted to $m \geq 1/2$. The parameter m is known as the shape factor of Nakagami or gamma distribution. The instantaneous power of the Nakagami distributed envelope will have gamma distribution.

It is worth mentioning that in contrast to other distributions, the Nakagami results in an approximate solution only. The PDF of the envelope in dB is expressed in the following relationship.

$$P(y) = \frac{2m^m}{M\Gamma(m\Omega)} \exp\left[\frac{2my}{M} - \frac{m}{\Omega}\exp\left(\frac{2y}{M}\right)\right] \tag{2.9}$$

where $y = 20\log r$, $M = 20/\ln 10$ and $r = \exp(y/M)$

2.3.4 Log-Normal Model

This distribution is applicable where the propagation environment has high rising structures like tall buildings and trees. The signal does not adopt different propagation paths immediately after it is transmitted from the antenna. Rather, it undergoes through multiple reflections or scattering through tall structures prior to adopting multiple paths to the receiver. Therefore, the signal reaching the receiver will not be the result of single scattering effect but will be the result of multiple scattering [23-26]. Multiple scattering introduces further fluctuation in the received signal. The probability density function and cumulative distribution functions are given by [27]

$$P(r) = \frac{1}{\sigma r\sqrt{\pi}} \exp^{-\frac{\left(\log_{10}(r)-\mu\right)^2}{2\sigma^2}} \quad , r>0 \tag{2.10}$$

$$P(r \leq R) = \frac{1}{2} + \frac{1}{2}\,\mathrm{erf}\,\frac{\left(\log_{10}(r)-\mu\right)^2}{2\sigma^2} \tag{2.11}$$

where σ and μ are the standard deviation and mean of $\log_{10}(r)$, and are expressed in decibel values. Suzuki [23] has shown that this distribution gives very good fit with data acquired in urban radio channels.

2.3.5 Suzuki Model

This model incorporates short-term fading and long-term fading in a single distribution. In this model, the short-term fading is modelled as Rayleigh and long term as Log-Normal. In fact it is a combination of Rayleigh and Log-Normal distribution. Suzuki gives the PDF of the envelope in dB as per the following relationship [23].

$$P(r_{dB}) = \sqrt{\frac{\pi}{8}} \frac{1}{M\sigma_{dB}} \int_{-\infty}^{+\infty} \exp\left[\frac{2}{M}\left(r_{dB} - \overline{r_{dB}}\right) - \frac{\left(\overline{r_{dB}} - m\right)^2}{2\sigma_{dB}}\right] \exp\left[-\frac{\pi}{4}\exp\left(\frac{2}{M}\left(r_{dB} - \overline{r_{dB}}\right)\right)\right] d\overline{r_{dB}} \qquad (2.12)$$

where, m is the mean of Rayleigh distribution in dB, σ_{dB} is the deviation of this mean in dB and $\overline{r_{dB}}$ is normally distributed.

2.3.6 Weibull Model

The Weibull Distribution is widely employed for radar sea clutter modelling. The probability density function in dB is expressed as [4]

$$P(y) = \frac{w}{M}\left(\frac{b}{V}\right)^w e^{\left[\frac{wy}{M} - \left(\frac{b}{v}\right)^w \exp\left(\frac{wy}{M}\right)\right]} \qquad (2.13)$$

where V is the RMS value of y in linear units, w is a measure of the signal variability and parameter W is defined as W=w/v. The Weibull distribution becomes Rayleigh when w = 2.

2.4 DOPPLER SHIFT AND SPECTRUM OF FADING SIGNAL

On account of the movement of mobile in a multi-path environment, there is a shift in the received carrier frequency. This shift is called Doppler shift and is denoted by f_m. This shift is caused due to a continuous change in the electrical length of every propagation path. These variations in the path lengths result in variations in the phases of the received signals. This phase change introduces an offset in the instantaneous received frequency.

The dynamic change in path length is a function of two parameters. One is the angle between the direction of arrival of the wave and the motion of the mobile unit and another is the velocity of the mobile unit. The waves arriving from ahead of the mobile yield positive Doppler shift and those reaching from the back produce negative shift. The change in frequency is given by the following relationship.

$$\Delta f = f_m = \frac{v}{\lambda}\cos\alpha \tag{2.14}$$

This shows that different waves arriving from different angles produce different shifts. The maximum value of the positive or negative shift will be produced when the angle between the motion of the mobile and the wave is zero. This value is v/λ. Consequently, the RF received signal will contain frequency components ranging from $f_c + f_m$ to $f_c - f_m$. However, the power spectrum density of frequency components confined within this range depends upon the probability density function of the spatial angles of arrival. There are three widely mentioned models that explain the RF power spectrum of fading signal. These are Clark's [28], Aulin's [29] and Parsons models [30]. They differ from each other on the basis of the assumption made in respect of the PDF of the spatial angels of arrival. The geometry of incoming wave along with its spatial angels with respect to the frame of reference is shown in Figure 2.4.

2.4.1 Clark's Model

The first one is a two dimensional model and was proposed by Clark [28]. Clark's model has been derived assuming that the spatial angel, β between the wave and the x-y plane is zero and the probability density function of alpha is uniform between 0-2π. It

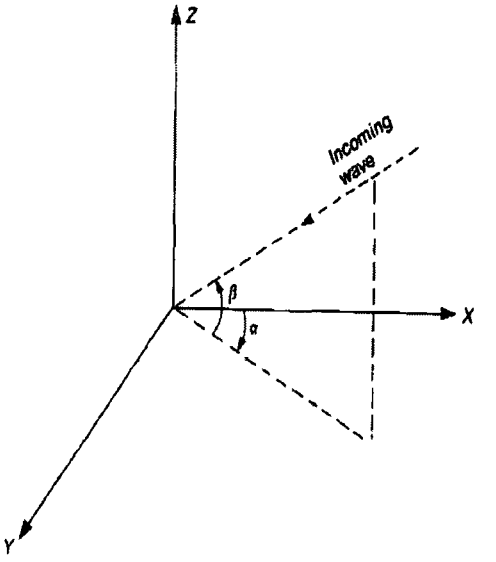

Figure 2.4 Spatial frame of reference [4]

assumes that all waves travel horizontally and the PDF of the angle of arrival is uniform. It also assumes that the receive antenna is omni-directional and the waves are vertically polarized. The shape of the spectrum obtained from this model is shown in Figure 2.5. Though the spectrum is band limited to a range of frequencies between $f_c + f_m$ to $f_c - f_m$ around the carrier it has infinite values at $f_c \pm f_m$

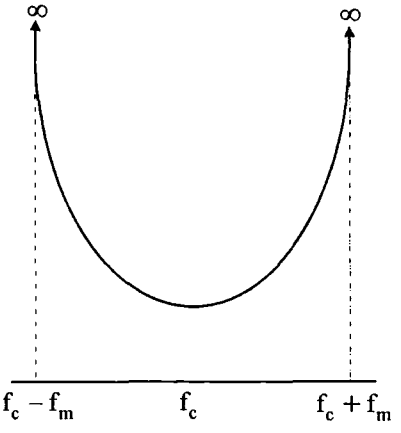

Figure 2.5 Doppler spectrum for Clark's model.

2.4.2 Aulin's Model

Aulin's model [29] is a three dimensional model. It differs from Clark's model in terms of the assumptions made for the PDF of the spatial angel of arrival β_n. It assumes that not all incoming waves travel horizontally. The waves also reach the receiver with spatial angle β with the x- axis. Instead of assuming the spatial angel of arrival β_n as zero, Aulin incorporated the following PDF relationship of β_n for calculating the signal spectra.

$$P(\beta) = \begin{cases} \dfrac{\cos\beta_n}{2\sin\beta_m} & |\beta| \le |\beta_m| \le \dfrac{\pi}{2} \\ 0 & \text{elsewhere} \end{cases} \tag{2.15}$$

The shape of spectra for Aulin's model is shown in Figure 2.6. The spectrum of Aulin's model is also confined within $f_c + f_m$ to $f_c - f_m$ range.

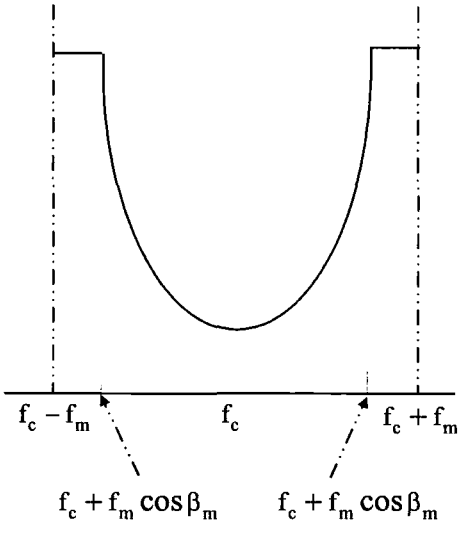

Figure 2.6 Doppler spectrum for Aulin's model

Unlike Clark's model, the spectrum does not have infinite values at $f_c \pm f_m$. These values are constant between $f_c + f_m \cos\beta_m$ to $f_c + f_m$ and $f_c - f_m \cos\beta_m$ to $f_c - f_m$. The constant values of spectra between these limits are also unrealistic.

2.4.3 Parson's Model

The last model is Parson's model [30]. The power spectra of this model is neither infinite at $f_c \pm f_m$ as in the case of Clark nor unrealistically flat between $f_c + f_m \cos\beta_m$ to $f_c + f_m$ and $f_c - f_m \cos\beta_m$ to $f_c - f_m$ like Aulin. The shape of the spectrum is shown in Figure 2.7. Parson based his model on the fact that the majority of the waves travel in a nearly horizontal direction and a realistic PDF for β is one that has a mean value of 0^0. It was numerically calculated incorporating the following relationship for the PDF of β.

$$P(\beta) = \begin{cases} \dfrac{\pi}{4|\beta_m|}\cos\left(\dfrac{\pi}{2}\dfrac{\beta}{\beta_m}\right) & |\beta| \le |\beta_m| \le \dfrac{\pi}{2} \\ 0 & \text{elsewhere} \end{cases} \tag{2.16}$$

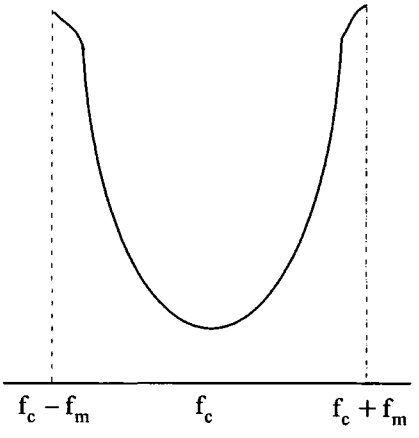

Figure 2.7 Doppler spectrum for Parson's model

2.5 AVERAGE LEVEL CROSSING RATE AND FADE DURATION

The Rayleigh and Rician fading statistics merely provide information on the overall percentage of time that the signal goes below a certain level. Information pertaining to the rapidity with which the signal level changes between different levels can not be obtained from these statistics. Whereas, this information is imperative in the context of

the bit error performance of the wireless communication link and is employed for designing error control codes and diversity schemes to be used in mobile communication systems [31]. Due to Doppler fading, the signal experiences deep fades occasionally as the vehicle is in motion [17, 32-35]. The presence of deep fades as well as their numbers change the instantaneous signal to noise ratio (SNR) and hence, the bit error rate (BER). Level crossing rate (lcr) and average fade duration (afd) are second order statistics used to quantify the deep fades experienced by the fading envelop. The level crossing rate is defined as the expected rate at which the fading envelope, normalized to local rms signal level, crosses a specified level in a positive direction. For Rayleigh fading, the number of level crossing per second is given by [6]

$$N_r = \sqrt{2\pi} f_d \rho e^{-\rho^2} \tag{2.17}$$

where f_d is the maximum Doppler frequency and $\rho = R/R_{rms}$ is the value of the specified level R, normalized to the local rms amplitude of the fading envelope [27] and N_r represents the average number of level crossing per second at R. This relationship indicates that it is a function of Doppler. There are few crossings at both high and low levels, with the maximum rate occurring at $\rho = 1/\sqrt{2}$, (i.e., at a level 3 dB below the rms level). It can further be observed that the signal envelope occasionally encounters deep fades, but shallow fades are more frequent.

Average fade duration, τ_{av} is the average period of time the signal remains below a certain level R. For Rayleigh fading, the average fade duration is given by

$$\tau_{av} = \frac{e^{\rho^2} - 1}{\rho f_d \sqrt{2\pi}} \tag{2.18}$$

The average fade duration decreases with an increase in Doppler frequency f_d. The level crossing rate and average fade duration, expressed by the above mathematical relationship, are direct consequences of the classical Doppler spectrum. Nevertheless, this is not the only spectrum which produces these results, as it may be shown that any Doppler spectrum having the same variance will share the same level crossing rate and

average fade duration. Figure 2.8 demonstrates the concept of level crossing rate and average fade duration [11].

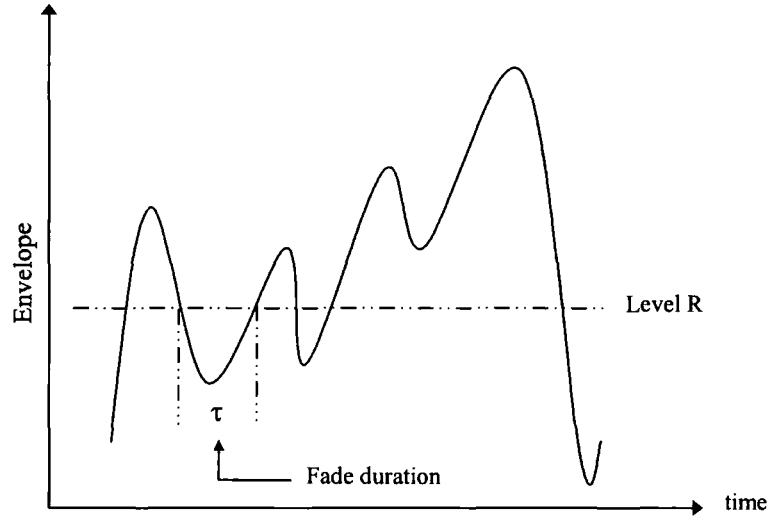

Figure 2.8 Level crossing rate and fade duration.

2.6 MOBILE RADIO CHANNEL

The mobile radio channel is typically characterised by the various propagation paths between the transmitter and the receiver. Many moving and still objects, which are part of the mobile channel environment, produce reflections, diffractions and scattering. This creates a constantly changing environment that constantly modifies the signal energy, amplitude and phase of the multi-path signal over time. This makes the behavior of the channel dynamic and time variant. Such a channel is classified as multi-path time variant channel.

2.6.1 Impulse Response of the Channel

The impulse response is used to describe completely the behavior of a channel in the time domain. It is the response of the channel to an impulse $\delta(t)$. This impulse is theoretical and cannot be generated in reality. However, it is possible to generate extremely short duration pulses of very high amplitude to approximate to the theoretical

pulse δ (t). In order to measure the impulse response of the channel, a very narrow pulse (delta) is transmitted. The impulses corresponding to multi-path arrive at the receiver at different times with different amounts of power depending upon the nature of reflections, scattering, refractions and diffractions. These received pulses are the time-delayed replicas of the original pulse. These multiple arrival times of the signals with different powers can be used to define the impulse response of the channel [11, 12, 16]. The transmitted and the received impulses are shown in Figures 2.9 and 2.10 respectively.

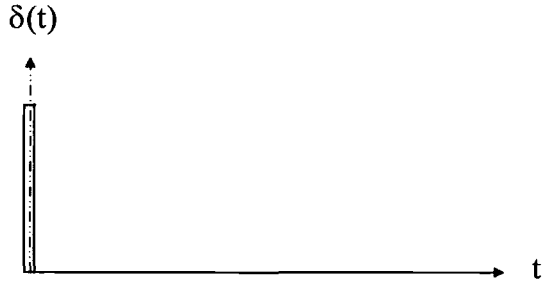

Figure 2.9 Transmitted pulse at t = 0

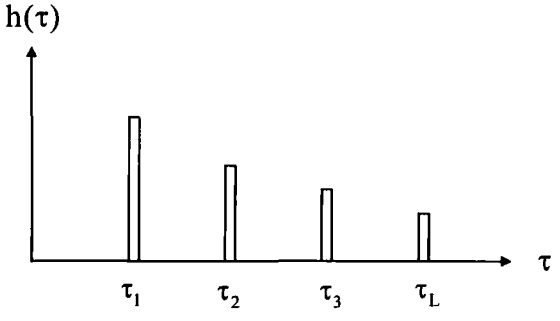

Figure 2.10 Channel impulse response.

As the environment is dynamic, the arrival times, magnitudes and numbers of received impulses vary as a function of time. Therefore, the impulse response also varies and becomes a function of time. In reality there exists a large number of multi-path components and their differential times of arrival are so close that it is not possible to distinguish one path from another and the graph of impulse response appears

continuous instead of discrete. The time delay axis is usually partitioned into equal delay segments, called delay bins. Each delay bin contains those multi-path components whose times of arrival are within the bin duration and can be considered unresolved. These multi-path components when vectorially combined can be represented by a delta function occurring in the centre of the bin having a weight that is Rayleigh distributed [12, 14]. Smaller impulses whose levels are less than the desired threshold are ignored. The channel impulse response is a bandpass function, but can also be expressed by its equivalent complex baseband notation. The time variant impulse response of a wideband channel is given by

$$h(t,\tau)=\sum_{i=1}^{L}\beta_i(t)e^{j\phi_i(t)}\delta\left[\tau-\tau_i(t)\right] \tag{2.19}$$

where t is time, τ is delay variable, L is the number of paths, $\beta_i(t)$ is the amplitude of ith path signal at time t and τ_i is the delay of ith path. The measured impulse response of a typical multi-path channel [36] is produced below for the purpose of demonstration. As seen, some of the components which have more power are easily distinguishable.

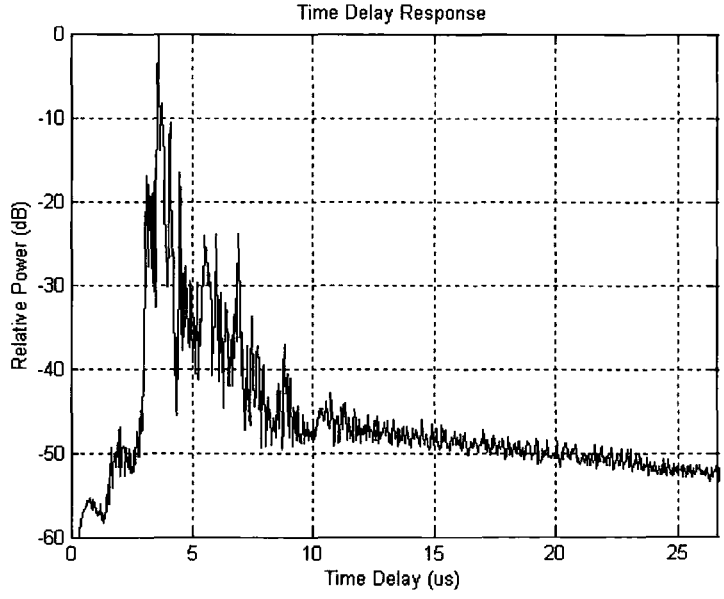

Figure 2.11 An example of a typical measured impulse response

2.6.2 Power Delay Profile (PDP)

The impulse response of a channel provides information pertaining to the distribution of received power in terms of delayed components. So the impulse response indicates the power of received components along with the delays associated with them. This plot is often called power delay profile or multi-path intensity profile. It is obtained by averaging a large set of impulse responses. The power delay profile $P_d(\tau)$ of the channel is the expected power per unit time received with a certain excess delay. It measures the average channel output power at delay τ in response to a channel input impulse at time zero.

$$P_d(\tau) \equiv E\left[\frac{1}{2}h(t,\tau)\, h^*(t,\tau)\right] \tag{2.20}$$

A typical shape of the power delay profile is shown in Figure 2.12. The time dispersive behavior of the multi-path channel can be characterised by estimating the average delay (AD), the root mean square (RMS) delay spread (DS), and the profile width (WD). These parameters are extracted from the power delay profile (PDF) of the multi-path channel and are used to characterize the behavior of the channel at different frequencies [37-39]. The following sections provide a brief description of these parameters.

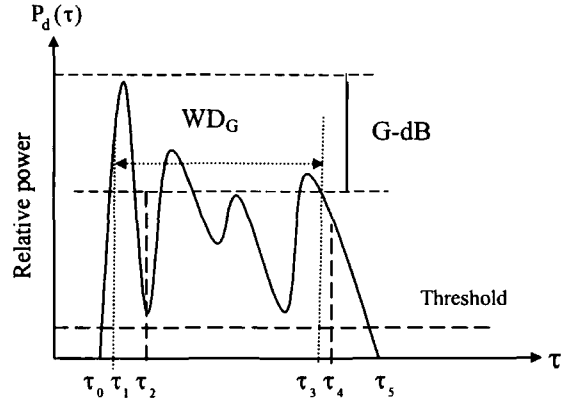

Figure 2.12 Profile width and delay window

2.6.2.1 Maximum Delay Spread (τ_m)

The maximum delay for which $P_d(\tau) > 0$ is defined as delay spread (τ_m) of the channel. In fact it is the time between the first and the last received component during which the multi-path signal's power falls to some threshold level below that of the strongest component. It represents the delay spread of the channel and is a function of the physical environment.

2.6.2.2 Average Delay Spread (ADS)

The average delay spread, also called first moment of the power delay profile (PDF), is defined by the following equation.

$$AD = \frac{\sum_i \tau_i \cdot P_h(\tau_i)}{\sum_i P_h(\tau_i)} \tag{2.21}$$

In the above equation, τ_i and $P_d(\tau_i)$ denote the time delay and power level of the i^{th} path, respectively.

2.6.2.3 RMS Delay Spread (DS)

The second central moment of the delay profile is RMS delay spread. The RMS delay spread characterizes the time dispersive nature of a channel and is given by

$$DS = \sqrt{\frac{\sum_i (\tau_i - AD)^2 \times P_h(\tau_i)}{\sum_i P_h(\tau_i)}} \tag{2.22}$$

The RMS delay spread impacts the bit error rate (BER) performance of systems. The irreducible BER was shown to depend upon the RMS delay spread rather than the shape

of the delay profile [40]. In [41], the effect of RMS delay spread on the BER performance of the system was studied and the influence of the PDF shape on the BER performance was investigated in [42].

2.6.2.4 Profile Width (PW)

Another parameter related to the PDF is the profile width (WD_G). It is defined as the delay interval between the points where PDP crosses the level G-dB below the peak for the first and the last time.

$$WD_G = (\tau_3 - \tau_1)_G \tag{2.23}$$

The delay window W_q is the duration of the middle portion of the profile that contains q % of the total energy [43].

$$W_q = (\tau_4 - \tau_2)_q \tag{2.24}$$

where the boundaries of $\tau_2 - \tau_4$ are defined as

$$\int_{\tau_2}^{\tau_4} P_h(\tau)\,d\tau = q \int_{\tau_0}^{\tau_5} P_h(\tau)\,d\tau = q \times P_{tot} \tag{2.25}$$

2.7 CHANNEL SYSTEM FUNCTIONS

The channel is considered as an element that transforms the input into the output. It is, therefore, analogous to a linear filter. The mobile radio channel can be described in terms of a two-port filter with randomly time varying transmission characteristics. The input and the output of a channel can be described either in time or frequency. As shown in Figure 2.13, the relationship between the input and the output can be explained in a number of ways using different time- frequency input-output relationships. This leads to the four system functions [45], known as Bello's functions.

1. Input delay-spread function h(t,τ).
2. Output Doppler-spread function H(f, v).
3. Time-variant transfer function T(f,t)
4. Delay Doppler-spread function S(τ, v).

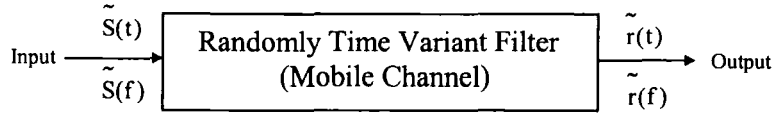

Figure 2.13 Linear filter model of mobile channel

2.7.1 Input Delay-Spread Function h(t,τ)

The Input delay-spread function $h(t,\tau)$ models the channel in the time-domain. It is interpreted as the response of a channel at time t to a unit impulse τ seconds in the past. It describes the channel in terms of t- τ domain, where t and τ are time and delay variables respectively. It is called input delay-spread function since the delay is associated with the input port of the channel. If the delay is associated with the output port of the channel then this function is referred to as output delay spread and is denoted by g(t,τ). The input delay spread function relates the complex envelope of the channel's input $\tilde{S}(t)$ and the output $\tilde{r}(t)$ through the following convolution relationship.

$$\tilde{r}(t) = \int_{-\infty}^{\infty} \tilde{S}(\tau)h(t-\tau)d\tau \qquad (2.26)$$

$$\int_{-\infty}^{\infty} \tilde{S}(t-\tau)h(t,\tau)d\tau$$

It is worth mentioning here that the limits of the integrals, $(-\infty,\infty)$, are not physically realizable. Therefore, for real world mobile propagation channels, τ is always greater than zero and less than some maximum value of τ_{max}, beyond which the impulse response of the channel is considered zero. However, $(-\infty,\infty)$ will be used for the

purpose of simplicity. The channel model based upon this function is called the tapped delay line model and will be described in section 2.8.

2.7.2 Output Doppler-Spread Function H(f, v)

The second function H(f, v) describes the channel in f-v domain. It is interpreted as the channel response at frequency v Hz above the cissoidal input at f Hz. This function relates the channel output spectrum $\tilde{R}(f)$ to the channel input spectrum $\tilde{S}(f)$ by the following relationship.

$$\tilde{R}(f) = \int_{-\infty}^{\infty} \tilde{S}(f - v)\, H(f - v, v)dv \tag{2.27}$$

2.7.3 Time Variant Transfer Function T(f, t)

The time variant transfer function relates the output in the time domain and the input in the frequency domain by the following relationship.

$$\tilde{r}(t) = \int_{-\infty}^{\infty} S(f)T(f,t)e^{j2\pi ft}df \tag{2.28}$$

It explains the frequency domain characteristics of the channel. This function will be described in detail in chapter 4.

2.7.4 Delay Doppler-Spread Function S(τ, v)

The last function, delay Doppler-spread, describes the channel in the time delay as well as in the Doppler shift domain. The output of the channel is expressed as

$$\tilde{r}(t) = \int_{-\infty}^{\infty} \int_{-\infty}^{\infty} \tilde{S}(t - \tau)\, S(\tau, v)\, e^{j2\pi vt} dv d\tau \tag{2.29}$$

2.7.5 Relationships Between the System Functions

The above stated system functions provide the same information in different forms and can be transformed from one to another through Fourier transform and inverse Fourier transform. Their inter- relationship is shown in Figure 2.14, where F denotes the Fourier transform and F^{-1} the inverse Fourier transform and the subscript represents the transformed variable.

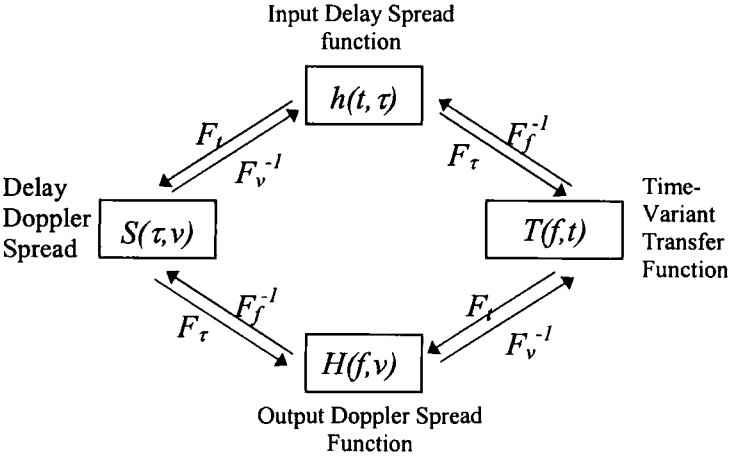

Figure 2.14 Inter-relationships between system functions.

2.8 MOBILE CHANNEL MODELS

Mobile channel simulators are usually designed on the basis of channel models which represent the random time varying behavior of a propagation channel. Therefore, it is imperative that the channel is modelled as accurately as possible. Great deal of work has been carried out on mathematical modelling of mobile channels [49-52]. The time-variant mobile propagation channel can be modelled either in the time domain or the frequency domain using the previously outlined four system functions [45]. The time domain description of the channel is expressed in terms of its impulse response. For the time varying channel, the impulse response is also time-variant. As it has already been stated that the channel impulse response is a bandpass function but it can be expressed in terms of its equivalent lowpass complex function. If the input to the channel is expressed in the notation of complex envelope of real bandpass signal $\tilde{S}(t)$, then the

relationship among the input, the output $\tilde{r}(t)$, and the complex impulse response of the channel $h(t,\tau)$ is expressed by the under mentioned relationship. The input and the impulse response convolve with each other to give the output [17].

$$\tilde{r}(t) = \int_0^t \tilde{S}(\tau)h(t-\tau)d\tau \qquad (2.30)$$
$$= \int_o^t \tilde{S}(t-\tau)h(t,\tau)d\tau$$

If the multi-path delay variable is expressed in discrete steps of multi-path excess delay, then this integral can be approximated as follows,

$$\tilde{r}(t) = \sum_{m=0}^{n} \tilde{S}(t-m\Delta\tau)h(t,m\Delta\tau)\Delta\tau \qquad (2.31)$$

The result can be realized by using a delay line with taps at delays $m\Delta\tau$ with output multiplied by the time-varying weights $h(t, m\Delta\tau)$. The structure is shown in Figure 2.15.

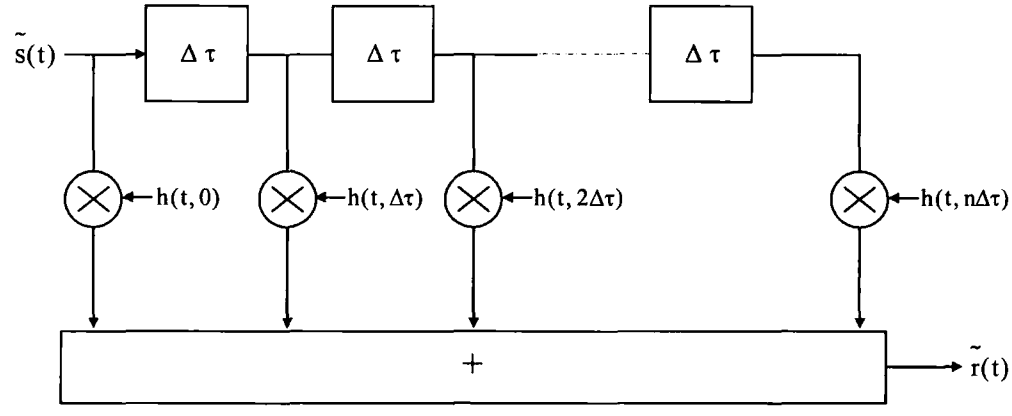

Figure 2.15 Tapped delay line model of the channel.

This kind of structure having delay line, tap weights and adder is called a transversal filter. The weights of each tap are random processes and can be generated by various techniques. Therefore, the time variant impulse response of the channel can be modelled as a tapped delay line transversal filter. Modelling the time-variant impulse response

through this filter shows that the received signal comprises delayed and attenuated replicas of the input signal. The tapped delay line model explains the multi-path phenomena in the time domain. In the frequency domain, the output frequency spectrum $\tilde{R}(f)$ and the input frequency spectrum $\tilde{S}(f)$ can be related as

$$\tilde{R}(f) = \int_{-\infty}^{\infty} \tilde{S}(f-v)\, H(f-v, v)dv \tag{2.32}$$

This integral can be represented in discrete form after approximation as

$$\tilde{R}(f) = \sum_{0}^{N} \tilde{S}(f - m\Delta v)H(f - m\Delta v, m\Delta v)\Delta v \tag{2.33}$$

The function H(f, v) is known as output Doppler-spread function in Bello's terminology[45] and shows the Doppler shift or frequency broadening on the output spectrum. In the above equation, the variable v expresses the Doppler shift introduced by the channel. The above equation shows that the channel can be represented by a bank of filters with transfer function $H(f, m\Delta v)\Delta v$ followed by a frequency conversion chain that produces the Doppler shift. The frequency domain model is shown in Figure 2.16.

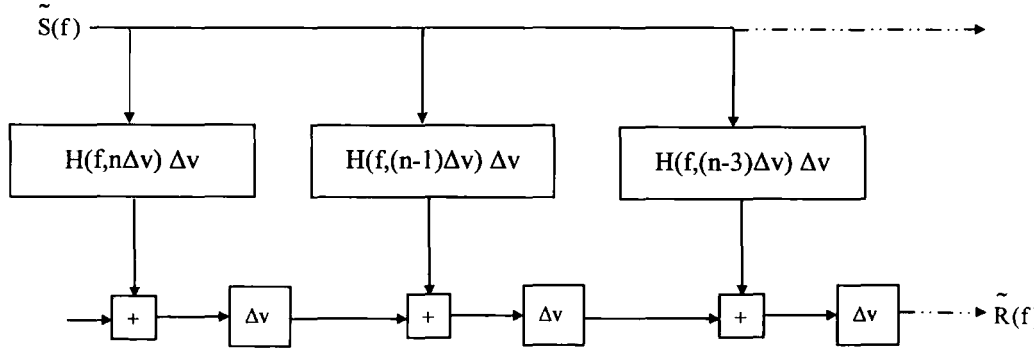

Figure 2.16 Frequency domain model for mobile channel.

The channel model based on the time variant transfer function is dealt in section 4.5.

2.9 WIDE SENSE STATIONARY UNCORRELATED SCATTERING (WSSUS) CHANNEL

The behavior of mobile radio channel is dynamic and time variant. Its characteristics change continuously. Under these circumstances, it is extremely difficult and too complicated to characterize and describe the channel using multidimensional probability density functions (PDFs) of the channel's system functions. Therefore, the assumption of wide sense stationary and uncorrelated scattering (WSSUS) is employed to simplify the mathematical modelling of the time varying nature of the mobile propagation channel both in time and frequency using stochastic processes. Under the assumption of WSS, the channel is assumed stationary over a short interval of time or over small spatial distances whilst it is not stationary in the strict sense. Therefore, the fading statistics of the channel are assumed stationary over short periods of time in order to characterize the channel. The Wide Sense Stationary channel has the property that the channel's correlation functions are invariant under a translation in time. Mathematically, the autocorrelation function does not depend on t and t', but only on the difference $\Delta t = t - t'$. Such a channel is referred to as Wide Sense Stationary (WSS). In WSS channel, if the contribution from elemental scatterers with different path delays is uncorrelated then the channel is called Wide Sense Stationary Uncorrelated Scattering channel (WSSUS).

WSSUS channel model requires only two sets of parameters to characterize fading and multi-path effects: the Power Delay Profile (PDP) and Doppler Power Spectra (DPS). Both parameters can be described by a single function called scattering function $S(\tau, f_D)$, where τ denotes the path delay and f_D denotes the Doppler frequency [46, 47].

2.9.1 Correlation Functions

The time variant nature of mobile communication channel can be explained by employing Bello's four system functions. Due to the random behavior of the channel, these system functions are modelled as random processes. In order to characterize the mobile channel, the joint probability density function of all these system functions is needed. It is not straightforward to obtain the joint probability density functions of these

system functions. Therefore, in order to describe the stochastic behavior of these system functions, it is more appropriate to employ the concept of autocorrelation and obtain statistical correlation functions for each system function. Since, each system function is modelled as Gaussian, then the autocorrelation function can completely describe the statistical nature of these system functions [44]. As there are four system functions, four autocorrelation functions are defined.

2.9.1.1 Time-Frequency Correlation Function $|R(\Delta f,\Delta t)|$

Time-frequency correlation function, also called spaced-frequency spaced-time correlation function, is the autocorrelation function of the time variant transfer function T(f, t). As the time variant impulse response is modelled as complex-valued, zero-mean Gaussian random process in the t variable and since the time variant transfer function is obtained by taking the Fourier transform of time variant impulse response in delay variable, it follows that T(f,t) possesses similar statistics[52,16]. By employing the assumption of wide-sense stationery, uncorrelated scattering (WSSUS), the frequency-time correlation function is obtained by taking the Fourier transform of multi-path power delay profile in the time delay variable [45]. It defines the correlation between two components of the channel transfer function with a frequency spacing of Δf and time spacing of Δt. The degree of correlation is expressed by normalized spaced–frequency spaced-time correlation function, denoted by $\rho(\Delta f,\Delta t)$ and expressed as [53]

$$\rho(\Delta f,\Delta t) = \frac{R(\Delta f,\Delta t)}{R(0)} \tag{2.34}$$

$$\rho(\Delta f,\Delta t) = \frac{E\left[T(f,t)T^{*}(f+\Delta f,t+\Delta t)\right]}{\sqrt{E\left[\left|T(f,t)\right|^{2}\right]E\left[\left|T(f+\Delta f,t+\Delta t)\right|^{2}\right]}}$$

where E [.] is the expectation operator.

It is assumed independent of the particular time t and frequency f and depends only on two variables, Δf and Δt. It is used to calculate both the coherence band width and coherence time. If $\Delta t = 0$ in the above relationship, then the correlation coefficient gives

the degree of similarity between any two frequency components which are separated by Δf. As Δf increases, the correlation decreases. At a particular separation, the frequency components become completely uncorrelated. At $\Delta f = 0$, it gives the degree of correlation of any frequency component at two different instants of times separated by Δt. As Δt increases, the correlation decreases and at a particular value of Δt, the envelope of the frequency component becomes completely uncorrelated. If A_1 and A_2 are the envelops of signals at frequency f_1 and f_2 respectively and at t_1 and t_2 respectively, then the envelope correlation coefficient is expressed as follows[11]

$$\rho(\Delta f, \Delta t) = \frac{E[A_1 A_2] - E[A_1]E[A_2]}{\sqrt{\left[E[A_1^2] - E[A_1]^2\right]\left[E[A_2^2] - E[A_2]^2\right]}} \tag{2.35}$$

In order to evaluate the above equation, the probability density function of delay (τ) of the signal has to be modelled. This has been modelled as an exponential distribution [12, 27].

$$P(\tau) = \frac{1}{\sigma}\exp\left(-\frac{\tau}{\sigma}\right)U(\tau) \tag{2-36}$$

where σ is the delay spread of the channel. The correlation coefficient can be derived by defining $\Delta f = |f_1 - f_2|$ and $\Delta t = |t_1 - t_2|$ as

$$\rho(\Delta f, \Delta t) = \frac{J_0^{\,2}(2\pi f_d \Delta t)}{1 + (2\pi \Delta f)^2 \sigma^2} \tag{2.37}$$

where $J_0(\cdot)$ is the zeroth-order Bessel function.

The above equation reveals that the time-frequency correlation function depends upon two parameters, the Doppler spread and the delay spread of the channel. The Doppler spread represents the rapidity of channel variation, whereas the delay spread indicates the time spreading of a channel. The time-frequency correlation function can be also derived by taking the double Fourier transform of the scattering function [16].

2.9.1.2 Spaced Frequency Correlation Function $|R(\Delta f)|$ and Coherence Bandwidth

The frequency correlation function describes the channel behavior in the frequency domain. It gives the degree to which the channel response at two carrier frequencies separated by $\Delta f = |f2 - f1|$ are correlated. It can be measured by transmitting a pair of sinusoids separated in frequency by Δf, and cross correlating the two received signals. It is derived from the autocorrelation function of T(f, t) by assuming the time separation between the observations as zero. The normalized spaced-frequency correlation function is expressed as

$$\rho(\Delta f) = \frac{R(\Delta f)}{R(0)} \tag{2.38}$$

Therefore, substituting $\Delta t = 0$ in equation 2.36 yields the following results

$$\rho(\Delta f, \Delta t) = \frac{J_0{}^2(2\pi f_d \Delta t)}{1+(2\pi\Delta f)^2 \sigma^2} \tag{2.39}$$

$$\rho(\Delta f, 0) = \frac{1}{1+(2\pi\Delta f)^2 \sigma^2} \tag{2.40}$$

The spaced-frequency correlation function can be obtained from the multi-path intensity profile as they form a Fourier transform pair.

The coherence bandwidth (B_c) is derived from the frequency correlation function of two fading signal's envelopes at frequencies f_1 and f_2 respectively. It is inversely proportional to the RMS delay spread of the channel. An exact relationship between the two is a function of the actual shape of multi-path delay profile [6], and must be derived from the measured channel data by employing signal analysis tools like Fourier techniques.

Several approximate relationships between the coherence bandwidth and RMS delay spread have been described in the literature on the basis of different values of frequency correlation functions. The choice of correlation value is arbitrary. The

correlation values of 0.9 and 0.5 have been widely used in the literature to describe the coherence bandwidth. However the correlation value of 0.5 is more common and has been used more frequently in the literature as threshold for defining coherence bandwidth. At the value of 0.9, it is defined as the frequency range over which the channel's complex frequency transfer function has a correlation of at least 0.9 and is expressed as [54]

$$B_c = \frac{1}{50\sigma_d} \tag{2.41}$$

For the correlation value of 0.5 B_c is expressed as [6,10, 55].

$$B_c = \frac{1}{5\sigma_d} \tag{2.42}$$

2.9.1.3 Spaced-Time Correlation Function $|R(\Delta t)|$ and Coherence Time

The spaced-time correlation function provides information about the time varying nature of the mobile channel. The temporal variations of the channel are either due to the relative motion between the transmitter and receiver or by movement of objects within the channel. The degree to which the response of the channel to a sinusoid at time instant t_1 and time instant t_2, separated by Δt, is related is expressed by this function. It gives the time duration over which the channel's response is essentially invariant. It is measured by transmitting a single sinusoid and auto correlating the signals received at two instants of times separated by Δt. In case of no relative motion between the mobile and the channel, provided the channel is static, the channel's response would be highly correlated for all values of Δt and the spaced-time correlation function, $R(\Delta t)$ would be constant. It can be obtained from the frequency-time correlation function by substituting the value of Δf as zero.

$$\rho(\Delta f, \Delta t) = \frac{J_0{}^2(2\pi f_d \Delta t)}{1+(2\pi\Delta f)^2\sigma^2} \tag{2.43}$$

The above equation reveals that the time-correlation function depends upon the Doppler shift which is a function of the relative velocity of the mobile. Clark [28] expressed its relationship with velocity assuming unmodulated carrier signal, dense scattering environment and constant velocity as follows,

$$\rho(\Delta t) = J_0(kv\Delta t) \tag{2.44}$$

where $J_0(.)$ is the zeroth-order Bessel function of first kind, Δt is the separation between time instants and k is the free space phase constant and is given by

$$k = \frac{2\pi}{\lambda} \tag{2.45}$$

The spaced-time correlation function can also be derived by taking the Fourier transform of the Doppler power spectrum. It is also defined on the basis of a certain value of correlation between the two responses. At the ρ value of 0.5, it is defined by the following relationship,

$$T_c = \frac{9}{16\pi f_d} \tag{2.46}$$

2.9.2 Classification of Mobile Radio Channels

2.9.2.1 Narrowband and Wideband Channel

Fading is primarily caused due to small variations in the path lengths of the received multi-path components. Fading can be characterized as either flat (multiplicative) or frequency selective (non-multiplicative). This classification is made on the basis of delay spread of the received signal and the transmitted signal bandwidth. In narrow band fading, the inverse signal bandwidth is much greater than the time spread of the propagation path delays. Under these conditions, all frequency components present within the transmitted signal bandwidth will experience the same random attenuation (fade) and phase shift. Therefore, no distortion will be introduced in the data signal. The

channel will offer the same characteristics to all the frequency components present in the transmitted bandwidth [44].

If the range in the propagation path delays is large compared to the inverse signal bandwidth, then the frequency components will experience different phase shifts along the different paths. Under these conditions, the channel introduces amplitude and phase distortion in the message bandwidth. Therefore, the frequency components present within the transmitted bandwidth will experience different fading. This kind of fading is called frequency selective, as it is a function of frequency.

The channel is called wideband if the bandwidth of the transmitted signal is greater than the coherence bandwidth of the channel. This channel is also called frequency selective fading channel. On the other hand if the bandwidth of the transmitted signal is smaller than the coherence bandwidth of the channel then the channel is classified as narrowband. The narrowband channel offers constant gain to the transmitted signal and no frequency selective fading is observed. The path geometry, shown in Figure 2.17, for multi-path propagation can be modelled as ellipses with the transmitter and receiver located at the foci.

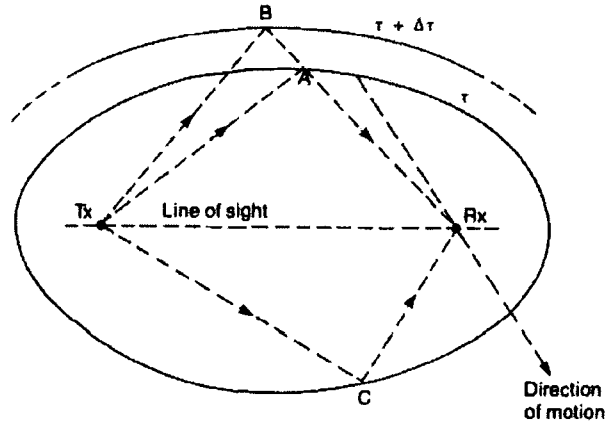

Figure 2.17 Path geometry for multi-path fading channel [4].

Different path delays can be associated with a particular ellipse. The scatterers associated with the flat fading channel are located on the ellipses that are either very close or overlapping with each other. In case of wideband, the scatterers are located on

several ellipses. These ellipses are not very close to each other and correspond to the differential delays that are significant as compared to the inverse signal bandwidth.

2.9.2.2 Slow Fading and Fast Fading

The rapidity with which the fading occurs or the time variant nature of the channel can be characterized as slow fading or fast fading. If the bandwidth of the transmitted signal is greater than the Doppler spread then the channel is classified as a slow fading channel with loss in signal to noise ratio. If the transmitted bandwidth is less than the Doppler spread, the channel is referred to as fast fading. The fast fading channel results in bit error rate.

2.10 SUMMARY AND CONCLUSIONS

The mobile radio channel is characterized by the multi-path propagation. This phenomenon results in constant variations in the received signal envelope, termed as fading, due to the movement of the mobile. There are two kinds of fading, fast fading or short-term and slow fading or long-term. The rapid fluctuations in the received signal amplitude due to the movement of the mobile over a small area are termed as fast or short-term fading, whereas the variations in the mean signal level observed over a large area is referred to as long-term fading. The received signal envelope obeys various distributions, such as Rayleigh, Rician, Nakagami, Lognormal, Suzuki and Weibull depending upon the existence of a direct line-of-sight component, the area surrounding the mobile and closeness of scattering objects. Due to the movement of the mobile in a multi-path environment, there is a shift in the received carrier frequency. This shift is called Doppler shift. There are three widely mentioned models that explain the RF power spectrum of fading signal. These are Clark's, Aulin's and Parson's models. They differ from each other on the basis of the assumption made in respect of the PDF of the spatial angels of arrival.

Channel system functions are employed to model and describe the channel in the time and frequency domain. Four system functions along their correlation functions were presented.

Second order statistics, such as level crossing rate and average fade duration were discussed. These are used for designing channel coding and interleaving schemes and greatly impact the BER system performance. Classification of the channel was made on the basis of narrow band, wideband, slow and fast fading.

This chapter emphasized the need for thorough understanding of the various phenomena associated with multi-path fading. These phenomena significantly impact the performance and play a pivotal role in the design and development of mobile communication systems for various operating environments.

2.11 BIBLIOGRAPHY

1. S.C. Gupta., R. Viswanathan, and R. Muammar, "Land mobile systems: A tutorial exposition," IEEE Commun. Mag., vol.23, no.6, June 1985, pp. 34-45.
2. B.H., Fleury and P.E., Leuthold, "Radio wave propagation in mobile communications: An overview of European research," IEEE Commun. Mag., vol.34, no.2, Feb 1996, pp. 1-13.
3. H. Hamuda, Cellular Mobile Radio Systems, Chichester, UK: John Wiley & Sons, 1998.
4. J.D. Parsons, The Mobile Radio Propagation Channel: John Wiley & Sons Ltd., 2000.
5. W.C.Y. Lee., Mobile Communications Engineering, New York: McGraw-Hill, 1976.
6. T.S Rappaport, Wireless Communications, Principles and Practice: Prentice Hall, 1996.
7. M.R.L., Hodges, "The GSM radio interface,"Br. Telecommun. Res. Lab.J., vol. 8, no.1, Jan 1990, pp. 31-43.
8. F. Ikegami., and S. yoshida, "Analysis of muiltipath propagation structure in urban mobile radio environments," IEEE Trans. Antennas and Propagation, vol., AP-28, no. 4, July 1980, pp. 531-537.
9. B. Sklar, "Rayleigh fading channels in mobile digital communication systems Part 1: Characterization," IEEE Commun. Mag., July 1997, pp. 90-100.

10. W.D., Rummler, R.P., Coutts., and M. Liniger, "Multipath fading channel models for microwave radio," IEEE Commun. Mag., vol.24, no.11, Nov 1986, pp. 30-41.
11. P.M. Shankar, Introduction to Wireless Systems, New York: John Wiley & Sons, 2002.
12. R. Steele, Mobile Radio Communications, London, England: Pentech Press Ltd., 1992.
13. W.R., Braun., and U.A., Dersch., "A physical mobile radio channel model," IEEE Trans. on Vehicular Technology, vol.40, no.2, May 1991, pp. 472-482.
14. L.W. Couch, Digital and Analog Communication Systems: Prentice Hall, 1997.
15. A. Papoulis, Probability, Random Variables, and Stochastic Processes, 3rd ed. New York: McGraw-Hill, 1991.
16. J.G. Proakis, Digital Communications, New York: McGraw-Hill, 1993.
17. J.D. Parsons and J.G. Gardinar., Mobile Communications Systems, Glasgow: Blackie & Sons, Ltd., 1989.
18. B. Sklar, Digital Communications: Fundamentals and Applications, Ch.4, Englewood Cliff, NJ: Prentice Hall, 1988.
19. S. Stein, "Unified analysis of certain coherent and non-coherent binary communications systems," IEEE Trans. on Information Theory, vol. IT-10, no.1, Jan 1964, pp. 43-51.
20. W.B. Davenport., and W.L. Root, An Introduction to the Theory of Random Signals and Noise, New York: McGraw-Hill, 1958.
21. H. Hashemi, "The indoor radio propagation channel," Proc. IEEE, vol.81, no.7, July 1993, pp. 943-968.
22. W.C., Hoffman, Statistical Methods on Radio Wave Propagation, New York, "The M-distribution: A general formula of intensity distribution in rapid fading" by M. Nakagami: Pergamon Press, 1960, pp. 943-968.
23. H. Suzuki, "A statistical model for urban radio propagation," IEEE Trans. on Communication, vol. COM-25, no.7, July 1977, pp. 673-679.
24. W.C.Y. Lee "Estimate of local average power of a mobile radio signal," IEEE Trans. on Vehicular Technology, vol.34, no.1, Feb 1985, pp.22-27.

25. F. Hansen, and F.I. Meno., "Mobile fading: Rayleigh and lognormal superimposed," IEEE Trans.on Vehicular Technology, vol.26, no.4, Nov 1977, pp.332-335.
26. R.C. French "The effect of fading and shadowing on channel reuse in mobile radio," IEEE Trans. on Vehicular Technology, vol.28, no.3, Aug 1979, pp.171-180.
27. W.C. Jakes, Microwave Mobile Communications, New York: IEEE Press, 1994.
28. R.H. Clarke, "A statistical theory of mobile radio reception", Bell Syst. Tech., no. J.47, 1968, pp. 957-1000.
29. T. Aulin, "A modified method for the fading signal at a mobile radio channel", IEEE Trans. on Vehicular Technology, vol. VT-28 (3), 1979, pp. 182-203.
30. J. D. Parson and A.M.D. Turkmani, "Characterization of mobile radio signals: model description", Proc IEE Part 1,138(6), 1991, pp. 549-56.
31. S. Haykin and M. Moher, Modern Wireless Communications, Upper Saddle River, NJ: Pearson Prentice Hall, Pearson Education, Inc., 2005.
32. W.C.Y. Lee, "Statistical analysis of the level crossings and duration of fades of the signal from an energy density mobile radio antenna," Bell Syst. Tech J., vol. 47, Feb. 1967, pp. 417-448.
33. R.S. Kennedy, Fading Dispersive Communication Channels, New York: John Wiley & Sons, 1969.
34. W.F. Bodtmann and H.W. Arnold., "Fade duration statistics of a Rayleigh distributed wave," IEEE Trans. on Communication, vol. COM-30, no. 3, Mar 1982, pp. 549-553.
35. F. Adachi, M.T. Feeney, and J.D. Parsons., "Level crossing rate and average fade duration for time diversity reception in Rayleigh fading conditions," IEE Proc., vol. 135, pt.F, no.6, Dec 1988, pp. 501-506.
36. S. Salous, G.H. Gokalp, "Simultaneous average power delay profile measurements for UMTS, " ICAP-2000, paper no., 2000, pp. 709 1-4.
37. L.J. Greenstein, V. Erceg, Y.S. Yeh, and M.V. Clark, "A new path-gain/delay-spread propagation model for digital cellular channels", IEEE Trans. on Vehicular Technology, vol. 46, no. 2, May 1997, pp. 477-485.

38. A.A.M. Saleh, and R.A. Valenzuela, "A statistical model for indoor multipath propagation", IEEE Jour. on Selected Areas in Communications, vol. SAC-5, no. 2, Feb 1987, pp. 128-137.
39. H. Hashemi, and D. Tholl, "Statistical modeling and simulation of the RMS delay spread of indoor radio propagation channels", IEEE Trans. on Vehicular Technology, vol. 43, no. 1, Feb 1994, pp. 110-120.
40. J. Chuang, "The effects of time delay spread on portable radio communications channels with digital modulation," IEEE Jour. on Selected Areas in Communications, vol. SAC-5, no. 5, June 1987, pp. 879-889.
41. P.A. Bello, and B.D. Nelin, "The effect of frequency selective fading on the binary error probabilities of coherent matched filter receivers," IEEE Trans. on Communications Systems, June 1963, pp.170-185.
42. M. Wittmann, J. Marti, and T. Kurner, "Impact of the power delay profile shape on the bit error rate in mobile radio systems," IEEE Trans. on Vehicular Technology, vol. 46, no. 2, May 1997, pp. 329-339.
43. E. Gurdenli, "Digital land mobile radio communication – on the presentation of results from wideband measurements," COST 207, Copenhagen, 11-13 May 1987.
44. G.L Stuber, Principles of Mobile Communication, Norwell, MA: Kluwer Academic Press, 1996.
45. P.A. Bello, "Characterization of random time-variant linear channels", IEEE Trans. on Communication Systems, Dec 1963, pp. 360-393.
46. M. Patzold, Mobile fading channels, 2rd ed. West Sussex, England: John Willey & Sons, Ltd, 2002
47. J. K. Caver, Mobile Channel Characteristics: Kluwer Academic Publisher, 2002.
48. G.L Turin, Clapp F. D., Johnston T. L., Fine S. B., and Lavry D., "A statistical model of urban multipath propagation," IEEE Trans. on Vehicular Technology, vol. VT-21, no. 1, Feb 1972, pp. 1-8,.
49. M. Lecours, Chouinard J., Delisle G. Y., and Roy J., "Statistical modelling of the received signal envelope in a mobile radio channel," IEEE Trans. on Vehicular Technology, vol. 37, no. 4, Nov 1989, pp. 204-212.

50. S. Kozono., "Received signal-level characteristics in a wide-band mobile radio channel," IEEE Trans. on Vehicular Technology, vol. 43, no. 3, Aug 1994, pp. 480-486
51. U. Dersch, and E. Zollinger, "Propagation mechanisms in microcell and indoor environments," IEEE Trans. on Vehicular Technology, vol. 43, no. 4, Nov 1994, pp. 1058-1066.
52. M.K. Simon and S.M. Alouini, Digital Communication over Fading Channels, A Unified Approach to Performance Analysis, New York: John Willey & Sons, Inc., 2000.
53. S. Saunder, Antenna and Propagation for Wireless Communication Systems: John Wiley & Sons Ltd.
54. W.C.Y. Lee, Mobile Cellular Telecommunications Systems, New York: McGraw Hill Publications,1989.
55. S. Stein, " Fading channel issues in syetem engineering," IEEE Jour. On Selected Areas in Communications, vol. SAC-5, Feb1987, pp.68-89.

CHAPTER 3

MOBILE CHANNEL SIMULATORS

3.1 INTRODUCTION

The process involved in the design and development of mobile communication system demands its excessive field testing in order to gauge its performance. Testing of a mobile system in the field is not only costly but also time consuming. Due to the time variant behaviour of the channel, it is required to test the system in all possible circumstances to quantify its performance against the worst scenario. The major issue is the repeatability of a certain scenario that degrades the system performance beyond acceptable level. Such propagation conditions are difficult to be experienced again. Therefore, the need was felt to come up with a solution that could test the system under a controlled propagation environment in the laboratory. The process of replicating a multi-path fading environment is termed as simulation.

The simulation can be carried out by a personal computer using software that can simulate the time varying behaviour of the mobile radio channel. Such simulators are called software simulators. Also, hardware can be built to simulate the channel. The hardware simulators are called Emulators. However, most of the literature have used the term 'simulator' in both cases. Therefore, this report will also be using the term simulator for hardware as well as for software simulators.

The channel simulator allows us to replicate the varying and troublesome characteristics of the RF mobile communication channel at our workbench to assess and quantify the performance of mobile communication systems. It produces randomly time-variant channel impulse response corresponding to the real propagation environment. It is in fact a radio channel in a box. This chapter presents a literature review of some of the popular narrowband and wideband simulators built over the last three decades. In this chapter, various analogue and digital techniques adopted by those simulators in replicating the real world mobile channels will be discussed in details.

On the basis of the classification of mobile propagation channels, simulators can be divided into two types: narrowband and wideband. As the wideband channel is considered

as a combination of many narrowband channels at different delays, it is appropriate to first review the principles of narrowband simulation and then consider the simulation of wideband channels.

3.2 NARROWBAND SIMULATOR

A narrowband simulator implements a narrowband fading model. Its operating principles are based upon the multi-path fading phenomena and its effects on the propagating signal. In narrowband fading, the arrival times of the multi-path components are unresolvable by the receiver and their vectorial sum results in fading. The impulse response of narrowband fading is modelled as a single delta function whose weight varies in time and obeys a certain statistical distribution depending upon the physical construction of the channel. As all frequencies confined within the signal bandwidth undergo the same fading, the narrowband channel can be simulated by simply multiplying the input signal with the output of the fading generator. The fading generator needs to produce an output in accordance with the known first and second order statistics of the mobile channel. Basically, the fading generator produces a complex random process with the desired mean, variance and autocorrelation function. There can be three main methods for narrowband channel simulation [1-4]. These are briefly discussed below.

3.2.1 Uniform Phase Modulation

In this method [1] the signal is split into many paths and then each path is randomly phase modulated. The random phase must be uniformly distributed. Uniformly distributed phase modulation is accomplished by appropriately shaping the amplitude distribution of the low-pass Gaussian noise source. As shown in Figure 3.1, the addition of several such uniformly distributed phase modulated paths will approximate to Rayleigh fading. This implementation has a draw back that the power spectrum of the output signal cannot be easily controlled and calculated. Due to this drawback, it is not practically employed for construction of multi-path fading simulators [1].

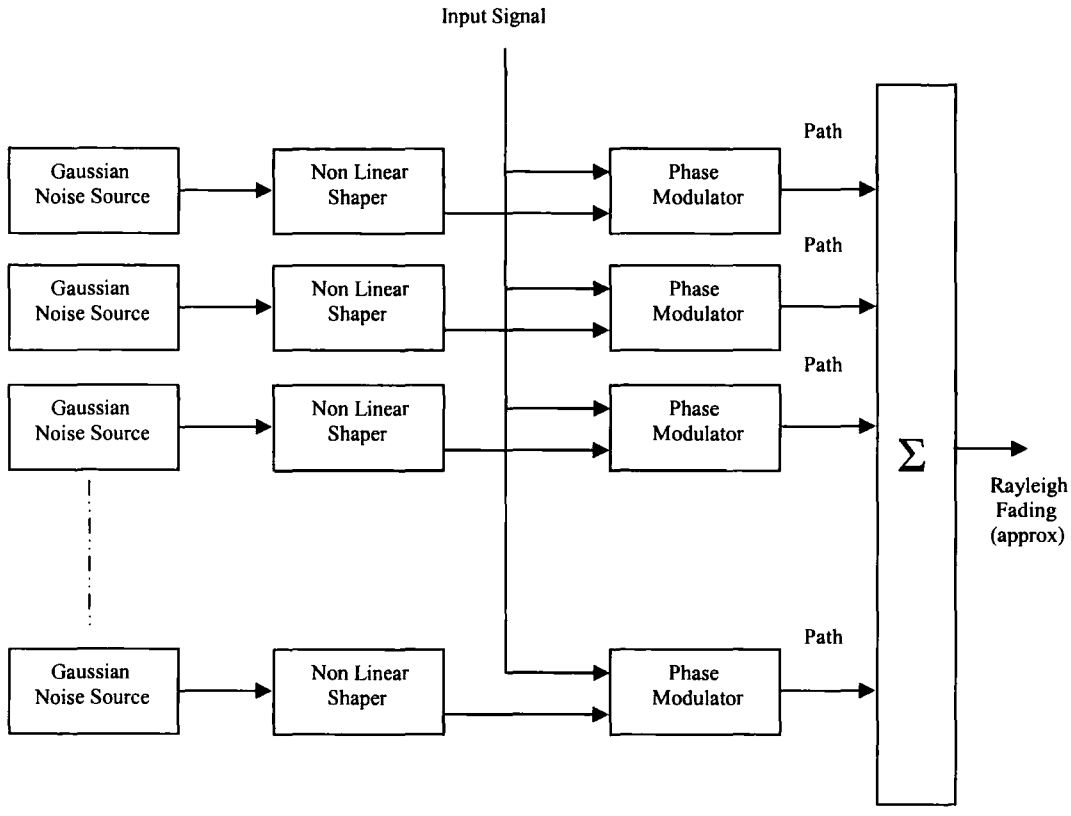

Figure 3.1 Simulator using uniform phase modulation

3.2.2 Quadrature Amplitude Modulation

This method of narrowband simulation is based upon equations 3.1-3.2 which represent the output of the multi-path fading channel in complex lowpass notation. Equation 3.1 states that the input signal is first converted into two quadrature components called in-phase and quadrature. Each component is modulated/multiplied separately by a normalized Gaussian random process having zero mean and variance σ^2. The combination of the modulated quadrature signals gives the Rayleigh fading output. The block diagram of the narrowband fading simulator is shown in Figure 3.2.

$$E(t) = E_0\left[\cos\omega_c t\sum_{n=1}^{N} C_n\cos\theta_n - \sin\omega_c t\sum_{n=1}^{N} C_n\sin\theta_n\right] \tag{3.1}$$

where $$I(t) = \sum_{n=1}^{N} C_n\cos\theta_n \text{ and } Q(t) = \sum_{n=1}^{N} C_n\sin\theta_n \tag{3.2}$$

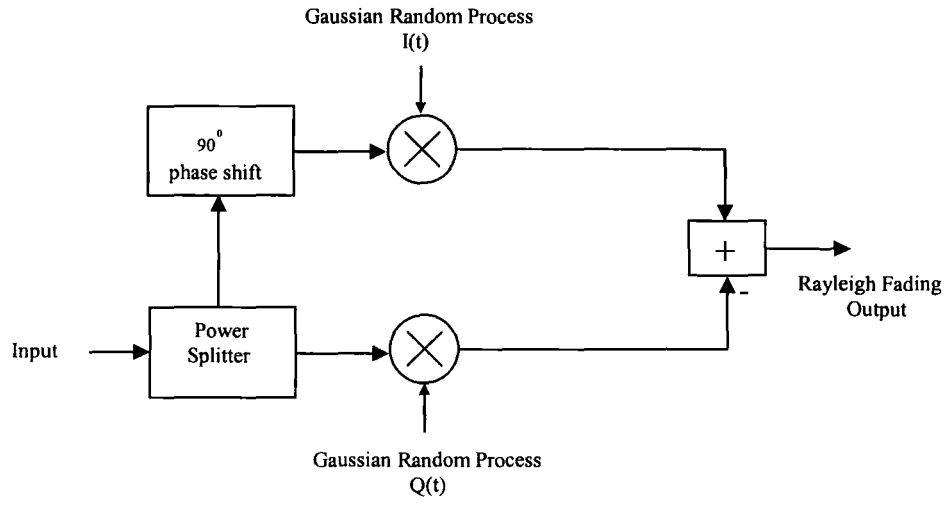

Figure 3.2 Block diagram of narrowband simulator

There are two time domain and one frequency domain methods to generate a complex Gaussian random process with the desired statistical properties. Time domain methods are: filtered Gaussian noise and sum of sinusoid, which are also referred to as Jakes's method. These methods are briefly explained below.

3.2.2.1 Filtered Gaussian Noise

The filtered Gaussian noise method is shown in Figure 3.3. In this method, two uncorrelated Gaussian random processes with zero mean and same variances are passed through identical lowpass filteres to limit and reshape its spectrum. A Gaussian random process is completely characterized by its mean value and colour, which can be described either by the power spectral density or, alternatively by the autocorrelation function[5-10]. The purpose of filtering is to achieve the maximum possible resemblance of the simulated spectrum with the theoretical one [11]. These filters only limit and shape the spectrum but do not alter the probability density function (PDF) of the random process. However, these filters reduce the variances of the processess [12]. The filter transfer function is the square root of the desired spectrum shape. As stated in section 2.4, the theoretical spectrum is U shaped with limits equal to the maximum

positive and negative Doppler shifts, which are equal to v/λ, where v is the velocity of the mobile unit and λ is the wavelength of the signal. It is practically not possible to shape the spectrum as per the theoretical one, however it can be approximated to the desired one by controlling the characteristics of the shaping filter. The cut-off frequencies of these filters are equal to the maximum Doppler shift. These filters can be implemented in the analogue as well as in the digital domain. Digital implementation is flexible and gives very close approximation to the desired U shaped spectrum. Whereas, in the analogue domain the shape have to be approximated. In practical digital implementations, the filters operate at a lower sampling frequency. In order to bring the sampling rate up to the value required by the signal representation, the spectrum shapping filters are followed by interpolators. The interpolation involves up sampling and lowpass filtering. It is efficient to perform interpolation in stages. Therefore, an overall interpolation factor is usually split into a number of cascaded stages to avoid large numbers of filter coefficients.

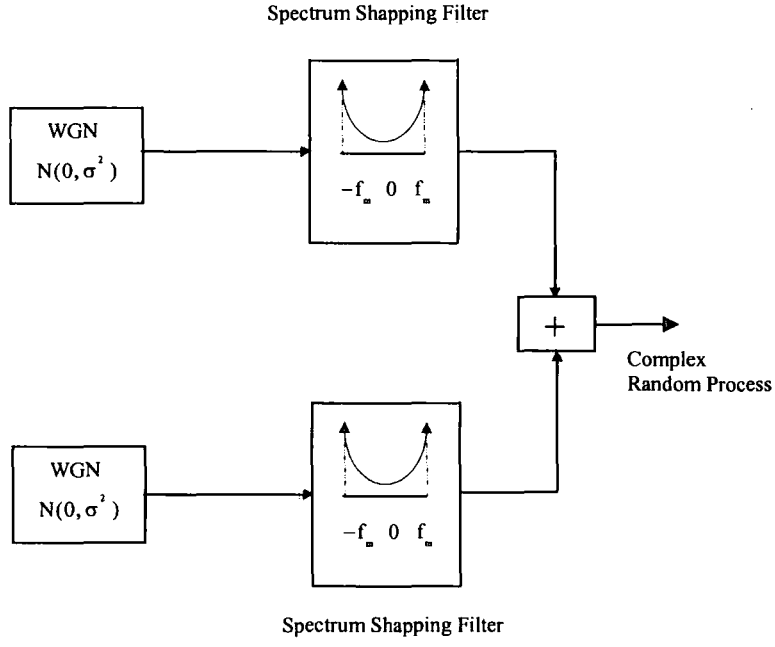

Figure 3.3 Filtered noise method of random process generation.

A number of narrowband channel simulators have been built on the basis of the above mentioned block diagram. These have been implemented using analogue and

digital techniques. A very simple multi-path fading simulator for mobile radio obtains the Gaussian process using a noisy Zener diode [2]. Close approximation to the theoretical spectrum is obtained by passing the output of each noisy diode through filters that are realized by using operational amplifiers. It uses a transistor to build a modulator which modulates the I and Q components of the signal with the filtered Gaussian random noise. In order to simulate various vehicle speeds, it uses a number of filters with different cut-off frequencies. These filters were needed to be replaced each time the simulation speed was changed. The whole implementation was in analogue hardware.

Anaother implementation [13] employed a fixed-point 16 bit digital signal processor to construct a narrowband real time Rayleigh fading simulator. All blocks comprising Doppler filters, Gaussian random process generators, and required multipliers and adders were implemented on a single chip. This implementation simulates short-term as well as long-term fading effects. Long term fading was based on lognormal probability density function. The simulator consits of three Gaussian noise sources, two for Rayleigh fading and one for log-normal shadowing effects. For simulating log-normal shadowing, the output of the Gaussian generator is applied to anti-log block convertor which converts the Gaussian random processs into a lognormal random process with the specified variance. The spectrum shaping filters were implemented as FIR with adjustable bandwidth to accommodate different values of Doppler. A classical U shaped spectrum was employed and all blocks were designed to operate on a variable sampling rate.

3.2.2.2 Sum of Sinusoids Method

This method is also called Jakes method [1]. It uses a number of low frequency oscillators whose outputs are added together to form the I and Q fading signals. The total number of oscillators is N_o plus one with frequency ω_m and amplitude $1/\sqrt{2}$. The amplitudes of N_o oscillators are unity and their angular frequencies are given by the following expression.

$$\omega_m \cos(2\pi\, n/N) \quad \text{where } n=1,2,3,\ldots\ldots N_o \tag{3.3}$$

and $N_o = \frac{1}{2}\left(\frac{N}{2} - 1\right)$

The architecture of Jakes method is shown in Figure 3.4. These oscillators have a phase βn. In order to have a uniform distribution of the complex envelope's phase, the phase

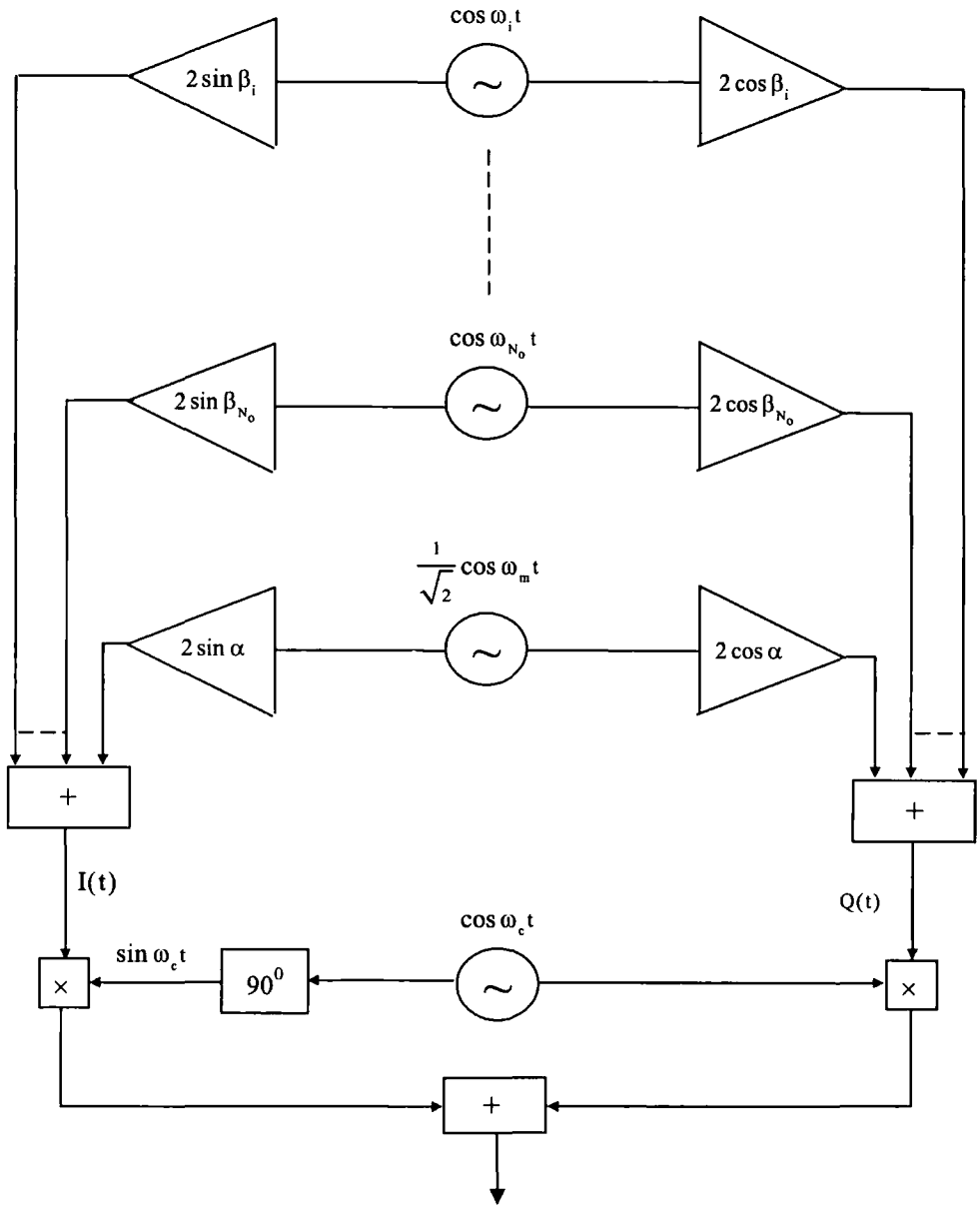

Figure 3.4 Jakes method of simulation

angles of the oscillators have to be chosen appropriately. The phase relationship is obtained by passing the output of these oscillators through the amplifiers having gains of 2cos βn or 2sin βn. The I and Q components are expressed in the following manner.

$$I(t) = 2\sum_{n=1}^{N_0} \cos\beta_n \cos\omega_n t + \sqrt{2}\cos\alpha\cos\omega_m t \tag{3.4}$$

$$Q(t) = 2\sum_{n=1}^{N_0} \sin\beta_n \cos\omega_n t + \sqrt{2}\sin\alpha\cos\omega_m t \tag{3.5}$$

where $\beta_n = n\pi/N_0$,

$\omega_n = \omega_m \cos(2\pi n/N_0)$

It is not necessary to replicate the diagram shown in Figure 3.4 a number of times in order to produce a number of independent processess. The method suggested by Jakes was to give the nth oscillator in the jth process an additional phase shift $\beta_{nj} + \Upsilon_{nj}$, where one possibility was

$$\beta_{nj} = \frac{\pi n}{N_0 + 1} \quad \text{and} \quad \Upsilon_{nj} = 2\pi(j-1)/N_0 + 1 \tag{3.6}$$

Jakes method is simple and popular. It has been developed particularly for the Jakes power spectral density. The spectrum of the process generated by this method matches exactly with the ideal spectrum. However, when this method is employed to generate a number of processes for the frequency selective fading, some of the sources may suffer from quite strong correlation. Correlation coefficients greater than 0.5 have been reported [14,15]. Moreover, when the maximum Doppler shift frequency increases, the limited number of discrete frequency components can no longer approximate the specified spectrum. Therefore, it is difficult to create multiple uncorrelated fading waveforms without modifying the original Jakes method.

A number of improvements in the Jakes method have been proposed in the literature [14-16, 5,7]. Patzold [5] studied the statistaical properties of Jakes method in detail and reported that the two deterministic processes were not optimally Gaussian distributed for the given number of harmonics. He proposed to increas the number of harmonics higher than 9. The method presented in [16] introduces the randomness to Doppler frequency and initial phases of sinusoids to have non determinstcs characteristics. Caver [7] improved the Jakes sum of sinusoids method by ensuring that the set of arrival angles of the simulated plane waves are disjoint for different

generators. The result is that the different generators become uncorrelated, regardless of the choise of initial phases.

A number of implementations [14,17,18] have employed Jakes method to generate fading waveforms. An implementation [17] of narrowband multi-path VHF/UHF channel simulator employed 8088 microprocessor to implement Jakes method of fading. The processor generates two Gaussian control signals I & Q in the digital domain. These control signals are the weighted sums of the outputs from nine sinusoidal oscillators. It could simulate a Doppler rate from 2 to 126 Hz, in steps of 2 Hz. Two digital to analog converters D/A's were used to convert the control signals in analogue form. These were filtered using two analogue filters that were built around operational amplifiers. It employed analog modulators. The whole implementation, except the generation of Gaussian processes, was analogue. The generation of Gaussian processes using a microprocessor had an advantage over the previous implementation in respect of the simulation of various vehicle speeds. Instead of changing the filters, the speed could be controlled by programming the microprocessor.

Chen and Chung [14] employed Texas Instrument's Digital Signal Processing (DSP) microprocessor, TMS320C31, to produce fading waveforms using Jakes method. It incorporated modifications in the phase angles in order to generate multiple uncorrelated fading processes. The jth pair of Gaussian noise processes was given by

$$I(t) = 2\sum_{n=1}^{N_0} \cos\beta_n \cos\left\{\omega_d t \cos\left[\frac{2\pi n}{N} + \frac{2\pi(j-1)}{mN}\right]\right\} + \sqrt{2}\cos\left[\omega_d t \cos\frac{2\pi(j-1)}{mN}\right] \quad (3.7)$$

$$Q(t) = 2\sum_{n=1}^{N_0} \sin\beta_n \cos\left\{\omega_d t \cos\left[\frac{2\pi n}{N} + \frac{2\pi(j-1)}{mN}\right]\right\} \quad (3.8)$$

where $\beta_n = n\pi / N_o$,

$\omega_d = 2\pi f_d$ and $N = 4(N_o + 1)$

and m denotes the total number of processes. It was shown that I(t) and Q(t) were approximately Gaussian for $N_o = 8$. In this implementation, the correlation coefficients between the individual Gaussian processes could readily be adjusted between 0 to 1. This feature is very useful for the study of diversity techniques and MIMO systems.

Patzold, Garcia and Laue [18] developed a narrowband simulator employing sum of sinusoids method using table look-up techniques. This technique exploits the periodicity of the harmonic functions. During the set up phase of the simulation, each of N_i harmonic functions of the sum of sinusoids is sampled only once within its basic period. The samples are then stored in N_i tables. During the simulation phase, the register of each table is read out cyclically and added to produce a Gaussian process. The resulting table system acts like a simulator. This method does not require the use of time consuming trigonometric and multiplication operations. The simulator is realized by using only adders, storage elements, and a simple address generator [19-21]. This simulator employs Rice's sum of sinusoids method to realize a Gaussian noise processes [11,12]. Rice principle states that a Gaussian noise process $\mu_i(t)$ can be modeled by supperposition of an infinite nomber of weighted harmonic functions with equidistant frequencies and random phases according to

$$\mu_i(t) = \lim_{N_i \to \infty} \sum_{n=1}^{N_i} c_{i,n} \cos\left(2\pi f_{i,n} t + \theta_{i,n}\right) \tag{3.9}$$

where the gains $c_{i,n}$ and discrete Doppler frequencies $f_{i,n}$ are given by

$$c_{i,n} = 2\sqrt{\Delta f_i . S_{\mu i \mu i}(f_{i,n})}$$

$$f_{i,n} = n.\Delta f_i$$

The random phases $\theta_{i,n}$ are uniformly distributed over the interval $[-\pi, \pi]$ and the quantity Δf_i is chosen such that equation 3.9 encompasses the whole frequency range of interest, where $\Delta f_i \to 0$ if $N_i \to \infty$. The Gaussian process modelled by equation 3.9 cannot be implemented on computer due to the infinite number of sinusoids. If N_i is made finite, then the resulting Gaussian process, expressed in equation 3.10, will be non-Gaussian distributed in the strict sense. However for $N_i \geq 7$, its PDF will approach close to Gaussian. Now it can be implemended practically on a computer and regarded as a stochastic simulation model. Patzold and Laue [22] assume phases

$\theta_{i,n}$ and other model parametrs constant during simulation. This assumption makes this process completely deterministic for all time t. Figure 3.5 depits the deterministic channel model based on equation 3.10. Its implementation using the table look-up method is presented in Figure 3.6

$$\tilde{\mu}_i(t) = \sum_{n=1}^{N_i} c_{i,n} \cos\left(2\pi f_{i,n} t + \theta_{i,n}\right) \tag{3.10}$$

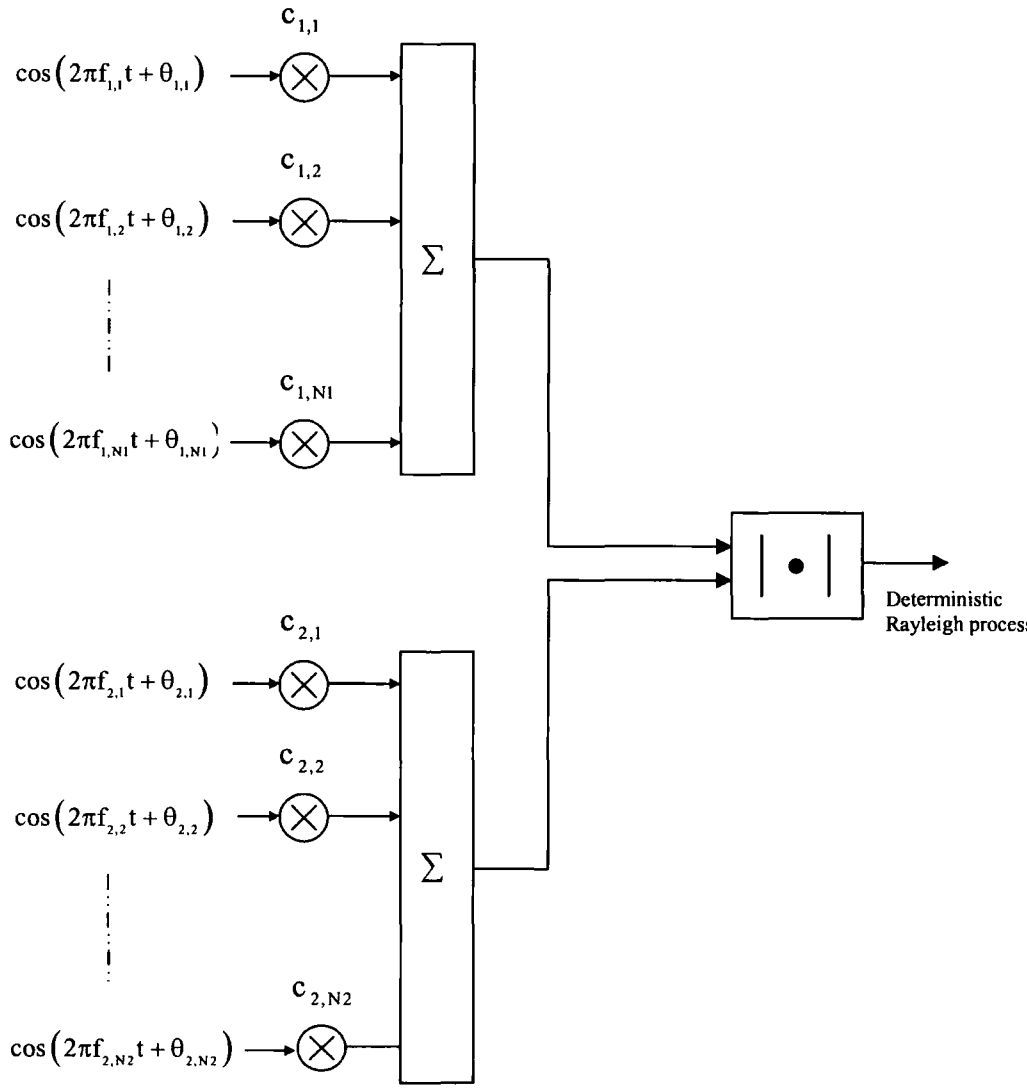

Figure 3.5 Deterministic channel model

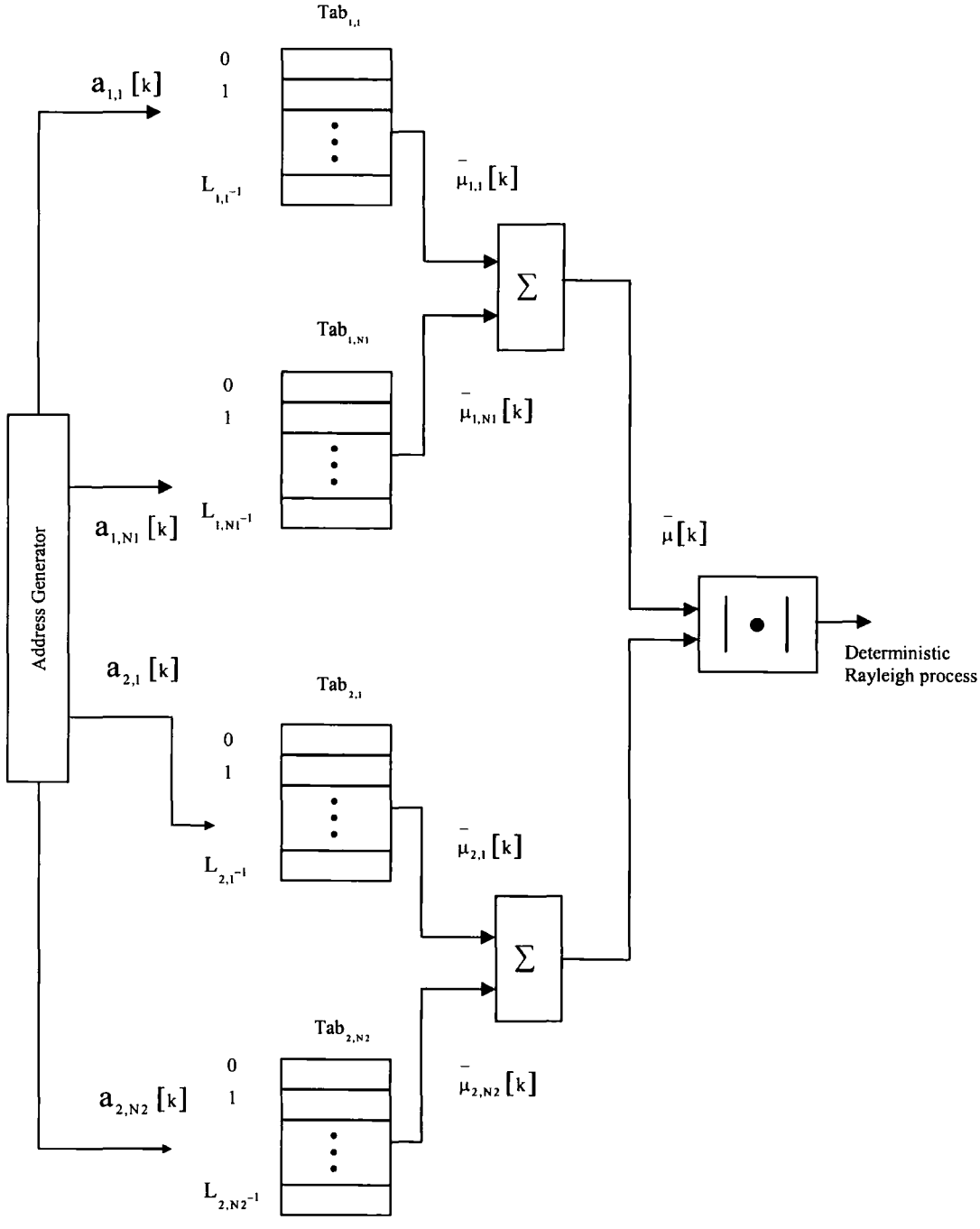

Figure 3.6 Channel simulator using look up table technique.

The discrete deterministic Gaussian process $\overline{\mu_i}[k]$ is obtained by sampling the continuous Gaussian process $\tilde{\mu}_i(t)$ at $t = kT_s$ (k=0,1,2....). The discrete Doppler frequencies $f_{i,n}$ and phases $\theta_{i,n}$ are replaced by $\bar{f}_{i,n}$ and $\bar{\theta}_{i,n}$ respectively as

$$= \sum_{n=1}^{N_i} \bar{\mu}_{i,n}[k] \tag{3.11}$$

$$= \sum_{n=1}^{N_i} c_{i,n} \cos\left(2\pi \bar{f}_{i,n} k T_s + \bar{\theta}_{i,n}\right), \tag{3.12}$$

where i = 1, 2 and T_s denotes the sampling interval

3.2.2.3 Frequency Domain Method

Frequency domain method is based on the idea proposed by Smith [23]. He implemented this method through a computer program in FORTRAN. Figure 3.7 depicts the frequency domain implementation of Rayleigh fading simulator at baseband. In this method, a complex Gaussian random number generator produces a baseband line spectrum with complex weights in the possitive frequency band. Basically these spectral components at discrete frequencies represent a series of frequency components confined in the Doppler spectrum in the range of maximum Doppler shift of f_d. The negative frequency spectrum is created by complex congugate operation on the possitive frequency components. This operation constructs a double sided frequency spectrum from $-f_d$ to $+f_d$. This line spectrum is multiplied by the discrete realization of the Doppler spectrum $\sqrt{S_{E_z}(f)}$. The IFFT operation on the complex double sided spectrum produces a real value time domain Gaussian random process [24].

Benelli, Li and Ikeda [25,26] utilized Smith method to simulate wireless systems. Young and Beaulieu [27] modified Smith method by modifying the filters coefficients. Two branches were combined first and then a single IFFT operation produced a complex Gaussian sequence. The elimination of one IFFT operation reduces the execution time as the IFFT operations are the most computationally intensive part of the Smith method.

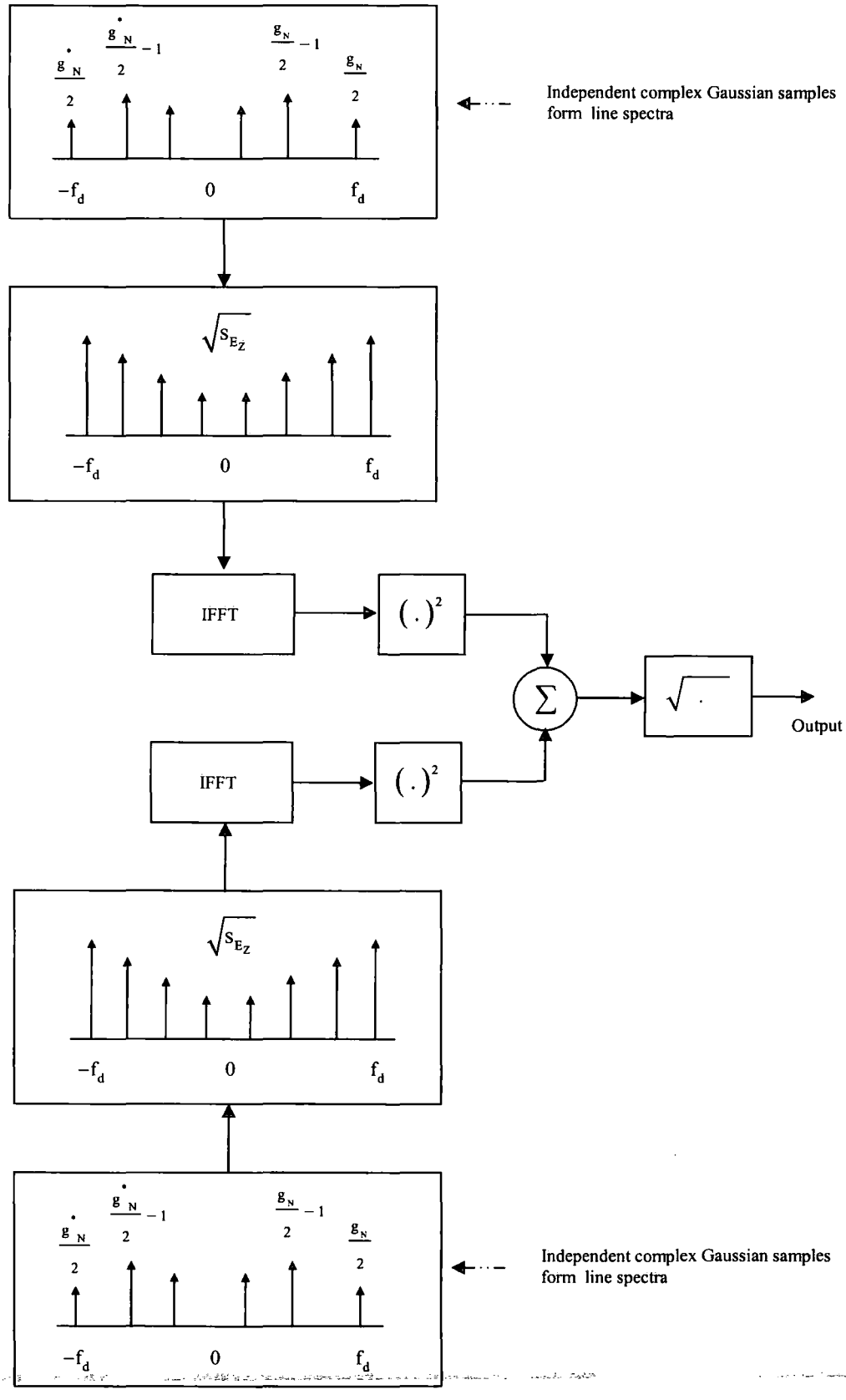

Figure 3.7 Frequency domain method of channel simulation.

Comparing IFFT based frequency domain method with the direct FIR filtering method and sum-of-sinusoids method, the IFFT method requires that all samples be generated using a single fast Fourier transform operation. Whereas, the advantages of the other methods are that the samples can be generated as they are needed. However, the IFFT method has been shown to be the most efficient and high quality method among the other tested methods for the generation of correlated Rayleigh fading [27].

3.3 SIMULATION OF WIDEBAND CHANNEL

The mobile radio channel can be modelled as a linear filter with randomly time varying transmission characteristics. In the time domain, the output of a wideband channel $\tilde{y}(t)$ is the convolution of the input signal $\tilde{x}(t)$ and the time variant impulse response of the channel $h(t, \tau)$.

$$\tilde{y}(t) = \int_0^t \tilde{x}(\tau)h(t-\tau)d\tau = \int_o^t \tilde{x}(t-\tau)h(\tau)d\tau \tag{3.13}$$

It has already been shown in section 2.8 that this convolution can be realized by a tapped delay line transversal filter. Therefore, the channel in the time domain is simulated by delaying the input signal and then multiplying by the time varying weights. The weights of each tap are random processes and can be generated by various techniques. All wideband channel simulators are based upon the tapped delay line transversal filter.

The wideband channel is considered as many narrowband channels at different delays. These delays are expressed with respect to the first significant path. Basically, the delays model the time spreading of the signal. Each narrowband channel at differential delay is a resultant of many unresolved components and models one fading path. In wideband channel simulations, the power of each path is relative and the total power of the channel is usually normalized to unity to preserve the power of the input signal [7]. Therefore, the sum of variances of all random processes in the tapped delay

line model should be unity. This unit variance is distributed among each tap depending upon the delay spread of the simulated power delay profile.

3.4 LITERATURE REVIEW OF WIDEBAND CHANNEL SIMULATORS

Various hardware and software implementations of wideband mobile radio channel simulators have been studied. The literature review of some of the popular simulators built over the last thirty years is being provided in the following section.

3.4.1 Software Implementation

In 1979, Homayoun Hashemi [28] developed a computer program in FORTRAN to create a wideband channel simulator. This program generates time varying impulse responses of the mobile radio propagation channel. The implementation was based on a wideband channel model proposed by Turin [29], which models the channel as a linear filter (shown in Figures 3.8 and 3.9) with complex impulse response h(t) given by the following equation.

$$h(t) = \sum_{k=o}^{\infty} a_k \delta(t - t_k) e^{j\theta_k} \tag{3.14}$$

where k denotes the multi-path number, a_k, θ_k and t_k are the amplitude, phase angle and arrival time of the kth path respectively.

It employed propagation parameters obtained experimentally by Turin [29] at frequencies of 488 MHz, 1280 MHz and 2920 MHz. These parameters pertain to four kinds of urban areas around San Francisco. These areas were classified as heavy built-up, medium size city, small to medium-size town and residential suburbs of cities. The experimental data were processed to obtain values of a_k, θ_k and t_k. It simulates the movement of the mobile by generating different profiles of impulse responses each for one spatial point. Each spatial point has a set of a_k, θ_k and t_k.

The simulation of arrival time is based upon the model developed by Suzuki and refined by Hashmi and is termed as Δ-k model. Basically it is a modified version of a

Poisson process and assumes that echoes arrive in groups from closely spaced buildings.

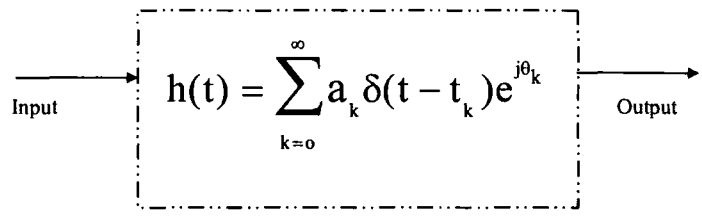

Figure 3.8 Linear filter model of channel

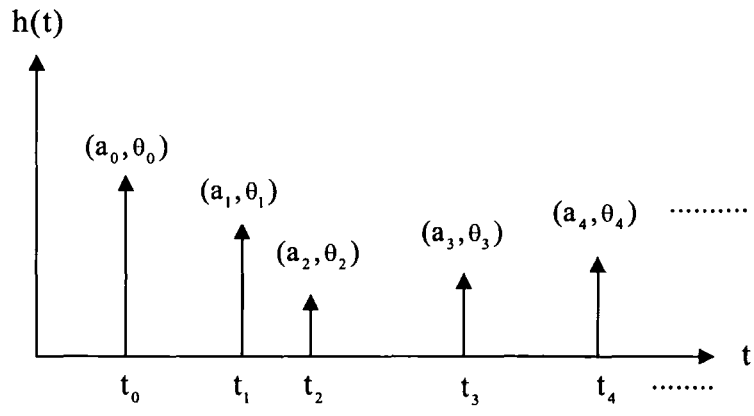

Figure 3.9 Mathematical simulation model

3.4.2 Analogue Hardware Implementation

Various implementations in respect of hardware simulators have also been reviewed. These implementations are based upon the tapped delay line model and vary in terms of the methods used for the generation of fading signals (random processes) and techniques employed in realizing delay lines. In 1980 [30], an UHF channel simulator was built to simulate the mobile propagation channel at a radio frequency of 1780 MHz. It was used for performance evaluation of digital packet radio whose output frequency range was between 1710-1850 MHz. It was designed to operate over a bandwidth of 40 MHz with differential delays of $10\,\mu s$.

The simulator was capable of generating up to four multi-path components with fading bandwidth of 1800 Hz for each path. This fading bandwidth corresponds to a simulation speed of 675mi/h at 1780 MHz. The input signal was converted into intermediate frequency band of 230-370 MHz and then delayed subsequently by employing Surface Acoustic Wave (SAW) delay lines. The SAW delay lines were constructed using piezoelectric substrate of lithium niobate that gave a delay of 9.3 μs for 7.3 cm of substrate. The application of SAW devices permitted the realization of long relative delays due to low propagation velocity of acoustic waves on the surface of the substrate. The SAW delay line was capable of supporting a bandwidth of 140 MHz. After delaying the input IF signal, it was fed to different Rayleigh generators. The architecture of the simulator is shown in Figure 3.10.

Each Rayleigh fading generator works independently and converts the IF signal into I and Q components and then modulates each with an independent Gaussian random process. Each Rayleigh generator consists of a phase shifter, a pair of mixers and a signal combiner. The phase shifter converts the delayed input signal into the I and Q components. The mixer achieves the modulation and signal combiner combines the I and Q output of the mixers to give Rayleigh fading at the output. The block diagram of the Rayleigh generator is shown in Figure 3.11. The output of the Rayleigh fader, denoted by S, is expressed as

$$S = x(t)\cos\omega_c t - y(t)\sin\omega_c t = R = \sqrt{x^2 + y^2} \tag{3.15}$$

$$\text{where} \quad x(t) = \sum A_i \cos(\omega_i t + \Phi_i) \quad \text{and} \quad y(t) = \sum A_i \sin(\omega_i t + \Phi_i) \tag{3.16}$$

$$\text{and} \quad \theta = \tan^{-1}\frac{y}{x} \tag{3.17}$$

The amplitude R follows a Rayleigh distribution. This simulator employs four fading generators to impose independent fading characteristics on the delayed incident signals. x(t) and y(t) are the Gaussian random processes and are obtained from noisy zener diodes (1N 4105) operating near cut off. The noise power spectrum is approximately flat from 0-200 kHz. The spectrum of noise is approximated to the theoretical fading spectrum by passing it through transversal shaping filter. These filters are realized by

charge couple devices (CCD). The bandwidth of these filters can be varied by changing the clock frequency to charge the couple devices in order to simulate different Doppler frequencies.

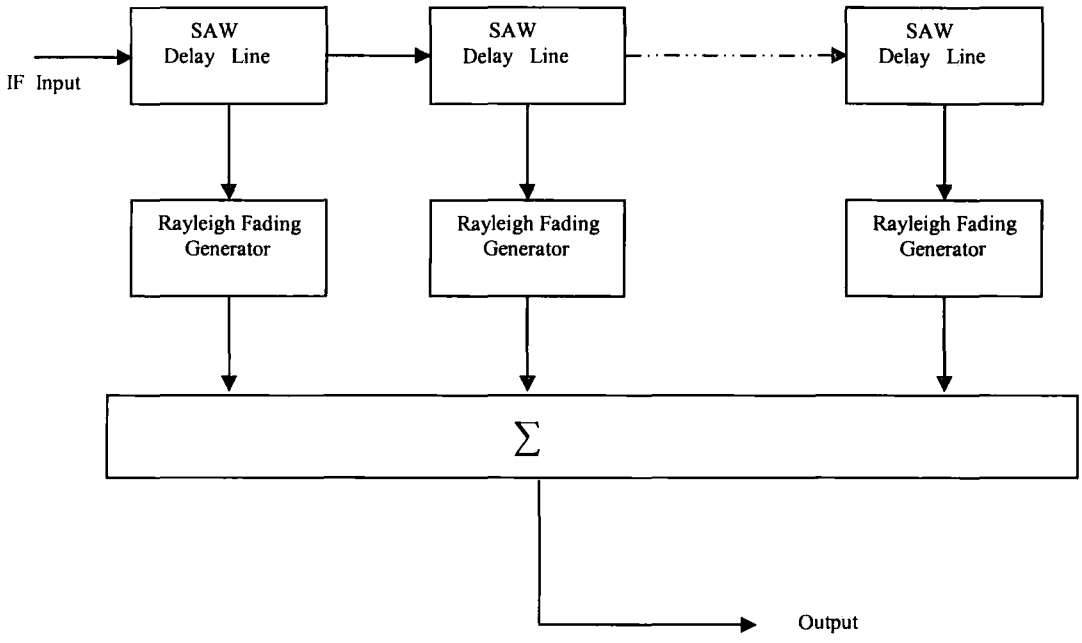

Figure 3.10 Block diagram of simulator.

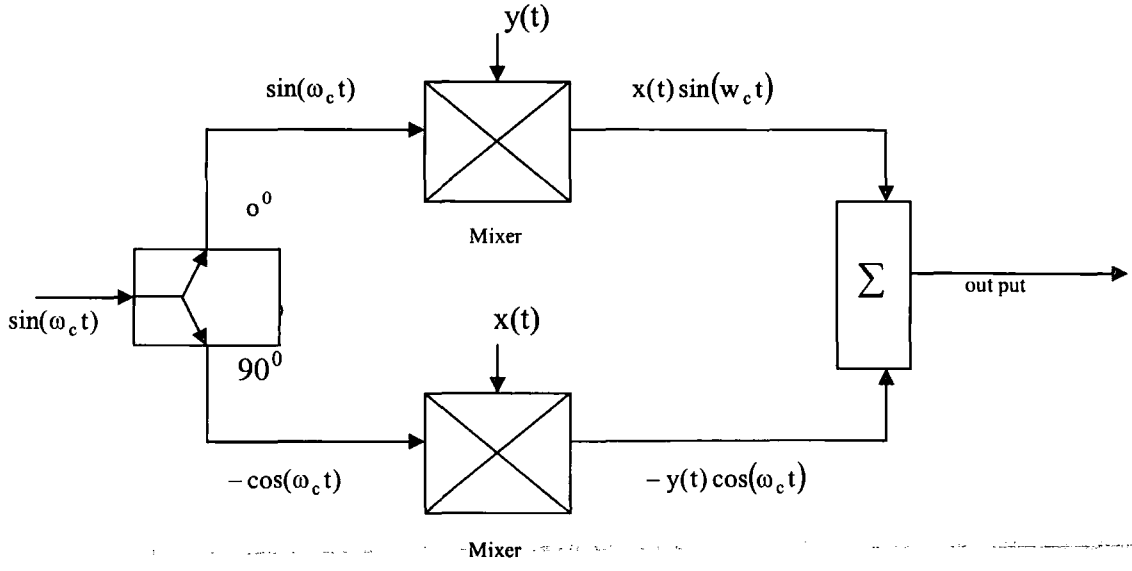

Figure 3.11 Rayleigh fading generator

In order to produce two Gaussian processes from one filter and noise source, the output of the shaping filter is delayed by 12 milliseconds which decorrelates one output from another. This reduces the total number of shaping filters and noise sources required, as they require considerable hardware and physical space. The process is illustrated in Figure 3.12.

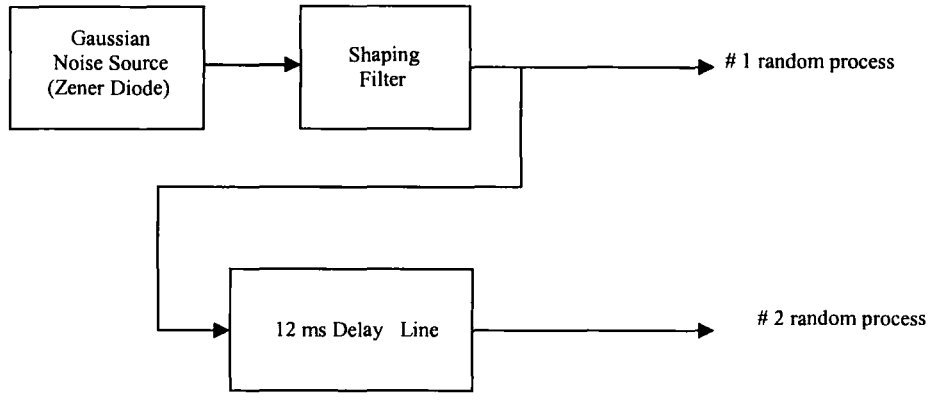

Figure 3.12 Method of obtaining more than one random processes.

3.4.3 Digital Techniques for Noise Generation

The introduction of Digital Signal Processor (DSP) brought revolution in processing of the signal in the area of communications. In earlier implementations, some simulators used a number of spectral shaping filters with different cut-off frequencies to simulate different speeds. These implementations either used a number of analogue filters with different cutt-off frequencies or variable bandwidth analog transversal filters to simulate different speeds. As these transversal filters employed analogue delay lines, their characteristics could not be changed over a wider range. The subsequent implementations of channel simulators took advantage of DSP techniques and started incorporating DSPs in the realization of the spectral shaping filters in order to have effective control over the features of simulation. One of the implementations [31] employed a DSP chip to filter the Gaussian random process. The channel simulator had

eight RF outputs. It simulated the fading observed in urban propagation environment at 900 MHz band.

It simulates the fading by modulating the quadrature components of RF with independent random processes. The input signal was converted to IF in the 50-60 MHz range. The delay of each multi-path component was independently achieved by using glass bulk acoustic wave delay lines capable of operating at 60 ± 10 MHz. The delays could vary between 3 to 36 μs.

It used digital techniques to generate the random processes. The processes were generated by employing a 19-stage maximal length feed-back register as a noise source [32]. The length was chosen to have the desired statistical properties. In order to generate a white spectrum over the desired region of interest, the shift register was clocked at a rate much higher than the Nyquist rate of the final noise waveform. For a vehicle speed of 60 mile/hr, cut-off frequency of the lowpass Doppler spectrum is 81 kHz at 900 MHz carrier frequency. It was chosen to clock the register at a rate of 8 kHz.

A DSP was employed to synthesize a lowpass filter to shape the spectral components of the noise to achieve close approximation with the desired parabolic frequency response. The desired response is non rational and cannot be realized. It was approximated by synthesizing an eight pole, 1 dB ripple, Chebyshev filter cascaded with two adjustable resonators. By adjusting the resonators, the shape of the spectrum was approximated. In order to produce multiple independent noise processes, the output from the DSP was delayed by a series of 1024 word length. The delays were achieved by using 1024-word RAM.

The implementation used analogue techniques to modulate the I and Q components of the input RF signal, therefore, the random processes were finally converted from the digital to analogue using 12-bit D/A converters. The architecture for the generation of the noise process is shown in Figure 3.13.

This simulator used an N-input and N-output network at the output of modulators to create multiple independent fading paths. The function of the network is to change the phase of each input appropriately and combine them in such a manner that each output is an appropriate phased combination of all inputs. Then each output becomes independent from the rest. The network is called Butler matrix [33]. It is all pass

2^k input and 2^k output network comprising cascaded quadrature hybrids and phase shifters. The signal applied at each input reaches equally at all outputs with a given unique linear input -to-output phase progression.

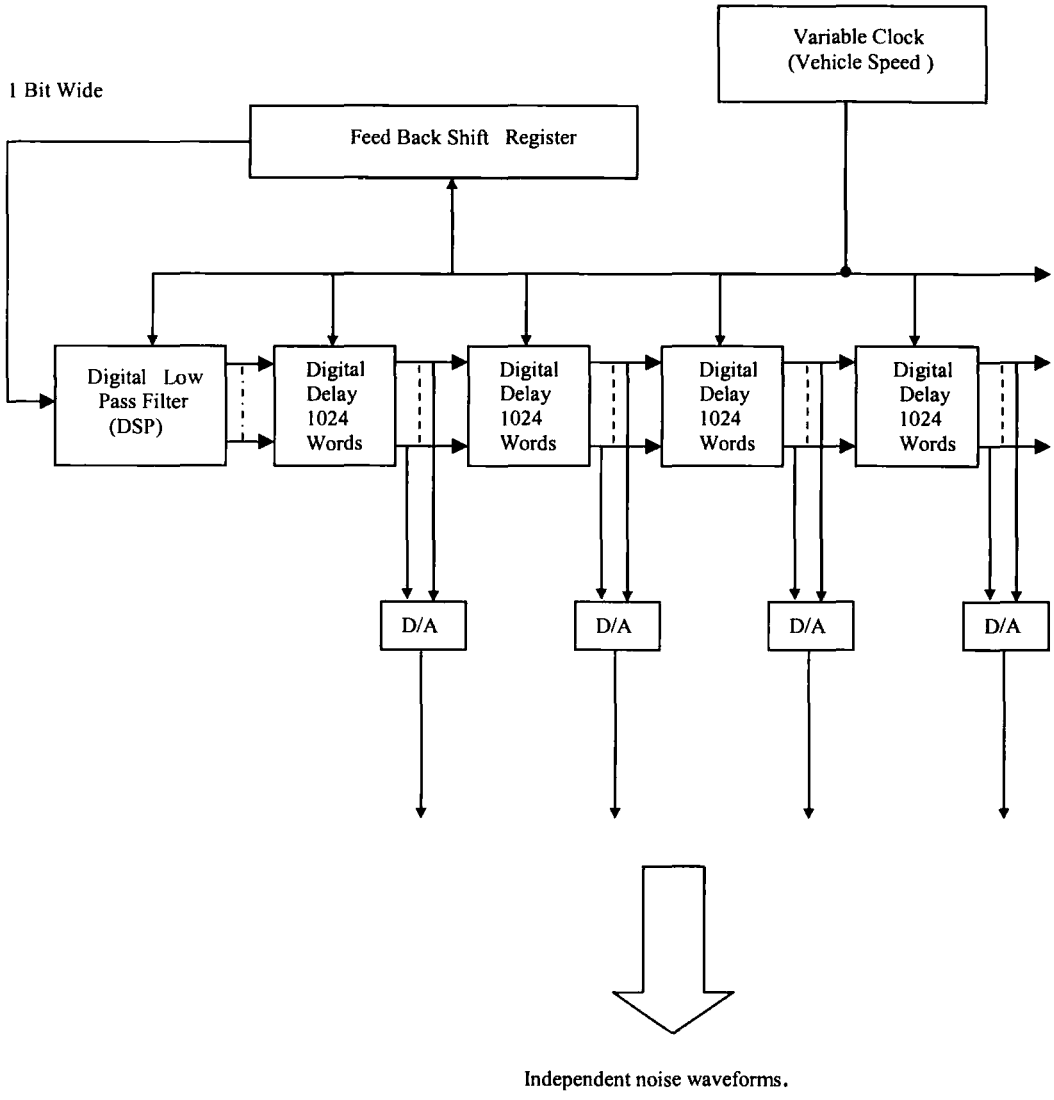

Figure 3.13 Digital method for noise generation.

3.4.4 Total Digital Implementation

The implementations that have been preseneted so for have used analogue techniques to obtain in-phase and quadrature components of the input signal and to modulate them

with the Gaussian random processes. Many implementations adopted digital methods to extract the I and Q components and to modulate them digitally. One such implementation [34] used digital techniques to convert a bandpass signal with 5 MHz bandwidth centered at 5 MHz to extract the I and Q components. This implementation converted the input signal into the digital domain and implemented all the functional blocks of the transversal filter digitally. The signal was sampled at 20 MHz using Datel ADC-304 8-bit flash A/D converter and modulated by 5 MHz bipolar sequence followed by interpolation/filtering for extracting I and Q components of the signal. The interpolation filter was realized as FIR 22-tap and implemented using IMSA110 integrated circuit. The schematics of the simulator and quadrature demodulator are shown in Figures 3.14 and 3.15 respectively.

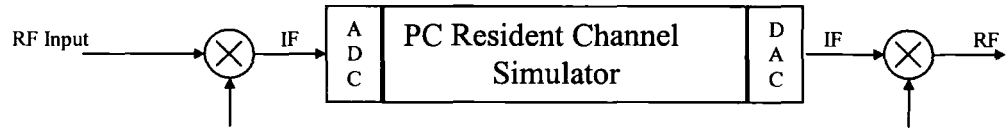

Figure 3.14 Schematic of the simulator

This implementation is based upon the transversal filter model of the channel. As the input I and Q components are in the digital domain, the tap processes are needed to be generated digitally. It generates the Gaussian processes by passing the output of the uniform noise generator through the nonlinear operator. The nonlinear operator converts them into Gaussian. These are then passed to a pair of spectrum shaping filters to closely approximate the spectral shape with the classical one. These filters are realized as moderate order ARMA IIR filters. The sum and differences of these outputs are obtained and the difference is Hilbert transformed. In this way the spectrum of upper side band and lower side band is realized by two spectral shaping filters. Figure 3.16 demonstrates the whole process in detail.

The above-mentioned technique of noise process generation was implemented by a fixed-point digital signal processor TMS320C50A. The processor has 9 kilobyte of RAM on board. It also shares the 32 K static RAM of a PC. The noise processes are

generated at a sampling rate of 20 kHz and stored in the FIFO RAM, which stores 512 values (128 complex samples) for each tap process. As the sampling rate of the input quadrature components is 10 MHz, the zero-order hold interpolation of noise process leads to a factor of 500.

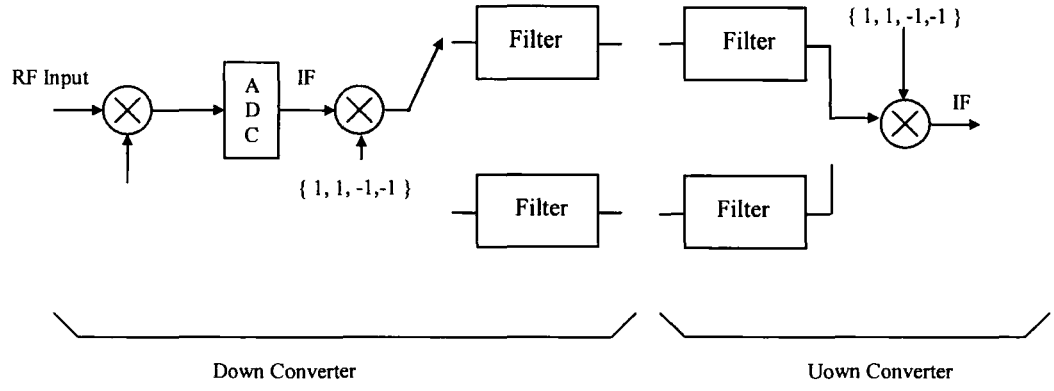

Figure 3.15 Block diagram of digital quadrature demodulator and modulator.

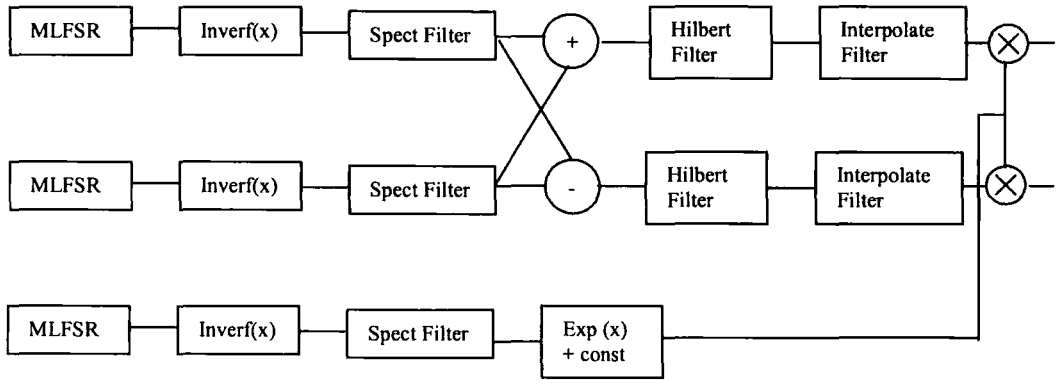

Figure 3.16 Schematic for noise generation.

This simulator employed IMSA110 integrated circuit to realize delays and multiplications of the input samples with the random processes. The same integrated circuit was configured to realize an interpolation filte for the extraction of I and Q components of the bandpass signal. The IMSA110 consists of three 7-stage multiply-accumulate (MAC) array (transversal filter) separated by three programmable lengths 1120-stage shift registers (delay lines). It is treated as three (seven-tap) filters, each preceded by a programmable delay line. As each complex tap of simulator needs two real taps of A110, three to nine paths can be simulated. If it is desired to simulate nine paths, then the power delay profile is required to be split into three groups of paths separated by arbitrary delays with inter-tap delay of 0.1 second within the group.

Another implementation [35] has realized the delays digitally and carried out multiplication of the incoming digital samples with digital noise process by employing FPGA 'XC4044XL' from Xilinx. Due to the limitations of this FPGA, three taps and a maximum delay of 20 μs could be realized. Moreover, the spacing of delays could not be configured dynamically. A new file pertaining to another delay configuration was needed to be loaded to the FPGA for realizing another delay configuration. This simulator had 5 MHz bandwidth and employed one A/D converter at 70 MHz IF to obtain digital samples. It used the Hilbert transform method to extract the I and Q components.

The Texas instrument's DSP TMS33320C6701 was used to generate a random number, implement cascaded 2^{nd} order Chebyshev and 5^{th} order Butterworth IIR Doppler spectrum shaping filters and to realize first interpolation stage. The first interpolation stage was implemented by the DSP as FIR polyphase linear filter. Realizing FIR as polyphase reduces the required sampling rate of the filter. As it is efficient to perform interpolation in stages, this implementation used two cascaded interpolators. The first interpolation was performed by DSP, whereas the second interpolation was performed by the FPGA due to high sampling rate. The FPGA accelerates the interpolation and multiplication process by implementing them in parallel. Although the FPGA performed the second interpolation process, the slope value between the previous and the current samples output from the first interpolator was calculated by the DSP and provided to the FPGA. In turn, the FPGA increments an accumulator by the slope value on each sample clock cycle to obtain the output signal.

The block diagram of the noise process generation and interpolation is shown in Figure 3.17

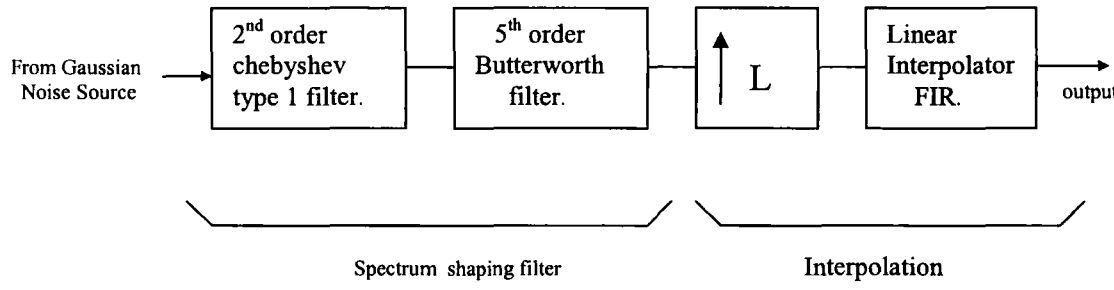

Figure 3.17 Noise process generation, filtration and interpolation.

Although the shaping filter was implemented by DSP, a PC was used to carry out its synthesis. The PC calculated the coefficients of IIR spectral shaping filter and transferred it to the DSP via a PCI bus.

In fact this implementation used three built-in system components to construct the entire channel simulator. One is the daughter board from Signalware which contained A/D, D/A, FPGA for delay lines, multipliers and final interpolation stage. The second one is the DSP board to implement a noise process, its filtering and first interpolation stage. The last one is the PC to calculate coefficients of Doppler shaping IIR filter and to provide user interface.

3.4.5 Application of First-In-First-Out Memory in Delay Implementation

If the duration of maximum impulse response is significantly long, then simulation by employing FIR tapped delay line model yields quite a large number of filter taps if they are equally spaced. In outdoor environment, impulse response duration of 80 μs has already been recorded [36]. For this duration of impulse response, the digital implementation for 10 MHz RF bandwidth would require 1600 equally spaced taps. It is not feasible to realize such a high number of taps. Therefore, for such long duration impulse responses, the delay of each particular tap is usually obtained independently. If the signal is in digital form, then the programmable first-in-first-out memory can be

used to realize the desired amount of delay. Many implementations have used FIFO memory to realize taps. In an implementation [36], the channel impulse response of 80 μs has been simulated by using independent taps. This implementation models the channel as complex FIR filter. The model is shown in Figure 3.18 and its impulse response is given by the following equation.

$$h(t,\tau)=\sum_{i=1}^{M} E_i(t).\delta(\tau-\tau_i) \tag{3.18}$$

This simulator has 20 complex propagation paths with delay resolution of 50 ns. It accepts RF signal with 10 MHz bandwidth and converts it into 70 MHz IF. This 70 MHz IF, as shown in Figure 3.19, is further down converted to be centered at 10 MHz and digitised at four times the carrier frequency i.e. at 4 MSPS. The I and Q samples are extracted digitally at a rate of 20 MSPS by the application of double Nyquist digital product detector [37]. The schematic is shown in Figure 3.20. These I and Q samples are multiplied by the samples of random process by digital multipliers. Finally the samples from various paths are added digitally to give fading. The final signal is again converted up in the same manner as it was done at the input.

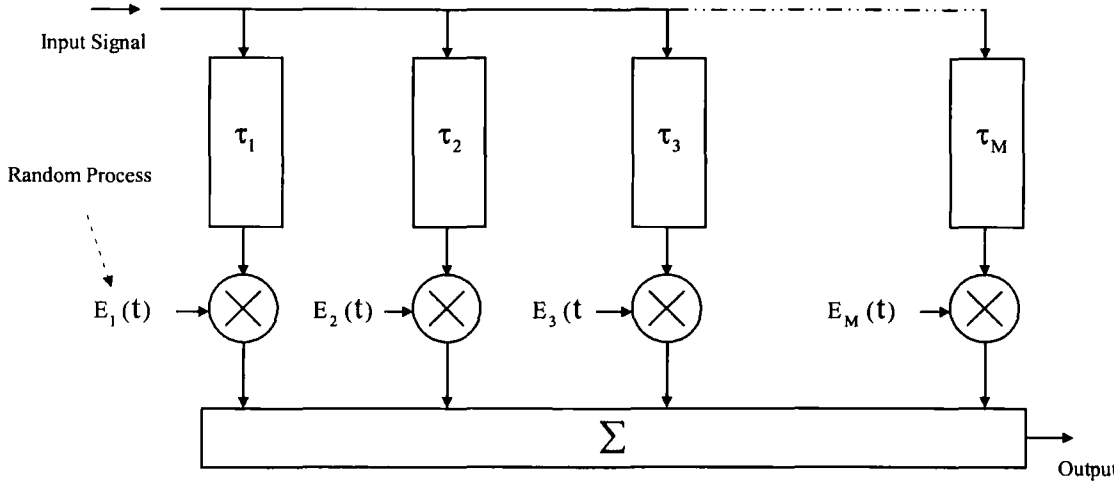

Figure 3.18 FIR filter model of the emulator.

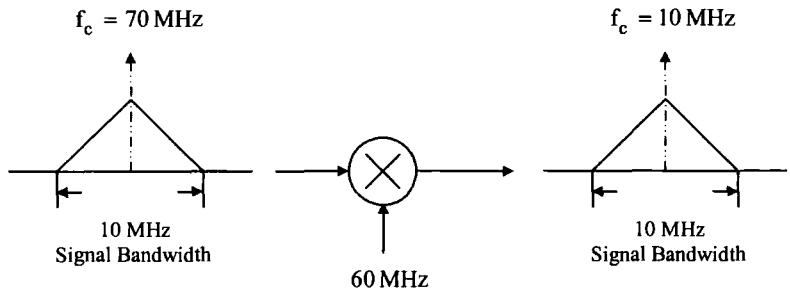

Figure 3.19 Signal spectrum before and after down conversion.

3.4.5.1 Application of Double Nyquist Digital Product Detector for I&Q Components Extraction

The digital product detector consists of a switch and a pair of interpolators (one for each I & Q branch), hence called in-phase and quadrature interpolators respectively. The switch separates odd and even samples from the stream. The even samples correspond to the in-phase branch and the odd samples to the quadrature branch. The two-cascaded flip-flops act as a switch and introduce a total delay of one sampling period. This pair of flip flops is inserted between the the ADC and the in-phase interpolator. The two interpolators operate at half the sampling speed of the ADC. The quadrature interpolator reads the samples directly from the ADC whereas the in-phase interpolator through the flip-flops. As these interpolators operate at half the sampling speed of the ADC, one interpolator will always read the even samples and the other will read only the odd samples. The delay of one sampling period through the flip-flops and operation of the interpolator at half the sampling speed of the ADC forms the basis of the separation of odd and even samples. The separation of odd and even samples of the stream into two branches is a process of two-decimation. As a result of this, two band pass signals (the Q and the I channels), centered at the Nyquist frequency, are created.

The Nyquist frequency after decimation, $f_s/2$, is equivalent to the carrier frequency f_0. Therefore, the decimated Q and I channel spectra can be down converted to baseband with simple sign alternation. These samples are then passed through interpolators to align them in time to obtain correct Q and I samples.

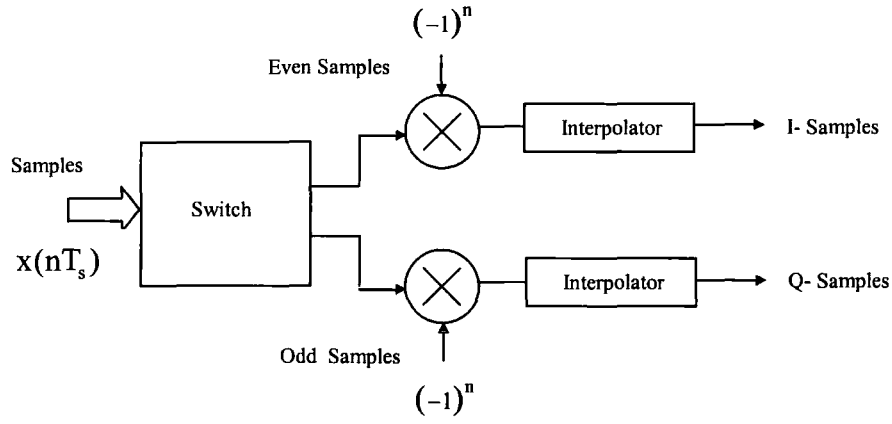

Figure 3.20 Block diagram of double Nyquist digital product detector.

The programmable FIR filters operating at half the sampling speed of the ADC can be employed to implement interpolators. These filters can store two different sets of coefficients and be configured to work with one set of coefficients for the even samples and another set for the odd samples. The FIR filter not only implements an interpolator, but it also multiplies the samples by $(-1)^n$.

In order to combine these non-aligned decimated samples into one stream, these samples are passed through interpolators to delay the quadrature signal with respect to the in-phase signal by half the sampling period. They are then multiplied by $(-1)^n$ to center them at f_o. Since there is a delay between the in-phase and quadrature samples, they can be multiplexed onto a single channel with double the sampling rate.

In this implementation, the generation of random processes Ei are based upon the WSSUS channel assumption. The samples of the channel impulse responses in respect of various environments such as, urban, suburban, rural, suburban-hilly, rural-hilly, and microcell are generated off line by a personal computer. They are based on the previously measured channel impulse responses for various environments. These samples are stored on the hard disk of a computer. As the sampling rate of the I and Q components is 20 MSPS, these samples are needed to be interpolated so that the FIR coefficients could be updated after every 50 ns. This implementation employs two cascaded software interpolators and two-cascaded hardware interpolators to achieve an overall interpolation ratio. Two software interpolators, one based on zero padding plus

filtering and another on Zero-order hold, have been cascaded to avoid a large number of filter coefficients. One hardware interpolator is also based on Zero-padding plus filtering and is realized by the DSP. The second hardware interpolator is based on zero order hold and implemented by a programmable FIR filter realized by PDSP16256/A from Plessey Semiconductors Ltd. The operation of the overall interpolation is explained below.

Before the start of the simulation process, the impulse response samples are interpolated by the two cascaded software interpolators and are stored in the 1M-word RAM of DSP card. This DSP interpolates these original samples and fills the RAM of each tap. Each tap has a RAM memory where these samples are stored prior to the start of the simulation. The functional schematic of the tap is shown in Figure 3.21.

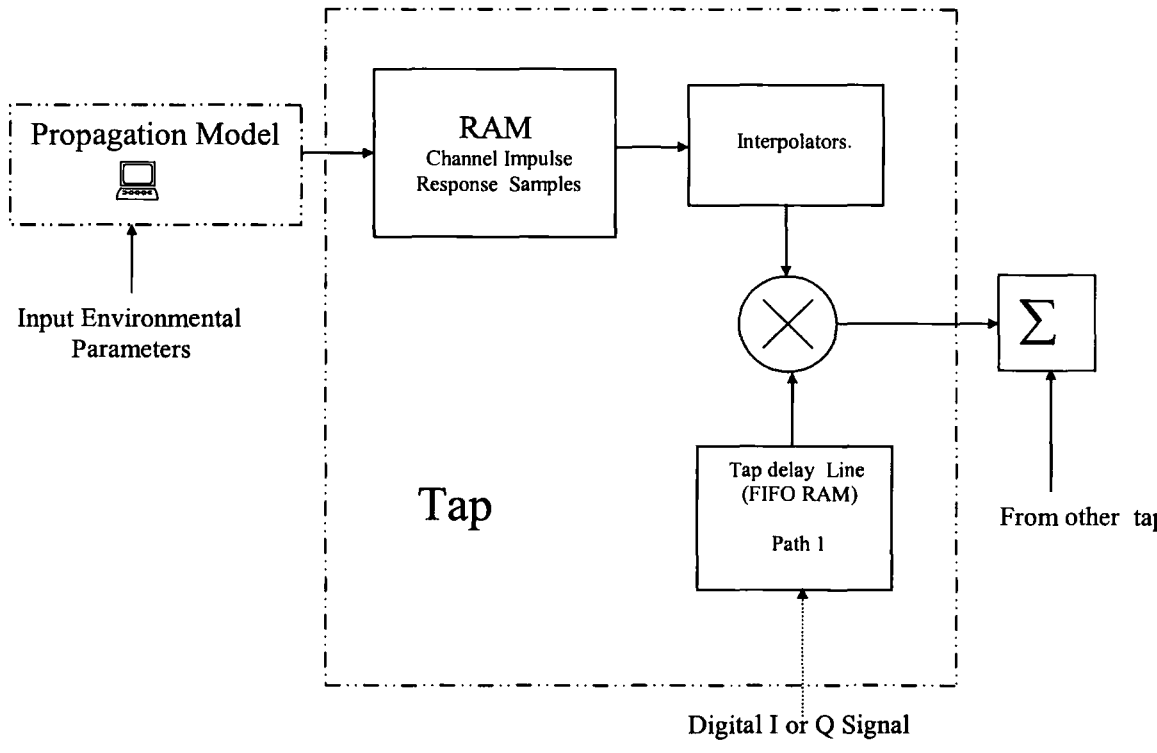

Figure 3.21 Functional diagram of each tap.

As the taps are complex, an independent RAM bank and interpolator are required for each real and complex part of the samples. This phase is called setup phase. When the simulation starts, the impulse response samples from the memory bank of taps are interpolated in real time by the four term interpolator and update the tap coefficients.

Therefore, the two software interpolators and one of the hardware interpolators perform their role in the setup phase and the fourth interpolator functions in the real time execution phase. The interpolation ratio of the first hardware interpolator is kept constant at 32, whereas the interpolation ratio of the second hardware interpolator is made a variable power of 2 ranging between 8-8192 in order to simulate different Doppler frequencies.

3.4.6 Application of Demultiplexing in Delay Implementation

The First-in-First-out memories are used by channel simulators to obtain delays. High-speed FIFO memories are more expensive than the low speed memories. In order to use low speed FIFO memories for high-speed applications, the input data are demultiplexed into a number of low speed channels. After the implementation of delays in each channel separately using low speed FIFO, these channels can be multiplexed again onto one channel having the original data rate. One implementation [38] has applied demultiplexing to separate the A/D output at 100 MHz into two 50 MHz channels and used a FIFO operating at a speed of 50 MHz instead of 100 MHz. Basically, the process of demultiplexing separates every alternative data bit into a channel.The schematic is shown in Figure 3.22.

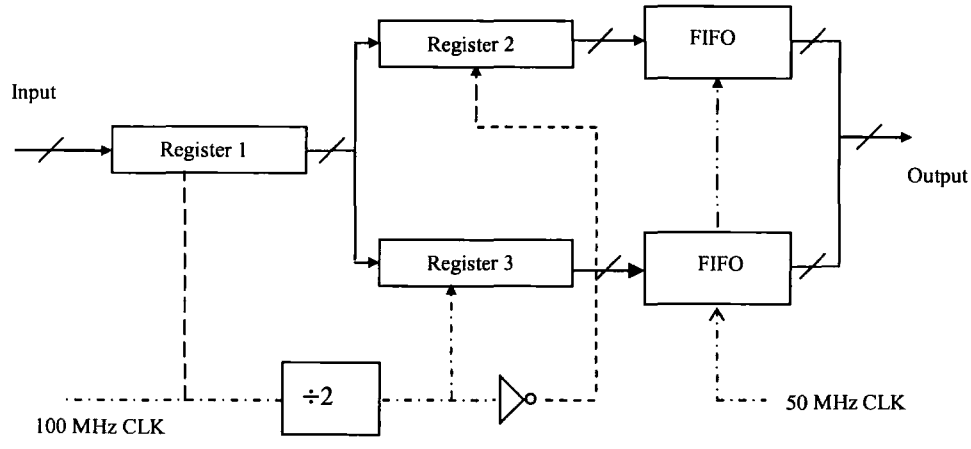

Figure 3.22 Application of demultiplexing in digital delays

This implementation generates lowpass Gaussian noise sources by employing a DSP TMS320C31. The characteristics of these sources are varied through software modifications.

3.4.7 Application of Numerically Controlled Oscillator in Hardware Simulators.

The total digital implementations of channel simulators have employed FIFO to generate delays, DSP techniques to generate channel fading parameters, digital multipliers to multiply the incoming signal samples with the samples of random processes and an adder to obtain the sum of various paths. Some of the implementations revealed the use of analogue multipliers and adders to simplify the hardware. The use of analogue multipliers and adders does not affect the performance of the system. One such implementation [39] has been studied and found that the delays were obtained by employing FIFO memory and the signal was again converted into the analogue domain using digital to an analogue converter and multiplied with the channel propagation parameters by an analogue multiplier. This implementation generated the channel fading in analogue form using numerically controlled oscillator (NCO). The architecture of this simulator is shown in Figure 3.23.

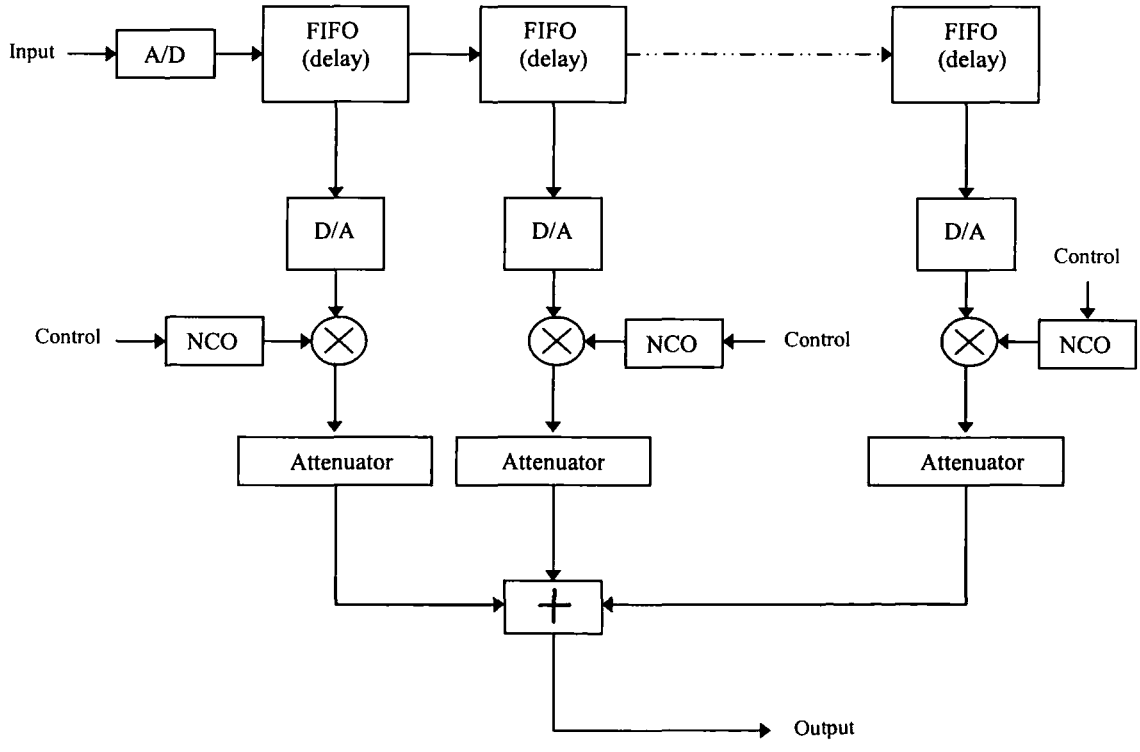

Figure 3.23 Schematic of channel simulator employing numerically controlled oscillator.

The NCO digitally generates a signal whose frequency, phase and amplitude can be controlled accurately and changed instantaneously. It is a programmable device and can be programmed to achieve accurate Doppler shifts, amplitude fading and phase variations with fine resolution of 0.01 Hz, 0.1 deg phase and amplitude of 0.1 dB respectively.

In this implementation, a PC was used to carry out real time calculation of propagation data. The data were finally used to control the delays and program the NCO for the generation of vector with the desired amplitude, phase and frequency (Doppler). Basically, the PC contains a software simulator whose data control the hardware to achieve hardware simulation.

In another implementation [40], an NCO has been employed to generate the Doppler spread for the IS-95 terrestrial CDMA system and bulk Doppler shift to simulate satellite link for the Global star satellite system. The block diagram of one propagation path is depicted in Figure 3.24 for demonstration. It imposes the Doppler spread and amplitude variation on the input signal in two steps. It does not multiply the I and Q components by the random process in order to achieve Doppler spread and Rayleigh fading envelope.

After achieving the delays using FIFO memories, the signal is converted into I and Q basebands in the digital domain and multiplied by the digitally generated sine and cosine signals respectively. These signals are generated by NCO and their phase angles and frequencies can change instantaneously for simulating the Doppler spread and bulk Doppler frequency. The sine and cosine signals generated by the NCO are $\cos[(\omega_c + \omega_d(t)t + \phi(t))]$ and $\sin[(\omega_c + \omega_d(t)t + \phi(t))]$ respectively. In these expressions, ω_d is the bulk Doppler frequency generated by the motion of satellite and $\phi(t)$ is the time varying phase shift that represents the Doppler spread. After multiplication, the I and Q signals are combined. Finally, the resultant is multiplied by k(t) to scale the magnitude in accordance with the appropriate envelope probability density function.

This implementation has employed Xilinx programmable chips to generate sine and cosine signals used in the quadrature down/up converter and carry out the multiplication in the digital domain. These oscillators are Numerically Controlled (NCO) and are built inside the Xilinx programmable chips. The Xilinx logic have built-in RAM look-up-table from where the contents of sinusoids are read out and applied

internally to digital multipliers. In order to reduce the total size of the look up table, the table is read with 90^0 offset for the quadrature arm. This NCO has a resolution of 22-bits and uses two look-up-tables with 256 bytes each giving a sine wave output with frequency resolution of 3.7 Hz. The RAM is made to act as FIFO by controlling its read- write operation. This read-write operation is also performed by Xilinx logic.

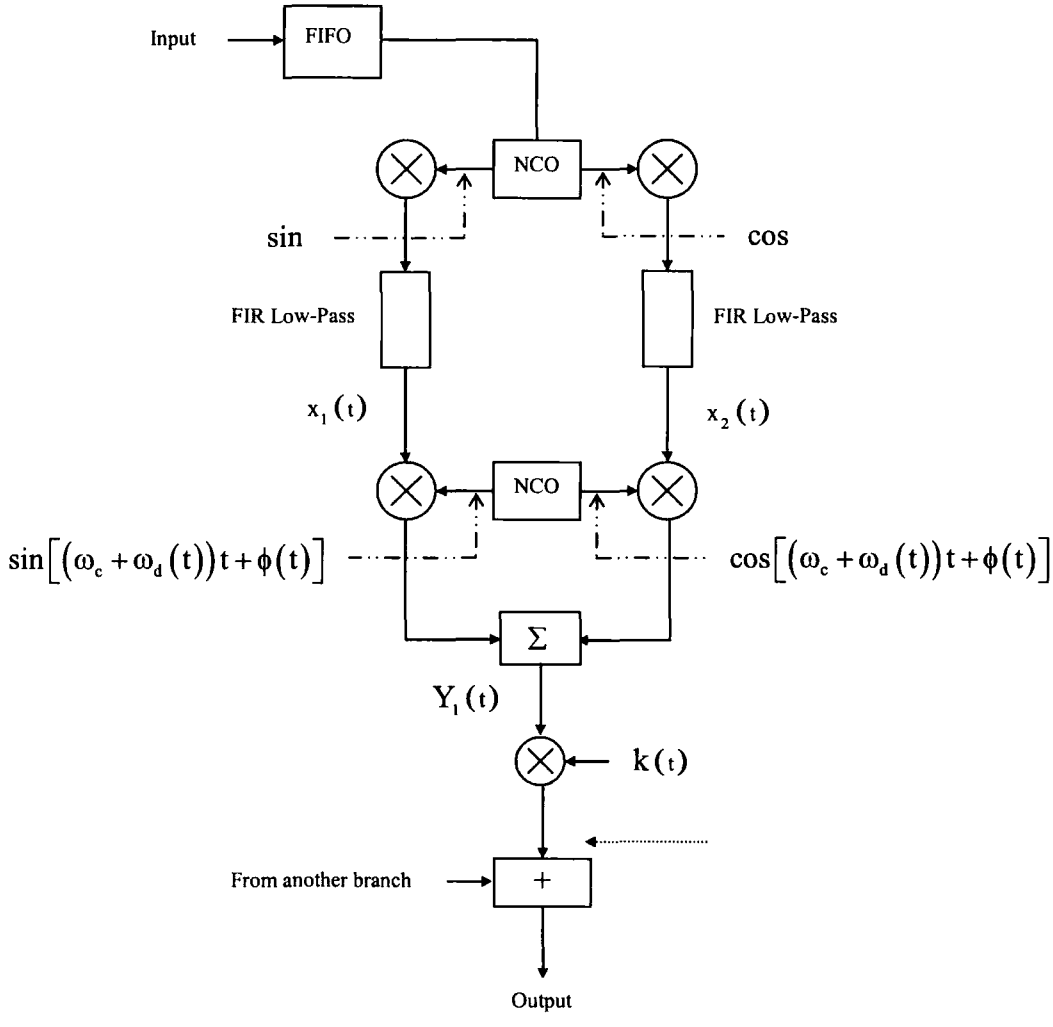

Figure 3.24 Channel simulator employing FIFO and NCO.

3.5 SUMMARY AND CONCLUSIONS

Mobile channel simulators are used to assess and quantify the performance of communication systems in a controlled environment at a work bench. Such testing is

less expensive, more conclusive and repeatable than field trials. There are two types of mobile channel simulators: narrowband; and wideband.

In this chapter, simulation techniques for narrowband and wideband channels were discussed in detail. Architectures of various analogue and digital channel simulators were presented. Earlier implementations were analogue in nature. They were less accurate as compared to digital implementations due to components intolerance. They employed zenor diodes and analogue filters to generate random processes. A number of filters with different cutt-off frequencies had to be used to simulate different Doppler frequencies. Surface Acoustic Wave (SAW) devices were used in analogue implementations to realize delays. Digital implementations incorporated Digital Signal Processors (DSP) to generate and reshape random processes and First-In-First-Out (FIFO) memories to implement delays. FIFO memories are capable of providing very accurate and long delays as compared to analogue SAW devices. The Doppler frequency and delays could easily be changed through programming.

Digital implementations offer many advantages over analogue. They are low cost, fast, more accurate, and flexible. Moreover, they provide effective control over the various simulation parameters through friendly interface.

3.6 BIBLIOGRAPHY

1. W. C. Jakes, Microwave Mobile Communications, New York: IEEE Press, 1994.
2. A. Gaston., H.W. Chriss and H.E. Walker, "A Multi path fading simulator for Mobile Radio," IEEE Trans. on Vehicular Technology, vol. 22, no. 4, Nov 1973, pp. 241-244.
3. R.A. Goubran, H.M. Hafez and A.U.H. Sheikh, "Implementation of real time mobile channel simulator using a single DSP chip," IEEE Trans. on Instrumentation and Measurement, vol. 40, no. 4, Aug 1991, pp. 709-714.
4. E. F. Casas and C. Leung, "A simple digital fading simulator for mobile radio," in Proc. IEEE Vehicular Technology Conference, Sep 1998, pp. 212-217.
5. M. Patzold, Mobile fading channels, 2rd ed. West Sussex, England: John Willey & Sons, Ltd, 2002

6. G.L. Stuber, Principles of Mobile Communication, Norwell, MA: Kluwer Academic Press, 1996
7. James K. Caver, Mobile Channel Characteristics: Kluwer Academic Publisher, 2002.
8. R. Steele, Mobile Radio Communications, London, England: Pentech Press Ltd., 1992.
9. J. D. Parsons, The Mobile Radio Propagation Channel: John Wiley & Sons Ltd., 2000.
10. L.W. Couch, Digital and Analog Communication Systems: Prentice Hall, 1997.
11. R.H. Clarke, "A statistical theory of mobile radio reception," Bell Syst. Tech.J.47, 1968, pp. 957-1000.
12. L. Hanzo, W. Webb and T. Keller, Single and Multi-carrier Quadrature Amplitude Modulation, West Sussex, England: John Wiley & Sons, Ltd., IEEE Press, 2000.
13. R.A. Goubran, H.M. Hafez and A.U. Sheikh., "Implementation of a real-time mobile channel simulator using a DSP chip," IEEE Trans. on Instrumentation and Measurements, vol. 40, no. 4, Aug 1991, pp. 709-714.
14. X. F. Chen and K. S. Chung, "Generation of noise sources for a digital frequency selective fading simulator," International Symposium on Signal Processing and its application, ISSPA, Gold Coast, Australia, Aug 1996.
15. Y. Lee and X. Huang, "The simulation of independent Rayleigh faders," IEEE Trans. Commun., vol. 50, Sep 2002, pp. 1503-1512.
16. R. Y. Zheng and X. Chengshan, "Improved models for the generation of multiple uncorrelated Rayleigh fading waveforms," IEEE Commun. Letter, vol. 6, June 2002, pp. 256-258.
17. C. Eduardo and L. Cyril, "A simple digital fading simulator for Mobile radio," IEEE Trans. on Vehicular Technology, vol. 39, Aug 1990, pp. 205-212.
18. M. Patzold, R. Garcia and F. Laue, "Design of high speed simulation models for mobile fading channels by using table look-up techniques ," IEEE Trans. on Vehicular Technology, vol. 49, no. 4, July 2000, pp. 1178-1190.
19. M. Patzold, Mobile fading channels, 2rd ed. West Sussex, England: John Willey & Sons, Ltd., 2002.

20. M. Patzold and R. Garcia, "A new procedure for the design of fast simulation models for Rayleigh fading channels," in Proc. IEEE Int. Symp. on Wireless Communications, ISWC'98, Montreal, Quebec, Canada, May 1998.
21. M. Patzold and R. Garcia, "Design and performance of fast channel simulators for Rayleigh fading channels," in Proc. 3rd European Personal Mobile Communications Conference, EPMCC'99, Paris, March 1999, pp. 280-285.
22. M. Patzold and F. Laue, "Statistical properties of Jakes fading channel simulator," in Proc. IEEE 48th Veh. Technol. Conf., VTC'98, Ottawa, Ontario, Canada, May 1998, pp. 712-718.
23. J.I. Smith., "A computer generated multipath simulator for mobile radio," IEEE Trans. on Vehicular Technology, vol. 24, no. 3, Aug 1975, pp. 39-40.
24. T. S. Rappaport, Wireless Communications, Principles and Practice: Prentice Hall, 1996.
25. G. Benelli, "A Go-Back-N protocal for mobile communications," IEEE Trans. on Vehicular Technology, vol. 40, Nov 1991, pp. 714-720.
26. H.B. Li, Y. Iwanami, and T. Ikeda, "Symbol error rate analysis for MPSK under Rician fading channels with fading compensation based on time correlation," IEEE Trans. on Vehicular Technology, vol. 44, Aug. 1995, pp. 535-541.
27. J.D. Young and N.C. Beaulieu, "The generation of correlated Rayleigh random varietes by discrete Fourier transform," IEEE Trans. Commun., vol. 48, no 7, July 2000, pp. 1114-1127.
28. H. Hashemi, "Simulation of Urban Radio Propagation Channel," IEEE Trans. on Vehicular Technology, vol. 28, no. 3, Aug 1979, pp. 213-225.
29. G. L. Turin et al, "A statistical model of urban multi path propagation," IEEE Trans. on Vehicular Technology, vol. 21, Feb 1972, pp. 1-9.
30. L.C. Edgar, K. Massad and R.M. Timothy, "A UHF Channel Simulator for Digital Mobile Radio," IEEE Trans. on Vehicular Technology, vol. 29, no. 2, May 1980.
31. W.A. Hamilton and W.F. Bodtmann, "A Hybrid Multichannel Hardware Simulator for Frequency-Selective Mobile Radio Paths," IEEE Trans. on Commun, vol. 31, no. 3, March 1983, pp. 370-377.

32. S.W. Golomb, Shift Register Sequences, San Francisco, CA: Holden-Day, 1967.
33. J.L. Butler, "Digital matrix and intermediate frequency scanning," Microwave Scanning Antenna, vol III, R.C Hansen, Ed, New York Academic,1966.
34. P.J. Cullen, P.C Fannin, and A. Garvey, "Real-Time Simulation of Randomly Time-Variant Linear Systems: The mobile Radio Channel," IEEE Trans. on Instrumentation and Measurement , vol. 43, no. 4, Aug 1994, pp. 583-591.
35. Jeff. R Papenfuss and Mark A. Wickert, " A TMS320C6701/FPGA Based Frequency Selective RF Channel Simulator using IF Sampling," Texas Instruments DSPS FEST , Houston, Tx, August 2-4, 2000, pp. 1-6.
36. J.J. Olmos, A. Gelonch, F.J. Casadevall and G. Femenias,"Design and Implementation of Wide-Band Real-Time Mobile Channel Emulator," IEEE Trans. on Vehicular Technology, vol.48, no. 3, May 1999, pp. 746-764.
37. L.E. Pellon, "A double Nyquist digital product detector for quadrature sampling," IEEE Trans. on Signal Processing, vol. 40, no. 7, July 1992, pp. 1670-1681.
38. X.F. Chen and K.S. Chung, "Implementation of a digital frequency selective fading simulator," Digital Signal Processing for Communication Systems, edited by Tadeusz Wysocki, Hashem Razavi and Bahram Honary, Kluwer Academic Publishers London.
39. C. Briso and J.I. Alonso, "Development and applications of multipath hardware emulator for satellite communications," IEEE Trans. on Antennas and Propagation, AP-2000, pp. 1-4.
40. M. Tykesson, L. Sabel, R. D. Wozniak Tran, and P.Koufalas, "On the development of real time wideband channel simulator for LEO satellite channels," Digital Signal Processing for Communication Systems, edited by Tadeusz Wysocki, Hashem Razavi and Bahram Honary, Kluwer Academic Publishers London.

CHAPTER 4

TRANSFER FUNCTION MODELLING AND SIMULATION

4.1 INTRODUCTION

The main aim of this chapter is to present the advantages of time variant transfer function modelling over impulse response modelling and to demonstrate that a wide band mobile channel simulator can equivalently be constructed in the frequency domain using the time variant transfer function T(f,t) of the channel. Although the transfer function modelling has been envisaged by several researchers as an alternative to the commonly used tapped delay line model so far it has not been implemented. Its main advantage however, arises for ultra wideband systems, where the number of taps in the time domain becomes very large as the bandwidth permits the resolution of more components, therefore limiting the applicability of the central limit theorem.

This chapter proposes a suitable implementation for the transfer function model using Digital Signal Processing (DSP) techniques in SIMULINK and verifies the bit error rate (BER) results with the published results and the simulation results from the commonly used tapped delay line model employing a two-ray power delay profile and differential quadrature phase shift keying (DQPSK) modulation scheme. In this chapter, the design of the simulator will also be optimised to permit future implementation in DSP for real time ultra wideband systems.

4.2 CURRENT APPROACH TO CHANNEL SIMULATON

The time variant behaviour of the mobile communication channel can be explained and modelled either in the time or frequency domain using Bello's four system functions: input delay-spread function, output Doppler-spread function, time variant transfer function and delay Doppler-spread function [1]. Accordingly, the mobile channel simulator can be constructed on the basis of any one of these four system functions. A literature research revealed that the channel simulators that have been built so far are based on the impulse response modelling approach which employed the Bello's input delay spread function $h(t,\tau)$. This function models the channel in the time domain. The

impulse response approach employs the time variant Finite Impulse Response (FIR) transversal filter, called a tapped delay line filter, to model and build a mobile channel simulator.

The impulse response modelling approach is not only widely accepted and a popular approach but also gives good understanding of the physical phenomena of multi-path fading in mobile communication channels. Each tap delay line shows the arrival of delayed replicas of the transmitted signal and the number of taps is based upon the number of propagation paths. After each delay, the signals are weighted by random processes in order to impose the fading. These random processes are generated on the basis of fading statistics. In case of statistical modelling, the statistical characteristics of random processes are typical and not related to any environment. However, in the case of modelling a specific environment, these statistical characteristics are usually obtained experimentally using various sounding techniques.

4.3 ADVANTAGES OF TRANSFER FUNCTION MODELLING

In the tapped delay line model, the various parameters associated with the fading statistics are bandwidth dependent. These parameters are valid only for a certain bandwidth. The reason behind this bandwidth dependency is based upon the fact that the increase in bandwidth will result in the resolution of more constituent components of fading. As the bandwidth increases, the number of resolved components in the time variant impulse response increases, thereby affecting the statistical parameters of fading and making it a function of bandwidth. Moreover, larger bandwidths may result in a situation where the number of unresolved components may not be enough to fulfil the criteria of the central limit theorem which requires the superposition of a large number of components. Therefore, for ultra wideband channels, it is not possible to establish a standard statistical model that can be rightly employed to all bandwidths [2]. In this context, researchers are of the view that conventional modelling approaches can not be applied to ultra wideband channels without modifications [3]. However, in the case of the channel transfer function, it is the only system function among the four Bello's system functions for which there is a superposition of all available multi-path components for all frequencies and instants with respect to all domains [4]. In case of

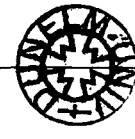

all other system functions, there is a resolution of multi-path components with respect to at least one domain [4,5]. Therefore, due to the fulfilment of the central limit theorem for all frequencies, the time variant transfer function is considered to be the most appropriate and preferred system function for statistical modelling of the time variant channels.

The time variant transfer function is a superposition of phasors rotating both over time and frequency. Therefore, frequency selective fading is completely analogous to the time selective fading. Moreover, the temporal small scale fading in the transfer function is similar to the fading that occurs for the single pulse in the impulse response. This implies that, for a wideband channel model based on the time variant transfer function, all established principles known for narrowband modelling can be applied directly to both the time and frequency domains simultaneously. This demonstrates that transfer function modelling is a more consistent extension from narrowband to wideband modelling as compared to impulse response modelling. It has been shown in [6] that transfer function modelling also has advantages for deterministic modelling, especially in the context of ultra wideband channels.

4.4 BRIEF DESCRIPTION OF THE TIME VARIANT TRANSFER FUNCTION

The channel transfer function models the frequency domain characteristics of a channel. It shows the power in the received signal as a function of frequency [7]. As shown in Figure 4.1, the transfer function is obtained by taking the Fourier transform of the input delay spread (impulse response) with respect to the delay variable τ and inverse Fourier transform of the output Doppler Spread function with respect to the Doppler shift variable, v [1,8].

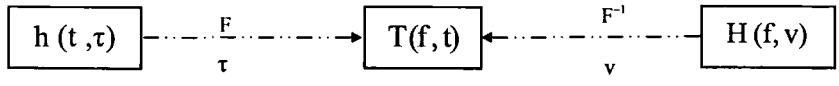

Figure 4.1 Relation ship of transfer function.

$$T(f,t) = \int_{-\infty}^{+\infty} h(t,\tau) e^{-j2\pi f\tau} d\tau \tag{4.1}$$

$$T(f,t) = \int_{-\infty}^{+\infty} H(f,v) e^{j2\pi vt} dv \tag{4.2}$$

In the context of the output of the channel, it can be used to express the output time function in terms of the input spectrum to the channel equivalent filter using the following relationship and interpreted as the complex envelope of the received signal for a cissoidal input at the carrier frequency [1].

$$Y(t) = \int_{-\infty}^{+\infty} X(f) T(f,t) e^{j2\pi ft} df \tag{4.3}$$

As per Zadeh's classical definition [9], the channel transfer function is defined as

$$T(f,t) = \left.\frac{Y(t)}{X(t)}\right|_{X(t)=e^{j2\pi ft}} \tag{4.4}$$

where X(t) is the input signal to the channel and Y(t) is the output signal from the channel. If the channel is excited simultaneously at all frequencies, the output signal Y(t) of the time variant channel is expressed as [5]

$$Y(t) = \sum_i a_i e^{j2\pi(ft - f\tau_i + f_d t)} \tag{4.5}$$

$$= \sum_i a_i e^{j2\pi ft}\ e^{-j2\pi f\tau_i}\ e^{j2\pi f_{di} t} \tag{4.6}$$

$$= e^{j2\pi ft} \sum_i a_i e^{-j2\pi f\tau_i}\ e^{j2\pi f_{di} t} \tag{4.7}$$

where t denotes time, f is frequency, and a_i, τ_i, f_{di} are the amplitude, multi-path delay and Doppler shift respectively for the i^{th} path.

By applying equation 4.4, the time-variant transfer function of the multi-path channel can be described as

$$T(f,t) = \sum a_i e^{-j2\pi f\tau_i} e^{j2\pi f_{di} t} \tag{4.8}$$

4.5 CHANNEL MODEL FOR TIME VARIANT TRANSFER FUNCTION

A channel model based on the time variant transfer function has been developed by Bello[1] employing the sampling theorem. According to the sampling theorem, if the function, h(x), is zero for values of x outside an interval $-X/2 < x < X/2$, then its Fourier transform H (y) can be expressed as the following series [1].

$$H(y) = \sum H\left(\frac{k}{X}\right) \text{sinc}\left[X \left(y - \frac{k}{X} \right) \right] \tag{4.9}$$

where

$$H(y) = \int h(x)\, e^{-j2\pi xy} dx \tag{4.10}$$

Equation 4.9 assumes that h(x) is centered at zero. But when h(x) is centered at x_1 instead of zero, and does not exist for the values of x outside the interval $x_1 - X/2 < x < x_1 + X/2$, then equation 9 becomes

$$H(y) = \sum H\left(\frac{k}{X}\right) e^{\pm j2\pi x_1 (y - \frac{k}{X})} \text{sinc}\left[X \left(y - \frac{k}{X} \right) \right] \tag{4.11}$$

Equation 4.11 can be used to derive the sampling model for the time variant transfer function. The time variant transfer function, T(f, t), is a Fourier transform of $h(t,\tau)$ with respect to the delay variable τ. Real mobile channels do not have delays smaller than zero and greater than certain maximum value τ_{max}. Therefore, the delay constraint interval Δ, can be expressed as

$\nabla = \tau_{max} - \tau_{min}$, when $\tau_{min} = 0$ and τ_{max} is centered at τ_0, then

$$\nabla = \frac{\tau_{max}}{2}$$

On the basis of equation 4.11, T(f, t) with delay constraint of τ_0 can be expressed as

$$T(f, t) = \sum_m T\left(\frac{m}{\tau_{max}}, t\right) e^{-j2\pi\tau_0\left(f-\frac{m}{\tau_{max}}\right)} \operatorname{sinc}\left[\tau_{max}\left(f-\frac{m}{\tau_{max}}\right)\right] \quad (4.12)$$

If the input to the channel has a spectrum X(f), then using equation 4.3, the output of the channel Y(t) is expressed as

$$Y(t) = \int X(f)T(f,t)e^{j2\pi ft}df \quad (4.13)$$

Substituting the value of T(f,t) from equation 4.12

$$Y(t) = \sum_m T\left(\frac{m}{\tau_{max}}, t\right) \int X(f)\, e^{-j2\pi\tau_0\left(f-\frac{m}{\tau_{max}}\right)} \operatorname{sinc}\left[\tau_{max}\left(f-\frac{m}{\tau_{max}}\right)\right] df \quad (4.14)$$

where X (f) is the input spectrum, τ_{max} is the delay of the last significant multi-path component in the power delay profile of the channel, τ_0 is equal to $\tau_{max}/2$, and m refers to the branch number. This equation represents a summation of weighted outputs of a number of elementary parallel channels, where each channel can be treated as a narrowband filter that filters the input and then multiplies its output by a gain factor $T(t, m/\tau_{max})$. The transfer function of such a filter is denoted by $I_m(f)$ [5] and is expressed below. The channel model based on this filter structure is shown in Figure 4.2.

$$I_m(f) = e^{-j2\pi\tau_0\left(f-\frac{m}{\tau_{max}}\right)} \operatorname{sinc}\left[\tau_{max}\left(f-\frac{m}{\tau_{max}}\right)\right] \quad (4.15)$$

The impulse response of this filter can be calculated by taking the inverse Fourier transform of equation 4.15 and the same is expressed below. This impulse response is the complex envelope of a rectangular RF pulse of frequency $f_c + \frac{m}{\tau_{max}}$ and of widt τ_{max} seconds centered at $\tau_{max}/2$ and f_c is the carrier frequency. This filter has frequently been called as bandpass integrator [1].

$$\exp\left[j2\pi\frac{m}{\tau_{max}}t\right]\frac{1}{\tau_{max}}\text{Rect}\left(\frac{t-\tau_0}{\tau_{max}}\right) \tag{4.16}$$

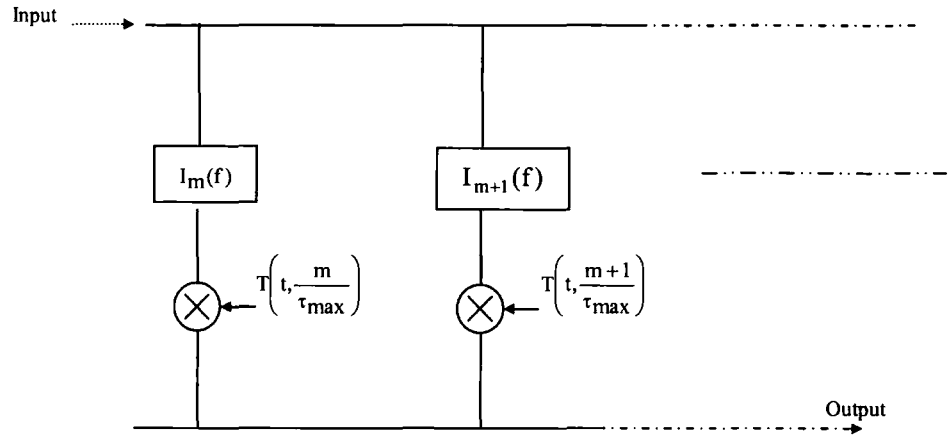

Figure 4.2 Channel Model for Time-Variant transfer function.

The width of each branch, i.e. the range of frequencies which each branch passes, is determined by the ratio of the input signal bandwidth B to the total number of branches, N, used in the model. Bello speculated that about $10B\tau_{max}$ branches might result in a very good approximation of the channel. A literature search revealed that the exact number of branches required has not been reported any where as this model has not yet been implemented.

4.6 SIMULATION OF MOBILE RADIO CHANNEL BASED ON TRANSFER FUNCTION MODEL

The model presented in Figure 4.2 shows that when the input signal is passed through the filter structure, its bandwidth B is sliced into a number of pieces depending upon the number of branches employed in the model. Figure 4.3 explains this concept. Each piece is then multiplied by the random process. At any instant of time, the combination of all these slices in the dimension of frequency will form a random process in f and viewed as a transfer function at that instant. If any one of the slices is viewed in the dimension of time, it will also be a random process in time with the correlation of its

adjacent values being determined by the spaced-time correlation function. Hence, combination of all the adjacent slices will yield the time variant transfer function, which can be viewed as a two dimensioned complex random process.

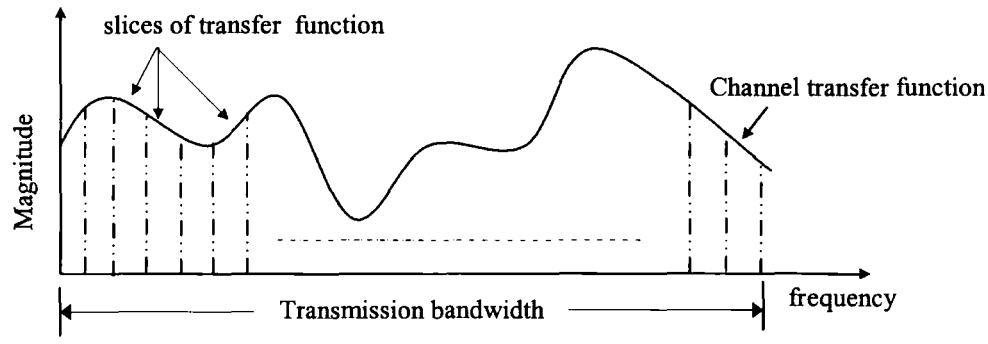

Figure 4.3 Slicing of channel transfer function into pieces.

As the time variant impulse response is modelled as a complex-valued, zero-mean Gaussian random process in the t variable and the fact that the time variant transfer function is obtained by taking the Fourier transform of the time variant impulse response in the delay variable, it can be assumed that the T(f,t) possesses similar statistics and hence can be modelled as a Gaussian random variable for any selection of time or frequency, i.e., it is a random process in both time and frequency [10]. In the case of no movement of the mobile, it becomes a function of frequency only and can be modelled as a Gaussian process in frequency. The movement of the mobile results in Doppler and it becomes a function of frequency as well as time. In that case, it is modelled as a Gaussian process both in time and in frequency. The autocorrelation function of the time variant transfer function T(f,t), called spaced-time, spaced-frequency correlation function, can be employed to determine the properties of T(f,t) in both dimensions i.e., time and frequency. On account of the assumption of WSS, the autocorrelation function of T(f,t) in time is a function of only the time-difference $\Delta t = t_2 - t_1$ and under the assumption of uncorrelated scattering, it is a function of only the frequency difference $\Delta f = f_2 - f_1$ [11].

Multiple random processes are needed to simulate the transfer function channel model. Each branch of the model, consisting of the filter and a complex multiplier, needs its own complex random process. Therefore, the total number of required complex random processes are equal to the number of pieces into which the input signal is sliced. These random processes are characterized by their means and autocorrelation functions [12]. In case of Rayleigh fading, the mean is zero. The autocorrelation function determines the correlation between the fading values spaced in time. This explains the rapidity with which the fading takes place. The rate of fading can also be viewed as a Doppler shift in the frequency domain. Since the power spectrum density and autocorrelation function form a Fourier pair, the correlation properties can be induced in the random processes by passing the white random process through the filter which can transform the power spectral density into the desired shape. The white random process contains the frequency components that have the same amount of energy and the spectrum is flat. The power spectral density (PSD) at the output of the filter is determined by the squared amplitude response of the filter's transfer function. The transfer function of the filter is obtained from the Doppler power spectrum. This work employs classical Doppler power spectrum in simulations. Almost all of the non-measurement based channel simulators [13-16] have employed this classical Doppler spectrum to simulate the mobile propagation channel. The shape of the Doppler spectrum resembles the classical bowl, therefore, it is usually called U shaped spectrum and is defined by the following relationship [17] assuming un-modulated signal, dense-scattering environment, a vertical receiving antenna with uniform azimuth gain, and a uniform distribution of the angle of arrival (0 to 2π).

$$S_{xx} = \frac{1}{\pi f_d \sqrt{1-\left(\frac{f}{f_d}\right)^2}} \tag{4.17}$$

This relationship is valid for values of f ranging $\pm f_d$ about the carrier frequency. The correlation between the random processes depends upon the frequency spacing between the branches and the power delay profile of the channel. For a channel with large delay

spread, there will be less correlation between these random processes and coherence bandwidth (B_c) will be low.

Idealized power delay profiles are usually employed to evaluate the BER performance of mobile radio channels [10]. There are two kinds of commonly used power delay profiles, a two-ray profile and an exponential profile. This work has employed a two-ray power delay profile to calculate the correlation between these random processes. The two-ray power delay profile has been recommended by the Telecommunications Industry Association (TIA) Standards Committee [18] to evaluate the tolerance of delay spread in digital cellular systems. Moreover this model is simple and also has been employed by a number of channel simulators to simulate frequency selective fading [19-21]. It is worth mentioning that BER performance depends most strongly on the root mean square (RMS) value of delay spread, regardless of the shape of the averaged power delay profile [22-24]. In the case of a two-ray model, different delay spread values can easily be realized by simply changing the delay between the two rays. The power delay profile of a two-ray model is expressed as [10]

$$P(\tau) = P_0\delta(\tau) + P_1\delta(\tau - \tau_d) \tag{4.18}$$

where P_0 and P_1 are the powers in the path without delay and with delay respectively and τ_d is the delay between the these path. The RMS delay spread is expressed by the following relationship

$$\tau_{rms} = \tau_d \frac{\sqrt{r}}{1+r} \tag{4.19}$$

where r = ratio of powers between the two paths = $\frac{P_1}{P_0}$ (4.20)

The spaced-frequency correlation function of the two-ray model as a function of τ_d can be expressed as

$$\rho(\Delta f) = P_0 + P_1 e^{-j2\pi(\Delta f)\tau_d} \tag{4.21}$$

If the two paths are equal, then at a correlation threshold of 0.5, the coherence bandwidth (B_c) is given by [10]

$$B_c = \frac{1}{6\tau_{rms}} \tag{4.22}$$

In the context of the bit error rate performance of the system in a wideband channel, it is worth stating again that there is no fixed definition of coherence bandwidth [25]. It is always defined on the basis of correlation coefficient. In some literature, it is defined at a correlation coefficient of 0.9 [25-27] and in some [28-30] at 0.5, which is more popular and widely employed [25, 31].

Though, the coherence bandwidth (B_c) and maximum excess delay (τ_m), are reciprocally related, the maximum excess delay is not necessarily the best indicator for gauging the performance of a given system in a channel. The reason is that different channels with the same value of τ_m can yield very different profiles of signal intensity over the delay span. Therefore, it is more useful to use delay spread for characterizing the dispersive effects of channels [25].

The required degree of correlation between these random processes has been established by mapping a pair of uncorrelated Gaussian random processes, X and Y, to a pair of random processes X and Z having a specified correlation level ρ. The relationship among X, Y, Z and ρ is based upon the following mathematical equation [32]

$$Z = \rho X + Y\sqrt{1-\rho^2} \tag{4.23}$$

4.6.1 Design of Channel Simulator using SIMULINK

Based on the channel model presented in Figure 4.2, the mobile channel simulator has been designed in Simulink by employing Digital Signal Processing (DSP) techniques. The block diagram of the simulator is depicted in Figure 4.4. In order to implement the transfer function model of the channel, the spectrum of the applied complex signal has to be sliced into number of pieces. This slicing can be achieved by passing the complex

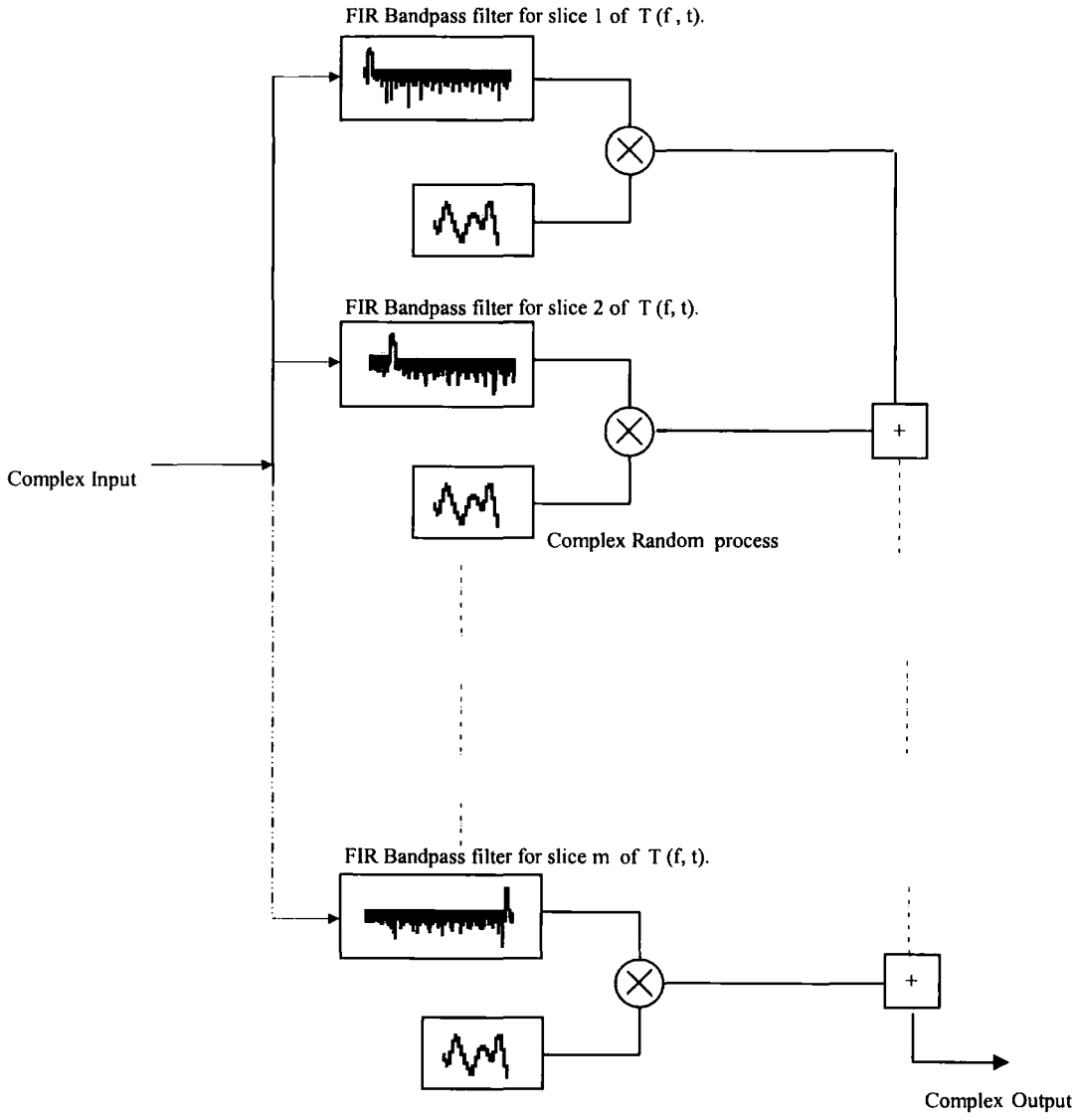

Figure 4.4 Block diagram of the simulator .

signal through a bank of bandpass filters. Each filter passes its own slice and attenuates the remaining portion of the signal. Each bandpass filter has been implemented as FIR filter, whose bandwidth and center frequency is programmable. Though a FIR filter requires a much higher filter order as compared to an IIR filter to achieve a given level of performance, it has been selected due to its stability and linear phase response [33-34]. For data transmission applications, the non-linearity causes frequency dispersion and results in errors [35,36]. In order to separate closely spaced frequency components and accurately slice the given spectrum into pieces, the FIR bandpass filter must have a steep and very narrow transition band. This requires fast roll-off [37]. For passband

frequencies to move through the filter unaltered, there must be no pass band ripples. Moreover, to adequately block the stop band frequencies, it is important to have very good stop band attenuation. These design requirements can only be met with higher order FIR filters.

A number of algorithms are available in MATLAB to realize FIR filters. It was observed that the frequency sampling method yielded lower order design as compared to the rest of the methods. A filter with 160 coefficients resulted in close approximation to the desired frequency response without introducing errors. The accuracy of the filter bank was checked by measuring the bit error rate between the input of the filter bank and the output after recombining all the elementary channels.

MATLAB function ' fir2 ' from the signal processing tool box has been used to calculate the filter coefficients. This function designs frequency sampling based digital FIR filters with arbitrarily shaped frequency response. It accepts a vector comprising frequency points and desired magnitudes at the points specified in the frequency vector. The desired frequency response is then interpolated onto a dense and equally spaced grid comprising 512 points. The filter coefficients are obtained by applying an inverse Fast Fourier transform (FFT) to the grid and multiplying by a window. This work has employed the Hamming window. The frequency vector should be in the range from 0 to 1, where 1 corresponds to the Nyquist frequency. This algorithm always uses an even filter order to configure the passband at the Nyquist frequency.

Figures 4.5-4.8 present the amplitude and phase response of some of the FIR filters designed with ' fir2 ' algorithm for normalized passband of 0.33, 0.2, 0.1 and 0.066 respectively. These filters operate at a sampling frequency of 24300 Hz and have been used to slice the input bandwidth of 12.15 kHz into 3, 5, 10, and 15 elementary channel.These filters are employed in the simulations. It is evident from Figures 4.5-4.8 that the frequency responses of these filters are flat and the transition band is steep. Moreover, the phase response is linear throughout the passband region. Figure 4.9 depicts the measured spectrum at the output of branch 2, 3 and 4 of the simulator which employs 15 band pass filters, each with normalized passband of 0.066 (response shown in Figure 4.8), to slice the input bandwidth of 12.15 kHz into 15 pieces. As evident from Figure 4.9, each branch passes its own band of frequencies and attenuates the remaining portion of the spectrum.

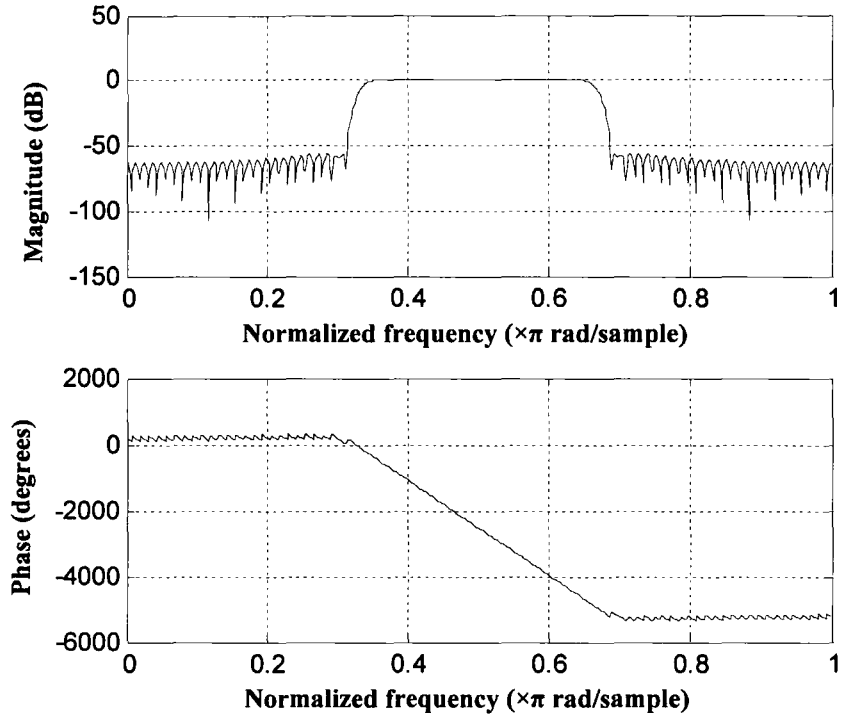

Figure 4.5 Amplitude and phase response of a bandpass filter with normalized bandwidth of 0.33

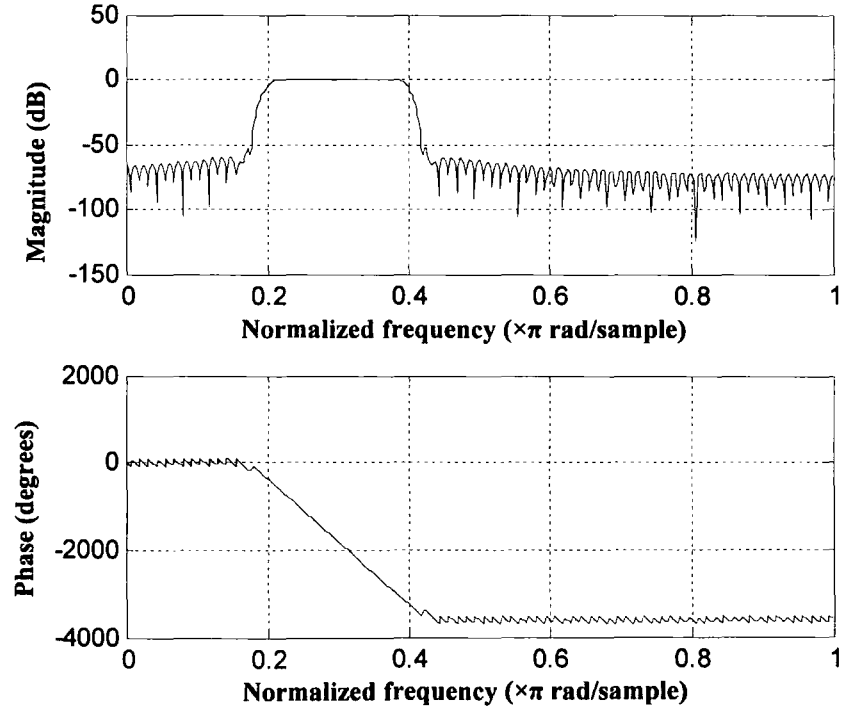

Figure 4.6 Amplitude and phase response of a bandpass filter with normalized bandwidth of 0.2

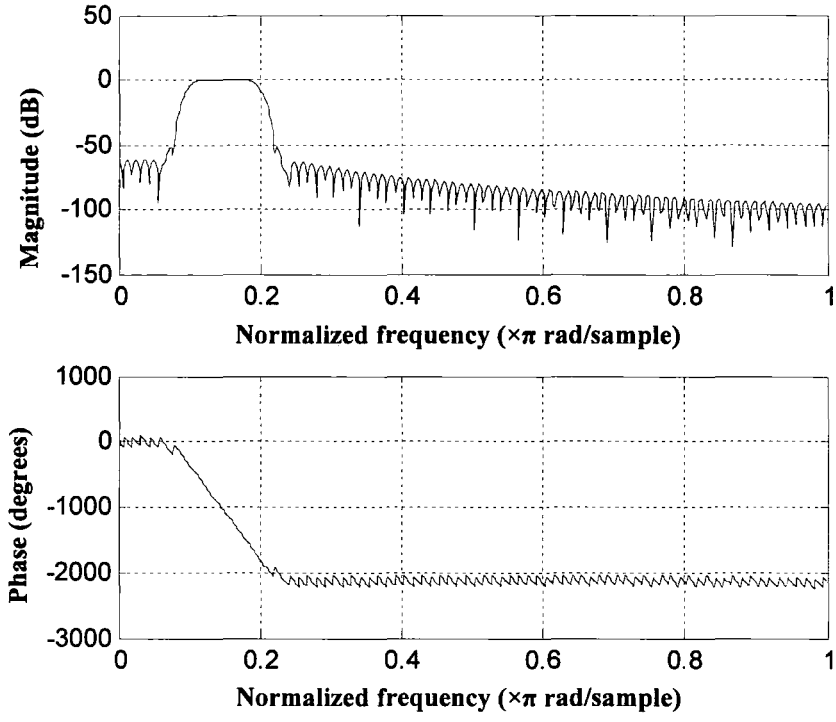

Figure 4.7 Amplitude and phase response of a bandpass filter with normalized bandwidth of 0.1

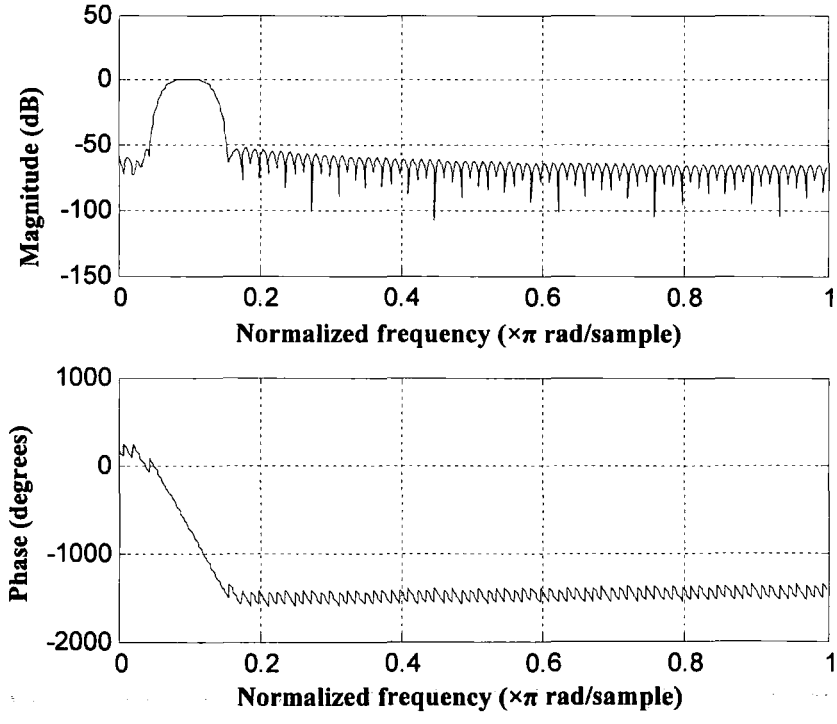

Figure 4.8 Amplitude and phase response of a bandpass filter with normalized bandwidth of 0.066

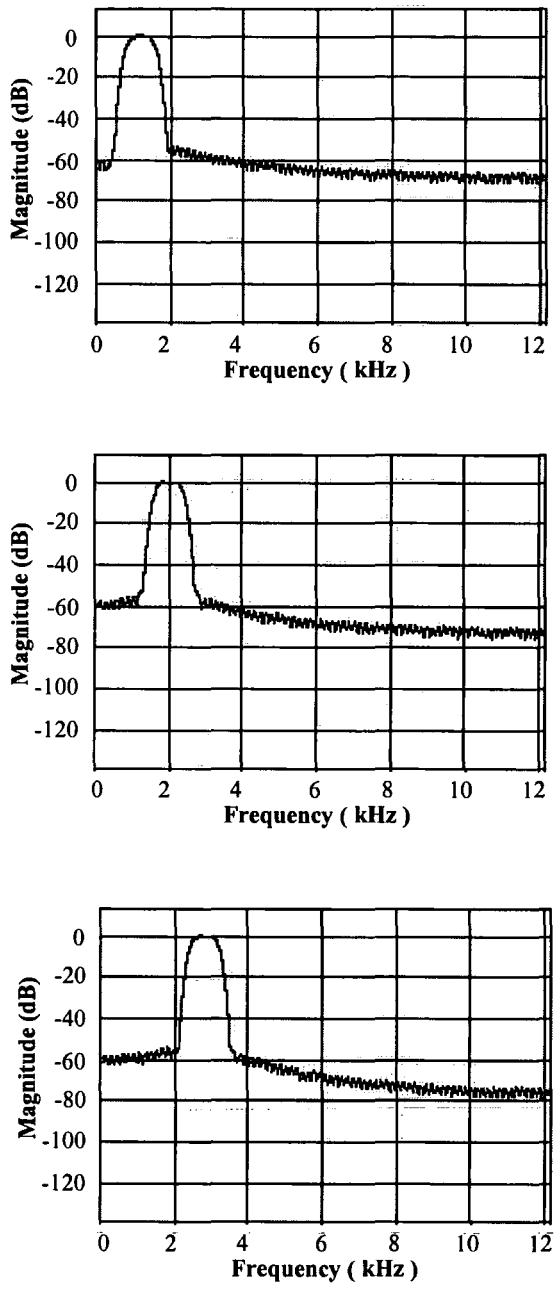

Figure 4.9 Measured spectrum at the output of the branch 2,3 and 4 (from top to bottom) of simulator. Each filter has normalized passband of 0.066. These filters operate at the Nyquist frequency of 12.15 kHz.

By comparing the measured spectrum with the calculated frequency response of the filter (shown in Figure 4.8), it can be noticed that both match each other. Moreover, the required features like, good stop band attenuation, narrow and steep transition band

are visible in Figure 4.9. The spectrum has been measured using the spectrum scope from the DSP library of SIMULINK.

4.6.2 Generation of Random Processes

Rayleigh fading generators have been used to generate complex random processes for each branch of the transfer function model. These generators employ filtered noise methods (explained in chapter 3) to produce classical Doppler spectrum as defined by equation 4.17. The generator accepts Doppler values as an input to control the autocorrelation function of the random process.

Figure 4.10 depicts the real and imaginary parts of the complex random processes produced by the generator for 40 Hz Doppler. The envelope of the complex process, which follows a Rayleigh distribution, is also shown in the figure.

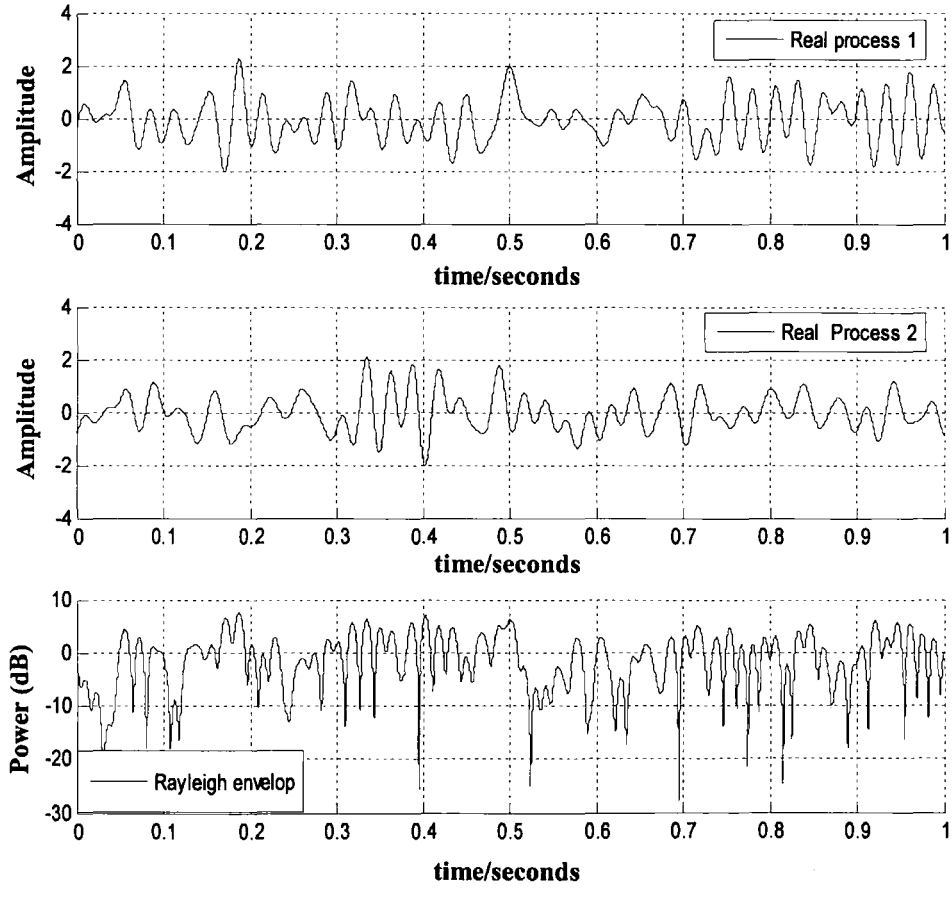

Figure 4.10 Complex random process (two real processes) along with its Rayleigh fading envelope

The accuracy of the fading generator has been verified by comparing the second order statistics like, level crossing rate (lcr) and average fade duration (afd) of the complex envelope of the simulated process against the theoretical curve. These parameters provide useful information about the time variations of the fading and are employed in the design and analysis of forward error control strategy for mobile communication systems where the time variations are used to specify the size of interleaver [11, 30, 38]. Figures 4.11 and 4.12 present a comparison between the measured and theoretical level crossing rate (lcr) and average fade duration (afd) [30] for the simulated random process with 40 Hz Doppler. These Figures reveal good agreement between them. A circuit was developed in SIMULINK using digital signal processing block sets to measure these statistics. The details of the circuit are provided in appendix 2.

As stated previously when these multiple processes are viewed together at any particular instant, they represent the channel transfer function. As each process changes in time, they form a time variant transfer function. The required amount of correlation between these processes have been established by employing equation 4.23. A SIMULINK block was built using multipliers and adders to implement this equation. A block diagram of the correlator is given in appendix 2. Figure 4.13 demonstrates the two correlated processes with correlation coefficient of 0.6.

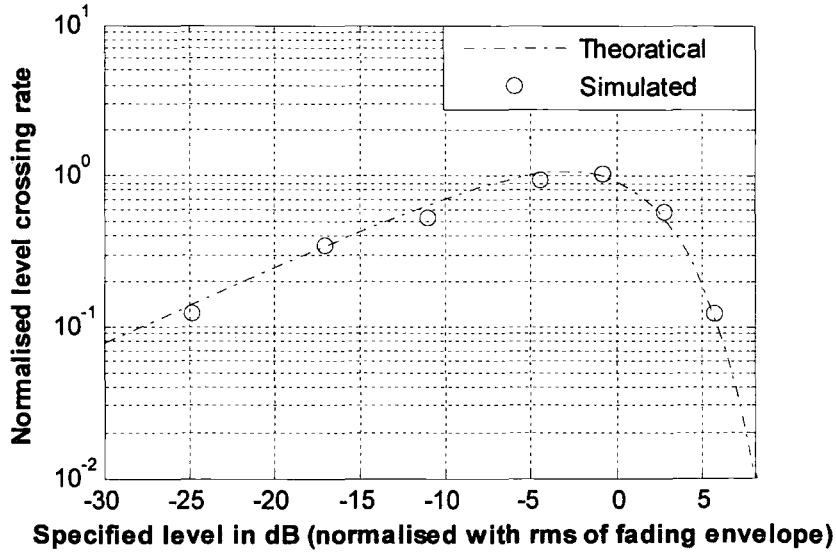

Figure 4.11 Comparison between the measured and theoretical level crossing rate (lcr) of the envelope of the simulated complex process with 40 Hz Doppler.

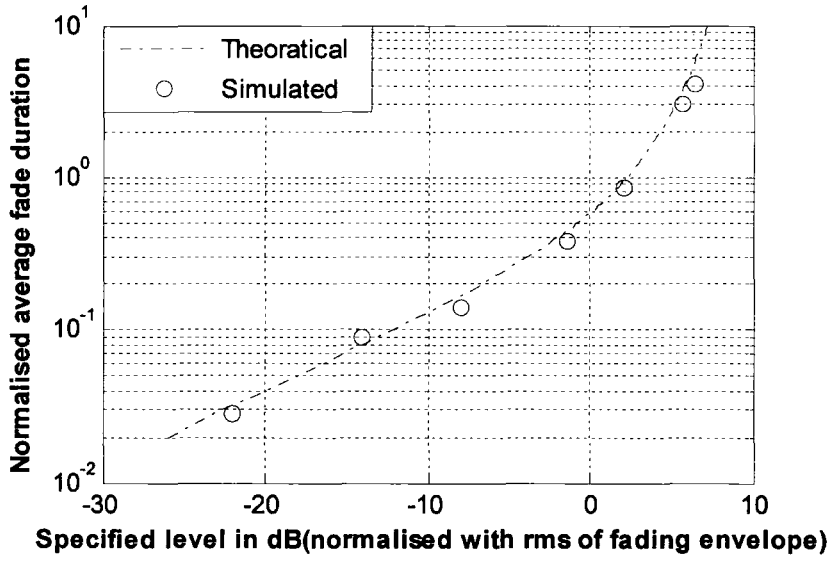

Figure 4.12 Comparison between the measured and theoretical average fade duration (afd) of the envelope of the simulated complex process with 40 Hz Doppler.

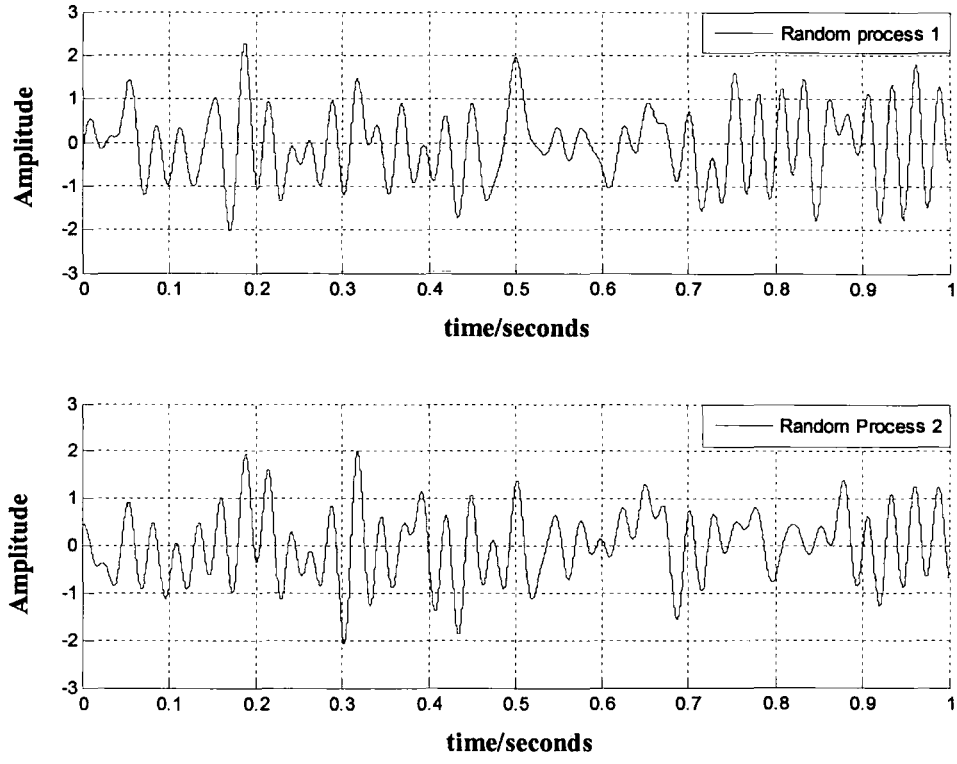

Figure 4.13 Two correlated random processes with correlation coefficient of 0.6

The correlation coefficient between these random processes was measured by storing the samples in the work space and then applying MATLAB command 'corrcoef'.

4.7 SIMULATION RESULTS

In a two-ray power delay profile, BER is usually studied and expressed as a function of τ/T, where τ is delay between the two-rays and T is the Symbol period. The value of τ/T can be varied by either changing the value of τ and keeping the symbol duration constant or keeping τ constant and varying the symbol duration T. This work has used both ways to obtain the BER results. In the first case, a fixed data rate of 24300 symbols/second has been employed to study the BER performance of DQPSK modulation scheme in an outdoor Rayleigh channel environment. The main reason for using this data rate and modulation scheme was to compare and validate the simulation results with those published in [39] for tapped delay line model. Moreover, this data rate has been specified in the U.S. Digital Cellular Standard IS-54.

Figure 4.14 shows the system block diagram employed to measure the bit error rate (BER). As seen in the figure, the pseudorandom generator produces a binary sequence. The DQPSK baseband modulator maps this sequence onto complex symbols at a rate of 24300 symbols/second. These symbols enter the bank of filters which slice the signal spectrum into a number of pieces. Each piece is then multiplied by the random process. These pieces are added to produce the channel output. The demodulator de-maps these complex symbols onto a binary bit stream. The BER tester, connected between the output of the binary source and the demodulator, compares the transmitted and received sequence and calculates the bit error rate (BER).

In order to determine the actual required number of branches for the time variant frequency model, simulations were performed by varying the value of τ/T. The data rate of 24300 symbols/second was kept constant while the delay between the two-rays was varied to realize different values of τ/T and rms delay spread. For each value of τ/T, the frequency correlation coefficient was calculated using equation 4.21 and was used to generate random processes for all the branches of the transfer function. For equal power of the two rays, the RMS delay spread of the channel depends only on the

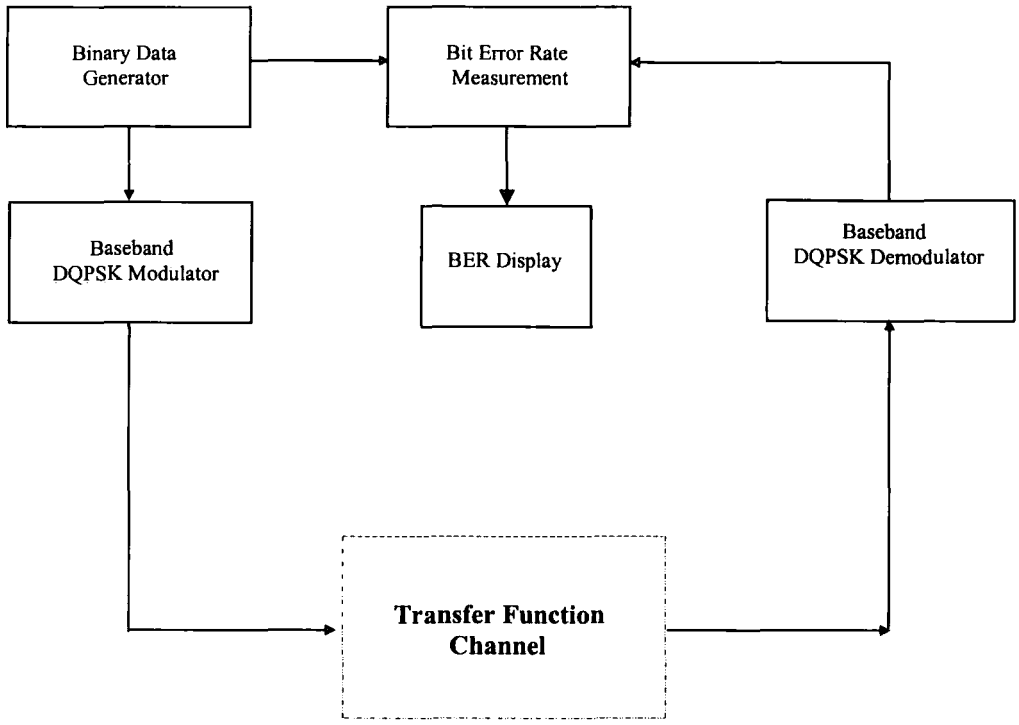

Figure 4.14 System block diagram for bit error rate (BER) measurement.

delay between the two rays. As the coherence bandwidth and RMS delay spread are related to each other, the coherence bandwidth can easily be varied by simply changing the delay between the two rays.

Table 4.1 shows different values of τ, τ/T, RMS delay spreads and coherence bandwidths employed in the simulations. In the context of the frequency domain description of the channel, BER performance is dependent upon the coherence bandwidth of the channel. Therefore, it seems more appropriate to link and define the total number of frequency branches (N) to the coherence bandwidth of the channel. Although, there is no fixed definition of coherence bandwidth it is always defined with reference to a correlation coefficient, where 0.5 is the most widely used. Therefore, different values presented in table 4.1 for coherence bandwidths were calculated based on a correlation coefficient of 0.5 using $B_c=1/2\pi\tau_{rms}$ [10].

BER results were obtained by varying the number of branches (N) between 3 to 10 times B/Bc, where B is the input signal bandwidth. For a data rate of 24300 symbols/second, the bandwidth of the signal is 12.15 kHz i.e., one half the symbol rate [40]. The BER was measured for values of τ/T ranging from 0.1 to 1 since the BER remains constant for values of τ/T greater than 1 [39]. This corresponds to varying the delay between the two rays from 4.11 μs to 41.15 μs and the coherence bandwidth of the channel from 8.10 to 81.30 kHz. The value of E_b/N_o was assumed to be 100 dB and was kept constant throughout the simulations. In all the simulations, a Doppler frequency of 40 Hz was assumed since as shown in [39], the BER is not a strong function of Doppler for this range of τ/T. In Figure 4.15, the simulation results for values of N equal to $10B/B_c$, $8B/B_c$, $5B/B_c$, $3B/B_c$ and $2B/B_c$ are compared with those published in [39] for the tapped delay line model. These results reveal that the transfer function channel model requires $10B/B_c$ branches to achieve close approximation to the channel output, whereas $5B/B_c$, $3B/B_c$ and $2B/B_c$ branches are insufficient to simulate the channel for values of τ/T less than 0.2, 0.3, and 0.4 respectively since at these values, the total number of branches becomes less than 1. This shows that the number of branches used need to be π times the value $10B\tau_{max}$ speculated by Bello [1].

Table 4.1 Parameters used in the simulations.

S.N0	Time delay between the two rays in μs (τ)	Time delay between the two rays/ symbol duration in μs (τ/T)	τ_{rms} in μs	Coherence BW B_c in kHz
1.	4.11	0.1	2.05	81.30
2.	8.23	0.2	4.11	40.55
3.	12.34	0.3	6.17	27.00
4.	16.46	0.4	8.23	20.25
5.	20.57	0.5	10.28	16.21
6.	24.69	0.6	12.34	13.50
7.	28.80	0.7	14.40	11.57
8.	32.92	0.8	16.46	10.12
9.	37.03	0.9	18.51	9.00
10.	41.15	1.0	20.57	8.10

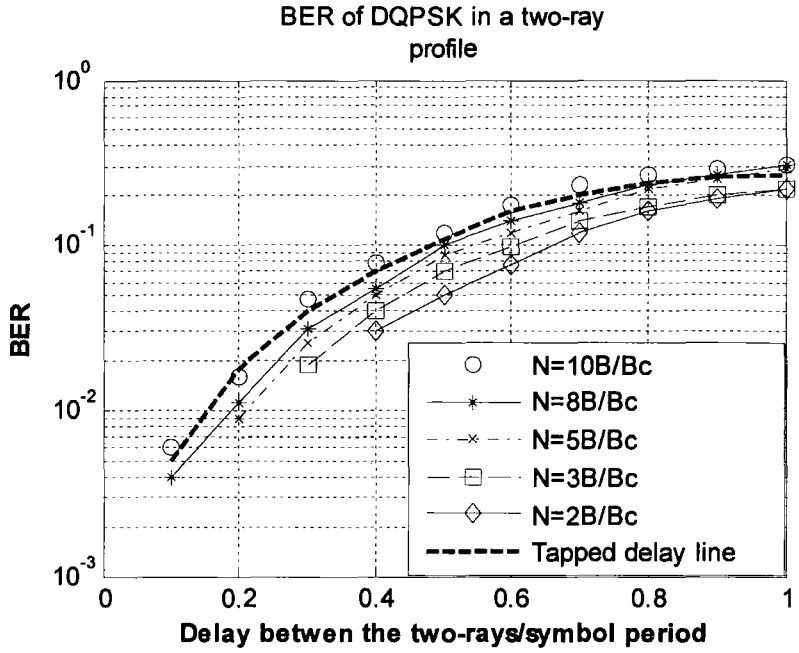

Figure 4.15 BER comparison for transfer function model with different values of N and tapped delay line model (published results).

BER results for tapped delay line model have also been obtained through simulations in SIMULINK and compared with those obtained using the transfer function model with $10B/B_c$ branches. Communication block set library of SIMULINK contains a tapped delay line model which was configured to implement a two-ray Rayleigh fading environment. This block employs noise filtered method to generate the classical U shape Jakes PSD with a user defined Doppler.

Figure 4.16 and Table 4.2 present a comparison between these results. The close match between them further validates the design and demonstrates that a mobile channel simulator can be built using the transfer function of the channel.

It is worth mentioning that the main advantage of the transfer function modelling arises for ultra wideband systems, where the number of taps in the time domain becomes very large as the bandwidth permits the resolution of more multi-path components, therefore limiting the applicability of the central limit theorem. However, the main aim of the simulations were to present a suitable implementation in SIMULINK and to optimize the design by determining the actual number of branches needed in the time variant frequency model for close approximation of the channel.

Table 4.2 BER comparison between tapped delay line model and transfer function model with $10B/B_c$ branches for DQPSK using a two-ray power delay profile at a data rate of 24300 symbols/second

S.N0	Time delay between the two rays in μs (τ)	τ/T in μs	BER (Tapped delay line model)	BER (Transfer function model)
1.	4.11	0.1	0.005	0.006
2.	8.23	0.2	0.020	0.016
3.	12.34	0.3	0.050	0.047
4.	16.46	0.4	0.085	0.079
5.	20.57	0.5	0.131	0.119
6.	24.69	0.6	0.173	0.173
7.	28.80	0.7	0.220	0.230
8.	32.92	0.8	0.260	0.265
9.	37.03	0.9	0.290	0.290
10.	41.15	1.0	0.300	0.310

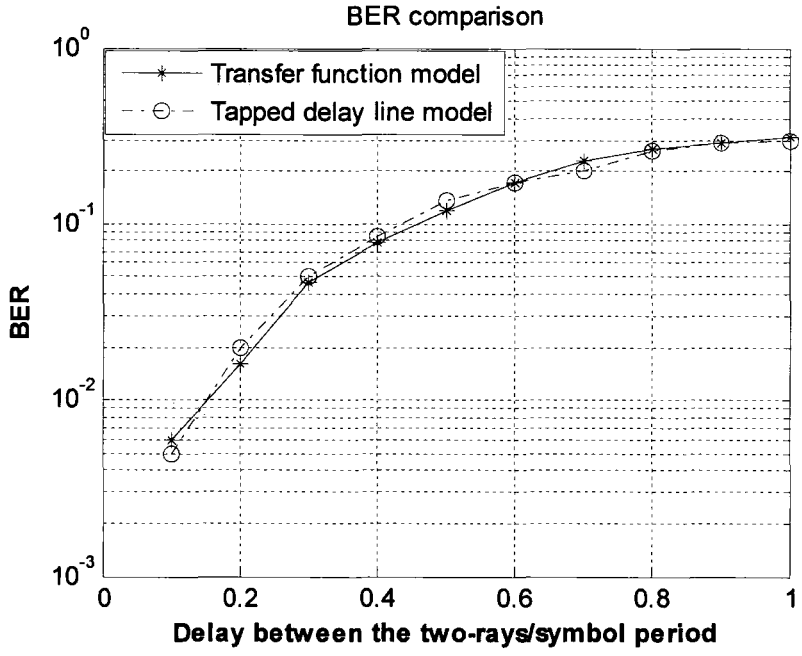

Fig. 4.16 BER comparison for transfer function model with $10\,B/B_c$ branches, and tapped delay line model. Both results were obtained through simulations in SIMULINK .

This design can be used for future implementations in DSP for real time simulations of ultra wideband systems.

As stated earlier that the BER performance as a function of τ/T can also be studied by keeping τ constant and varying the symbol duration. Simulations were further carried out to obtain BER results by employing both modelling approaches under the same channel conditions. Transfer function model with $10B/B_c$ branches was employed for frequency domain simulations, whereas the 2 taps model was used for the time domain model. At each value of τ, the symbol period, T, was varied to realize different values of τ/T. DQPSK modulation scheme was retained in all simulations because it did not require any explicit channel estimation since the preceding symbol acts as a phase reference for the current symbol. However, in case of non-differential modulation technique, the channel estimation is required at the receiver end to correctly demodulate the symbol.

Tables 4.3- 4.7 present different values of τ/T and data rates (symbols/second) for which the simulations were performed. Figures 4.17-4.21 present a comparison of simulated BER results for the time domain and the frequency domain model. The comparison shows good match between them.

In all the simulations, the gain functions for each branch of the transfer function model were generated statistically. For system performance in a particular channel environment, these gain functions can be taken from the wideband measurements. For SIMULINK implementation, these gain functions can be stored in the MATLAB work space prior to commencing the simulations. During the simulation stage, these can be retrieved and fed to the channel.

Table 4.3 BER comparison for different data rates using a two-ray power delay profile at excess delay of 1 μs

$$\tau = 1\,\mu s\,,\ \tau_{rms} = 0.5\,\mu s\,,\ B_c = 333.33\ \text{kHz}.$$

S.N0	Data rate (k symbols/s)	τ/T in μs	BER (Tapped delay line model)	BER (Transfer function model)
1.	100	0.1	0.006	0.008
2.	200	0.2	0.020	0.017
3.	300	0.3	0.041	0.048
4.	400	0.4	0.060	0.070
5.	500	0.5	0.100	0.110
6.	600	0.6	0.160	0.150
7.	700	0.7	0.240	0.220
8.	800	0.8	0.280	0.270
9.	900	0.9	0.310	0.290
10.	1000	1.0	0.330	0.330

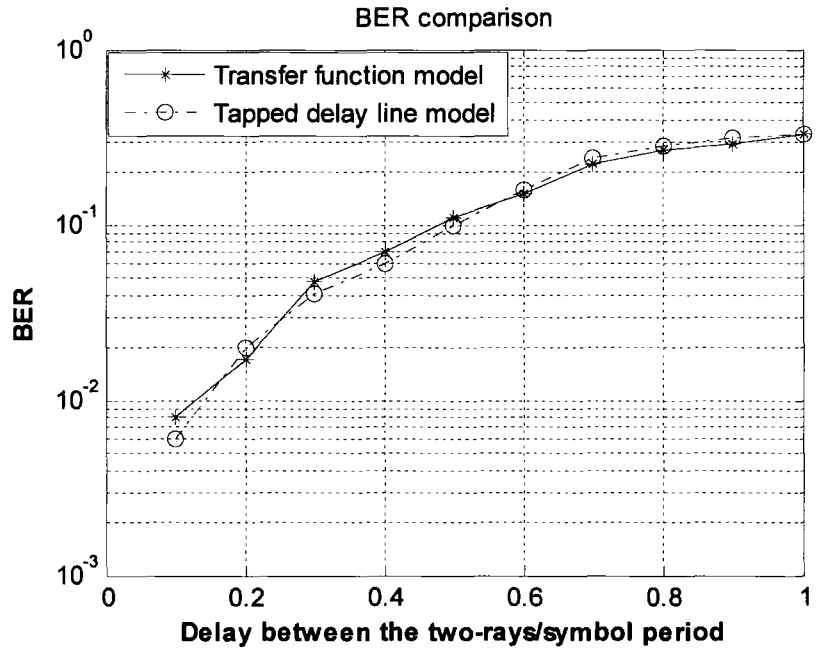

Figure 4.17 BER comparison for transfer function model and tapped delay line model. The delay between the two rays is 1 μs.

Table 4.4 BER comparison for different data rates using a two-ray power delay profile at excess delay of 2.2 μs

$\tau = 2.2\,\mu s\,, \tau_{rms} = 1.1\,\mu s\,, B_c = 151$ kHz.

S.NO	Data rate (k symbols/s)	τ/T in μs	BER (Tapped delay line model)	BER (Transfer function model)
1.	46	0.12	0.005	0.004
2.	100	0.22	0.024	0.028
3.	150	0.33	0.060	0.070
4.	200	0.44	0.100	0.110
5.	250	0.55	0.140	0.160
6.	280	0.61	0.180	0.200
7.	300	0.66	0.200	0.220
8.	350	0.77	0.250	0.280
9.	400	0.88	0.300	0.310
10.	450	1.00	0.310	0.320

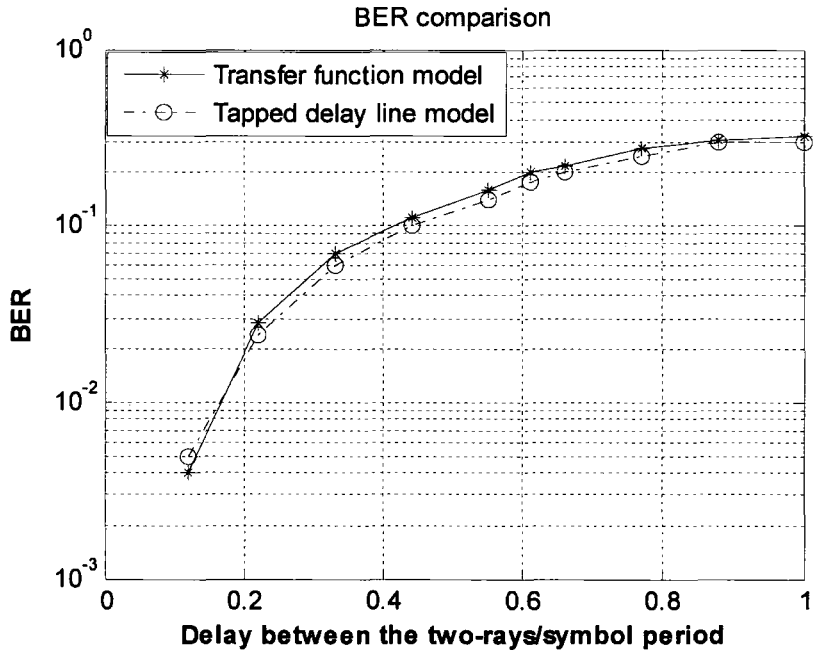

Figure 4.18 BER comparison for transfer function model and tapped delay line model. The delay between the two rays is 2.2 μs .

Table 4.5 BER comparison for different data rates using a two-ray power delay profile at excess delay of 3 μs

$$\tau = 3\,\mu s\,,\ \tau_{rms} = 1.5\,\mu s\,,\ B_c = 111.11\ \text{kHz}.$$

S.N0	Data rate (k symbols/s)	τ/T in μs	BER (Tapped delay line model)	BER (Transfer function model)
1.	35	0.105	0.005	0.0035
2.	60	0.180	0.018	0.0230
3.	80	0.240	0.030	0.0350
4.	100	0.300	0.041	0.0470
5.	150	0.450	0.090	0.1000
6.	180	0.540	0.130	0.1500
7.	210	0.630	0.190	0.2100
8.	260	0.780	0.260	0.2400
9.	300	0.90	0.310	0.2700
10	334	1.00	0.340	0.3000

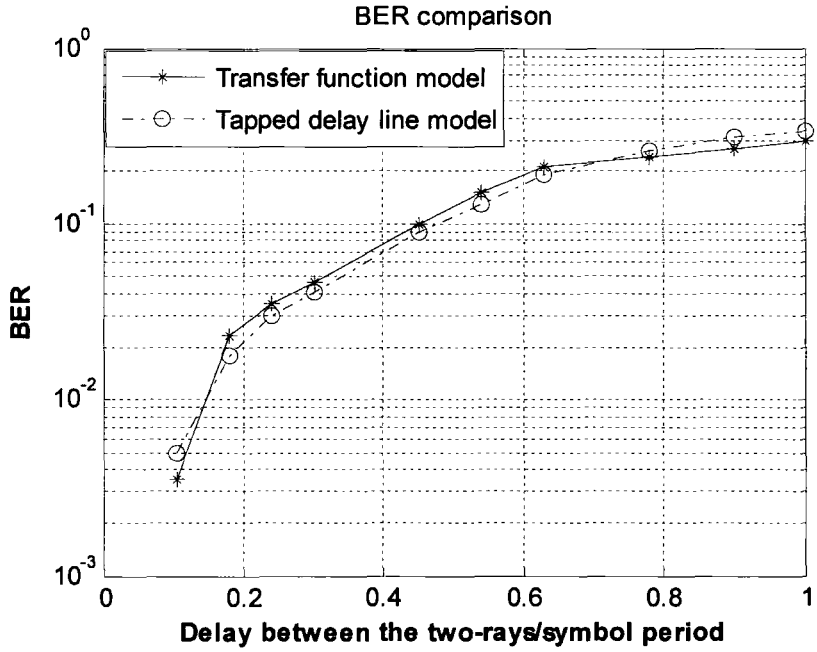

Figure 4.19 BER comparison for transfer function model and tapped delay line model. The delay between the two rays is 3 μs .

Table 4.6 BER comparison for different data rates using a two-ray power delay profile at excess delay of $6\mu s$

$$\tau = 6\mu s, \tau_{rms} = 3\mu s, B_c = 55.55 \text{ kHz}.$$

S.N0	Data rate (k symbols/s)	τ/T in μs	BER (Tapped delay line model)	BER (Transfer function model)
1.	16.66	0.10	0.005	0.007
2.	33.33	0.20	0.021	0.018
3.	50.00	0.30	0.045	0.036
4.	66.66	0.40	0.080	0.066
5.	83.33	0.50	0.100	0.120
6.	100.0	0.60	0.150	0.140
7.	118.0	0.70	0.210	0.200
8.	133.33	0.80	0.250	0.230
9.	150.0	0.90	0.280	0.250
10.	166.0	1.00	0.330	0.290

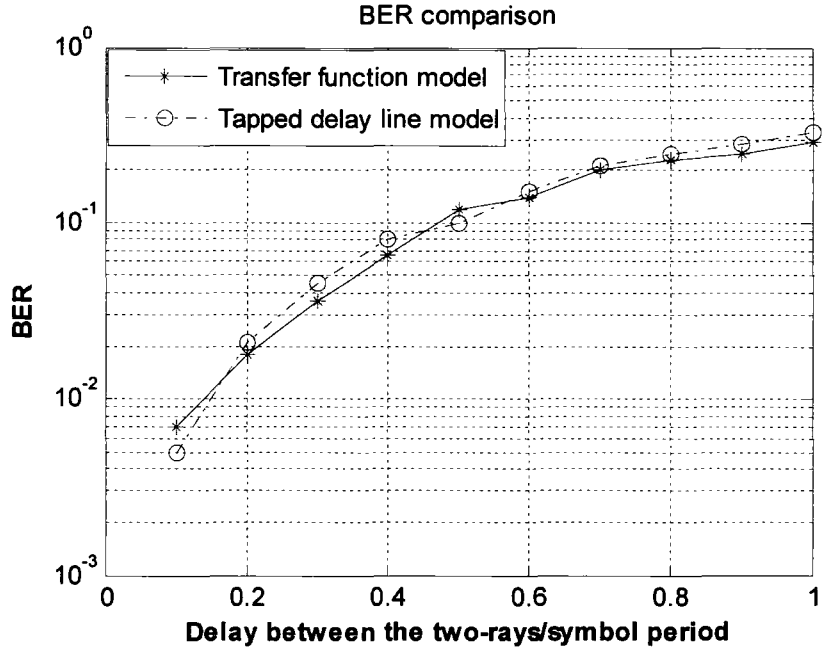

Figure 4.20 BER comparison for transfer function model and tapped delay line model. The delay between the two rays is $6\mu s$.

Table 4.7 BER comparison for different data rates using a two-ray power delay profile at excess delay of $10\,\mu s$

$$\tau = 10\,\mu s\,,\ \tau_{rms} = 5\,\mu s\,,\ B_c = 33.33\ \text{kHz}.$$

S.N0	Data rate (k symbols/s)	τ/T in μs	BER (Tapped delay line model)	BER (Transfer function model)
1.	10	0.1	0.006	0.006
2.	20	0.2	0.018	0.015
3.	30	0.3	0.045	0.039
4.	40	0.4	0.070	0.085
5.	50	0.5	0.130	0.120
6.	60	0.6	0.150	0.160
7.	70	0.7	0.220	0.210
8.	80	0.8	0.250	0.240
9.	90	0.9	0.290	0.280
10.	100	1.0	0.300	0.300

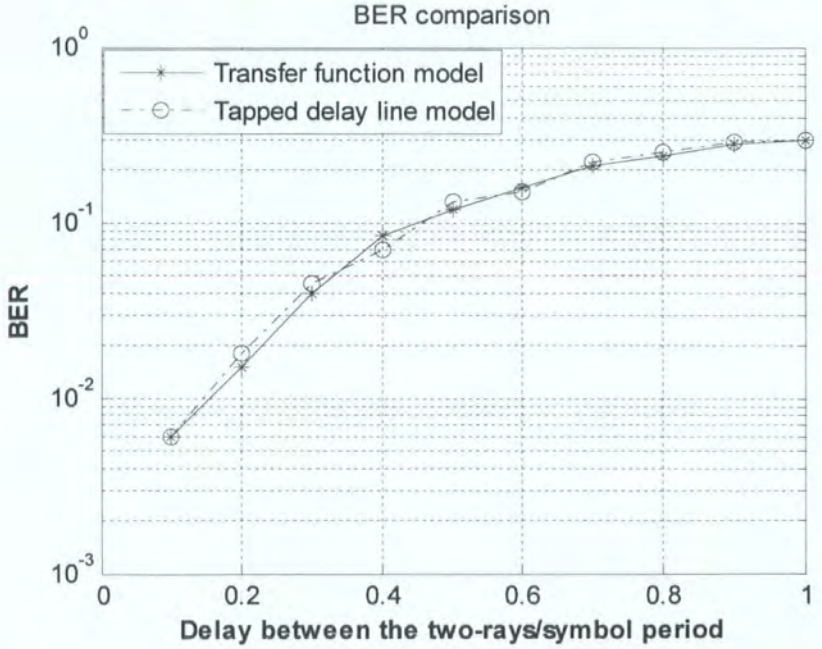

Figure 4.21 BER comparison for transfer function model and tapped delay line model. The delay between the two rays is $10\,\mu s$.

4.8 SUMMARY AND CONCLUSIONS

A mobile channel simulator can be constructed either in the time domain using the tapped delay line model or in the frequency domain using the time variant transfer function of the channel. Transfer function modelling approach has many advantages over impulse response modelling. These include: non independence of fading statistics over the bandwidth, fulfilment of central limit theorem for all frequencies and instants with respect to all domains, and consistent extension from narrowband to wideband. However, its main advantage arises for ultra wideband systems, where the number of taps in the time domain becomes very large as the bandwidth permits the resolution of more components, therefore limiting the applicability of the central limit theorem.

In the transfer function modelling approach, the wideband channel is split into a number of elementary parallel channels, where each channel can be treated as a narrowband filter that filters the input signal and then multiplies its output by a gain factor. The gain factor can be modelled as a random process. The combination of all parallel narrowband channels at any particular time can be viewed as the transfer function of the channel. As each narrowband channel fades in time, therefore, the transfer function becomes time variant and can be treated as a two dimension random process whose correlation properties are completely specified by the spaced-time, spaced frequency correlation function.

The transfer function channel model was presented and implemented using DSP techniques in SIMULINK. FIR filter bank was used to slice the signal into many narrowband channels. The filters were designed using the frequency sampling method with 160 taps. Bello speculated that about $10B\tau_{max}$ branches might result in a very good approximation of the channel. To determine the actual required number of branches for the time variant frequency model, simulation of a two- ray power delay profile with equal power was performed by varying the number of branches between 3 to 10 times the B/B_c, where B_c is the coherence bandwidth of the channel specified at a correlation coefficient of 0.5. DQPSK modulation scheme with the U.S. Digital Cellular Standard IS-54 symbol rate of 24300 symbols/second was employed to enable the comparison of simulation results with published results from the commonly used tapped delay line model under the Rayleigh channel conditions. BER was recorded as a

function of τ/T, where τ is the delay between the two rays and T is the symbol period. At each value of τ/T, the frequency correlation coefficient between the branches was calculated and used to generate random processes for all branches. Rayleigh fading generators were employed to generate colored random processes having commonly used U-shaped spectrum. Simulation results were presented and compared against the tapped delay line results for values of N equal to $10B/B_c, 8B/B_c, 5B/B_c$, $3B/B_c$ and $2B/B_c$. The results revealed that $10B/B_c$ branches gave close agreement with the tapped delay line model. This number was π times higher than $10B\tau_{max}$, previously speculated by Bello.

Simulations were further carried out using the transfer function model with $10B/B_c$ branches to obtain BER results. Instead of varying τ, the symbol period was varied between 10 K to 1000 K to realize different values of τ/T. The BER results were compared against those obtained using the tapped delay line simulations in SIMULINK. The close agreement with the tapped delay line results further validated the optimized design. This design will permit future implementation in DSP for real time ultra wideband systems.

4.9 BIBLIOGRAPHY

1. P.A. Bello, "Characterization of random time-variant linear channels", IEEE Trans. on Communication Systems, Dec 1963, pp. 360-393.
2. T. Englert and H. Fruchting,"Bandwidth dependence of the characteristics of time variant impulse response," Proceeding of 2000 European Conference on Wireless Technology (ECWT 2000), Paris, France, Oct 5-6, 2000, pp. 230-233
3. D. Cassioli, and A.F. Molisch, "A statistical model for UWB indoor channel," IEEE Vehicular Technology Conference(VTC 2001 Spring), Rhodes, Greece, May 6-9, 2001, pp. 1159-1163.
4. R. Kattenback, "Statistical modeling of small scale fading in directional radio channel," IEEE Jour. on Selected Areas in Communications, Vol. 20, No.3, April 2002, pp. 584-592.

5. R. Kattenback, "Transfer function modeling and its application to ultra-wide band channels," COST 273 TD (02) 136 Lisbon, Purtugal, Sep 19-20, 2002, pp. 1-20.
6. T. Englert, L. Layer, R.Kattenback, and H. Fruchting, "Deterministic wideband modelling of time variant transfer function," Proc of IEEE International Symposium on Personal, Indoor and Mobile Radio Communicatopns (PIMRC 99), Osaka, Japan, Sep 12-15, 1999, pp. 106-110.
7. S. Saunder, Antenna and Propagation for Wireless Communication Systems: John Wiley and Sons Ltd.
8. J.D. Parson, The Mobile Radio Propagation Channel, second ed.: John Wiley & Sons Ltd., 2000.
9. L.A. Zadeh, " Frequency analysis of variable networks, " Proceeding of the IRE, March 1950, pp.291-299.
10. J.K. Caver, Mobile Channel Characteristics: Kluwer Academic Publisher, 2002.
11. P.M. Shankar, Introduction to Wireless Systems, New York: John Wiley & Sons, 2002
12. W.B. Davenport and W.L. Root, An Introduction to the Theory of Random Signals and Noise, New York: McGraw-Hill, 1958.
13. A. Gaston, H.W. Chriss and H.E. Walker, "A Multi path fading simulator for Mobile Radio", IEEE Trans. on Vehicular Technology, vol. 22, no. 4, Nov 1973, pp. 241-244.
14. L.C. Edgar, K. Massad and R.M. Timothy, "A UHF Channel Simulator for Digital Mobile Radio", IEEE Trans. on Vehicular Technology, vol. 29, no. 2, May 1980, pp. 281-293.
15. R.A. Comroe, "All digital fading simulator", in Proc. Nat. Electron. Conf. , vol. 32, 1978, pp. 136-139.
16. C. Eduardo and L. Cyril, "A simple digital fading simulator for Mobile radio", IEEE Trans. on Vehicular Technology, vol. 39, Aug 1990, pp. 205-212.
17. R.H Clark, "A statistical theory of mobile radio reception," Bell SysTec.J. vol. 47, no. 6, Jul-Aug 1968, pp. 957-1000.
18. Electronics Industries Association Specification IS-54, " Dual-mode subscriber equipment compatibility specification," EIA project Number 2215, Dec 1989.

19. C.L. Liu and K. Feher, "Bit error rate performance of $\pi/4$-DQPSK in a frequenct-selective fast Rayleigh fading channel", IEEE Trans. on Vehicular Technology, vol. 40, no. 3, Aug 1991, pp. 558-568.
20. S. Yoshida, F. Ikegami, and T. Takeuchi, "A mechanism of burst error performance due to multipath propagation in digital mobile radio," in Proc. ISAP' 85 Conf., Aug. 1985, pp. 561-564.
21. M.C. Jeruchim, P. Balaban, and K.S. Shanmughan, Simulation of Communications Systems, 2nd ed., New York: Kluwer Academic/Plenum Publisher, 2000.
22. J. Chuang, "The effects of time delay spread on portable radio communications channels with digital modulation," IEEE Jour. on Selected Areas in Communications, vol. SAC-5, no. 5, June 1987, pp. 879-889.
23. P.A. Bello and B.D. Nelin, "The effect of frequency selective fading on the binary error probabilities of coherent matched filter receivers," IEEE Trans. on Communications Systems, June 1963, pp.170-185.
24. C.I. Justin, "The effects of delay spread on 2-PSK, 4-PSK, 8-PSK and 16-QAM in portable radio environment", IEEE Trans. on Vehicular Technology, vol. 38, no. 2, May 1989, pp. 43-45.
25. B. Sklar, "Rayleigh fading channels in mobile digital communication systems Part 1: Characterization," IEEE Commun. Mag., July 1997, pp. 90-100.
26. W.C.Y. Lee, Mobile Cellular Telecommunications Systems, New York: McGraw Hill Publications, 1989.
27. R.W. Lowdermilk and F. Harris, "Design and performance of fading insensitive Orthogonal Frequency Division Multiplexing (OFDM) using polyphase filtering techniques," Proc. 30th Annual Asilomar Conf. Signals, Sys., and Comp., Pacific Grove, CA, Nov. 3-6, 1996.
28. W.D., Rummler, R.P., Coutts., and M. Liniger, "Multipath fading channel models for microwave radio," IEEE Commun. Mag., vol.24, no.11, Nov. 1986, pp. 30-41.
29. S. Stein, "Fading channel issues in system engineering," IEEE Journ. On Selected Areas in Communications., vol.SAC-5, Feb 1987, pp.68-89.

30. T.S. Rappaport, Wireless Communications: Principles and Practice: Prentice Hall, 1996.
31. R.L. Bogusch, F.W. Guigliano, and D.L. Knepp, "Frequency-selective scintillation effects and decision feedback equalization in high data rate satellite links," Proc. IEEE, vol.71, no.6, June 1983, pp. 754-67.
32. H. William Tranter, K.S. Shanmugan, T.S. Rappaport & K.L. Kosbar, Principles of Communication System Simulation with Wireless Applocations: Prentice Hall Communications Engineering and Technologies Series, 2003.
33. A. V. Oppenheim and R. W. Schafer, Discrete-Time Signal Processing, New Jersey: Prentice-Hall Inc., 1999.
34. L.R. Rabiner and B.Gold, Theory and Applications of Digital Signal Processing. New Jersey: Prestice-Hall, 1975.
35. B. Windsor and P. Toldalagi, "Digital FIR filter design without tears," Analog Devices application note no. AN-344, DSP product 9-19, 1983.
36. S. J. Orfanidis, Introduction to Signal Processing, New York: Prentice Hall, Upper Saddle River, 1996.
37. S.W. Smith, The Scientist and Engineer's Guide to Digital Signal Processing, San Diego: California Technical Publising, California, 2005.
38. S. Haykin and M. Moher, Modern Wireless Communications, New Jersey: Pearson Prentice Hall, Pearson Education, Inc. Upper Saddle River, 2005.
39. V. Fung, T.S. Rappaport, " Bit error simulation of $\pi/4$ DQPSK mobile radio communications using two-ray and measurement based impulse response model, " IEEE Journ. on Selected Areas in Communications ,vol. 11, no.3, April 1993, pp. 393-405.
40. W. Tomasi, Advanced Electronic Communications Systems, New Jersey: Prentice Hall, Inc., 1987.

CHAPTER 5

SIMULINK IMPLEMENTATION OF FREQUENCY DOMAIN CHANNEL SIMULATOR FOR OFDM WirelessMAN

5.1 INTRODUCTION

Orthogonal frequency division multiplexing (OFDM) scheme has gained significant importance over the last few years due to its resilience against frequency selective fading and simplicity of frequency domain channel equalization. It is becoming popular for the transmission of wideband signals over dispersive channels. OFDM is considered as a potential candidate for fourth generation (4G) mobile wireless systems. This chapter pertains to the design and development of frequency domain channel simulator for OFDM based physical (PHY) layer of WirelessMAN. The simulator comprises 256 carriers OFDM transmitter, receiver and a frequency domain channel based on measured transfer function. FFT convolution is employed to implement the channel. The simulator is developed in SIMULINK using digital signal processing techniques (DSP). Though, the simulator is designed mainly for measurements based channel simulations, it can be equally employed to carry out statistical simulations after some modifications. This chapter also presents the salient features of the physical layer of IEEE 802.16-2004 WirelessMAN.

5.2 ORTHOGONAL FREQUENCY DIVISION MULTIPLEXING (OFDM)

Orthogonal frequency division multiplexing (OFDM) has been adopted in several standards such as Hiperlan/2[1], IEEE 802.11a [2], Digital audio broadcasting (DAB) [3, 4], and Digital video broadcasting (DVB-T) [5, 6]. It is a frequency division multiplexing scheme for orthogonal carriers. It is considered as a special form of multicarrier modulation scheme where the carrier spacing is selected in such a way that they become orthogonal to each other and overlap. The nulls from adjacent carriers coincide with the centres of neighbouring carriers. Despite of overlapping, these carriers do not interfere with each other. Such overlapping permits to pack more carriers into a given bandwidth and increases the spectral efficiency of the system. Whereas, in a normal frequency division multiplexing (FDM) scheme, guard bands

must be placed between the adjacent carriers to prevent interference. These guard bands reduce the spectral efficiency of the system. The term orthogonality refers to a precise mathematical relationship between the frequencies of the carriers. If the the integral of the product of two signals over an interval is zero then the signals are called orthogonal. For an OFDM system, each carrier has a different frequency. These frequencies are chosen such that there is an integral number of cycles in a symbol period and the spacing between the carriers is equal to the reciprocal of the OFDM symbol period. Furthermore, the number of cycles between the adjacent subcarriers differs by exactly one [7]. This spacing makes the carriers orthogonal to each other and at the same time permits them to overlap. At the receiver, the individual carrier can be recovered from the overlapped spectrum provided the orthogonality remains preserved during the course of transmission through the channel.

In OFDM, the total data to be sent through the channel is split into parallel streams equal to the number of carriers. This reduces the data rate and increases the symbol duration in each parallel channel. This increase in symbol duration is the main cause for reducing the intersymbol interference (ISI) and mitigating the effects of frequency selective fading. Each parallel stream at the lower baud rate can be modulated by a separate modulator and the summation of all the outputs of the modulators results in an OFDM signal [8-11]. Figure 5.1 presents the concept of OFDM modulation [10].

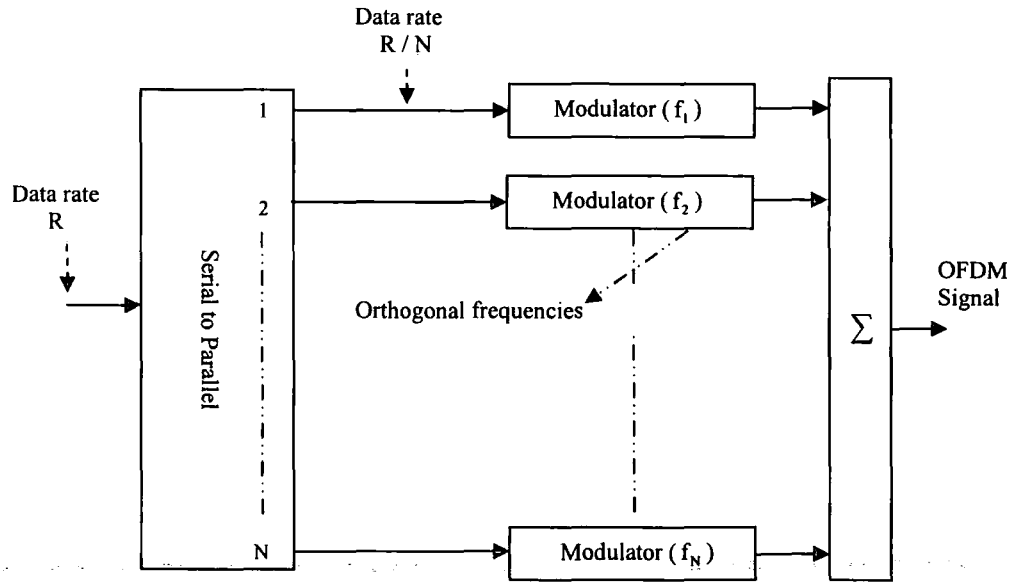

Figure 5.1 Basic concept of Orthogonal Frequency Division Multiplexing (OFDM) scheme.

5.2.1 OFDM Implementation using FFT

The OFDM signal can be produced using the implementation shown in Figure 5.1. This scheme employs a bank of modulators to generate the OFDM signal. However, such implementation becomes very complex with increasing number of carriers. Therefore, the OFDM is not implemented in practice by this method. It is implemented by using discrete Fourier transform (DFT) [12,13,14]. It was shown in [14] that multicarrier signal is effectively the Fourier transform of the original serial data train, and that the bank of coherent demodulators is effectively an inverse Fourier transform generator. In practice these transforms can be implemented very efficiently by a pair of fast Fourier transform (FFT) and inverse fast Fourier transform (IFFT) algorithms. IFFT is normally used in the modulator to generate the OFDM signal whereas, FFT is employed at the receiving end. A typical OFDM implementation based on IFFT/FFT is presented in Figure 5.2 [15].

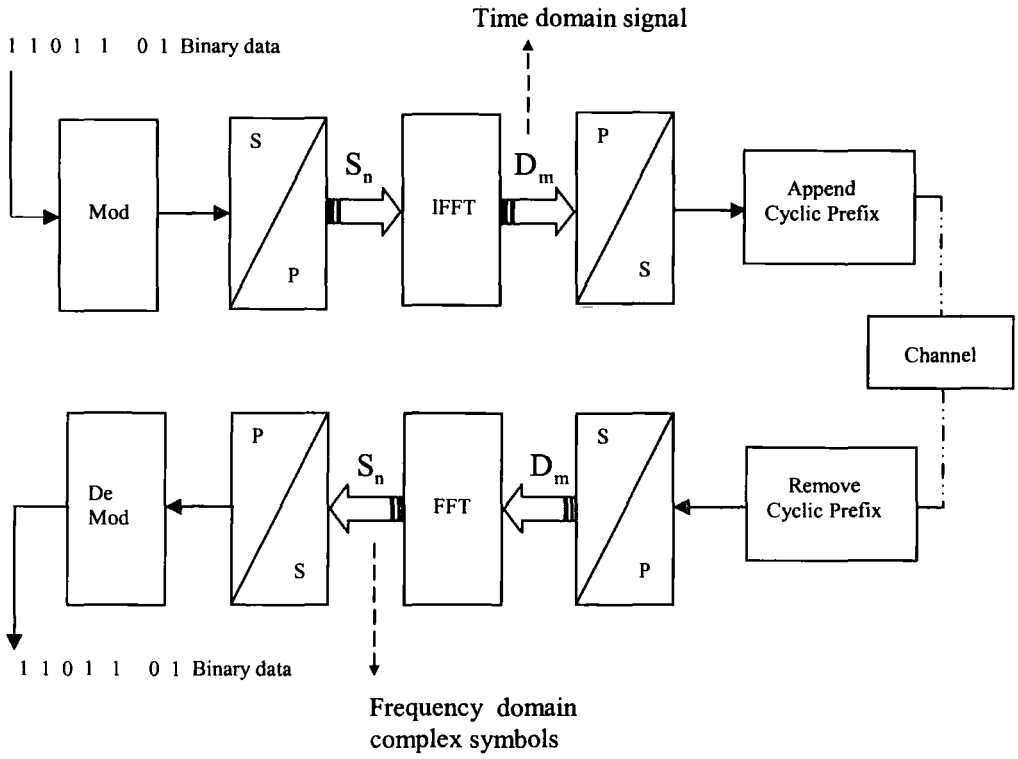

Figure 5.2 OFDM implementation using Fourier transforms.

A modulator generates the serial complex data symbols S_n spaced in time by $\Delta t = 1/f_s$, where f_s is the symbol rate. They form a constellation in the complex plane. These symbols are converted from serial to parallel. The symbol rate in each parallel branch then becomes $T = 1/N\Delta T$, where N is equal to the number of carriers in the OFDM system and T is the OFDM symbol period. The frequency separation between the carriers is $1/T$, making the subcarriers orthogonal to each other. These N parallel symbols, often called a block, are fed to IFFT. The IFFT treats these symbols as being in the frequency domain, contrary to the usual engineering interpretation [11], and produces a time domain waveform which is the summation of all N carriers. As known from signals and system theory, the basic functions for an IFFT are N orthogonal sinusoids. These sinusoids have different frequencies and the lowest frequency is DC. Each input symbol acts like a complex weight for the corresponding sinusoidal basic function. Since the input symbols are complex, the value of the symbol determines both the amplitude and phase of the sinusoid for that subcarrier. The output of the IFFT is then converted from parallel to serial and appended by the cyclic prefix to produce the final OFDM signal.

The process is reversed at the receiving end. After removing the cyclic prefix, the FFT block is employed to process the received signal and recover the frequency domain symbols. The FFT block produces the same original symbols that were fed to the IFFT block at the transmission end if sufficient measures are taken to preserve the orthogonality of the carriers and channel effects are equalized.

Consider Figure 5.2, the block of N complex symbols $\{S_0, S_1, ...S_{N-1}\}$ produces the data block D_m at the output of IFFT. The subscript m is the index of the composite time domain symbols and assumes values from 0 to (N-1).

$$D_m = IFFT\{S_n\} = \frac{1}{N}\sum_{n=0}^{N-1} S_n e^{j(2\pi/N)\,nm} \tag{5.1}$$

At the receiving end, the FFT generates the original block of symbols

$$S_n = FFT\{D_m\} = \sum_{m=0}^{N-1} D_m e^{-j(2\pi/N)\,nm} \tag{5.2}$$

5.2.2 Cyclic Prefix and Intersymbol Interference

Cyclic prefix is used in OFDM to reduce intersymbol interference (ISI) and intercarrier interference (ICI) introduced by the time dispersive muti-path channel [16-20]. It is a copy of the last portion of the time domain OFDM waveform which is transmitted first before the effective part of the OFDM symbol. After an IFFT operation at the transmitter, the last L-1 samples are copied from the end of each OFDM time domain waveform and appended in the same order to the beginning of the OFDM symbol. It does not only act as a guard period between OFDM symbols but it also eliminates intercarrier interference by preserving the orthogonality among subcarriers during the course of propagation through a multi-path channel. Figure 5.3 shows the concept of cyclic prefix. The length of cyclic prefix is chosen to be large enough so as to exceed the maximum excess delay of the channel.

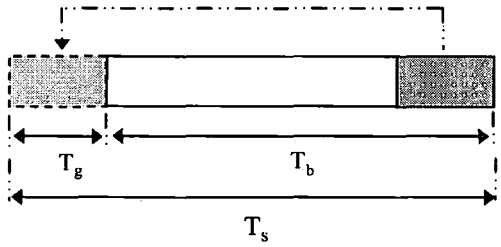

Figure 5.3 Description of cyclic prefix for OFDM symbol

OFDM transmission encounters two types of interference in a multi-path channel: intersymbol interference (ISI) and intercarrier interference (ICI). Intersymbol interference occurs when the received OFDM symbol is distorted by the previously transmitted OFDM symbol. It is analogous to the intersymbol interference (ISI) that is encountered in a single carrier system. In single carrier system, the ISI is a result of many previously transmitted symbols as the symbol period is much shorter than the time span of the channel. However in the case of OFDM systems, the OFDM symbol is made up of many symbols and therefore its period is much longer as compared to the single carrier's symbol period due to which only a portion of an OFDM symbol is distorted by the replicas produced by the multi-path channel. As the few samples of an OFDM symbol are affected, one could consider the use of guard interval to eliminate

the effect of intersymbol interference. The guard interval could comprise zero samples having a length equal to the maximum excess delay of the channel's impulse response. This guard period would prevent intersymbol interference and can be discarded at the receiver prior to the FFT operation. However, it will not prevent the OFDM symbol from interfering with itself. This kind of interference is called intrasymbol or intercarrier interference (ICI). ICI is crosstalk between different subcarriers which destroys the orthogonality of the subcarriers. Therefore, the guard period is not used in practical systems. Instead, the OFDM symbol is cyclically extended in the guard period time by replicating part of the OFDM time domain signal from back to the front in the same order. This extension ensures that delayed replicas of the OFDM symbol always have an integer number of cycles within the FFT interval as long as the delay is smaller than the guard time. This results in complete elimination of intercarrier interference. Due to the cyclic prefix, the linear convolution of the transmitted OFDM time domain signal and multi-path channel is converted into a circular convolution [15,18-20]. This stems from the discrete time properties of signals. In continuous time, a convolution in time domain is equivalent to a multiplication in the frequency domain [19]. This property is true in discrete-time only if the signals are of infinite lengths or if at least one of the signals is periodic over the range of convolution. It is not practical to have an infinite length OFDM signal, however, it is possible to make the OFDM symbol appear periodic by using cyclic prefix. Due to the periodic nature of cyclically extended OFDM symbol, the time domain convolution will result in the multiplication of the spectrum of the OFDM signal with the frequency response of the channel. This employs that each subcarrier's symbol will be multiplied by a complex number which represents the channel's frequency response at that subcarrier. Each received carrier experiences a complex gain i.e. amplitude and phase distortion due to the channel. It means that the cyclic prefix transforms a wideband frequency selective channel into N parallel flat fading channels. Each channel fades independently. Therefore, the performance of OFDM over a frequency selective fading channel is the same as that of a single carrier scheme in flat fading provided there is no intercarrier and intersymbol interference. The use of cyclic prefix protects the OFDM system from being effected by these two impairments.

5.3 FREQUENCY DOMAIN CHANNEL IMPLEMENTATION FOR OFDM SYSTEMS

A communication channel is modelled as linear filter which, in the time domain, convolves the input signal with its impulse response to produce the output. In this modelling approach, the input and the output of the channel are described in the time domain and the channel is characterized by its impulse response. The research carried out until now has revealed that almost all of the channel simulators for OFDM systems have been designed and built using the impulse response modelling approach. All those employed a tapped delay line filter to simulate the channel. The OFDM signal, which is by default in the time domain (IFFT output), is convolved with the impulse response of the channel to produce the output. In general the channel actually performs linear convolution with the time domain signal. However in case of OFDM systems, due to the cyclic prefix this convolution is transformed into cyclic convolution and as a result the magnitude and phase of each subcarrier is point wise multiplied by the channel transfer function. As the information symbols S(n), generated by the complex constellation, are mapped onto the amplitudes and phases of the subcarriers during OFDM modulation, therefore the received symbols R(n) are the product of the transmitted symbols S(n) and the channel's frequency domain transfer function $T(f_n)$ plus the additive complex Gaussian noise n(n). Here, n refers to the subcarrier number.

$$R(n) = S(n).\ T(f_n) + n(n) \tag{5.3}$$

The transfer function is the Fourier transform of the channel impulse response. This implies that the convolution between the cyclically extended OFDM time domain signal and the channel's impulse response results in multiplication in the frequency domain. Hence, a channel can be represented as a bank of multipliers where each OFDM carrier is multiplied by its corresponding transfer function. Figure 5.4 depicts the channel representation for an OFDM system. This is applicable only if the orthogonality among the subcarriers is preserved and there is no intersymbol (ISI) interference. The addition of cyclic prefix ensures that the ISI is eliminated and the subcarriers maintain their orthogonality during transmission through a multi-path

channel. Therefore, cyclic convolution can be employed between the OFDM signal and the channel response to model the transmission system[21].

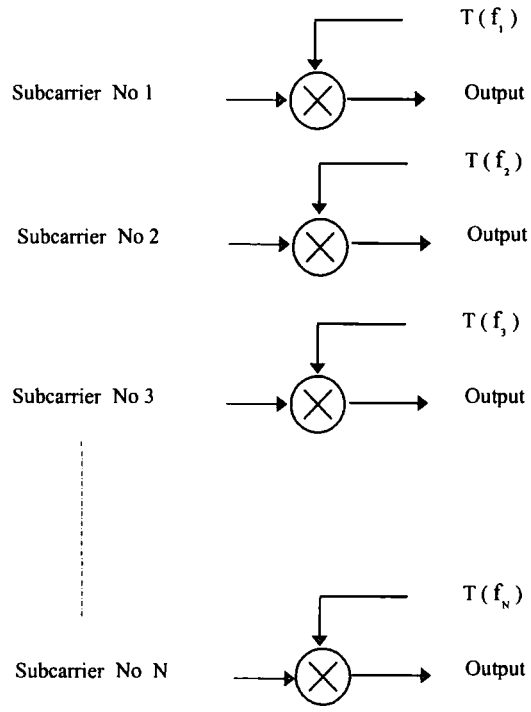

Figure 5.4 Frequency domain channel model for OFDM systems.

It is equally possible to implement the channel in the frequency domain by carrying out point wise multiplication of the spectrum of OFDM time domain signal with the transfer function of the channel. This point wise multiplication can be implemented by employing the FFT convolution between the OFDM time domain sequence and the channel impulse response. FFT convolution requires that the lengths of both sequences should not only be the same but also be a power of 2 for efficient implementation [22]. Therefore, before applying the FFT to the channel impulse response and the OFDM time domain signal generated by the transmitter, both are extended with enough zeros so that their lengths become equal and form a smallest power of 2. The FFT converts both the time domain sequences into frequency domain and then they are multiplied point by point. After multiplication, the frequency domain

signal is again converted into the time domain by inverse Fourier transform operation and the last M samples are removed. Figure 5.5 demonstrates the frequency domain channel implementation using FFT convolution.

In fact the operation of point by point multiplication of the frequency spectrum of two discrete time signals is a result of their circular convolution in the time domain [22-23]. This is due to the fact that discrete Fourier transform treats the functions being transformed are periodic, with period N [22-25]. The the output produced by the multiplication of two FFT operations is also periodic. It can be visualized as the placing of N samples of one function around the circumference of a cylinder, and N samples of another function in reverse order around a second concentric cylinder. One cylinder is rotated, and coincident sample values are multiplied together and summed. The resulting output signal is also periodic. As the discrete Fourier transforms are usually implemented by employing computationally efficient FFT algorithm, therefore, it is called FFT convolution.

It is worth mentioning that linear convolution of two finite duration sequences can also be performed by multiplying DFT's and taking the inverse if the sequences are first zero padded to sufficient length. Therefore, the circular convolution of two zero padded sequences yields the same results as those produced by regular convolution

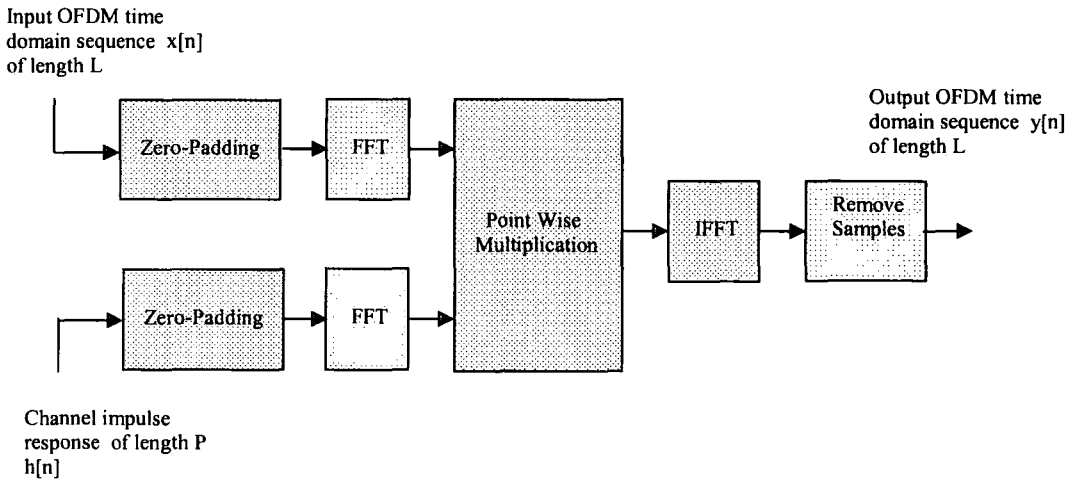

Figure 5.5 Frequency domain channel implementation for OFDM systems.

FFT based convolution has already been employed [24,25] for implementing FIR filters. It has speed advantage over normal time domain convolution [26,27]. This is due to the relative simplicity of multiplication and the speed advantage of FFT algorithm. Moreover, the zero padding of x[n] and h[n] employs that many of the transform multiplications do not, in fact, have to be carried out. Efficient fast convolution algorithms take these factors into account and give further speed advantage [24, 27].

5.4 DEVELOPMENT OF FREQUENCY DOMAIN CHANNEL SIMULATOR USING SIMULINK

SIMULINK has been employed to build FFT convolution based channel simulator for OFDM system based on the physical (PHY) layer's specifications of IEEE 802.16-2004 WirelessMAN [28]. Figure 5.6 depicts the block diagram of the channel simulator. It comprises 256 carriers OFDM transmitter, receiver and a frequency domain channel.

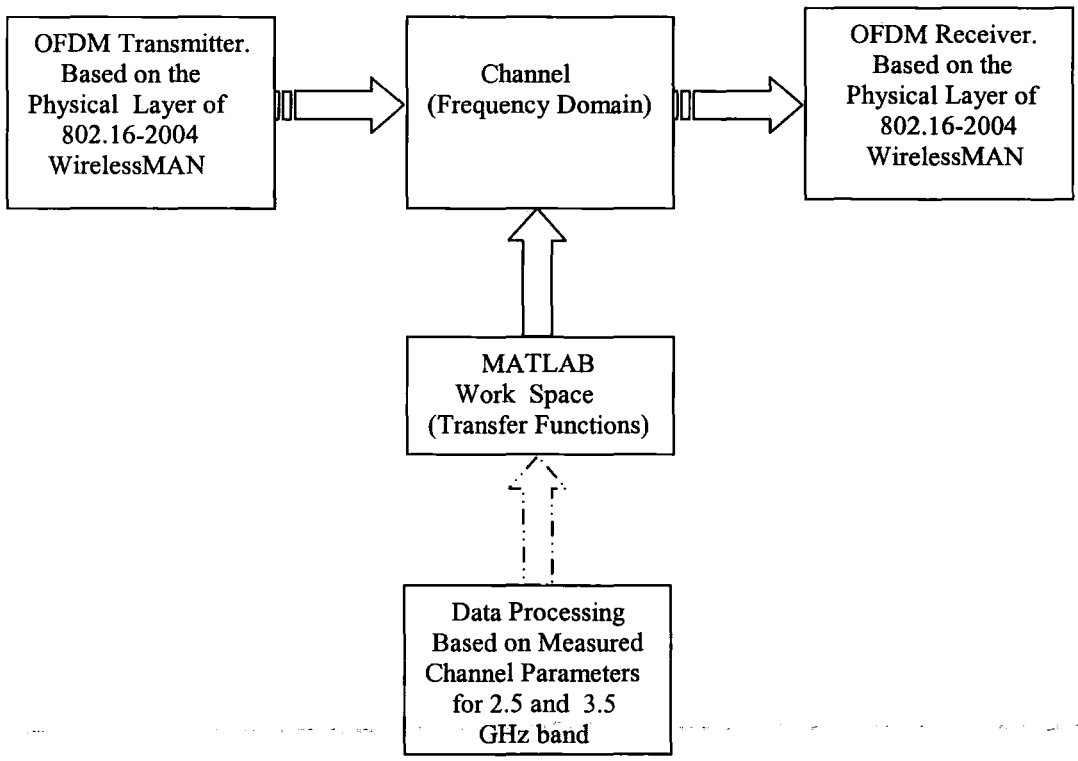

Figure 5.6 Frequency domain channel simulator for 256 carriers OFDM system.

FFT convolution requires that the two signals should be of finite length. This constraint can be met easily in OFDM systems. OFDM is a block based modulation scheme. Each OFDM block including the cyclic prefix form a finite length sequence in the time domain. Real mobile channels exhibit impulse responses of finite durations. Therefore, FFT convolution (cyclic convolution) can be employed to model and simulate a multi-path fading channel for OFDM systems [21].

This work uses measured channel data at the 2.5 GHz and 3.5 GHz bands.The data were measured using a chirp sounder. The sounder employed 10 MHz bandwidth to measure the channel at a sweep repetition frequency (SRF) of 250 Hz. Measured data were processed to extract the channel transfer function for 250 consecutive sweeps. The processed data were made available in the form of a matrix containing complex time frequency functions for 249 consecutive sweeps.The transfer functions contained in the matrix can be treated as a series of snapshots of the channel transfer functions that are separated by the sweep duration; 4 ms for SRF of 250 Hz. The transfer function for each sweep comprised 512 points. The 512 points are separated by 11.6 kHz. Therefore, 249×512 points matrix contained the time variant transfer function for the duration of approximately one second. IEEE802.16-2004 WBA system is flexible in terms of bandwidth, therefore, the required number of points from the 512 points can be taken to constitute a transfer function of variable bandwidths. This research has taken the first 256 points to construct a channel transfer function for approximately 3 MHz bandwidth for 256 carriers. Since the fast convolution based channel model requirs a transfer functions of zero-padded impulse responses, the available transfer functions are first converted into impulse responses by an inverse FFT operation (without windowing) to derive the impulse responses from the measured channel transfer functions. These impulse responses are zero padded and then again transformed into transfer functions to be used in the fast convolution based channel implementation. These steps are consistent with the duality of the impulse response and the transfer function [29-32]. All processing is carried out prior to the start of simulation. During the simulation phase, as shown in Figure 5.7, these transfer functions are moved from the MATLAB work space sweep by sweep at 4ms intervals and entered into the channel where they are first held and resampled to match the

sampling rate of the OFDM symbols and then point wise multiplied by the spectrum of the OFDM signal. Figure 5.7 describes the channel simulation process in detail.

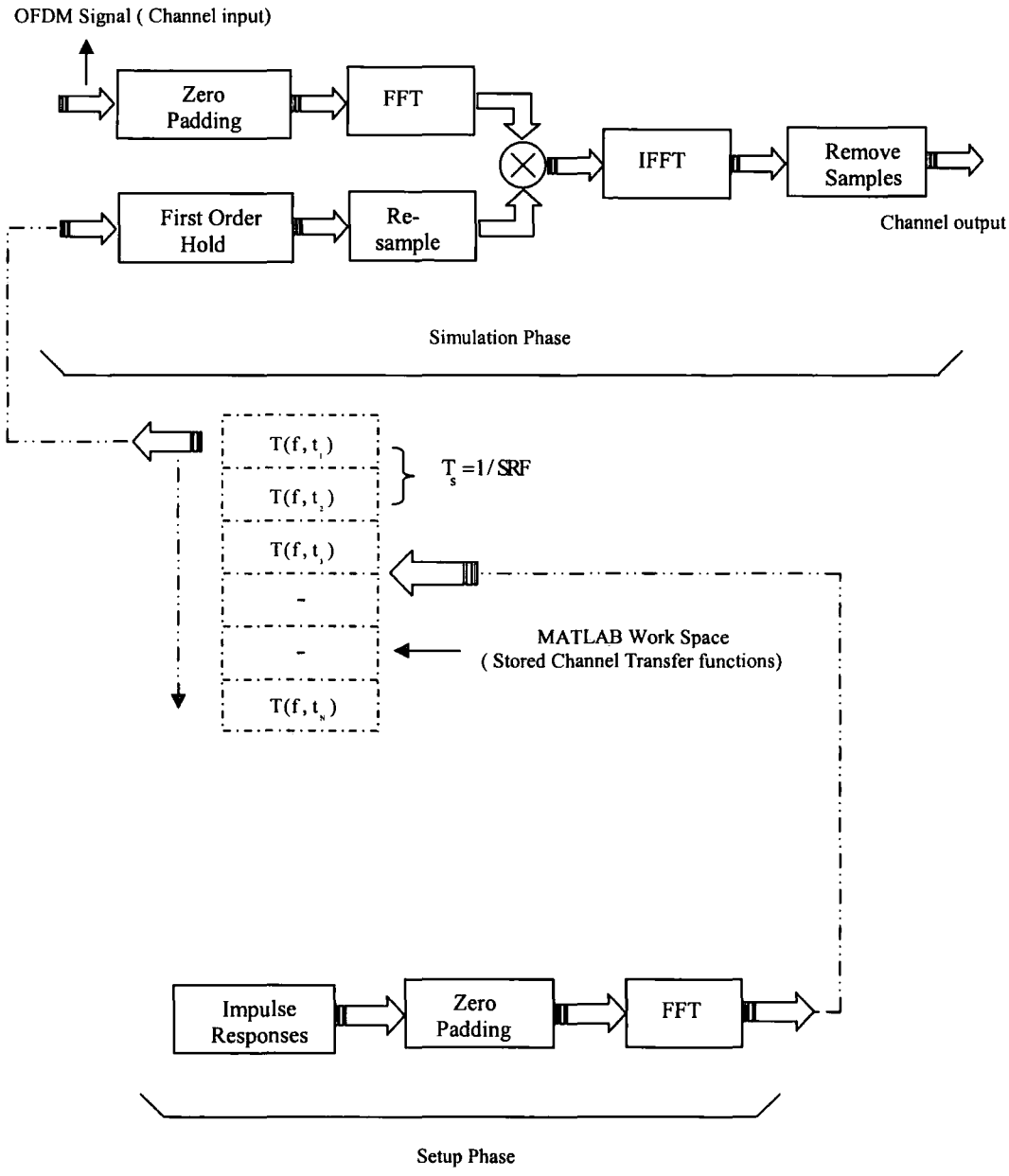

Figure 5.7 Block diagram of the channel simulator. Implemented in SIMULINK using digital signal procesing techniques (DSP)

The process of first order hold and resampling saves computational time and MATLAB workspace which otherwise is required in the case of interpolation. As the

sounder acquires the channel state at every 4ms, therefore, the channel is assumed stationary for this period. In this context it is to be mentioned here that the WBA system is meant for stationary sites, therefore, channel variations are very small. It will be seen in the next chapter that the maximum observable Doppler from the measured data will not be more than 2 Hz.

Though, this work has focused on measured channel data, the simulation architecture presented in Figure 5.7 can be equally employed to carry out statistical simulations. Either the channel transfer function could be directly generated using the frequency-time correlation properties of the channel and stored in the MATLAB workspace or impulse responses can be generated first and then converted to transfer functions using Fourier transformation.

5.5 SIMULINK IMPLEMENTATION OF PHYSICAL(PHY) LAYER FOR WIRELESS BROADBAND METROPOLITAN AREA NETWORK (MAN)

The wireless metropolitan area network, WirelessMAN™, is a fixed broadband wireless access system which provides high data rate network connections to stationary sites at microwave frequencies between 2 to 11 GHz bands through a multi-path channel environment. It is the technology of the future and is an alternate to broadband wired links such as, digital subscriber line (DSL), fiber optic and coaxial cable. Its main advantage is the rapidity and ease with which it can be deployed to provide access to sparsely located sites. These sites communicate with the central radio base station through radio antennas mounted on a roof top. The base station spans a cellular radius of 20-30 km.

The IEEE 802.16-2004 standards, approved in June 2004, define the WirelessMAN™ air interface specifications for wireless metropolitan area networks (MAN) [27]. These standards were first published on 8th April 2002 and were amended on January 30, 2003 to cover a licensed and unlicensed frequency spectrum between 2 to 11 GHz. These standards encompassed line of sight (LOS) propagation in the 10-66 GHz band and none line of sight (NLOS) propagation in the 2 to 11 GHz band. The IEEE 802.16-2004 standards specify three air interfaces: single carrier modulation, 256 point transform OFDM, and 2048 point transform OFDMA. This work has chosen to develop a simulator for 256 carriers OFDM system. This interface is mandatory for the

license exempt band. Moreover, only 256 carriers OFDM mode of IEEE 802.16-2004 has been adopted by the WiMax forum for fixed broadband services [33]. This interface seems to be favored by the vendor community for reasons such as lower peak to average ratio, fast Fourier transform (FFT) calculation, and less stringent requirements for frequency synchronization compared to 2048 carrier systems. Figure 5.8 shows the block diagram of OFDM-based physical layer for 802.16-2004 WirelessMAN.

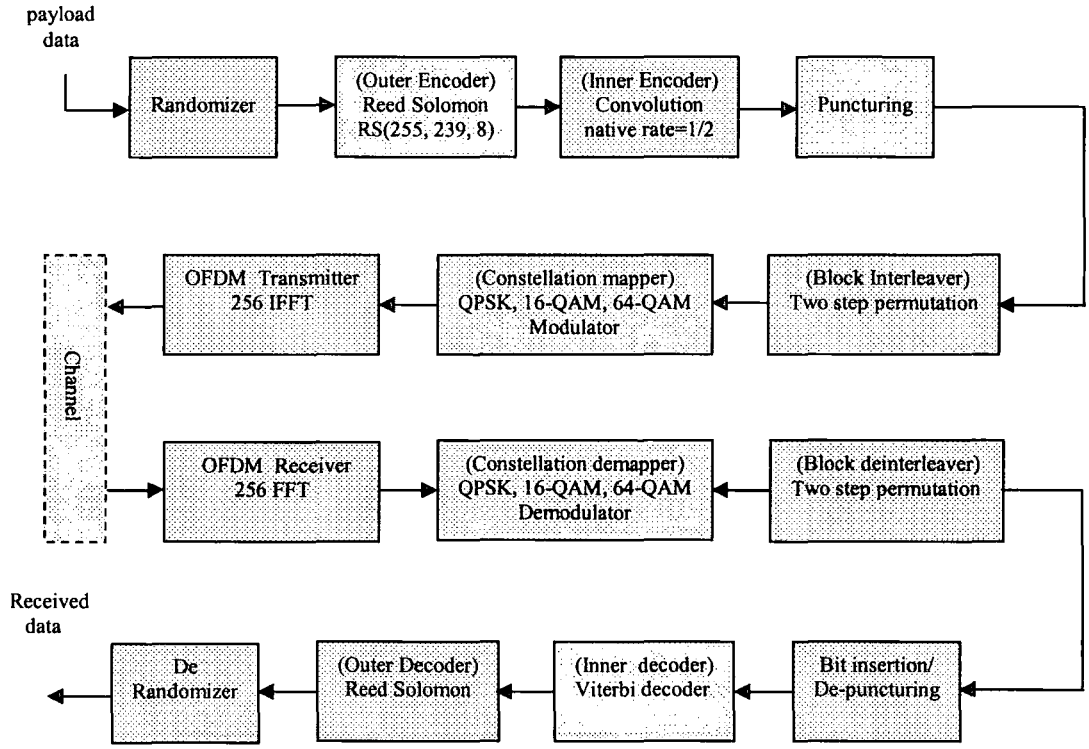

Figure 5.8 Block diagram of OFDM-based physical (PHY) layer for 802.16-2004 WirelessMAN.

5.5.1 Channel Coding for IEEE 802.16-2004 WirelessMAN

Channel coding is employed to achieve a reliable communication link from transmitter to receiver through the channel. The presence of additive white Gaussian noise (AWGN) and multi-path fading in the mobile communication channel degrades the bit error rate (BER) performance of the system to unacceptable level. [34]. The multi-path fading channels introduce bursts of errors in the data due to a drop in the signal strength

below the noise level [35]. The channel coding involves rearranging and addition of redundant data prior to the transmission and complementary operation at the receiving end. In IEEE 802.16-2004, channel coding is achieved in three steps: randomization, forward error correction (FEC) and interleaving.

5.5.1.1 Randomization

Randomizers are used to introduce randomness in the payload data by toggling some of the zeros to one or ones to zeros. As a result, the long sequences of ones and zeros in the payload data are eliminated. This randomness is needed to optimize the decision regions of maximum likelihood detector in the receiver. The randomizer XOR's the data with a pseudorandom bit sequence. In IEEE 802.16-2004 standards, 15 bit shift-registers with generator polynomial of $1+X^{14}+X^{15}$ are employed to implement randomization. The block diagram of the randomizer is shown in Figure 5.9. As per standards, randomization is performed on both the up and the down link for each allocation of data block independently. If the amount of data to be transmitted does not fit exactly the amount of data allocated, padding will be employed at the end of the transmission block up to the amount of data allocated, minus one byte, which shall be reserved for the introduction of tail byte. This tail byte is required by the convolution encoder to turn its register state back to zero.

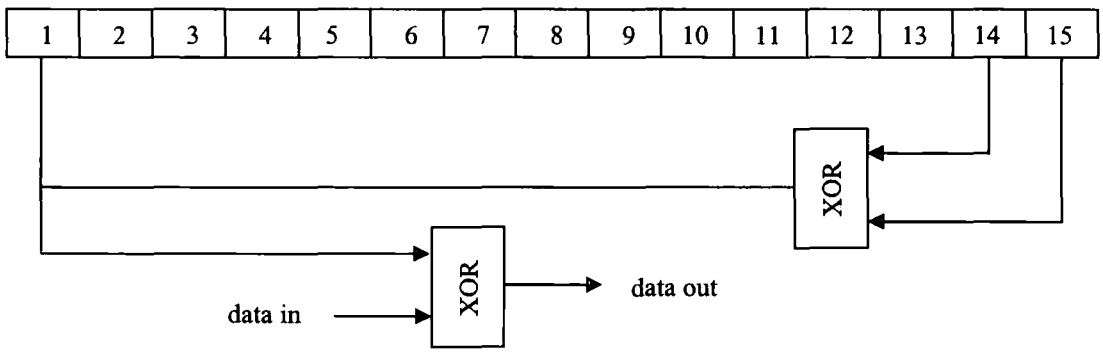

Figure 5.9 Block diagram of the randomizer for physical layer of 802.16-2004 WirelessMAN.

The PN sequence generator from the communication block set library has been employed to generate a sequence of pseudorandom binary numbers. This block accepts generator polynomial to configure its shift register connections. The generator polynomial can be provided by a vector comprising either the coefficients of the polynomial in descending order of power or exponents of X for the nonzero terms of the polynomial in descending order of power. The last entry should be 1 or 0 respectively.

This implementation has chosen the second method to configure the PN sequence generator. The initial state of the register can be set by specifying a binary vector. The generator has been configured to produce binary data in the form of a frame based column vector. The size of the column vector can vary to match the size of input data block to RS encoder specified in table 5.1. Moreover, the RS encoder block accepts only frame based column vector at its input. The output of PN generator has been zero padded to achieve tail byting.

5.5.1.2 Forward Error Correction Codes (FEC)

Forward error correction (FEC) codes are used to detect and correct the errors introduced by the channel. FEC is the only error correcting scheme that detects and corrects the errors at the receiver without requesting retransmission [36]. In FEC, extra bits are added to the original data at the expense of an increase in bandwidth. Forward error correction (FEC) codes have been classified into block codes and convolution codes [37]. This classification has been based on the presence or absence of memory in the encoders for the two codes. The IEE802.16-2004 standards employ concatenated Reed-Solomon encoder/decoder and convolution encoder/decoder in its forward error correction (FEC) scheme. Reed-Solomon (RS) code is called outer and convolution code is called inner code respectively. The concatenation of these codes provides large coding gain with less implementation complexity as compared to single coding scheme [37]. Reed-Solomon codes are block codes and can handle burst of errors introduced by the wireless channel but do not possess ability to handle a large number of distributed errors. Convolution codes are considered good for correcting random errors. Therefore, the combination of both effectively corrects most of the errors introduced by the wireless channel.

5.5.1.2.1 Reed-Solomon (RS) Codes

The Reed-Solomon (RS) codes are block based codes which take a block of data and add extra redundant bits. The code words are produced on a block-by-block basis. These are linear block codes and are a subset of BCH codes. These codes are based on a specialist area of mathematics known as Galois field or finite field. The RS encoder is specified as RS (N, K, T), where N, K refer to the number of overall bytes after and before encoding respectively and T denotes the number of data bytes which can be corrected. It is not required to use the natural size of Reed-Solomon code block. A technique called 'shortening' can produce a small code of any desired size from a large size by zero padding the unused portion of blocks in the beginning and not transmitting them. At the decoder end, the same length of zeros is appended locally. The RS codes are characterized by field polynomial and generator polynomial.

The Reed-Solomon coder specified in the IEEE802.16-2004 standards is based on N=255, K=239, T=8 over Galois Field GF (256). The standards recommend that the following polynomials are to be employed to generate systematic code.

Code Generator Polynomial: $g(x) = (x + \lambda^0)(x + \lambda^1)(x + \lambda^2)...(x + \lambda^{2T-1}),\ \lambda = 02_{HEX}$

Field Generator Polynomial: $p(x) = x^8 + x^4 + x^3 + x^2 + 1$

Table 5.1 presents the values of N, K and T of RS code specified in the standards for different modulation schemes. RS encoder and decoder blocks from the communication block set library of SIMULINK have been employed to implement RS encoding and decoding. The values of N, K, code generator and field polynomial can be specified directly in the dialog box. If N is less than $2^M - 1$, the block uses a shortened Reed-Solomon code, where M refers to the length of binary sequence for each symbol of the code. The block accepts the primitive polynomial as a binary row vector that represents a primitive polynomial over GF (Z) of degree M, in descending order of power. If the primitive polynomial is specified, then N must lie in the range $3 \le N < 2^{M-1}$. These two blocks accept only a frame based column vector at the input and produce the output in the same format. The length of the input column vector to the RS encoder should be an integer multiple of $M \times N$.

Table 5.1 Coding requirements for various modulation schemes for IEEE 802.16-2004 standards.

Modulation	Uncoded Block size (bytes)	Coded Block size (bytes)	RS code	CC code rate	Overall Coding rate
BPSK	12	24	(12,12,0)	1/2	1/2
QPSK	24	48	(32,24,4)	2/3	1/2
QPSK	36	48	(40,36,2)	5/6	3/4
16-QAM	48	96	(64,48,8)	2/3	1/2
16-QAM	72	96	(80,72,4)	5/6	3/4
64-QAM	96	144	(108,96,6)	3/4	2/3
64-QAM	108	144	(120,108,6)	5/6	3/4

5.5.1.2.2 Convolution Encoder/Viterbi Decoder

A convolution encoder operates in a continuous manner. It maps each k bits of continuous input stream onto n output bits by convolving the input bits with a binary impulse response. It employs M stage shift register and n modulo-2 adders to generate redundant bits. The output is usually in a multiplexed form. A convolution encoder is characterized by the constraint length K, generator polynomials and code rate r. The constraint length indicates the number of shifts over which a single message bit enters and leaves the shift register and also can influence the encoder output. The constraint length is equal to M+1. Whereas, the generator polynomials define the connection of each path from the output to the input of the convolution encoder.

The IEEE 802.16-2004 standards specify that a convolution encoder with native rate of 1/2, having a constraint length equal to 7, with the following generator polynomials, should be employed to generate two coded bits.

$G_1 = 171_{oct}$ FOR X

$G_{1=2} = 133_{oct}$ FOR Y

It is one of the most frequently applied encoders. It has a single data input and two outputs which are interleaved to form the coded output sequence. One bit enters the encoder and two are generated at the output. Each pair of output bits depends on seven

input bits. The number 7 refers to the current input bit plus six previously fed bits that are stored in the length 6 shift register. Figure 5.10 shows the block diagram of the convolution encoder specified in the IEEE 802.16-2004 standards. In order to realize different code rates, different puncturing methods are employed at the output of this native 1/2 rate encoder. Puncturing patterns and serialization order for different code rates are defined in Table 5.2

Table 5.2 Puncturing configuration for different code rates

	Code Rates			
Rate	1/2	2/3	3/4	5/6
d_{free}	10	6	5	4
X	1	10	101	10101
Y	1	11	110	11010
XY	X_1Y_1	$X_1Y_1Y_2$	$X_1Y_1Y_2X_3$	$X_1Y_1Y_2X_3Y_4X_5$

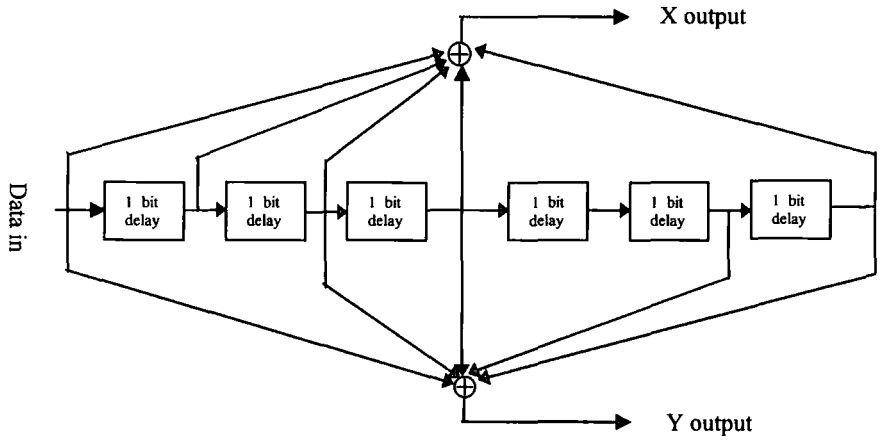

Figure 5.10 Block diagram of native rate 1/2 convolution encoder

As per specified standards, zero terminating convolution encoder should be used for convolution coding. This implies that the encoder's register state have to be brought back to zero before the start of the next data block. This can be achieved by employing

tail biting and zero tailing. The tail biting is implemented by initializing the encoder's memory with the last data bits of the RS encoded block. If these bits are zero, then these will reset the register state to zero. As the convolution encoder requires at least six zero bits to make its register state back to zero, there is a need to append a single 0×00 byte at the end of each block of data generated by the randomizer [28, 38, 39]. This appending is referred to as zero tailing.

The decoding of convolutionally encoded data is performed at the receiver end by employing a computationally efficient algorithm called Viterbi [40-42]. This algorithm estimates the maximum likelihood path through the trellis based on received symbols. The decoder reconstructs the action of the encoder by selecting the most likely path from a structured graph, corresponding to a tree or trellis that describes all possible states.

The communication block set library of SIMULINK contains convolution encoder, Viterbi decoder, puncture and insert zero blocks to achieve convolution encoding and decoding. The convolution encoder and decoder block have been configured by specifying a constraint length of 7, code generator polynomial of 171 and 131(in octal numbers) through the MATLAB command 'poly2trellis'. This command converts convolution code polynomials to trellis structure description to be used by the encoder/decoder. Puncturing has been performed by specifying a puncture vector pattern in binary form as an input parameter to the puncturing block. At the receiving end, the zeros were inserted in place of punctured bits prior to the decoding. The inserted zero block has been employed for this purpose. This block accepts a vector as a parameter to specify the positions of zeros and input elements.

5.5.1.3 Interleaving/Deinterleaving

Interleaving is used to spread the burst of correlated bit errors introduced by the fading channel. The channel coding schemes have a limited capability to correct a long string of errors [10]. Most FEC coding schemes are able to handle a limited number of bits errors if they are randomly distributed and statistically independent from one bit to the next. Even a powerful algorithm like Viterbi does not correct errors if there are $d_{free}/2$ closely spaced errors in the received signal [37]. Interleaving is basically a form of a scrambling scheme which rearranges the data prior to transmission. At the receiving

end, the deinterleaver takes the data which contains a burst of error and when it rearranges that data to its original order, the series of errors get distributed and are easily corrected by the forward error correction schemes (FEC). 802.16-2004 standards employ a block interleaver to distribute adjacent bits into data subcarriers. The size of the block interleaver depends upon the modulation type and the number of coded bits per the specified allocation, N_{cbps} and is listed in table 5.3.

Interleaving and deinterleaving is carried out in two steps. The first step rearranges the ordering of the bits so as to ensure that adjacent bits are not mapped onto adjacent carriers. This helps to eliminate the errors by reducing the chance that adjacent bits would be lost if a portion of the channel bandwidth is degraded due to frequency selective fading or with some sort of spurious or band limited noise. The second step of interleaving reorders the bits so that the original adjacent coded bits are alternatively mapped onto more or less significant bits of the constellation. This step avoids long runs of lowly reliable bits.

The first permutation is defined by the rule:

$$m=\left(N_{cbps}/16\right).k_{mod(16)}+\text{floor}\left(k/16\right) \qquad k=0,1,....N_{cbps}-1 \tag{5.4}$$

The second permutation is defined by the rule:

$$j=s.\text{floor}\left(m/s\right)+\left(m+N_{cbps}-\text{floor}\left(16.m/N_{cbps}\right)\right)_{mod\,s} \qquad m=0,1,....N_{cbps}-1 \tag{5.5}$$

where k and m are the input and output indices in the first permutation respectively, j and m are the output and input indices in the second permutation respectively. Let $s=N_{cpc}/2$, where N_{cpc} denotes the number of coded bits per carrier, i.e., 2, 4, or 6 for QPSK, 16-QAM, or 64-QAM respectively.

At the receiving end, the inverse operation is carried out. The first permutation in the deinterleaver is the inverse of the second permutation in the interleaver, and conversely. The deinterleaving is also performed in two steps. The first permutation is defined by the rule

$$m = s.\text{floor}(j/s) + \left(j + \text{floor}(16.j/N_{cbps})\right)_{\text{mod}\,s} \qquad j = 0,1,....N_{cbps} - 1 \tag{5.6}$$

The second permutation is defined by the rule:

$$k = d.m - (N_{cbps} - 1).\text{floor}(16.m/N_{cbps}) \qquad m = 0,1,....N_{cbps} - 1 \tag{5.7}$$

where j and m are the input and output indices in the first permutation respectively, k and m are the output and input indices in the second permutation respectively.

Table 5.3 Block sizes for various modulation schemes specified in IEEE 802.16-2004 standards

Modulation	Coded bits per bit interleaved block (N_{cbps})		
	(Default) 4 subchannels	2 subchannels	1 subchannels
BPSK	192	96	48
QPSK	384	192	96
16-QAM	768	384	192
64-QAM	1152	768	384

In implementing interleaving and deinterleaving in SIMULINK, a general block interleaver from the communication block set library has been employed for both operations. Two cascaded blocks are required for each interleaving and deinterleaving operation to perform the fist and second permutations. The block rearranges the elements of its input vector without repeating or omitting any element on the basis of the indices provided to it through its parameters mask. During the setup phase of the simulation, the indices of both permutations for interleaving and deinterleaving are calculated using equations 5.1-5.4 and stored in the workspace. An algorithm has been written in MATLAB to generate these indices (appendix 3).

It is worth mentioning that deinterleaving can also be carried out by employing a deinterleaver block instead of an interleaving block. The deinterleaving block needs indices from equation 5.1 and 5.2 rather than 5.3 and 5.4. It automatically generates

indices for the deinterleaving operation. Hence, only two permutation equations are sufficient for both operations. However, this implementation has employed only an interleaver block to perform both operations for the purpose of demonstrating the application of all four equations. Moreover, it has no bearing on the simulation run time whether the deinterleaving is performed by employing an interleaving block and equations 5.3-5.4 or a deinterleaving block and equations 5.1-5.2.

5.5.2 Data Modulation/Demodulation

Data modulation and demodulation is employed to map the data bits from the output of the interleaving block onto the complex constellation points and vice versa. Gray-mapped phase shift keying (PSK), Quadrature Phase Shift Keying (QPSK), 16 levels Quadrature Amplitude Modulation (16-QAM) and 64 levels QAM have been specified in the standards, where 64-QAM is optional. Figures 5.11 and 5.12 depict the complex constellation points for 16-QAM and QPSK respectively. The constellation points are multiplied by a constant value indicated in table 5.4 for QPSK, 16-QAM and 64-QAM respectively to achieve equal average power.

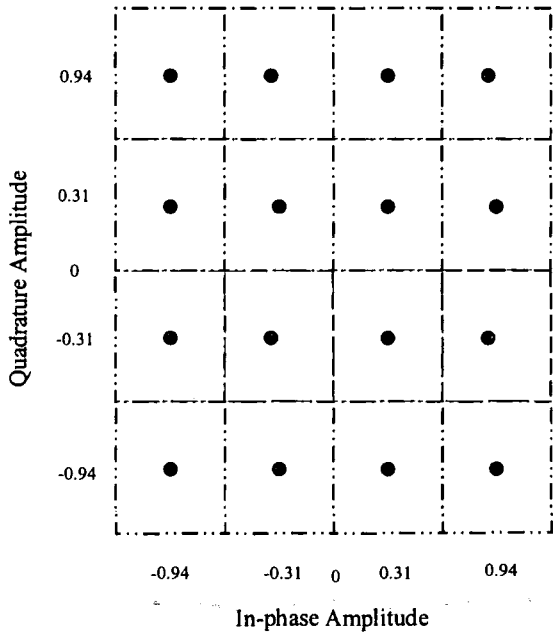

Figure 5.11 Complex constellation points for 16 level Quadrature Amplitude Modulation (16-QAM)

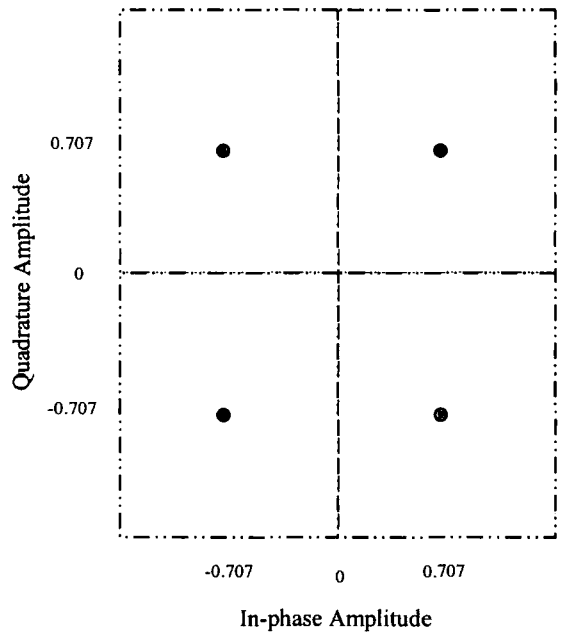

Figure 5.12 Complex constellation points for Quadrature Phase Shift Keying (QPSK)

Table 5.4 Normalized values of constellation points for different modulation schemes.

Modulation type	Normalized amplitude
QPSK	$1/\sqrt{2}$
16-QAM	$(1,3)/\sqrt{2}$
64-QAM	$(1,3,5,7)/\sqrt{2}$

The communication block set library contains various types of baseband modulators and demodulators. As per standards, 64-QAM is optional, therefore, this work employs only 16-QAM and QPSK for mapping binary data onto complex symbols. These base band modulators accept binary sequences as well as integers. There are two methods to achieve equal average power as specified in the standards. The first method involves the generation of output symbols based on minimum distance

between them, i.e., 2 and then multiplying them by the constants indicated in table 5.4. Another method is to specify the average power of the symbols to 1 using the mask of the modulator block. This implementation performs normalization by setting the average output power of the modulator to 1. This reduces one multiplication block which otherwise is needed at the output of the baseband modulator. Figures 5.11 and 5.12 show a gray coded constellation produced at the output of the demodulators for 16-QAM and QPSK

5.5.3 OFDM Modulation / Demodulation

Inverse Fast Fourier Transform (IFFT), Fast Fourier Transform (FFT), zero padding and selector blocks from the DSP block set library have been employed for implementing OFDM modulation and demodulation. Prior to the IFFT operation, the complex symbols are first zero padded and then arranged using a selector block. The 256 carriers OFDM system effectively uses 200 carriers to convey data. The remaining carriers are used for guard bands at lower and higher ends of the spectrum. The purpose of the guard bands is to enable the signal to naturally decay and create the FFT 'brick Wall' shaping [27]. Table 5.5 presents the main features of 256 carriers OFDM system.

5.5.4 Pilot Modulation

Pilots are inserted into each OFDM symbol for the purpose of tracking, channel estimation and frequency off-set estimation. Every OFDM symbol contains 8 pilots. The exact position of each pilot is shown in Figure 5.13. These pilots are power boosted by 2.5 dB and are transmitted using binary phase shift keying (BPSK) using the following formula. The binary sequence, w_k, for these pilots has been generated by employing the PRBS generator from the communication block set library with polynomial generator of $X^{11}+X^9+1$. The generator uses a vector, [1 1 1 1 1 1 1 1 1 1 1], for its initialization. The modulated sequence can be expressed as

$$R_e\{c_k\}=8/3(1/2-w_k) \tag{5.8}$$

$$I_m\{c_k\}=0 \tag{5.9}$$

Table 5.5 Symbol parameters for IEEE 802.16-2004 IEEE 256 OFDM system

Parameters	Values
N_{FFT}	256
N_{used}	200 (including 8 pilots)
F_s/BW	Licensed channel bandwidths are multiples of 1.75 MHz, licensed exempt 8/7 and any other bandwidth 7/6.
(T_g/T_b)	1/4, 1/8, 1/16, and 1/32.
Number of lower frequency guard carriers.	28
Number of higher frequency guard carriers.	27
Frequency offset indices of guard carriers	-128, -127,...., -101 +101, +102,...,+127
Frequency offset indices of basic fixed location pilots	-84, -60, -36, -12, 12, 36, 60, 84.
Subchannel number: Allocated frequency offset Indices of carriers	1:{-88,...,-76},{-50,...,-39},{1,...,13},{64,...,75} 2:{-63,...,-51},{-25,...,-14},{26,...,38},{89,...,100} 3:{-100,...,-89},{-38,...,-26},{14,...,25},{51,...,63} 2:{-75,...,-64},{-13,...,-1},{39,...,50},{76,....,88}

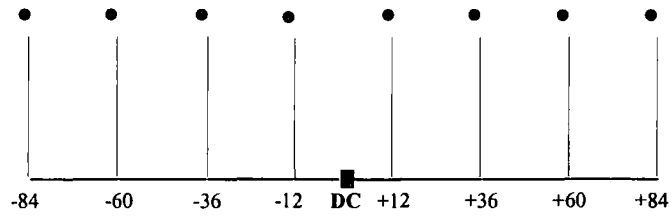

Figure 5.13 Positions of 8 pilots in the spectrum of OFDM symbol

In this implementation, the BPSK modulation has been carried out by passing the output of the polynomial generator through the unipolar to bipolar converter block from the DSP block set of SIMULINK.

5.5.5 Time and Frequency Domain Description of 256 OFDM Symbol

Prior to the IFFT operation, each OFDM symbol in the downlink subframe is always viewed in the frequency domain and contains

- 8 pilot tones at frequency offset of ± 12, ± 36, ± 60 and ±84.
- 192 data carriers at locations specified in table 5.5 and shown in Figure 5.14.
- 28 lower frequency guard carriers.
- 27 higher frequency guard carriers
- One DC.

Figure 5.14 presents the frequency domain description of the OFDM symbol containing 256 subcarriers.

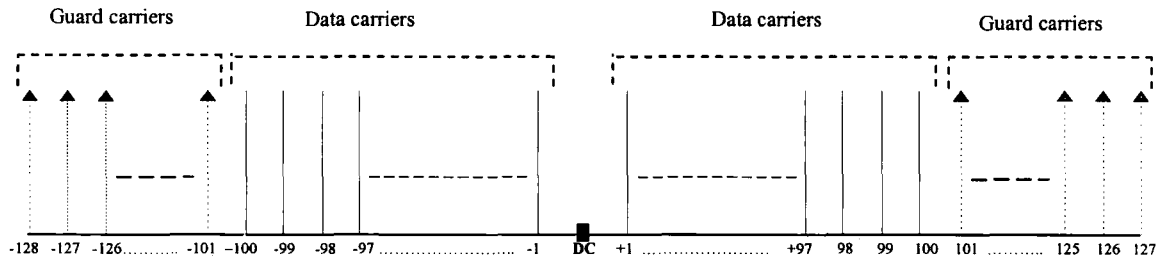

Figure 5.14 Frequency domain description of OFDM symbol.

Inverse Fourier transform operation converts the OFDM frequency domain symbol into the time domain waveform which represents the composite of 256 carriers. As shown in Figure 5.15, the time duration of this waveform is called the useful symbol time T_b. The cyclic prefix (CP), which is a copy of the last T_g μs of the useful symbol period, is appended in the same order at the beginning of this waveform to preserve the orthogonality of the carriers during propagation through multi-path fading channel. The time duration of the resulting waveform is referred to as the symbol time T_s. Figure 5.15 illustrates the time domain representation of the OFDM symbol.

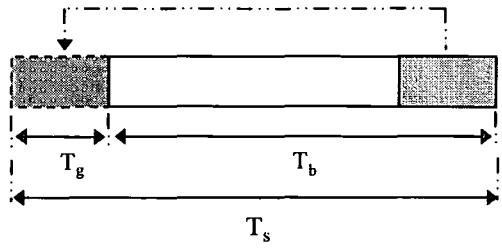

Figure 5.15 Time domain description of OFDM symbol.

Figure 5.16 illustrates the measured time domain waveform (absolute value) for one OFDM symbol of IEEE802.16-2004 system having 8.62 μs useful period. The corresponding frequency spectrum is also been shown in Figure 5.17. The time domain waveform and the spectrum of the signal have been measured using the vector scope and the spectrum analyzer respectively from the SIMULINK library of DSP block set.

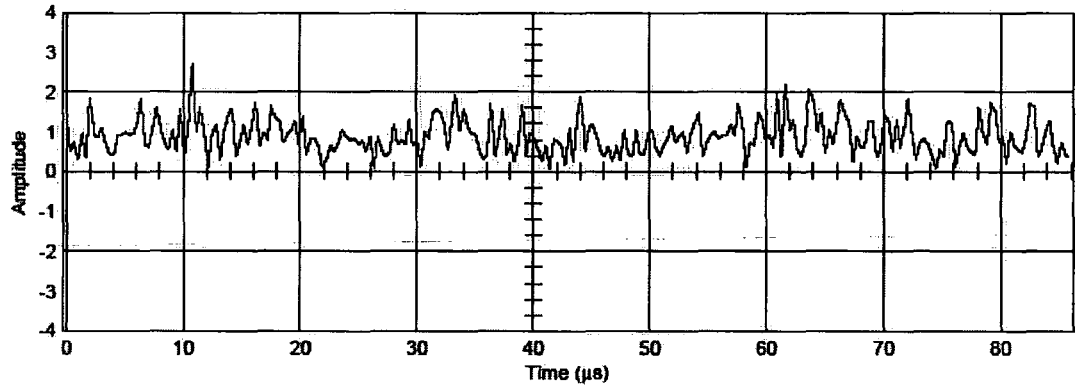

Figure 5.16 Measured time domain waveform for one OFDM symbol of 256 OFDM system implemented in SIMULINK

5.5.6 Frame Structure for 802.16-2004 OFDM System

Communications between the base station (BS) and the subscriber stations (SS) take place using either time division duplex (TTD) or frequency division duplex (FDD)

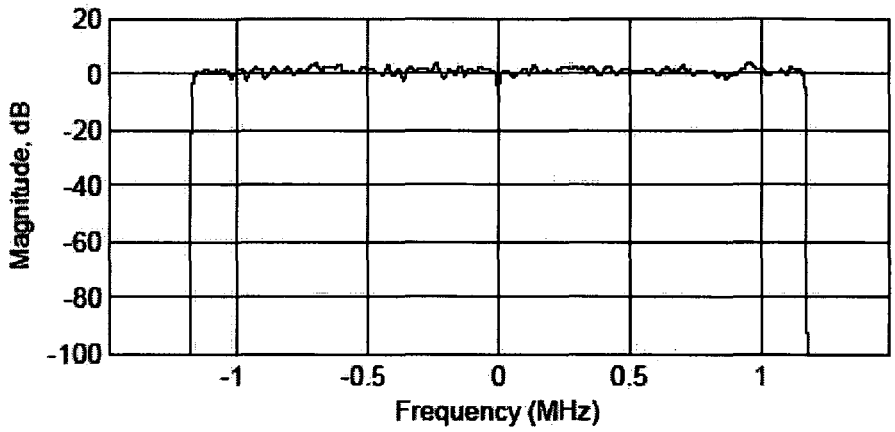

Figure 5.17 Measured spectrum for one OFDM symbol of IEEE 802.16-2004 system implemented in SIMULINK.

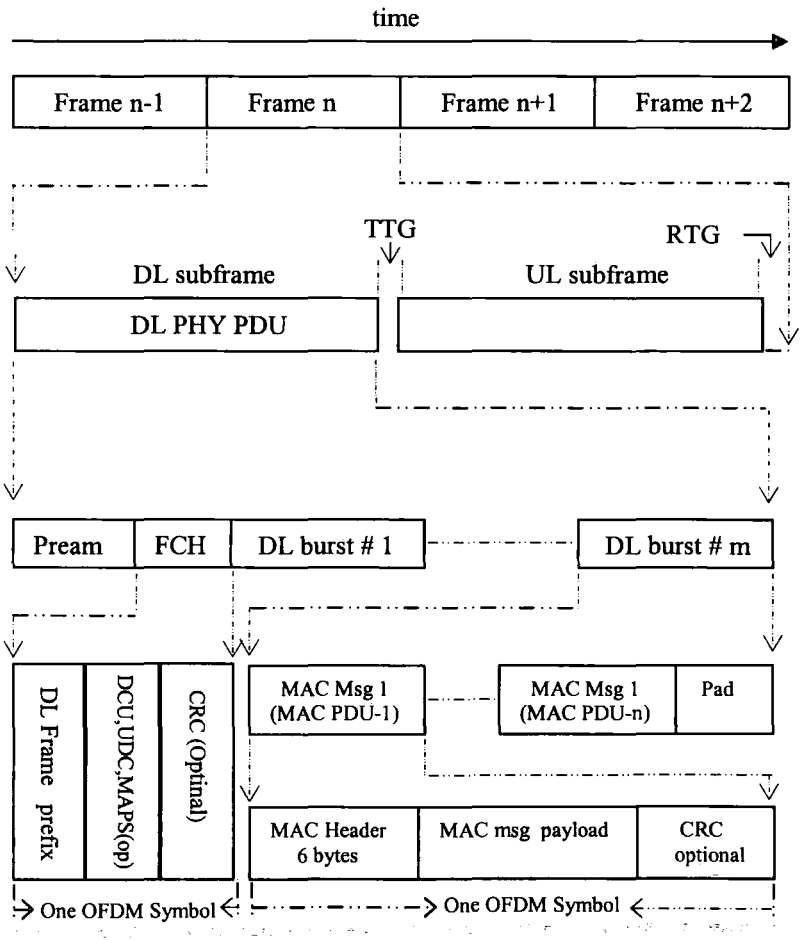

Figure 5.18 Frame structure for time division duplex (TDD) mode of operation .

mode of operation. A Subscriber station may operate in half duplex FDD (H-FDD) mode or in full duplex FDD mode. The license exempt band operates in TDD mode, whereas the licensed band operates either in FDD or TDD mode. As this work pertains to the license exempt band, only TDD mode will be considered. Uplink (UL) and downlink (DL) communications take place in frames. Each TDD frame, as shown in Figure 5.18, comprises downlink subframe and uplink subframe. In TDD mode of operation, base station and subscriber equipment transmit on the same RF frequency but separated in time. The base station transmits a downlink sub frame, followed by a short gap called transmit/receive transit gap (TTG), then the subscriber stations transmit the uplink sub frame. The subscribers are accurately synchronized such that their transmission does not overlap each other as they arrive at the base station. Following all uplink frames, another short gap called receive/transmit transition gap (RTG) is placed before the base station starts its transmission again. In the TDD mode of operation, the division point between the uplink and the downlink can also vary on frame to frame basis to facilitate asymmetric allocation of on air time between the uplink and the downlink. This work involves the simulation of downlink only. Each downlink subframe is depicted in Figure 5.19

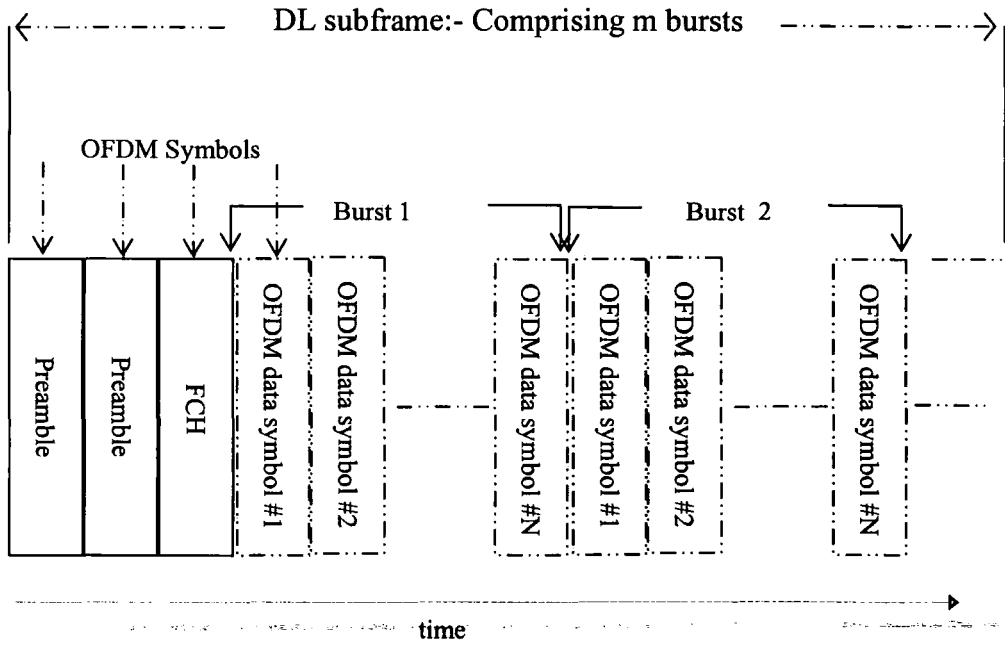

Figure 5.19 Structure of down link subframe for physical layer of IEEE802.16-2004 WirelessMAN

It consists of preamble, frame control header (FCH) and series of data bursts which contain user data and control messages. Frame control header consists of an OFDM symbol with known data values. The data in this symbol is encoded by rate 1/2 mandatory encoding scheme and modulated by QPSK modulation. The data in FCH describes system information such as base station ID, burst profile, and length of a burst. This information is needed by the receiver to decode the subframe. This work pertains to the simulation of a baseband OFDM system, it does not require FCH. In the simulation model, it will be replaced by the payload data. However, for the purpose of clarity and completeness, it will be shown in the downlink frame. Each data burst contains multiple OFDM symbols. Each OFDM symbol in the burst contains payload data depending upon the modulation type and coding gain. Table 5.1 has already presented the seven different combinations of modulation type and coding gain. For each of these combinations, a specific amount of payload data is needed for each symbol. The payload data may be padded, if required, to have correct block sizes. The modulation type remains constant within the burst, however it may change from burst to burst. Bursts using robust modulation types such as BPSK and QPSK are required to be transmitted first, followed by less robust modulation types, 16-QAM and 64-QAM. The structure of a data burst is shown in Figure 5.19. In the context of the networking layers, the data in the bursts is delivered to the physical layer by the medium access control (MAC) layer. It controls access of the base station and subscriber's stations through the air using a set of protocols. The scheduler in the base station controls the size of the frame and burst in order to effectively and dynamically allocate the on air resources to meet the connection demands with specified quality of service (QOS). Referring to the format of the burst in Figure 5.19, MAC PDU is the data unit exchanged between the MAC layer of base station and its subscriber station. Basically these are considered as packets transferred between the bottom of MAC and the physical layer [43]. A MAC PDU consists of fixed length MAC header, a variable length payload, and an optional cyclic redundancy check (CRC).

Each uplink and downlink subframe is always preceded by a preamble. It comprises one or more OFDM symbols of known values. Preamble is used for achieving synchronization between transmitter and receiver and for channel estimation. The preambles used in the uplink and downlink are referred to as short and long

preambles respectively. The uplink preamble consists of 2 times 128 samples preceded by a cyclic prefix. It is shown in Figure 5.20. It contains 100 QPSK carriers at even numbered locations and will form one OFDM symbol. The preamble in the downlink is called long preamble. It is equivalent to two OFDM symbols and consists of CP and 4 times 64 samples followed by a CP and 2 times 128 samples. The first symbol of this preamble uses 50 subcarriers (every 4^{th} subcarrier of the available 200) and the second symbol uses 100 subcarriers (all at even numbered positions). All subcarriers in the long preamble are QPSK modulated. Figure 5.21 depicts the structure of long preamble and appendix 3 contains its frequency domain sequence. This sequence is loaded into the MATLAB work space prior to the start of simulation.

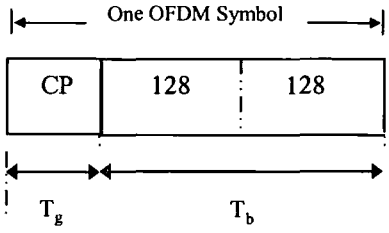

Figure 5.20 Short preamble

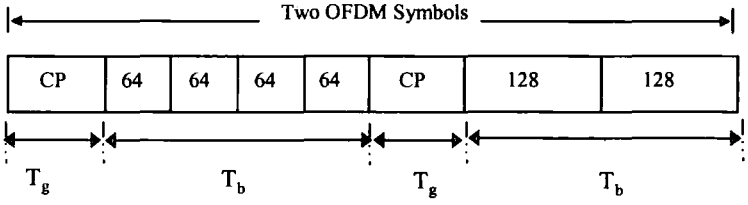

Figure 5.21 Long preamble

These preambles are transmitted with 3 dB more power as compared to all other symbols in the downlink subframe so that the receiver can easily and correctly demodulate and decode them. If the downlink bursts are extremely long, then the standards permits to insert a midamble in between the bursts to cater for time variations in the channel and help the receiver to resynchronize.

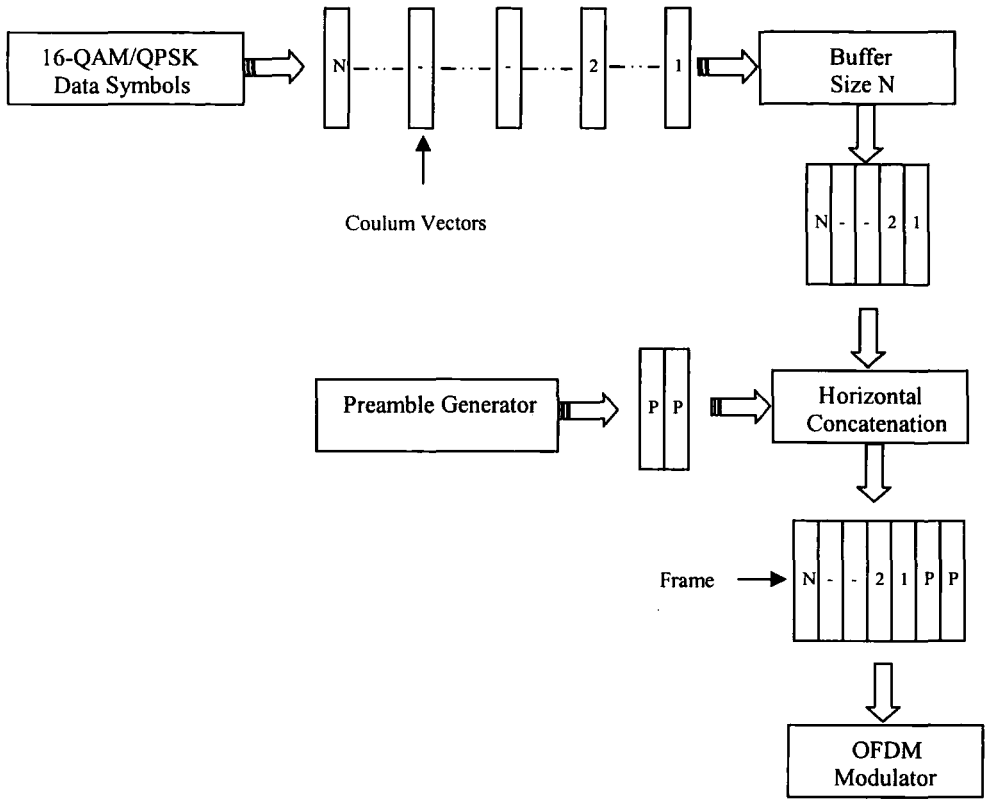

Figure 5.22 Process of frame formulation and preamble attachment

A buffer block from the signal processing block set of SIMULINK has been used to construct the OFDM frames. It combines column vectors into frames of specified sizes. The size of the frame is equal to the size of the buffer. The baseband demodulator produces complex symbols in the form of column vectors. These successive vectors are combined into frames and then appended with preambles. The size of the frame is set during the simulation setup phase. Figure 5.22 depicts the process of frame formulation and preamble appendment. SIMULINK block diagram is attached in appendix 4.

5.6 CHANNEL ESTIMATION AND EQUALIZATION FOR OFDM SYSTEMS

The frequency selective mobile propagation channel modifies the amplitude and phase of each subcarrier present in the OFDM symbol. Such distortion degrades BER performance of the system. In order to correct the effect of the channel, a frequency selective network having transfer function that is inverse of the fading channel is

required to be employed at the receiving end. This network is called frequency domain equalizer. Real mobile channels are time variant and their transfer functions keep changing in time and in frequency, therefore, the characteristics of the equalizer are required to vary in time in order to adapt these variations [44]. These channel variations are estimated by the channel estimator and provided to the equalizer to undo the effect of the channel. In contrast to single carrier equalizers, the equalizer employed in OFDM consists of only one independent tap per subcarrier. The total numbers of taps are equal to the total number of carriers in the OFDM signal. This is due to the cyclic prefix, where the dispersive multi-path channel results in point wise multiplication of the transmitted constellation by the channel transfer function.Therefore, the process of equalization also requires an element wise multiplication of the FFT output (OFDM demodulation) by the inverse of the channel transfer function [45].

There are a number of ways to estimate the channel's transfer function. OFDM systems employ known frequency domain pilot symbols to acquire information about the channel state. These pilot symbols are inserted in each OFDM symbol either at fixed locations or their positions may vary from one OFDM symbol to another. These pilot symbols may constitute one OFDM symbol. There are two types of pilot aided channel estimation techniques. These are called block-type and comb-type [7].

5.6.1 Block-Type Channel Estimation

In block-type channel estimation, pilot tones are inserted into all of the subcarriers of OFDM symbols at regular intervals [46]. These pilot tones constitute one OFDM symbol and are sent prior to the OFDM data symbol. The channel estimation at pilot tones can be performed using either Least Square (LS), Minimum Mean-Square Error (MMSE) or Least Mean Square (LMS) algorithm. It was shown in [47] that MMSE gives 10-15 dB gain in signal-to-noise ratio (SNR) for the same mean square error of channel estimates over LS. MMSE is more complex than LS. However, an application of low-rank approximation to linear MMSE by using the frequency correlation of the channel can reduce the complexity of MMSE [48]. The block-type channel estimation technique performs well in a slow fading channel where channel transfer function does not change during the time period of the block.

5.6.2 Comb-Type Channel Estimation

In comb-type channel estimation, pilot tones are inserted into each OFDM symbol. These can be interleaved with data symbols at fixed carrier locations in each successive OFDM symbol or their locations may vary from symbol to symbol. The channel at pilot frequencies can be estimated by using any one of Least Square (LS), Least Mean-Square (LMS) or Minimum Mean-Square (MMSE) methods. MMSE performs better than LS. It was shown in [49] that the complexity of MMSE can be reduced by deriving an optional low-rank estimator with singular value decomposition. The channel estimation at the rest of the carriers, other than pilots, can be done using either, linear interpolation, second order interpolation, low pass interpolation, spline cubic interpolation or time domain interpolation [46,50]. In terms of better performance, they are arranged as: low-pass, cubic-spline, time-domain, second order, and linear interpolation. Low pass interpolation outperforms the rest [46]. It is performed by inserting zeros into the original data sequence and then applying a low pass FIR filter that permits the original data to pass through unchanged and interpolates between such that the mean square error between the interpolated points and their ideal values is minimized. The channel is variant in time and in frequency. Therefore, in order to interpolate the channel estimates in both time and frequency, the pilot spacing has to meet the following criteria [7].

$$\Delta P_f < \frac{1}{\tau_{max}} \tag{5.10}$$

$$\Delta P_t < \frac{1}{B_d} \tag{5.11}$$

where ΔP_f and ΔP_t are pilot spacing in frequency and time respectively. τ_{max} and B_d are maximum delay spread and Doppler spread of the channel respectively. The frequency domain channel transfer function T(f) is the Fourier transform of the channel impulse response $h(\tau)$. Each of the impulses in the impulse response will result in a complex exponential function $e^{-(j2\pi\tau/T_s)f}$ in the frequency domain, depending on its time delay τ. In order to sample this contribution to T(f) according to the sampling theorem, the maximum pilot spacing ΔP_f in the OFDM symbol is governed by [15]

$$\Delta P_f \leq \frac{N}{2\tau/T_s}\Delta f \tag{5.12}$$

where Δf are the carrier spacing and N refers to the number of subcarriers in the OFDM symbol. Comb-type channel estimation is more suitable for fast fading channels. As the pilot tones are present in each of the OFDM symbols, therefore, the state of the channel can be estimated at every OFDM symbol. However, its performance suffers in frequency selective fading when the correlation between the pilots decreases and even the best interpolation technique fails to provide the channel estimates at the remaining carriers. Therefore, the number of pilots in OFDM symbol increases with the increase in delay spread of the channel.

5.6.3 Channel Estimation and Equalization for IEEE 802.16-2004 OFDM System

In IEEE 802.162004 system, the channel estimation can be carried out using either 8 pilot tones or long preamble which contains 100 subcarriers at even numbered positions. After channel estimation at pilot tones or at preambles's carriers, the estimates at the remaining subcarriers can be achieved by employing a suitable interpolation technique. Section 5.6.2 has focused on various channel estimation techniques. Two channel estimation techniques can be employed in 802.16-2004 system; Linear Minimum Mean Square Error (LMMSE) and Least Square (LS). As the channel varies slow, most implementations [51] and commercial systems [52] have carried out the channel estimation using long preamble. If the transfer function of a channel is more erratic due to the frequency selective nature then this technique proves more suitable since it provides estimates at 100 carriers, whereas the pilots provide estimates at 8 carriers and any interpolation technique will yield more accurate results for the remaining 100 carriers from 100 known values as compared to 8. Moreover, if the pilots become uncorrelated due to frequency selective fading then it will not be possible to interpolate the remaining channel values. On the other hand, if the channel is less frequency selective and fast changing then the pilot estimation technique proves better. This is due to the fact that each OFDM symbol contains pilots and channel variations even between OFDM symbols can be recorded and due to the strong

correlation between pilots which enables the interpolation of 100 unknown values from even 8 known values. However, the standards incorporate a provision for midamble which can be inserted in between the downlink bursts to cater for any channel variations within the burst. Moreover, initial channel estimation can be performed using long preamble and any variation in the channel can be tracked using pilots which are present in every OFDM symbol.

In this work, the preamble-aided Least Square (LS) channel estimation technique was used to estimate the channel at 100 known carriers. The transfer function at the remaining 100 carriers was obtained using a low-pass interpolation technique which outperforms other techniques [46]. Adaptive tracking of the channel using the embedded 8 pilots in each OFDM symbol is not required as the duration of each frame is small as compared to a very slow varying channel. For most fixed wireless applications, adaptive channel tracking is omitted since the channel is unlikely to change significantly during the frame [53].

A number of blocks from the DSP library of SIMULINK were employed to realize channel estimation and equalization. Figure 5.23 demonstrate this process in detail. As shown in this figure, the selector block separates the long preamble from the down link subframe. This preamble contains 100 complex values which are the products of the known values and the values of the channel transfer function at preamble's subcarriers. These 100 estimated values are provided to the channel estimator which simply divides these values by the known values to obtain channel transfer functions for 100 active subcarriers. Interpolation in real and imaginary part of the complex fading envelopes was reported to outperform the interpolation in amplitude and phase [11], therefore, this work separates these 100 complex values into real and imaginary parts and applies interpolation on each part separately and then combines them again into complex values (shown in Figure 5.23). S function has been written to design a custom made SIMULINK block to realize interpolation. This block accepts 100 values at its input and generates 200 values at its output. The S function uses MATAB command 'interp' to implement low-pass interpolation.. The equalizer comprising 200 taps, one for each subcarrier, uses the estimated transfer function to undo the effects of the channel for all OFDM symbols present in the frame.

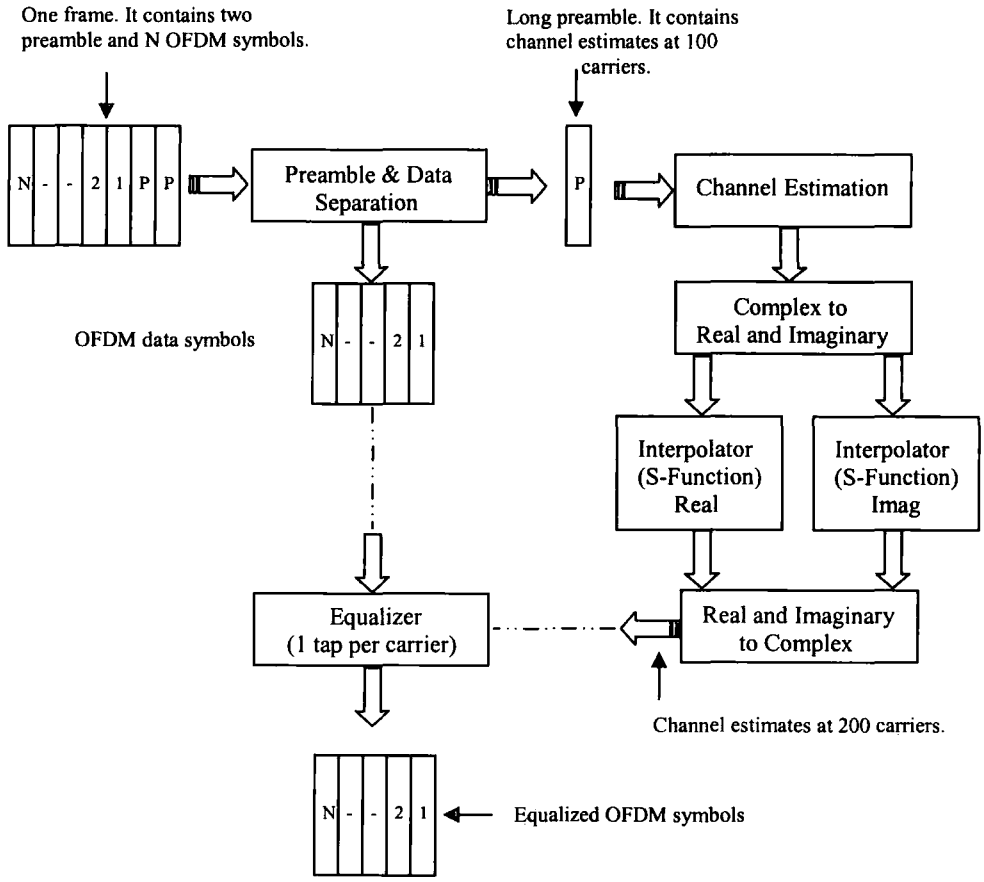

Figure 5.23 SIMULINK implementation of preamble-aided channel estimation technique.

This work employs measured channel transfer functions which are spaced at 4ms in time. The frequency components within the transfer function are 11.6 kHz apart. This spacing results in OFDM symbol duration of 8.62×10^{-5} seconds. As the channel is updated after every 4ms, the channel appears the same for approximately 46 OFDM symbols. This seems consistent with the coherence time of the channel. From the measured Doppler power spectrum (section 6.3.1 of chapter 6), a maximum Doppler of 2.5 Hz was observed. This value results in a coherence time of 0.169 seconds using $T_c = 9/16\pi f_d$ [54]. This implies that the channel will appear the same for 42 OFDM symbols. In block type channel estimation, the duration of the frame should always be less than the coherence time of the channel, i.e., 0.169 second. Therefore, in order for

preamble-aided estimation technique to deliver good estimates, the number of OFDM symbols in the down link burst should be less than 42.

5.7 SUMMARY AND CONCLUSIONS

This chapter presented a SIMULINK implementation of a frequency domain channel simulator for the physical (PHY) layer of IEEE802.16-2004 WirelessMAN. The simulator comprises 256 subcarriers OFDM transmitter, receiver and a frequency domain channel. Various blocks from different libraries of SIMULINK were employed to design and build the simulator using DSP techniques. The simulator was specifically designed for measurement based channel simulations, but it could also be used for statistical simulation after some modifications. The channel was implemented in the frequency domain by multiplying the spectra of OFDM time domain symbols with the measured channel transfer functions at 2.5 GHz and 3.5 GHz bands. The receiver employed long preamble for channel estimation. The preamble contained channel estimates at 100 subcarriers, whereas the estimates at the remaining 100 subcarriers were made using low-pass interpolation technique.

This chapter also provided a brief introduction to Orthogonal Frequency Division Multiplexing (OFDM). Its advantages over the single carrier modulation scheme were highlighted and the role of cyclic prefix in combating the effects of multi-path propagation was discussed in detail. This simulator can be used to study the performance of Wireless Broadband Access (WBA) systems in a measured channel environment.

5.8 BIBLIOGRAPHY

1. ETSI Documentation, "Broadband Radio Acess Networks (BRAN); HIPERLAN Type 2; Physical (PHY) layer," ETSI TS 101 475, v1.1.1, European Telecommunication Standard, April 2000.
2. B.P. Crow, I. Widjada, J.G.Kim and P.T. Sakai, "IEEE 802.11 wireless local area networks, " IEEE Commun. Mag., Sep 1997, pp. 116-126.

3. M. Alard and R. Lassalle, "Principles of modulation and channel coding for digital broadcasting for mobile receivers," EBU Review, Aug. 1987, pp. 47-69.
4. B.L. Floch, R. Halbert-Lassalle, and D. Castelain, "Digital sound broadcasting to mobile receivers," IEEE Trans. on Consumer Electronics, vol.35, Aug.1989, pp. 493-503.
5. T. de Couasnon, R. Monnier and J. B. Rault, "OFDM for digital TV broadcasting," IEEE Trans. on Signal Processing, 1994, pp.1-32.
6. ETSI, Digital video broadcasting (DVB); Framing structure, channel coding and modulation for digital terrestrial television. EN300 744 v1.2.1, European Telecommunication Standard, July 1999.
7. R.V. Nee and R. Prasad, OFDM for Wireless Multimedia Communications, Boston: Atech House, 2000.
8. J.A.C. Bingham, " Multicarrier modulation for data transmission: An idea whos time has come," IEEE Commun. Mag., vol. 28, no. 5, May 1990, pp. 5-14.
9. S.Hara, M. Okanda, and N. Morinaga, "Multicarrier modulation technique for wireless local area network," Proc. Fourth European Conference on Radio Relay Systems, Oct. 1993, pp. 33-38.
10. P.M. Shankar, Introduction to Wireless Systems: John Wiley & Sons Ltd., 2002.
11. L.J. Cimini, "Analysis and simulation of digital mobile channel using orthogonal frequency division multiplexing," IEEE Trans. on Communications, vol.33, no.7, July 1985, pp. 665-675.
12. S.B. Weinstein and P.M Ebert. "Data transmission by frequency division multiplexing using discrete Fourier transform," IEEE Trans. Communications, vol.COM-19, no. 5, Oct 1971, pp. 628-634.
13. J. Salz and S. B. Weinstein, "Fourier transform communication system," presented at the Ass. Comput. Machinery Conf. Computer and Communication, Pine Mountain, Ga., Oct. 1969.
14. B. Hirosaki, "Orthogonal multiplexed QAM system using the discrete Fourier transform," IEEE Trans. on Communications, vol. COM-29, no.7, July 1981, pp. 982-989.

15. L.Hanzo, W. Webb and T. Keller, Single and Multi-carrier Quadrature Amplitude Modulation, West Sussex, England : IEEE Press, John Wiley & Sons, Ltd, 2000.
16. A. Peled and A. Ruiz, "Frequency domain data transmission using reduced computational complexity algorithm," in Proceeding of the IEEE International Conference on Acoustics, Speech, and Signal Processing (ICASSP'80), Singaore, 1980, pp. 964-967.
17. M. Russel and G. Stuber, "Interchannel interference analysis of OFDM in a mobile environment," in Proceedings of the Vehicular Technology Conference (VTC'95), 1995, pp. 820-824.
18. A.Vahlin, and N. Holte, "Use of guard interval in OFDM on multipath channels," Electron. Lett., 30(24), 1994, pp. 2015-2016.
19. L. Louis and M. Pugel, "The principles of OFDM," www.rfdesign.com.
20. G.L. Stuber, R.J. Barry, S.W. Mclaughlin, Ye.Li, M.A. Ingram and T.G. Pratt, "Broadband MIMO-OFDM Wireless," in Proceeding of the IEEE, vol. 92, no.2, Feb 2004, pp. 964-96 7.
21. W.Y. Zou and Y. Wu, "COFDM: An overview," IEEE Trans. on Broadcasting, vol. 41, no.1, March 1995, pp. 1-8.
22. A. V. Oppenheim and R. W. Schafer, Discrete-Time Signal Processing, New Jersey: Prentice-Hall Inc., 1999.
23. J. Cartinhour, Digital Signal Processing: An Overview of Basic Principles, New Jersey: Prentice Hall, Upper Saddle River, 2000.
24. P.A. Lynn, and W. Fuerst, Introductory Digital Signal Processing with Computer Applications, revised edition, Chichester, West Sussex, England: John Wiley & Sons, Ltd., July 1994.
25. L.R. Rabiner and B.Gold, Theory and Applocations of Digital Signal Processing, New Jersey: Prestice-Hall, 1975.
26. S.J. Orfanidis, Introduction to Signal Processing, New York: Prentice Hall, Upper Saddle River, 1996.
27. R.J. Schilling and S.L. Harris, Fundamentals of DSP using MATLAB: Thomson, Canada, Ltd., 2005.

28. IEEE 802.16-REVD/D5-2004, "Draft IEEE standards for local and metropolitan area networks-part 16: Air interface for fixed broadband wireless access system," May 2004.
29. K. Witrisal, Y.H. Kim and R.J. Prasad, "A new method to measure parameters of frequency-selective radio channels using power measurements," IEEE Trans. on Communications, vol.COM-49, no.10, Oct 2001, pp. 1788-1800.
30. P.A. Bello, "Characterization of random time-variant linear channels", IEEE Trans. on Communication Systems, Dec 1963, pp. 360-393,
31. M. Patzold, Mobile fading channels, 2rd ed. West Sussex, England: John Willey & Sons, Ltd., 2002
32. G.L Stuber, Principles of Mobile Communication: Kluwer Academic Press, Norwell, MA, 1996.
33. Wimax forum website: www. Wimaxforum.org.
34. E.R. Berlekamp, R.E. Peile, and S.P. Pope, " The application of error control to communications," IEEE Commun. Mag., vol.25, no.4, April. 1987, pp.44-57.
35. J.G. Proakis, Digital Communications, New York: McGraw-Hill, 1993.
36. W. Tomasi, Advanced Electronic Communications Systems, New Jersey: Prentice Hall, Inc, 1987.
37. S. Haykin and M. Moher, Modern Wireless Communications, New Jersey: Pearson Prentice Hall, Pearson Education, Inc., Upper Saddle River, 2005.
38. S.G. Lee, "Performance of concatenated FEC under fading channel in Wireless-MAN OFDM system," Proceedings of the IEEE 19th International Conference on Advance Information Networking and Applications, 2005.
39. H. Yaghoobi, " Scalable OFDM physical layer in IEEE 802.16 WirelessMAN," Intel Technology Journal, vol. 8, issue 3, 2004.
40. A.J. Viterbi, "Convolution codes and their performance in communication systems," IEEE Trans. on Communications Technology, vol. COM-19, no.5, Oct.1971, pp.751-772.
41. D.G. Forney, "The Viterbi algorithm," Proc. IEEE, vol. 61, no.3, Mar 1973, pp.268-278.

42. A.R. Abdul, V.Szwarc, and T.A. Kwasniewski, "High speed Viterbi decoder for W-LAN and broadband applications," IEEE Inter. Conf. on Digital System Design, 2004.
43. C. Eklund, R.G. Mark, K.L. Stanwood, and S. Wang, "IEEE standards 802.16: A technical overview of the WirelessMAN Air interface for broadband wireless access," IEEE Commun. Mag, June 2002, pp. 98-107.
44. D.H. Morais, Fixed Broadband Wireless Communications: Principles and Practical Applications, Indiana: Prentice Hall, PTR, 2004.
45. U. Reimers, "Digital video broadcasting," IEEE Commun. Mag., vol. 36, no.6, June 1998, pp. 104-110.
46. S. Coleri, M. Ergen, A. Puri, and A. Bahal, "Channel estimation techniques based on pilot arrangement in OFDM systems," IEEE Trans. on Broadcasting, vol. 48, no. 3, Sep 2002, pp. 223-229..
47. J. van de Beek, O. Edfors, M. Sandell, S. K. Wilson, and P. O. Borjesson, "On channel estimation in OFDM systems," in Proc. IEEE 45th VT Conf., Chicago, IL, July. 1995, pp. 815-819.
48. O. Edfors, M. Sandell, J. van de Beek, S. K. Wilson, and P. O. Borjesson, "OFDM channel estimation by singular value decomposition," IEEE Trans. on Communications, vol. 46, no.7, Jul. 1998, pp. 931-939.
49. M. Hsieh and C. Wei, "Channel estimation for OFDM systems based on comb-type pilot arrangment in frequency selective fading channel," IEEE Trans. on Consumer Electronics, vol. 44, no. 1, Feb. 1998.
50. S. Coleri, M. Ergen and A. Bahal, "A study of channel estimation in OFDM systems," IEEE Vehicular Technology Conference 2002, Proceeding VTC, Fall, 2002, pp. 894-898
51. Y. Sang-Jung, L. Yi-Ching and C. Tzi-Dar."Design and Simulation of baseband transceiver for IEEE 802.16a OFDM mode subscriber station," The 2004 IEEE Asia-Pacific Conference on Circuit and Systems, Dec 6-9, 2004, pp. 697-700.
52. www.comsonic.com
53. A. Ghosh and D.R. Wolter, J.G. Andrews, and R.Chen, "Broadband Wireless Access with WiMax/802.16: Current performance benchmarks and future potential," IEEE Commun. Mag., Feb 2005, pp. 129-136.

54. T.S. Rappaport, Wireless Communications, Principles and Practice: Prentice Hall, 1996.

CHAPTER 6

MEASUREMENTS-BASED CHANNEL SIMMULATIONS FOR WirelessMAN

6.1 INTRODUCTION

Performance of any communication system is usually studied in terms of its bit error rate (BER) behaviour as a function of signal to noise ratio of the channel. This chapter pertains to the simulation of frequency selective channels for IEEE 802.16-2004 Wireless Broadband Access (WBA) systems using measured channel functions for 2.5 GHz and 3.5 GHz bands. Simulations were carried out to study the bit error rata (BER) performance in a variety of channel conditions. The BER performance results were obtained using the frequency domain channel simulator designed and developed in SIMULINK (presented in chapter 5). The designed system was first validated by studying its BER performance over an additive white Gaussian noise (AWGN) channel and comparing BER simulation results with the theoretical results and other published results. The close match between them validated the SIMULINK implementation of 256 OFDM system.

Seven sets of measurements were used in the simulations. Four sets belong to 2.5 GHz band and three to 3.5 GHz band. The channel profiles in these measurements differ from one another in terms of the frequency selective fading. For the purpose of reference, the four sets of 2.5 GHz measurements have been named as profile 1 to profile 4 and the three sets of 3.5 GHz measurements have been named profile 1 to profile 3. Corresponding profiles of both bands were measured simultaneously.

In the first phase of simulations, the BER results of rate 1/2 coded OFDM system employing QPSK and 16-QAM constellations were obtained for profiles 1-3 of both bands. The aim was to show that the difference in the system behavior for both bands. The BER results showed the effect of frequency selective fading on the system performance. Section 6.3 presents these results. In order to quantify the severity of frequency selective fading among these profiles, frequency domain level crossings and average fade bandwidth within the OFDM symbol were measured.

Profiles 2 and 3 of the 2.5 GHz band were used in the second phase of simulations to study the BER performance of rate 3/4 coded systems employing 16-QAM and QPSK constellations. These two profiles differ from each other in respect of the channel transfer function variations within the OFDM symbol bandwidth. Section 6.3.1.2 depicts the simulation results.

In order to study the effects of frequency selective fading on different channel coding schemes specified in the IEEE 802.16-2004 standards, profile 4 of the 2.5 GHz band was employed in the simulations. It represents the worst-case multi-path conditions amongst all profiles. The purpose of the simulation was to compare the performance of rate 1/2 and 3/4 coded system in a highly frequency selective environment. The BER performance results have been shown in section 6.3.1.2.

6.2 SYSTEM PERFORMANCE IN AWGN CHANNEL

The accuracy of the simulator is usually verified by comparing the simulated BER performance results with the theoretical results in additive white Gaussian noise (AWGN) channel [1,2]. Therefore, this work has first employed AWGN channel to validate the various digital signal processing (DSP) implementation techniques used to design and build the OFDM transmitter and receiver. It is worth mentioning that the SIMULINK library of communication block set does not contain OFDM transmitter and receiver. These were completely built using a number of DSP blocks from various SIMULINK libraries. In this perspective, it becomes imperative to verify the accuracy of the OFDM transmitter and receiver first and then employ channel coding. Achieving channel coding is not very complex in SIMULINK. All the necessary blocks are available in the communication block set library to realize the various channel coding requirements specified in the IEEE 802.16-2004 standards [3] for Wireless Broadband Access (WBA) systems and these blocks do not require any further validation. Figure 6.1 depicts the simulation block diagram used to measure the bit error rate. AWGN block from the communication block set library was used to add the required amount of noise to the output of the OFDM transmitter. This block accepts a complex input signal. The average power of the transmitter has been normalized to unity. The BER results were obtained by varying the value of signal to noise ratio (input parameter of

AWGN block). 16-QAM has been selected to map binary data onto the complex constellation.

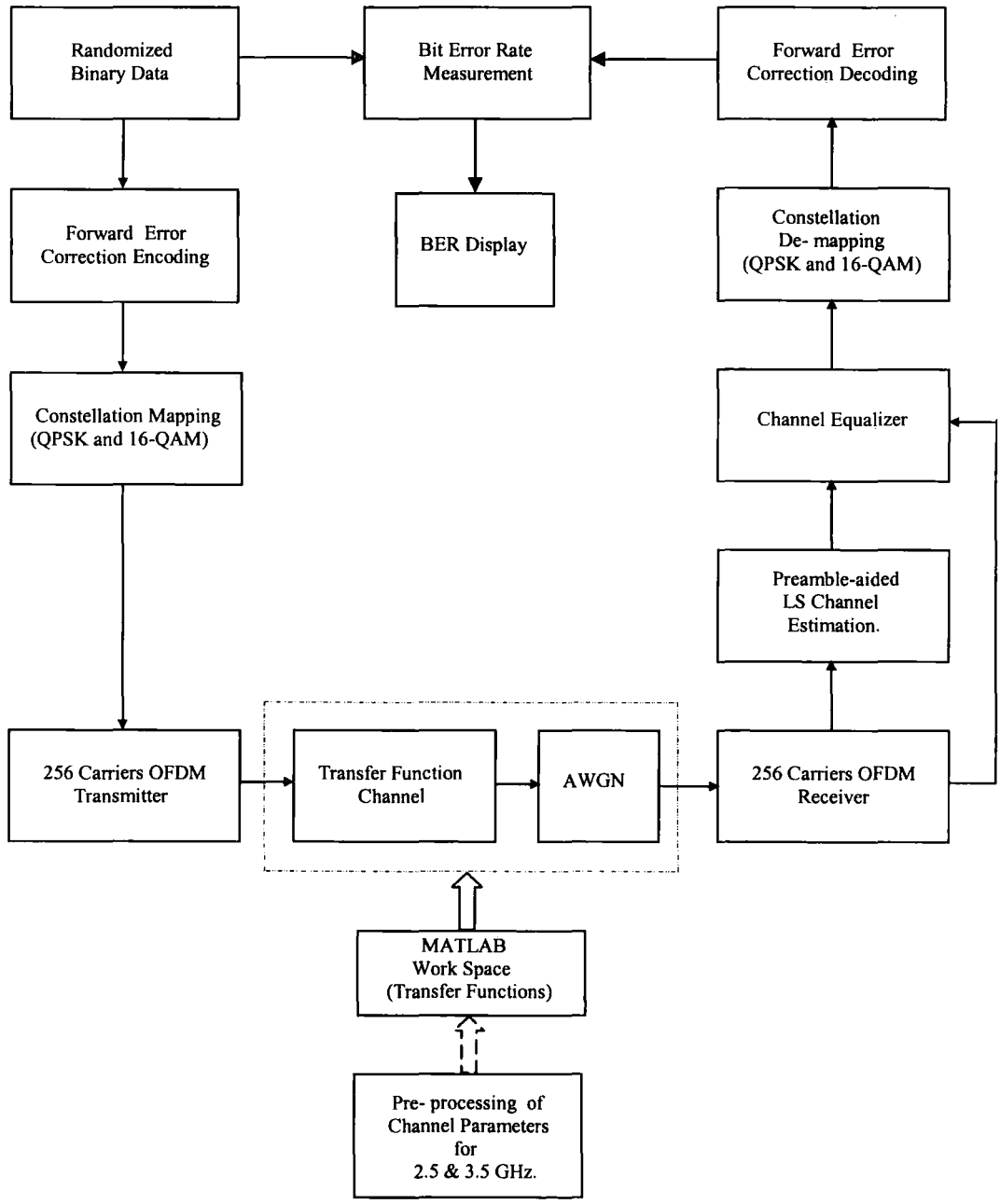

Figure 6.1 Simulation setup for the OFDM based physical layer of 802.16-20004 WirelessMAN

The main reason for selecting this modulation scheme is that the theoretical as well as simulated BER results are readily available in the literature [4] for comparison purposes. Moreover, 16-QAM is spectrally more efficient as compared to BPSK and QPSK. Referring to Figure 6.1, channel coding and transfer function channel blocks were by passed for recoding BER results in only AWGN channel.

The performance of OFDM system in an AWGN channel is identical to that of a serial modem since AWGN in the time domain corresponds to AWGN of the same average power in the frequency domain [4]. BER results presented in [4] for OFDM systems and for a serial modem proved that the performance of both systems was identical in an AWGN channel. Figure 6.2 presents simulated BER results as a function of average signal to noise ratio of the AWGN channel for 256 OFDM system employing 16-QAM. The length of cyclic prefix was set to zero as it was only meant to cater delays in the multi-path channel [5,6]. Each point in the curve was obtained by averaging 20 simulation results. Each result was obtained by running simulation for 10 minutes. At the beginning of every simulation run, the initial seed parameter in the AWGN block was changed to initialize the noise generator.

The theoretical BER performance is also shown in Figure 6.2 for comparison. These BER results for uncoded OFDM system closely match with the theoretical curve for the serial mode. These results also agree with the simulation results presented in [4] for 16-QAM OFDM system. The close match between these results validates the performance of designed SIMULINK OFDM simulator. The IEEE 802.16-2004 WirelessMAN system incorporates forward error correction coding (FEC) which significantly improves the system performance not only over fading channel but also over AWGN channel. Simulations have also been carried out to study BER performance of rate 1/2 and 3/4 coded 256 OFDM IEEE 802.16-2004 system in AWGN channel employing 16-QAM and QPSK constellations. Figures 6.3 and 6.4 present these results.

As evident from these results the FEC coding scheme, comprising concatenated Reed-Solomon (RS) and convolution, have significantly improved the BER performance of the system in an AWGN channel. Concatenated coding possess the ability to correct both types of errors; random and burst. The Reed-Solomon (RS) codes

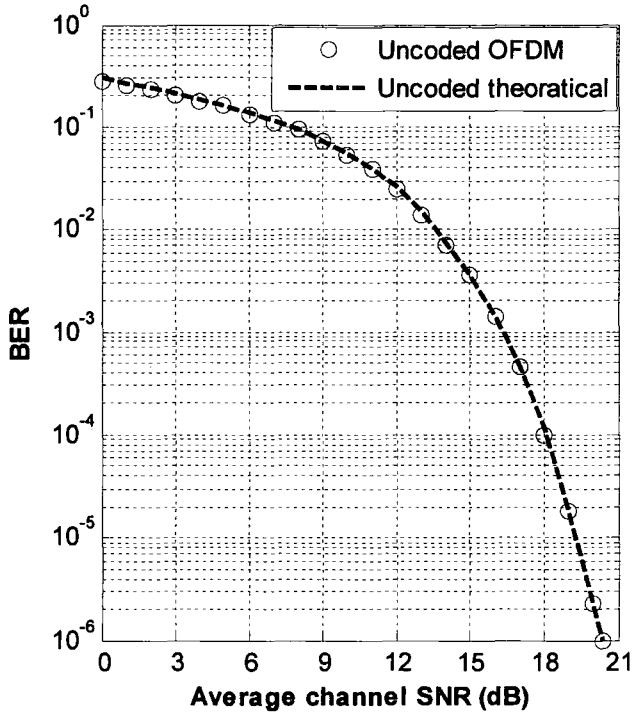

Figure 6.2 BER performance of uncoded 256 OFDM IEEE 802.16-2004 WirelessMAN employing 16-QAM

prove very effective in correcting burst errors, whereas random errors are dealt with by Convolution codes [7]. The BER curve for rate 1/2 coded system with 16-QAM reveals a coding gain of approximately 7 dB at BER of 10^{-6} as compared to uncoded system. This coding gain can be attributed to the error correcting ability of RS as well as convolution codes. Though, RS codes are meant for specifically burst errors thus can also correct random errors [7, 8]. In the simulations, a rate 1/2 convolution encoder with constraint length 7 was employed. In convolution coding, the coding gain increases towards the asymptotic limit as the signal to noise ratio (SNR) per bit increases [9]. This is apparent from the BER curves of Figures 6.3 and 6.4. If the decoder employs hard-decision decoding, then the coding gain reduces by approximately 2 dB as compared to soft decision decoding for AWGN channel. However, the soft decision Viterbi decoder would be computationally expensive [9,10].

The coding gain can also be increased by employing long-constraint length convolution codes. However, for long-constraint length codes, sequential decoding will be employed. The coding gain is also a function of QAM constellation. It was shown in [6] that coding gain relative to uncoded QAM becomes larger for larger constellations.

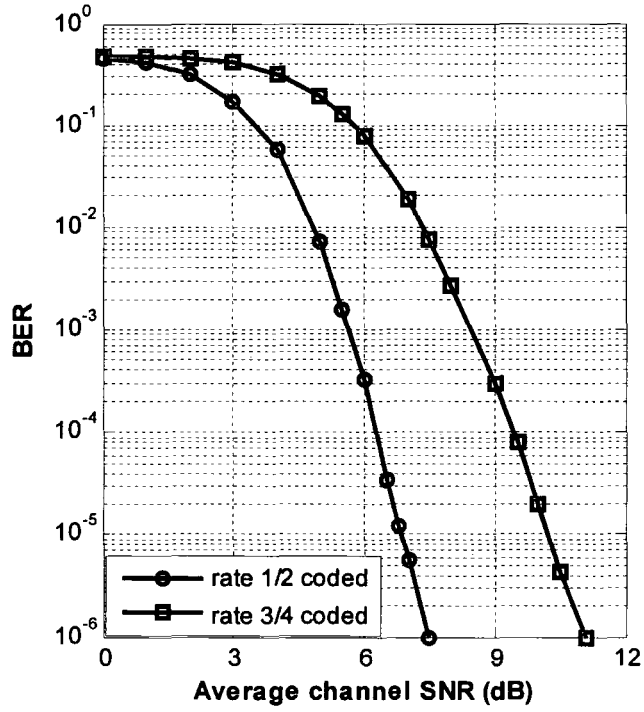

Figure 6.3 BER performance of rate 1/2 and 3/4 coded 256 OFDM IEEE 802.16-2004 WirelessMAN in AWGN channel employing QPSK.

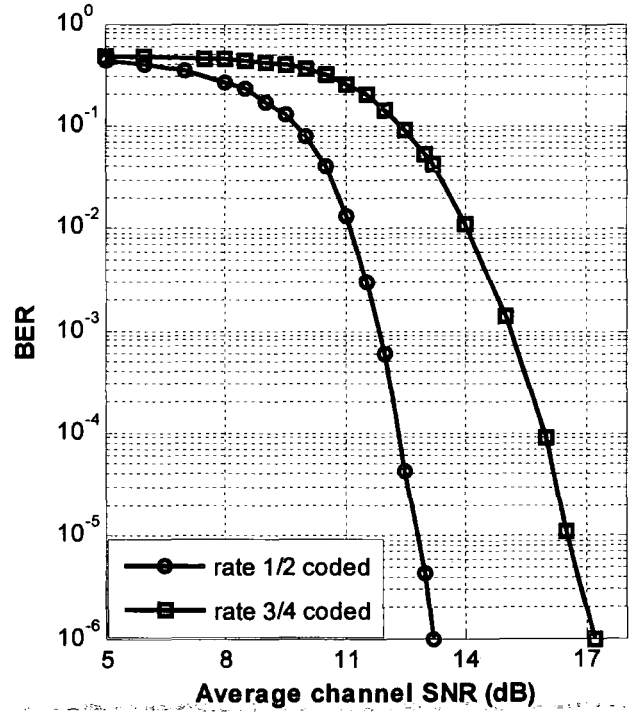

Figure 6.4 BER performance of rate 1/2 and 3/4 coded 256 OFDM IEEE 802.16-2004 WirelessMAN in AWGN employing 16-QAM.

The behaviour of the BER curve for coded system is consistent with the transfer function for rate 1/2 convolution code derived in [11]. The BER bounds are governed by the Viterbi decoding algorithm, which asymptotically approaches the maximum likelihood decoder performance. These bounds are based on the transfer function of the convolution code and can be derived from the state transition diagram of the code. The transfer function basically describes the distance properties of various paths in the trellis for the code that starts at state 0 and merges to state 0 later on.

6.3 SYSTEM PERFORMANCE IN FREQUENCY SELECTIVE CHANNELS

In a single carrier wireless communication system, the bit error rate (BER) performance is a function of the length of the channel impulse response and the duration of the transmitted symbol. The shape of the channel impulse response depends heavily on the propagation environment. Indoor channels exhibit only shorter delays but the outdoor channels can possess delay spread in the range of 15 μs. In the context of the time domain description of the channel, the channel is characterized by the rms delay spread which impacts the bit error rate of the communication system. BER depends upon the rms delay spread of the channel irrespective of the shape of the channel impulse response [12-13]. As a general rule, the effect of intersymbol interference (ISI) on the transmission error rate of the system is negligible as long as the delay spread of the channel is significantly shorter than the duration of the transmitted symbol. Otherwise, the multi-path propagation will lead to ISI and channel equalization has to be used to suppress the echoes caused by the channel. OFDM, unlike single carrier systems, overcomes the effect of frequency selective fading by dividing an entire channel bandwidth into many subchannels. The frequency response over each subcarrier becomes relatively flat. Each subchannel has an individual signal-to-noise ratio (SNR) depending upon the value of the channel transfer function for a particular carrier. Accordingly, the bit error performance varies significantly between different subcarriers. Therefore, the over all bit error performance heavily relies upon the performance of individual subcarriers. As the frequency response of the wideband channel is variant in frequency, each subcarrier will have different signal-to-noise ratio. Few carriers in deep fade may degrade the overall performance of the system. OFDM

systems are capable of yielding high performance as compared to single carrier systems in wideband channels by employing one-tap equalizer for each subchannel. Still the ability of channel estimator which is responsible for delivering the estimated channel transfer function for each subcarrier is dependent upon the time-frequency characteristics of the channel and the accuracy of the estimating algorithm. As the subchannel's frequency response is estimated through the use of pilots [14-15], the correlation of the channel transfer function amplitude both along the time and frequency axis is of significant importance. The correlation in the frequency domain is dependent on the impulse response of the channel. The delay spread of the channel manifests itself as frequency domain fading over the bandwidth of the OFDM symbol. The longer delays result in the rapid fading in the frequency domain and causes a decorrelation of the received signal envelopes at different frequencies, lessening the effectiveness of the pilot correction mechanism [16]. Consequently, the performance of the channel estimator decreases with a decrease in correlation between pilots. The simulation results presented in section 6.3.1.1 reveal that the bit error performance decreases with an increase in the variations in the channel transfer function.

The time variations in the channel transfer functions also have a great impact on the bit error performance of the OFDM system. These channel variations distort the orthogonality of the subcarriers and result in intercarrier interference which limit the attainable bit error rates. If the channel changes slowly as compared to the duration of an OFDM symbol, then the channel is considered stationary during the OFDM symbol period. Then the frequency selective effect of the channel will be a frequency dependent multiplicative distortion of the received symbol [4]. Whereas, a non stationary channel will introduce intercarrier interference due to the time variant impulse response. Hence, the time variant channel transfer function during the transmission of an OFDM symbol results in the loss of orthogonality between the OFDM symbols subcarriers. The amount of this interference is a function of the rate of change of the channel transfer function. However, as the Doppler spread is very small in WirelessMAN systems, the system performance is mainly dependent upon the frequency selective behaviour of the channel. The Doppler spectrum which will be presented in section 6.3.1 for measured channel parameters will show a maximum Doppler of 2 Hz. This implies that the channel transfer function remains stationary for

more than one OFDM symbol. Therefore, this work focuses mainly on the effect of the frequency selective behaviour of the channel on the bit error rate performance of the system.

It is worth mentioning that IEEE 802.16-2004 has specified 6 types of channel models to assess the performance of different transmission techniques in the 2-11 GHz band [17]. These models have been developed by Stanford University and are known as Stanford University Interim (SUI) channel models. These models have three taps and differ from one another in delay spread. Out of these six models, SUI-1, SUI-2 and SUI-6 are line of sight models with rms delay spread of 0.111 μs, 0.202 μs and 5.24 μs respectively. Whereas SUI-3, SUI-4 and SUI-5 are non-line of sight models having delay spread of 0.264 μs, 1.2 μs and 2.842 μs respectively. The channel data which have been employed in this work for simulations cover a delay spread range from 0.22 μs to 4.4 μs. The measurements were performed in the 2.5 GHz and 3.5 GHz bands in Martlesham, UK. The sounder employed 10 MHz bandwidth to measure the channel at a sweep repetition frequency (SRF) of 250 Hz. This work has employed processed data that was made available in the form of a matrix containing 512 points complex time frequency functions for 249 consecutive sweeps. As stated in chapter 5 that the fast convolution based channel simulator required transfer functions of zero-padded impulse responses, therefore, the available transfer functions were first converted into impulse responses by inverse FFT operation without applying windowing. If the window is applied, then the response will be superimposed on the shape of the window. Therefore, windowing is normally not applied in such cases prior to the IFFT operation[18]. These impulse responses were zero padded and then again transformed to transfer functions to be used in the fast convolution based channel implementation. All processing were carried out prior to the start of simulation. During the simulation phase, these transfer functions moved from the MATLAB work space sweep by sweep and entered into the channel where they were point wise multiplied by the spectrum of the OFDM signal. The detailed explanation in respect of the frequency domain channel implementation for measured channel data has already been provided in section 5.3 of chapter 5.

6.3.1 Channel Simulations using 2.5 GHz and 3.5 GHz Measured Data

IEEE802.16-2004 OFDM system is flexible in terms of bandwidth specifications. The channel bandwidth can be integer multiples of 1.25 MHz, 1.5 MHz, and 1.75 MHz with a maximum of 20 MHz. Therefore, the required number of points from 512 points can be taken to form a transfer function of variable bandwidths. In the case of 256 OFDM systems, the first 256 points can be used to simulate a 3 MHz wide channel where each carrier will be 11.6 kHz apart. This work has used the first 256 points out of 512 to construct the channel transfer functions for the both bands. The inverse FFT operation was performed on these points to extracts impulse responses which were then used to compute RMS delay spread of the channel using a threshold value of 20 dB. The 2.5 GHz band exhibited delay spread in the range 0.1 μs - 4.4 μs while the 3.5 GHz band showed delay spread in the range 0.1 μs - 3.8 μs. Figures 6.5 and 6.6 present the CDFs and PDFs for the distribution of the RMS delay spread for the two frequency bands.

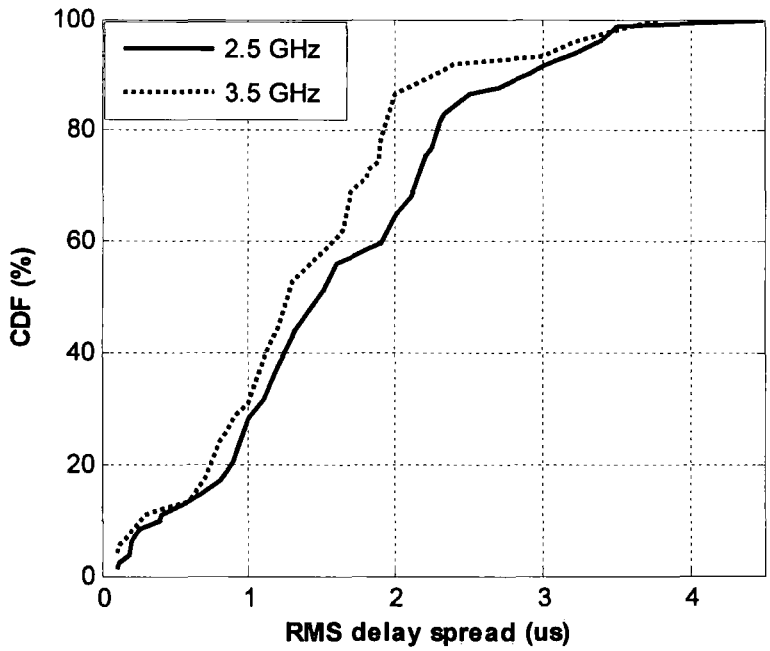

Figure 6.5 CDFs for the distributions of RMS delay spread for the 2.5 GHz and 3.5 GHz bands

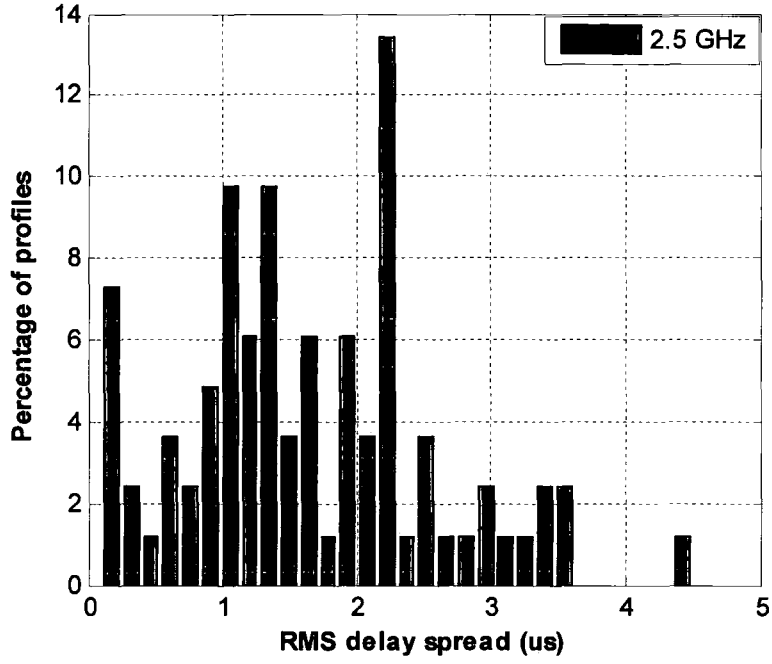

(a)

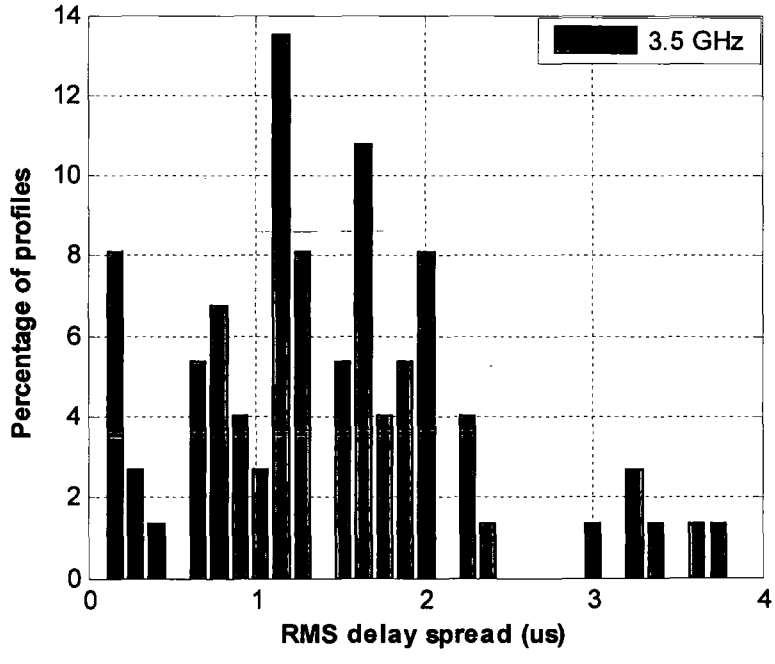

(b)

Figure 6.6 PDFs for the distributions of RMS delay spread for (a) 2.5 GHz and (b) 3.5 GHz

Seven types of measured channel data have been selected for the purpose of simulations. Figures 6.7-6.9 and 6.10-6.12 present some of the impulse responses and their corresponding channel transfer functions for three profiles of 2.5 GHz and 3.5 GHz bands respectively, employed in the first phase of simulations. These profiles were measured at three different locations. As shown in table 6.1, the profiles 1, 2, and 3 of the 2.5 GHz band exhibit RMS delay spread of 0.22 μs, 2.90 μs, and 3.30 μs respectively. Whereas for the 3.5 GHz band, the delay spread values are; 0.30 μs, 1.89μs, and 3.40 μs respectively. The impulse responses and the transfer functions depicted in these figures represent the channel state at 4 different sweeps. Only four out of the 249, have been shown here for the purpose of demonstration. They change from sweep to sweep if the channel is time variant. In case of static channel, they remain the same. The transfer functions contained in the matrix can be treated as a series of snapshots of the channel transfer functions that are separated by the sweep duration; 4 ms for sweep repitition frequency of 250 Hz. As IEEE 802.16-2004 system is meant for point to point communication between base station and stationary sites, the channel experiences very little variations in time. The data employed in the simulations were measured using stationary receiver. The measured data exhibited some variations in the channel transfer functions. Figures 6.13 and 6.14 depict the time variations in the transfer functions of three profiles for the 2.5 GHz and 3.5 GHz bands respectively. As the receiver was stationary, these variations were mainly caused due to moving objects in the channel. As evident from the average Doppler power spectrum of three profiles shown in Figures 6.15 and 6.16 for 2.5 GHz and 3.5 GHz respectively, the channel was very slowly varying with a maximum Doppler shift of approximately 2 Hz. This value results in a coherence time of 0.21 seconds. In [19], Doppler of 2 Hz was used to obtain BER performance results.

OFDM symbol duration is a function of frequency spacing between subcarriers, therefore, frequency spacing of 11.6 kHz results in an OFDM symbol duration of 8.62×10^{-5} seconds. Table 6.2 presents OFDM system parameters used in the simulations.

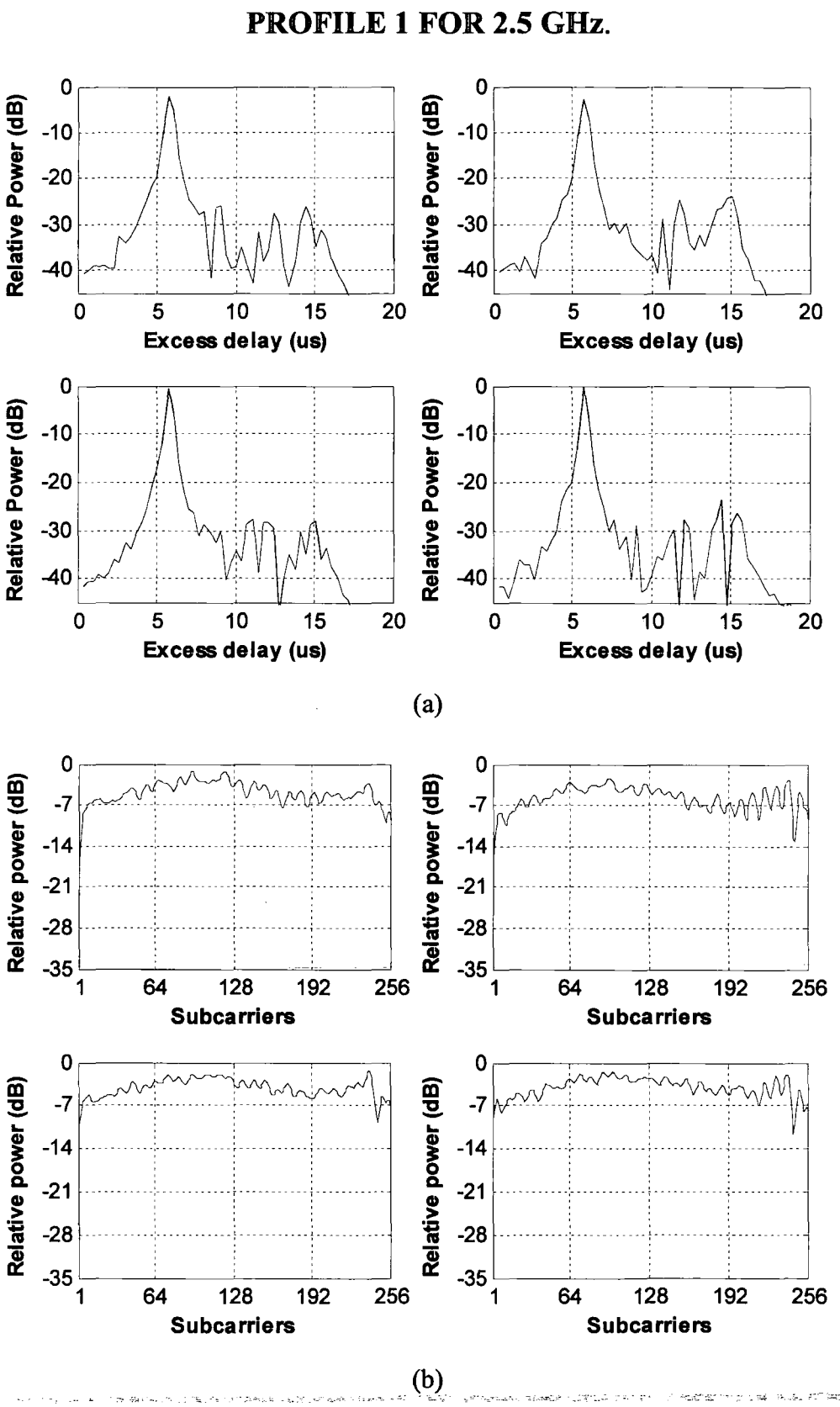

Figure 6.7 (a) Examples of channel impulse responses , (b) their corresponding channel transfer functions.

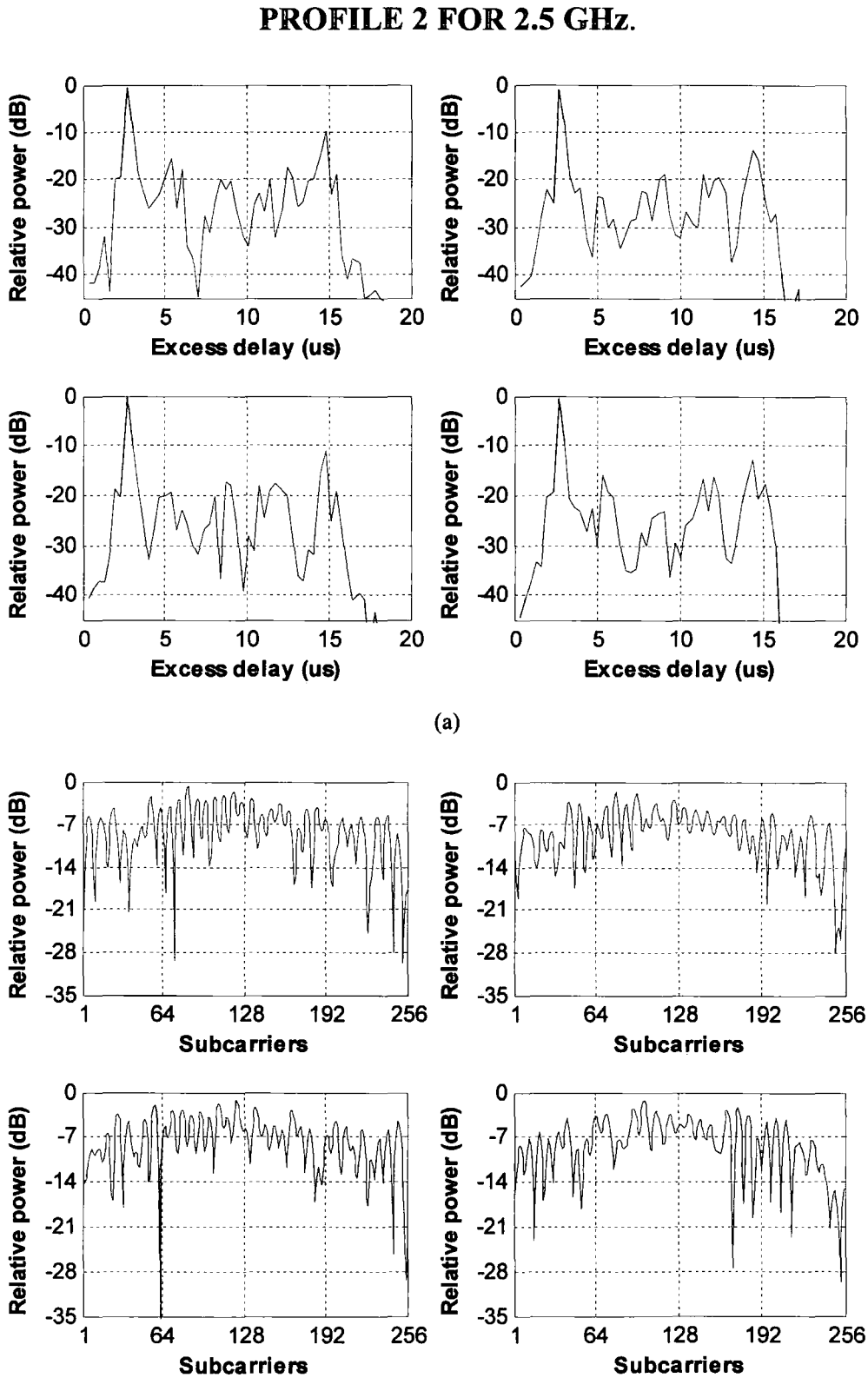

Figure 6.8 (a) Examples of channel impulse responses , (b) their corresponding channel transfer functions.

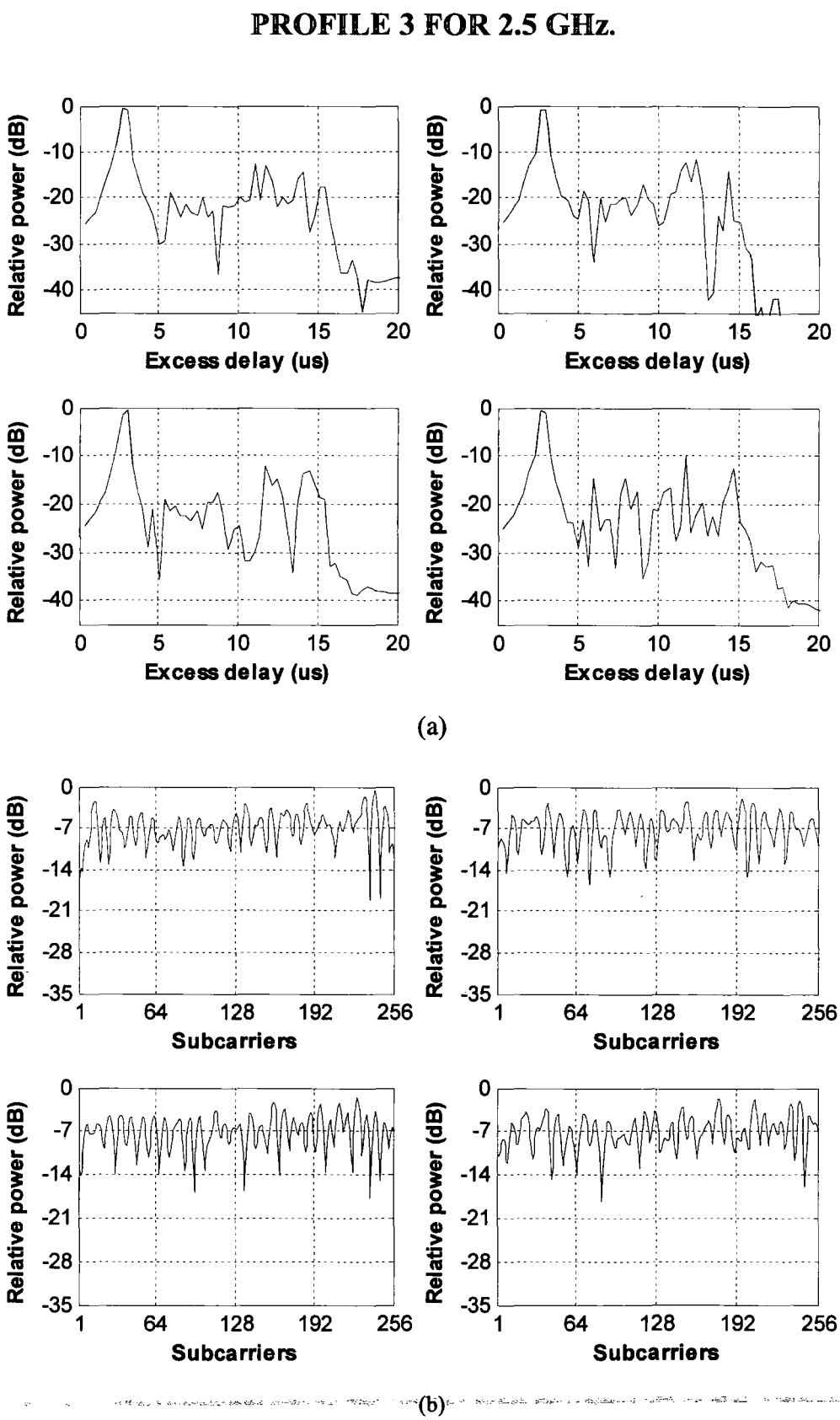

Figure 6.9 (a) Examples of channel impulse responses, (b) their corresponding channel transfer functions.

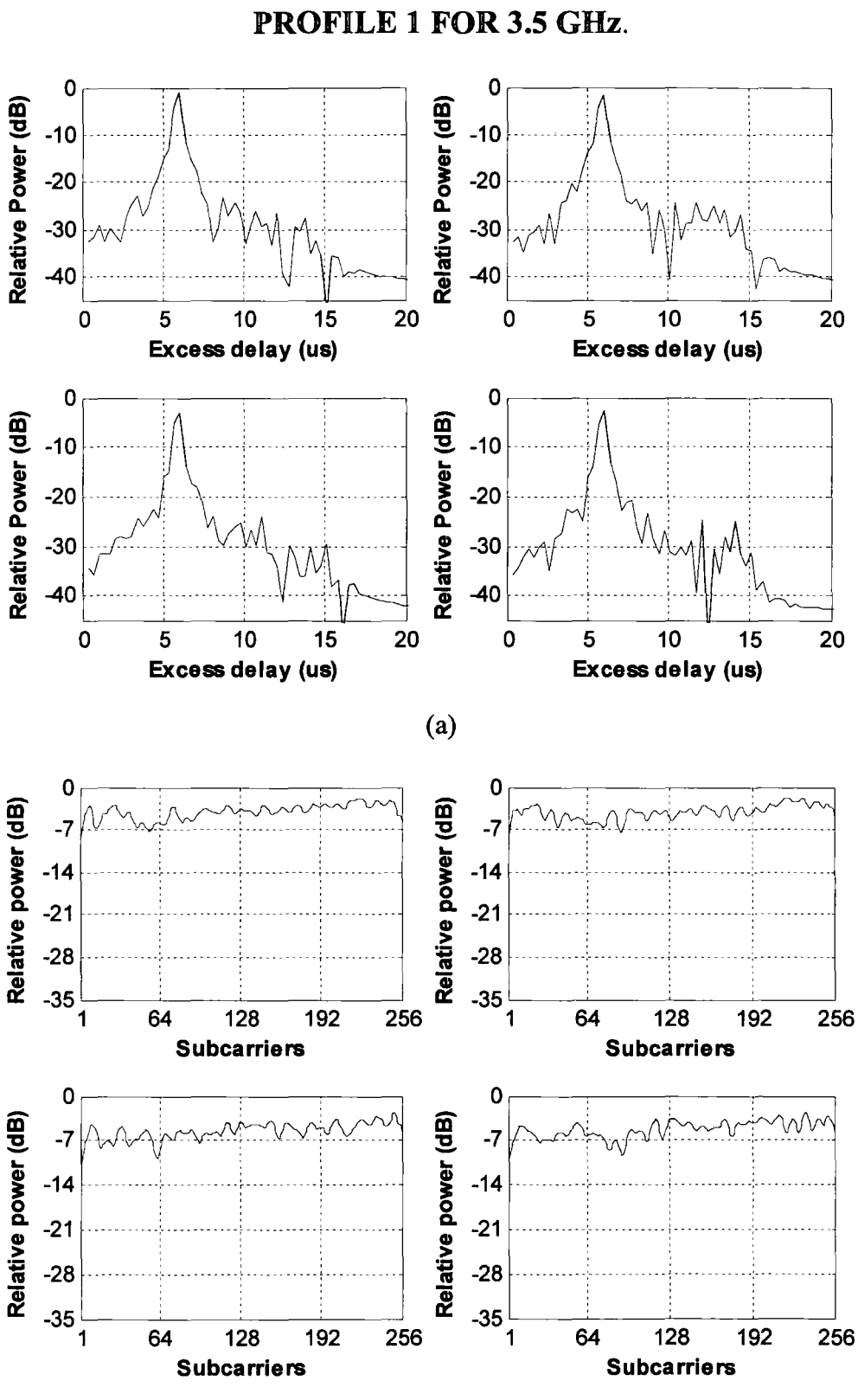

Figure 6.10 (a) Examples of channel impulse responses, (b) their corresponding channel transfer functions.

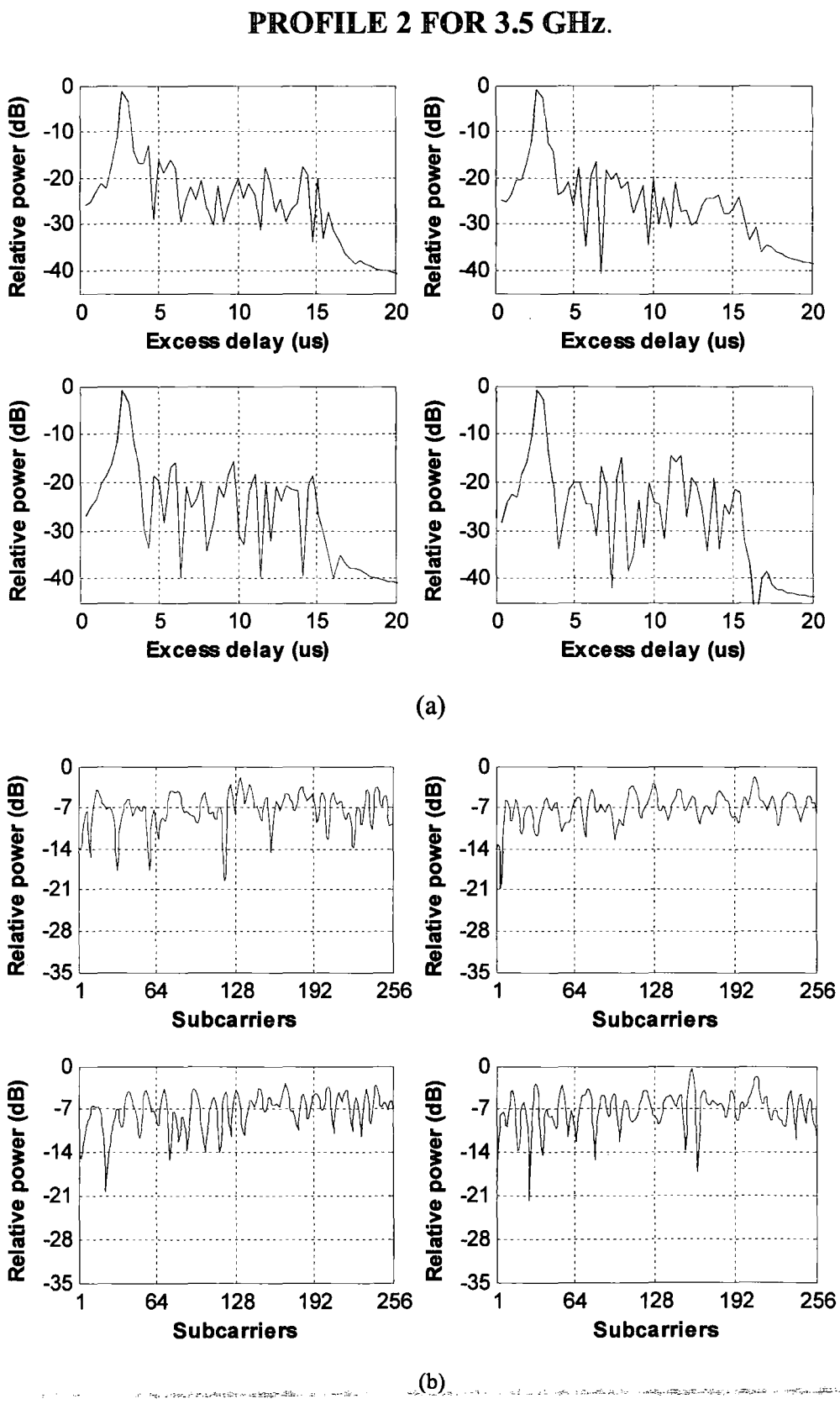

Figure 6.11 (a) Examples of channel impulse responses , (b) their corresponding channel transfer functions.

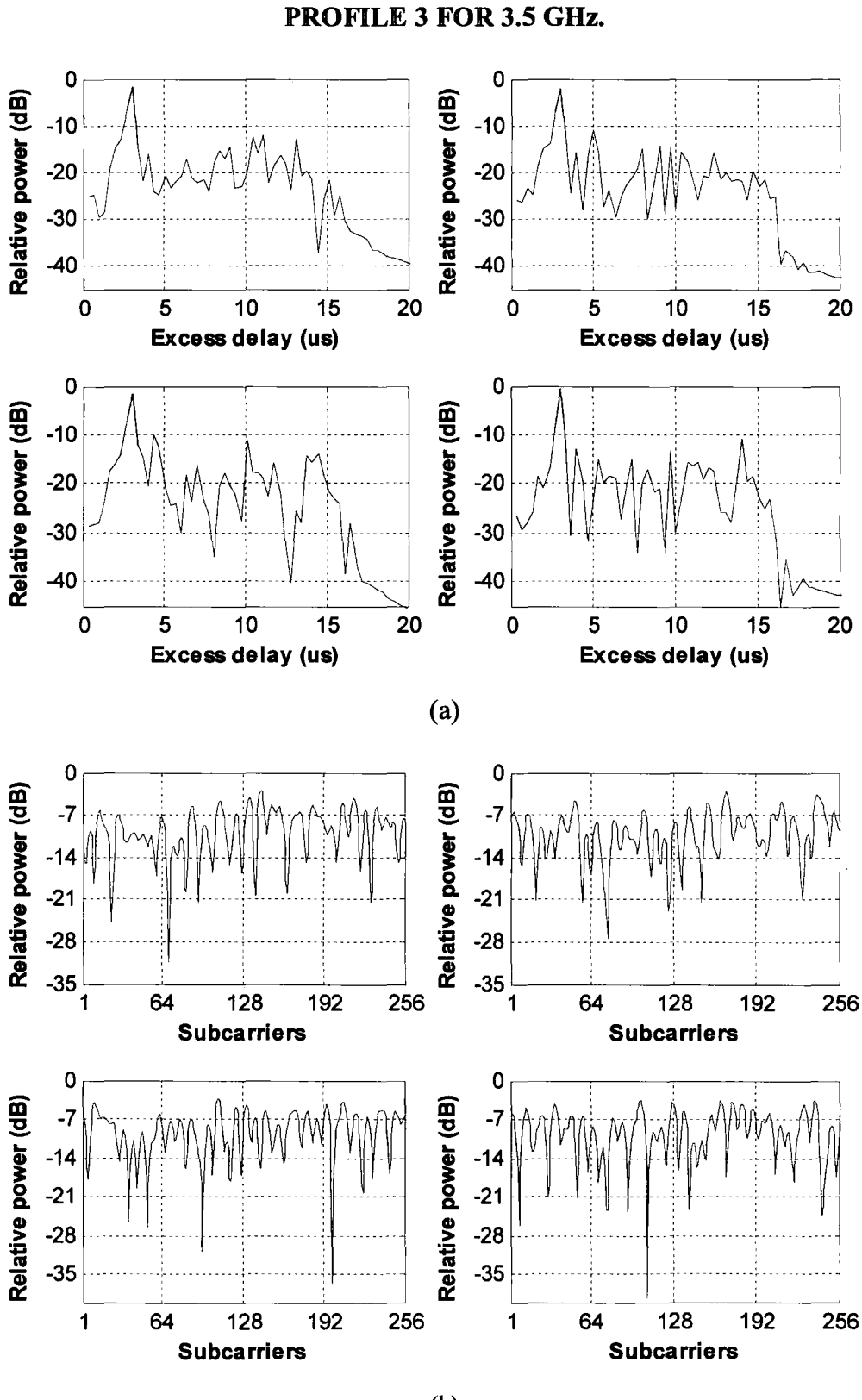

Figure 6.12 (a) Examples of channel impulse responses, (b) their corresponding channel transfer functions.

Table 6.1 RMS delay spreads for the three profiles of the 2.5 GHz and 3.5 GHz bands.

Frequency band	P1	P2	P3
2.5 GHz	0.22 μs	2.90 μs	3.00 μs
3.5 GHz	0.30 μs	1.89 μs	3.40 μs

Table 6.2 OFDM system parameters.

Parameters	Values
FFT Size (N_{FFT})	256
256 carriers bandwidth (F_S)	2.96 MHz
Sampling time (T_S) = $1/F_S$	0.34 μs
Subcarrier spacing (Δf) = $F_S / 256$	11.6 kHz
Useful symbol duration (T_b) = $1/\Delta f$	86.2 μs
Guard interval duration (T_g).	Based on measured impulse responses
Number of data subcarriers (N_D)	192
Number of pilot subcarriers (N_p)	8
Number of used subcarriers (N_{used})	200
Number of guard subcarriers (N_{guard})	55

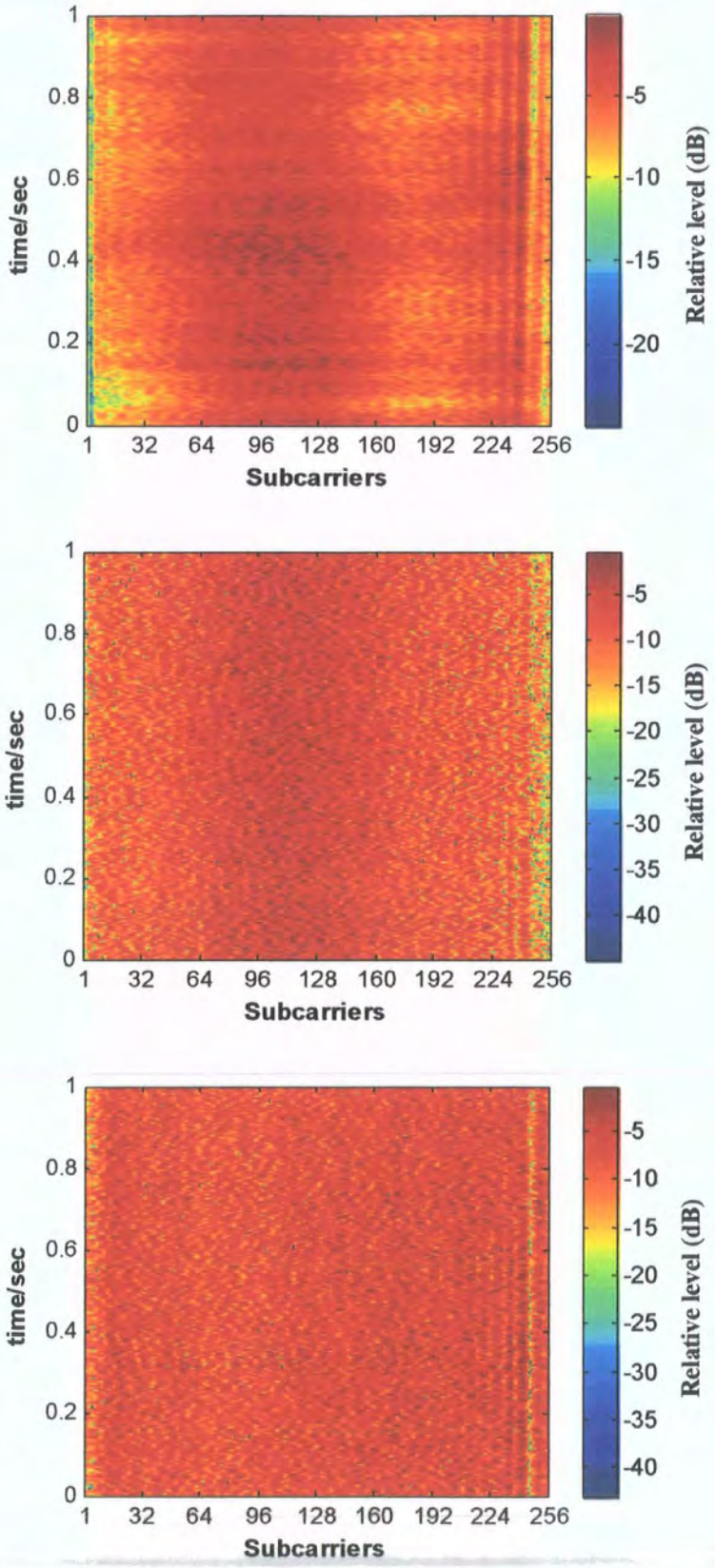

Figure 6.13 Time variant channel transfer functions of profile 1, 2 and 3 (top to bottom) for 2.5 GHz

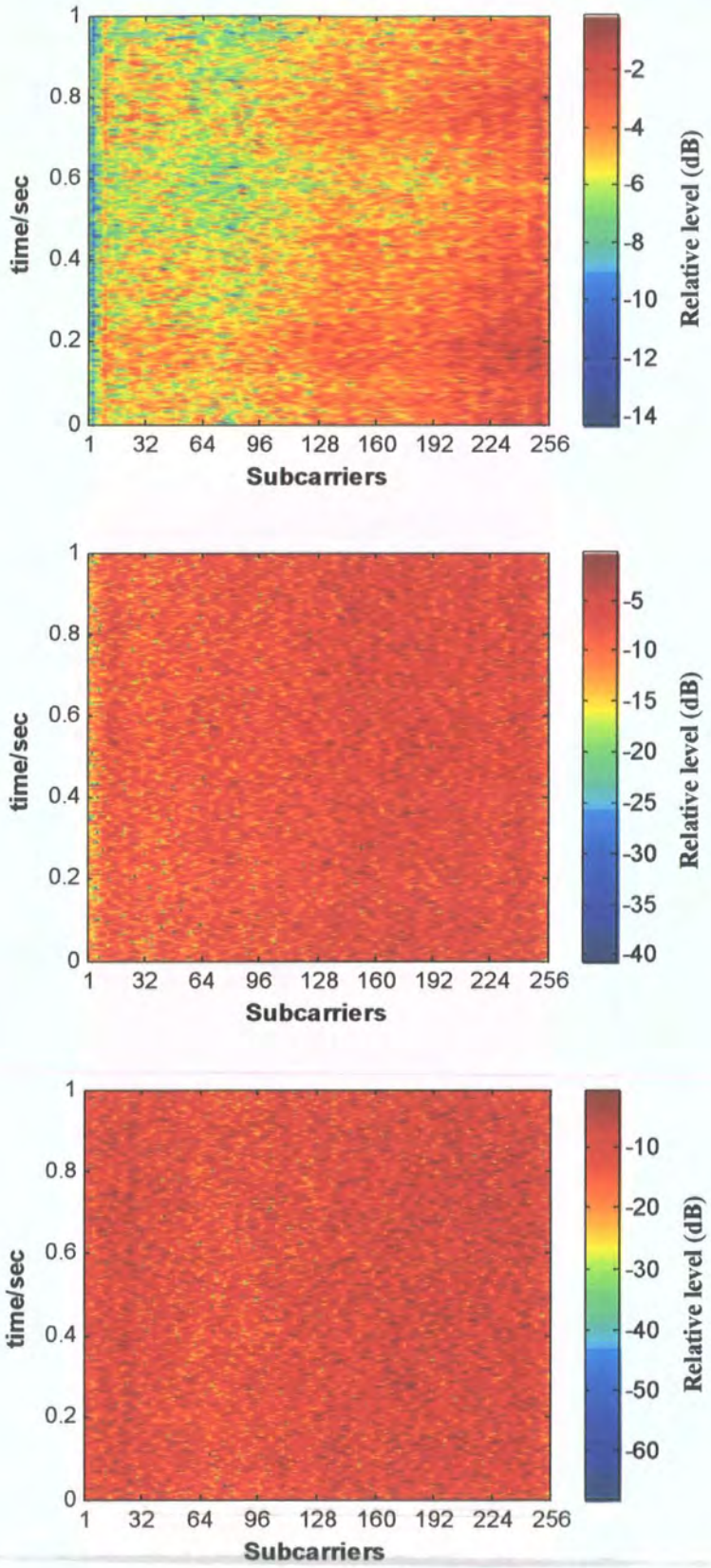

Figure 6.14 Time variant channel transfer functions of profile 1, 2 and 3 (top to bottom) for 3.5 GHz

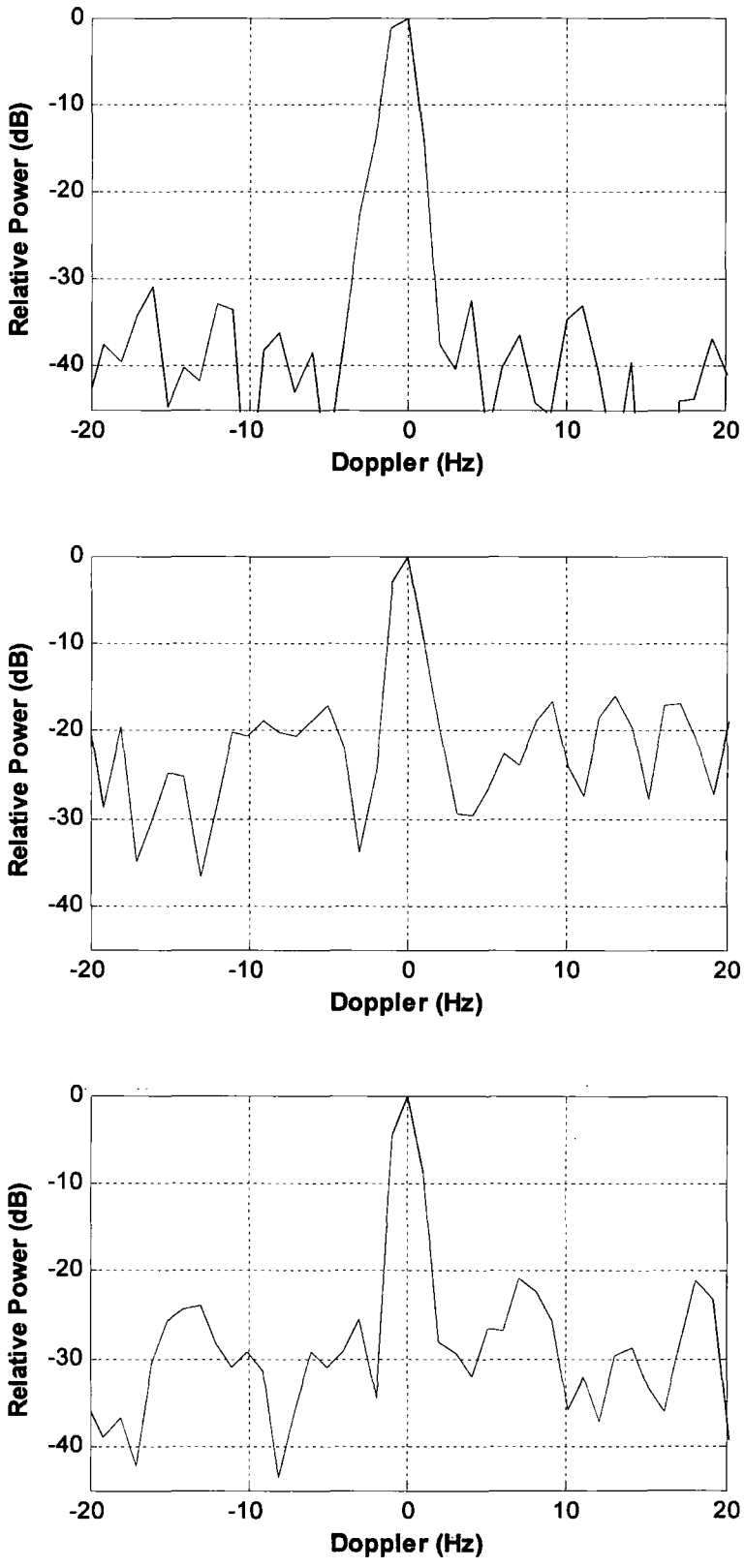

Figure 6.15 Average Doppler power spectrum of profile 1, 2 and 3 (top to bottom) for 2.5 GHz

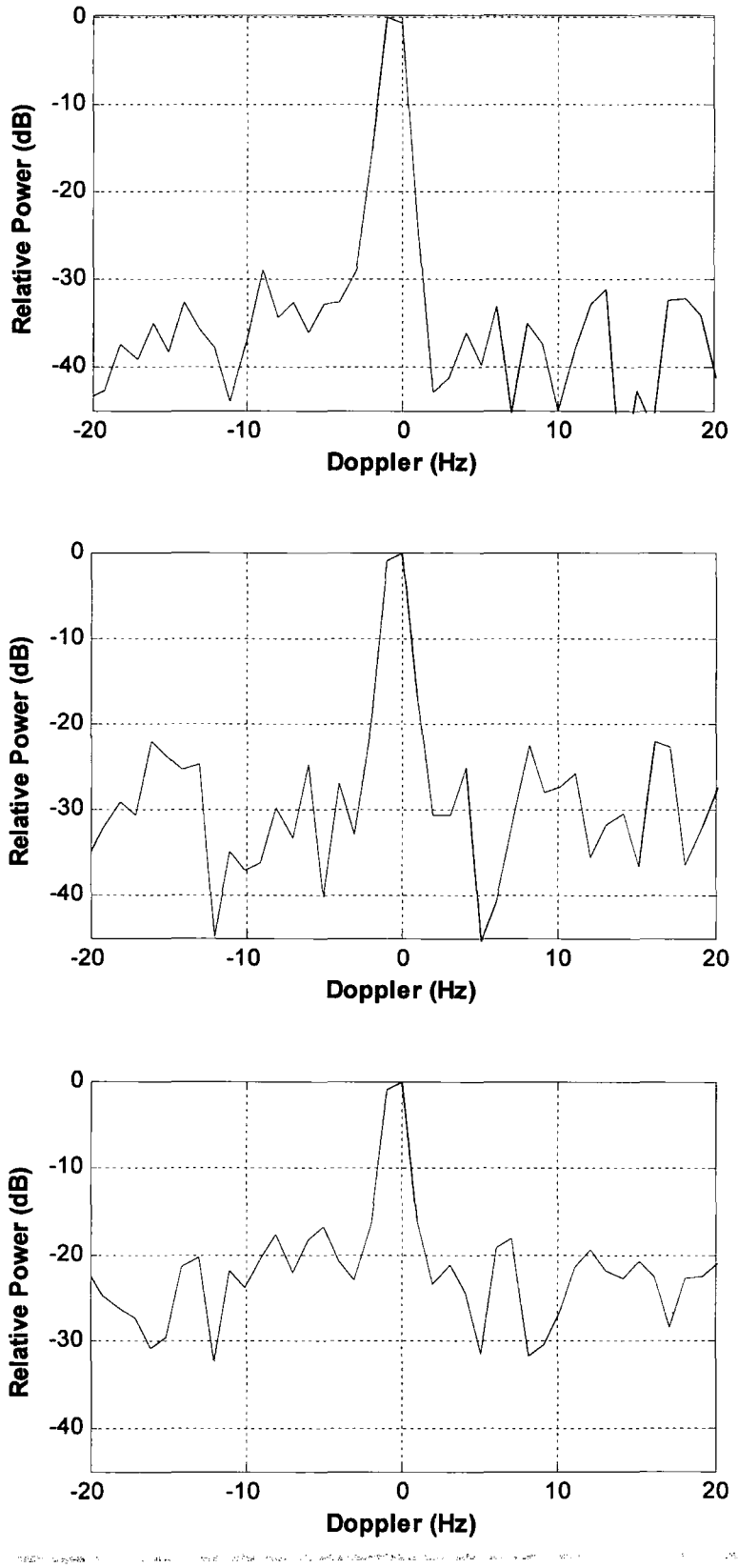

Figure 6.16 Average Doppler power spectrum of profile 1, 2 and 3 (top to bottom) for 3.5 GHz

6.3.1.1 Simulation Results and Analysis for Rate 1/2 Coded OFDM System

Figures 6.17 and 6.18 present BER performance results of rate 1/2 coded IEEE802.16-2004 OFDM system for profiles 1-3 in the 2.5 GHz band (Figures 6.7 to 6.9), employing QPSK and 16-QAM constellation. Whereas, Figures 6.19 and 6.20 depict BER performance results of the same system for profiles 1-3 of the 3.5 GHz band (Figures 6.10 to 6.12. Channel estimation employed long preamble aided Least Square (LS) technique.

The bit error rate (BER) results of the 2.5 GHz band reveal that profile 1 yielded the lowest BER as compared to profiles 2 and 3. As can be seen from the frequency transfer functions of these profiles the channel transfer function for profile 1 is less erratic and does not contain a series of deep fades. Most of the transfer function variations are confined within a 5 dB range. It exhibits less frequency selective fading since its impulse response has only one significant multi-path component (Figure 6.7) and the remaining two components have relatively very low power. These peaks are about 25 dB down as compared to the main peak. Due to this dominant component, the channel transfer function exhibits Rician fading in frequency and in time. Rician fading is characterised by the K factor. It can be used to obtain a clear picture about the fade depth on each subcarrier and the degree of variability in the frequency selective fading across the OFDM symbol bandwidth. When cumulative distributions of the amplitude of individual subcarriers of profile 1 were determined, it was found that the fading on almost all subcarriers exhibited a good fit with the Rice distribution. The Kolmogrov-Simirnov (K-S) goodness-of-fit test was employed to determine the best-fit distribution for the amplitudes of OFDM subcarriers. Figures 6.21 and 6.22 present the plot of K factor versus 256 subcarriers for the three profiles of the 2.5 GHz and 3.5 GHz bands. The plots for the 2.5 GHz band show that almost every subcarrier of the profile 1 has a very high K-factor which implies that there is less probability of encountering a deep fade and consequently the mean bit error rate will be low. Whereas, profile 2 causes more severe fading on the OFDM subcarriers as compared to profile 1. It can also be noticed from the K-factor plots that profile 2 has deep fades between subcarriers number 230 and 256. Moreover, more variations in the K factor have also been observed across the subcarriers of profile 2.

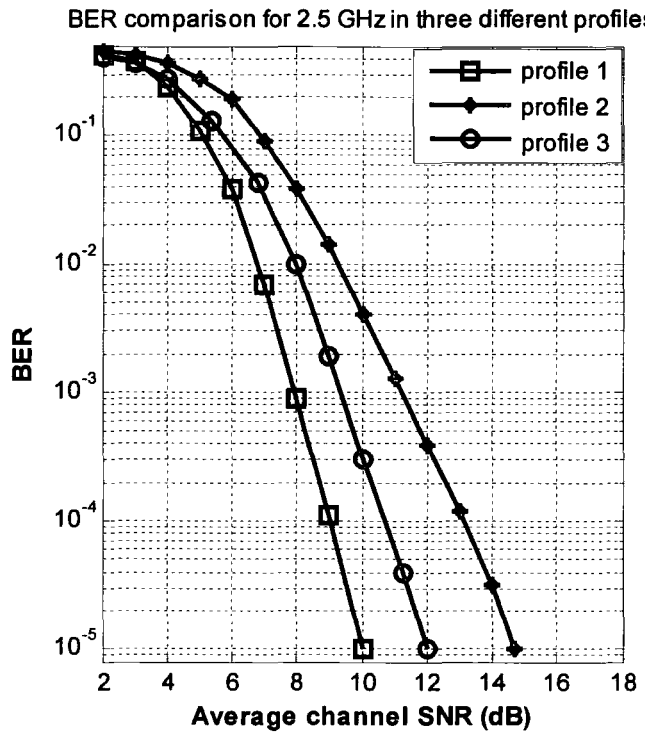

Figure 6.17 BER performance of rate 1/2 coded 256 OFDM IEEE 802.16-2004 WirelessMAN employing QPSK and measured channel profiles for 2.5 GHz depicted in Figures 6.7-6.9.

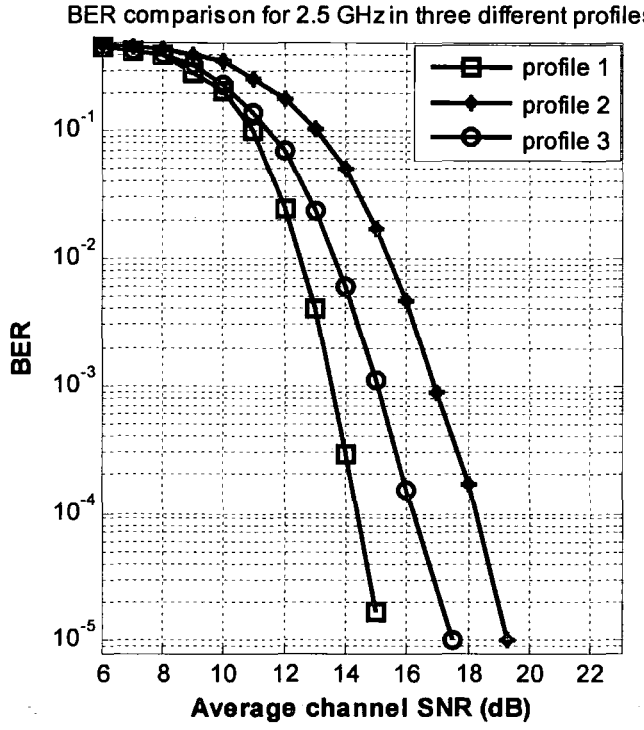

Figure 6.18 BER performance of rate 1/2 coded 256 OFDM IEEE 802.16-2004 WirelessMAN employing 16-QAM and measured channel profiles for 2.5 GHz depicted in Figures 6.7-6.9.

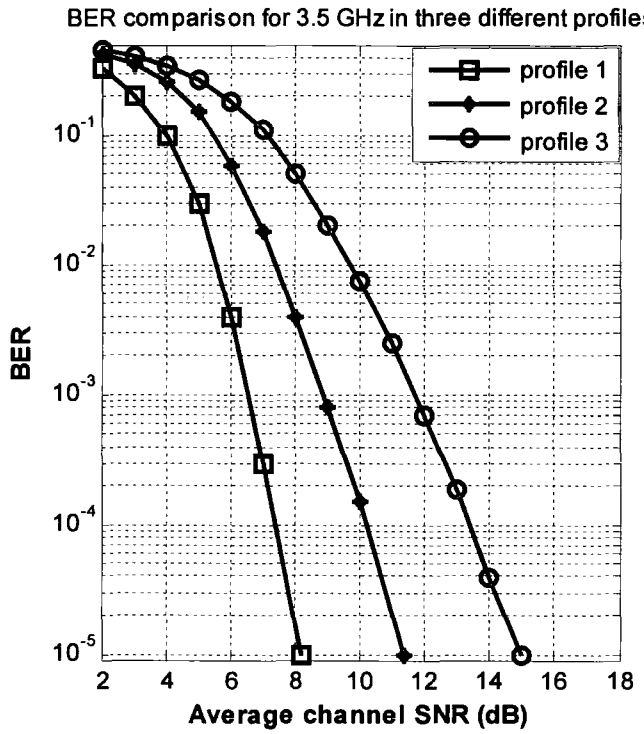

Figure 6.19 BER performance of rate 1/2 coded 256 OFDM IEEE 802.16-2004 WirelessMAN employing QPSK and measured channel profiles for 3.5 GHz depicted in Figures 6.10-6.12.

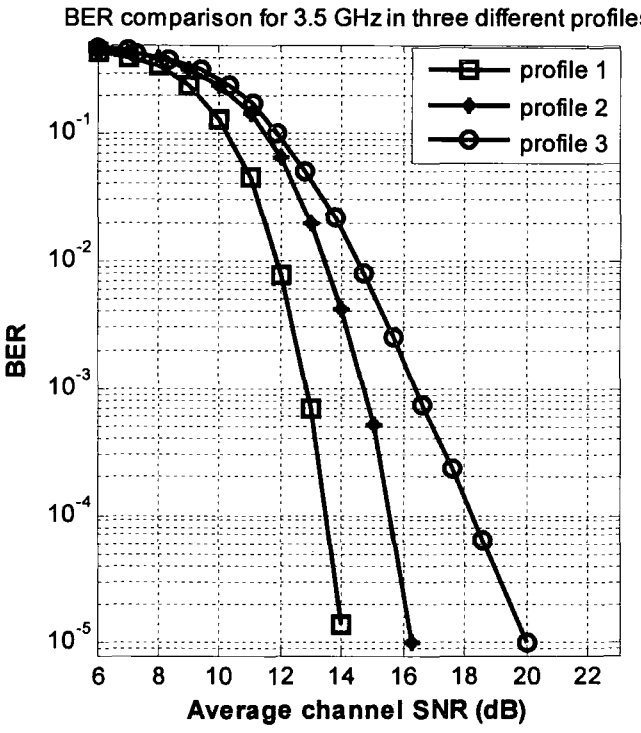

Figure 6.20 BER performance of rate 1/2 coded 256 OFDM IEEE 802.16-2004 WirelessMAN employing 16-QAM and measured channel profiles for 3.5 GHz depicted in Figures 6.10-6.12.

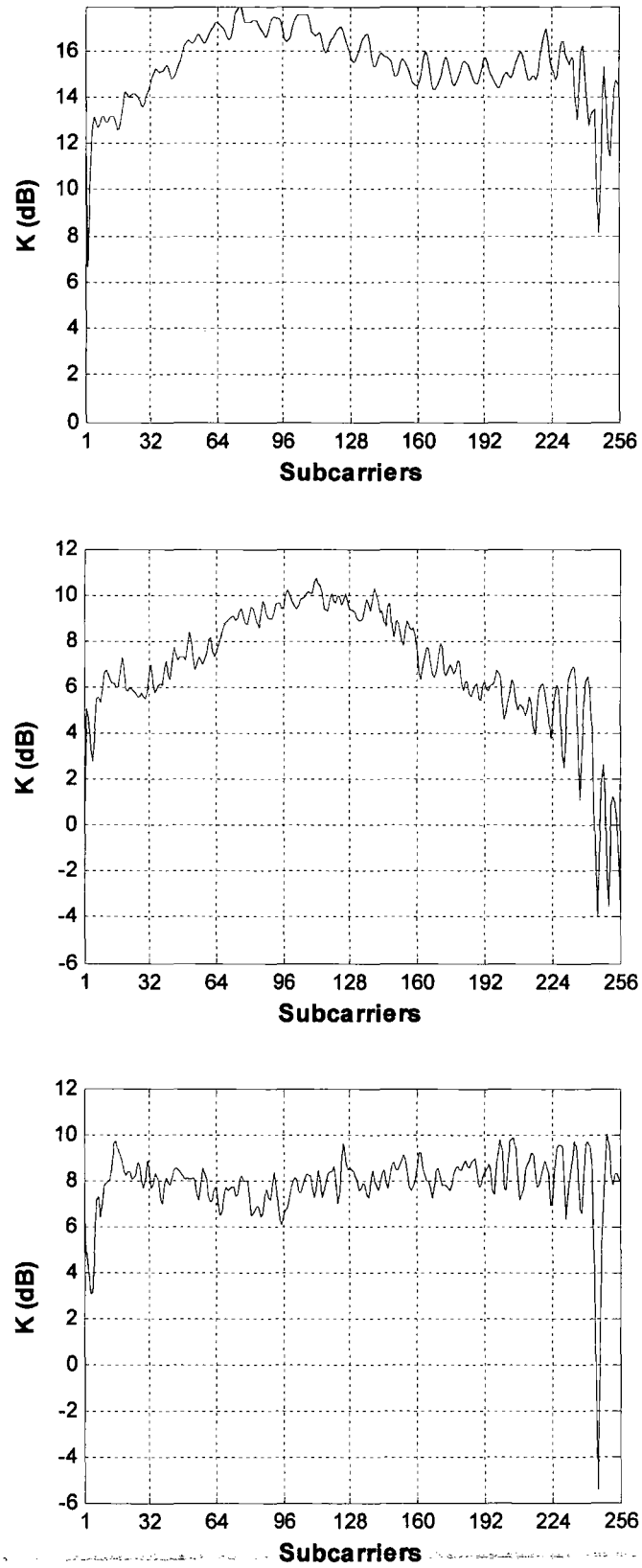

Figure 6.21 K-factor versus subcarriers for channel profiles 1,2 and 3 (from top to bottom) of 2.5 GHz.

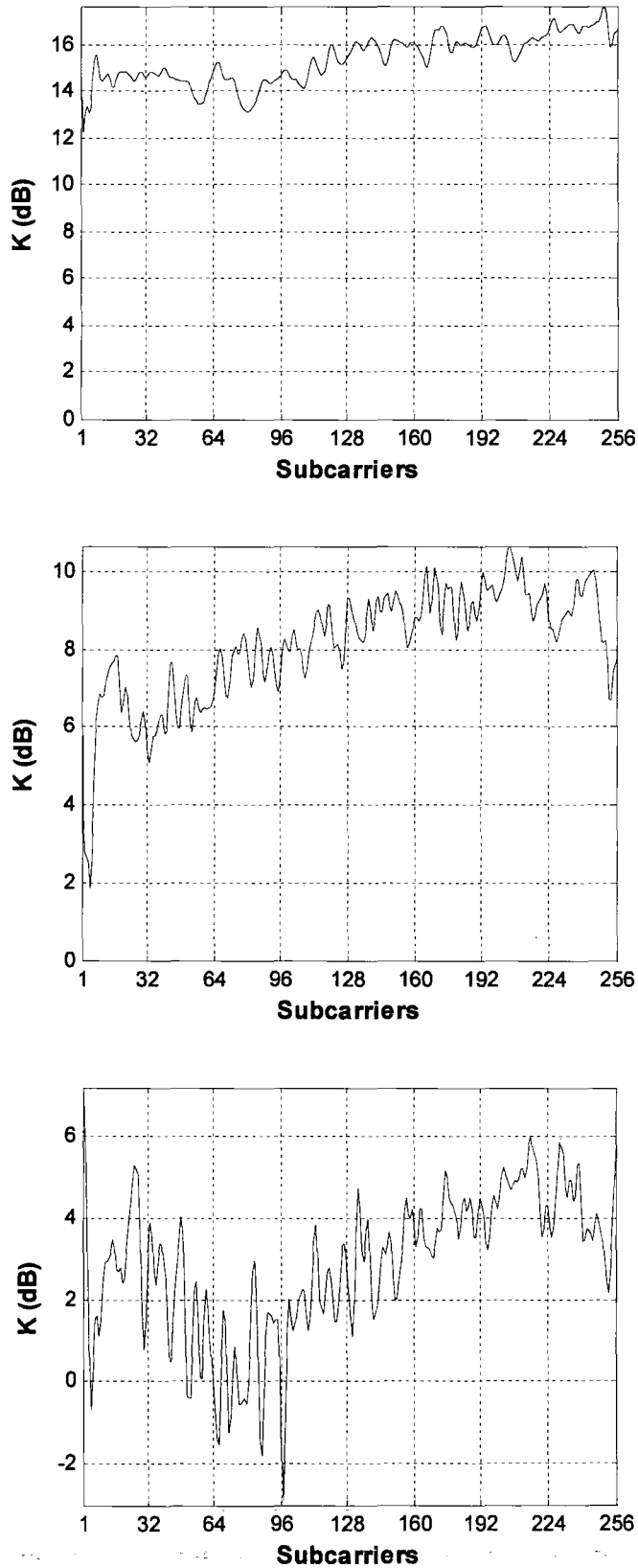

Figure 6.22 K-factor versus subcarriers for channel profiles 1,2 and 3 (from top to bottom) of 3.5 GHz

It was found that some subcarriers obeyed Rayleigh distribution and some Rician depending upon the value of K. Subcarriers with high values of K obeyed Rician, whereas Rayleigh distribution was noticed for subcarriers having low K factor. As an example, consider a K factor plot for profile 2 of 2.5 GHz band (Figure 6.21). Subcarrier number 245, which appears to be in a deep fade, has a low K factor of about -4 dB. As shown in Figure 6.23a, its amplitude exhibited a very good fit with Rayleigh distribution. Another subcarrier number 96 has a high K factor of about 11 dB, and hence obeyed Rician distribution. Figure 6.23 depicts the best-fit distribution for both carriers.

Moreover, channel estimator delivers better performance in profile 1 than profile 2. It may be recalled that 802.16-2004 system uses only 100 carriers for the purpose of channel estimation. These carriers are located at odd number positions. The channel estimates at the remaining even numbered carriers are made using interpolation techniques. Series of deep variations in the channel transfer function lower the performance of interpolation algorithm substantially. This is evident from Figure 6.24 which compares the equalized complex symbols for the system operating in profile1 and 2 against the original constellation for 16-QAM. It is apparent that the equalized constellation points in respect of channel profile 2 are more deviated from their original positions than those of profile 1. More frequency selective fading causes more drift from their original positions and results in more transmission errors.

Comparing the channel transfer functions for the profile 2 and 3, it can be observed that they appear different in terms of their frequency selective behaviour. The transfer function for profile 2 is more erratic and contains more deep fades as compared to that of profile 3. This can be related to the impulse response which contains some significant peaks in addition to the main peaks. These peaks are about 10 dB low as compared to main peak. Whereas, the impulse responses of profile 3 depicted in Figure 6.9a reveal that their peaks are more than 15 dB lower as compared to the main peak. Moreover, as evident in Figure 6.9b, the subcarriers of profile 3 have consistent variations in the K-factor across the whole bandwidth, whereas inconsistent variations in the K factor are noticed for profile 2. Therefore, profile 3 delivers better BER performance as compared to profile 2.

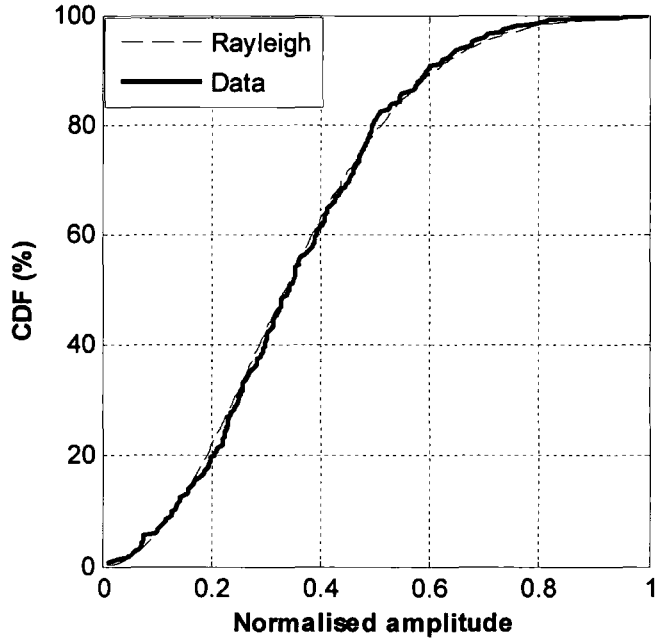

(a)

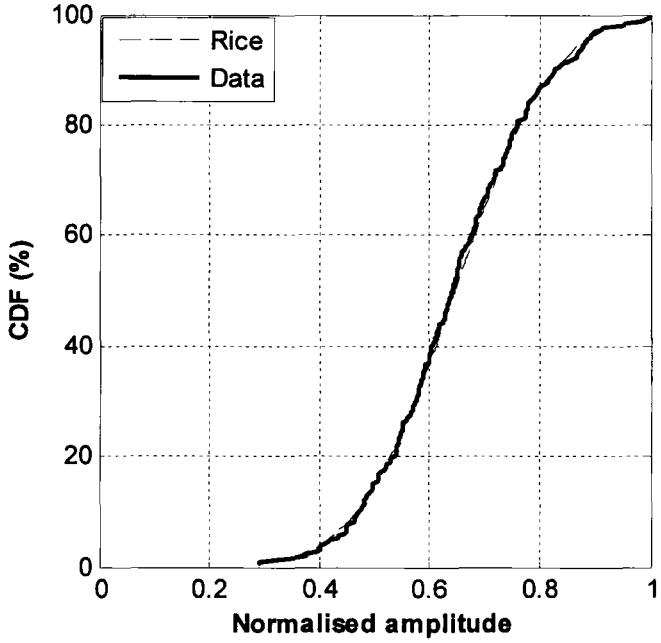

(b)

Figure 6.23 CDFs of amplitude of subcarrier number (a) 245, (b) 97 of channel profiles 2 of 2.5 GHz

Comparing the bit error rate (BER) performance of the system in three channel profiles of 3.5 GHz band (Figures 6.10-6.12), it can be seen that the channel transfer function for profile 1 is much smoother and consequently results in a lower BER as compared to profiles 2 and 3.

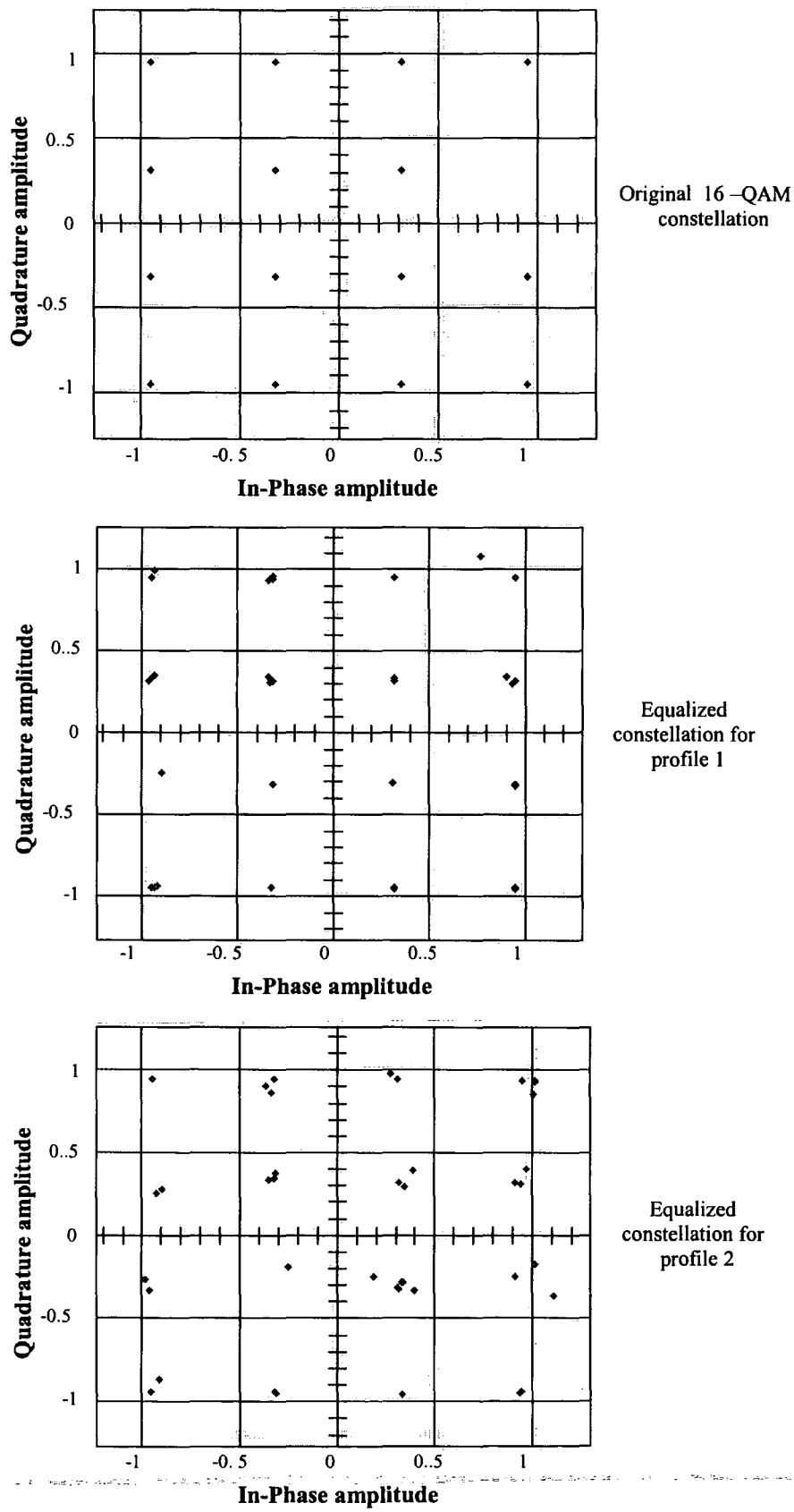

Figure 6.24 Comparison of equalized constellation against the original for the channel profiles 1 and 2 of the 2.5 GHz band.

As evident from Figure 6.22, all subcarriers have very high K-factor. Considering Figures 6.10 -6.12, it can be observed that the transfer function of profile 3 is more erratic and contains more of fluctuations as compared to profile 2. This can also be observed from its impulse response which contains some significant peaks in addition to the main peaks. These peaks are about 10 dB lower than the main peak. Whereas, the impulse responses of profile 2 depicted in Figure 6.11 reveal that their peaks are more than 15 dB lower than the main peak. Moreover, as evident in Figure 6.22, the subcarriers of profile 2 have a high K-factor as compared to profile 3. Therefore, profile 2 delivers better BER performance as compared to profile 3.

The BER results presented in Figures 6.17 and 6.19 for QPSK in three channel profiles of the 2.5 GHz and 3.5 GHz bands reveal that QPSK requires less signal to noise ratio as compared to QAM for equivalent bit error rate performance. However, it has been noticed that a relative bit error rate performance relationship between QAM and QPSK approximately remains the same over three channel profiles for both frequency bands. As evident from the simulation results there is a difference of approximately 5-6 dB in signal-to-noise ratio at BER of 1e-5 in all profiles for both bands.

Analogous to the time domain level crossing rate and average fade duration, the concept of level crossings (LC_f) per OFDM symbol bandwidth with respect to a specified level can also be employed in the frequency domain to quantify the severity of frequency selective fading. Similarly, the depth of fade can be defined in the frequency domain as the average bandwidth of fade (ABF) over which the amplitude of the transfer function remains below a specified level. Algorithms in MATLAB were written to calculate these statistics for the three channel transfer functions of both bands. The number of crossings and average fade bandwidth were determined for every transfer function and the results were averaged over 249 sweeps. The transfer functions depicted in Figures 6.7 to 6.12 were normalised such that the maximum absolute value contained in the matrix of transfer functions was 0 dB. Therefore, the frequency domain level crossings were determined by varying the threshold level from 0 dB to the value beyond which the envelop did not exist. For profiles 1 of both bands, most of the envelop variations are confined from 0 dB to -10 dB. Therefore, the reference level was varied from 0 to -10 dB to calculate the level crossings and average fade bandwidth.

Whereas, profiles 2 and three of both bands contain envelope variations up to -30 dB. Therefore, for these profiles, the reference level was varied between 0 to -30 dB. Figures 6.25 and 6.26 present the comparison of average level crossings (LC_f) and bandwidth of fade (ABF) over OFDM symbol bandwidth (3 MHz) for the three profiles of 2.5 and 3.5 GHz bands respectively.

From these results it can be noticed that profile 1 of both bands does not have any crossings beyond -5 dB. However, profile 2 of 2.5 GHz band have crossing beyond -11 dB. It is apparent from these results that profile 2 of 2.5 GHz is more frequency selective as compared to profiles 1 and 3. This can be verified from the BER performance results which showed that profile 2 resulted in worst performance. In case of profile 2 and 3 of 3.5 GHz band, level crossings can be observed even at -13 dB level.

Regarding average bandwidth of fade, it is also influenced by the frequency selective fading and obeyed the same order as of average level crossing results in respect of the three profiles of both bands. As noticed from the results that profiles with deep fades exhibit values of average bandwidth of fade even at low threshold level. Therefore, it can be concluded that the number of level crossings and average bandwidth of fades in the frequency domain are related to the frequency selective fading and can be used to quantify and distinguish one profile from another.

In the context of average level crossing rate and fade duration in time, it is worth mentioning that the measurements were made using a stationary receiver, therefore, the channel variations were very small and the maximum level crossing rate of less than 2 can be expected with a Doppler of 2 Hz. The effects of these parameters on the performance of IEEE 802.16-2004 system are therefore insignificant. Moreover, with available data of one second duration, it is difficult to get accurate average results. The level crossing rate is inversely proportional to the K factor. Every subcarrier has a different K factor. Envelope's variations about rms value are small and confined within ± 3 dB. For the purpose of demonstration, Figure 6.27 shows the time variations of the three subcarriers with different values of K factor (0.4 dB, 9.9 dB and 17.9 dB) . It can be noticed that as K increases, the variations about rms values decrease and level crossings occur only near the rms values.

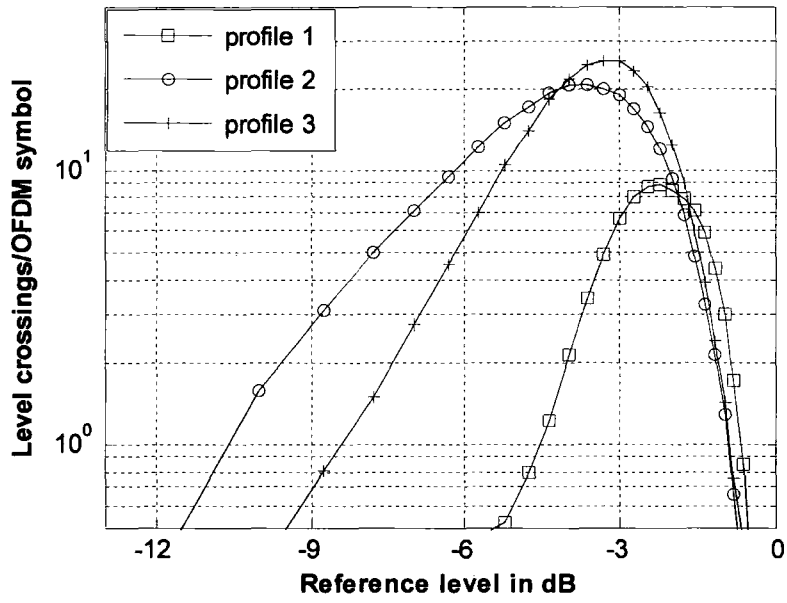

(a) 2.5 GHz band

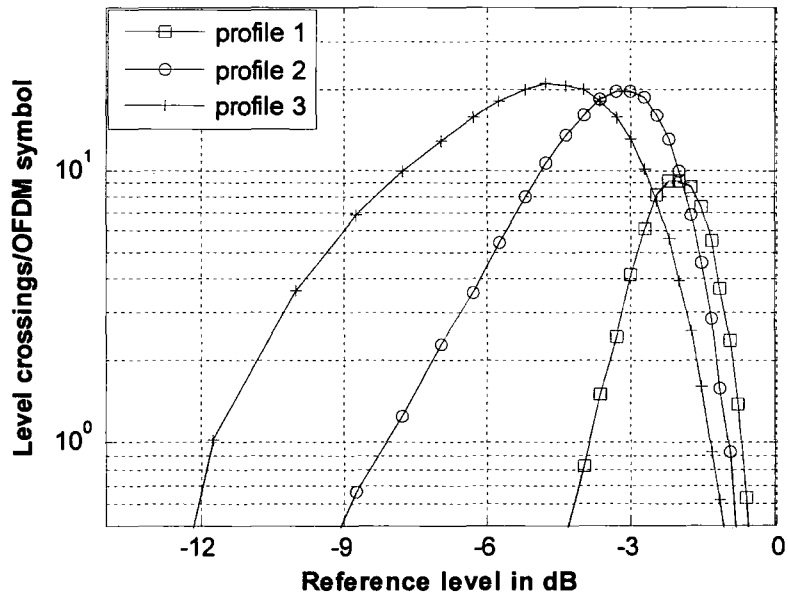

(b) 3.5 GHz band

Figure 6.25 Comparison of frequency domain level crossings for three profiles of 2.5 GHz band (a) and 3.5 GHz band (b).

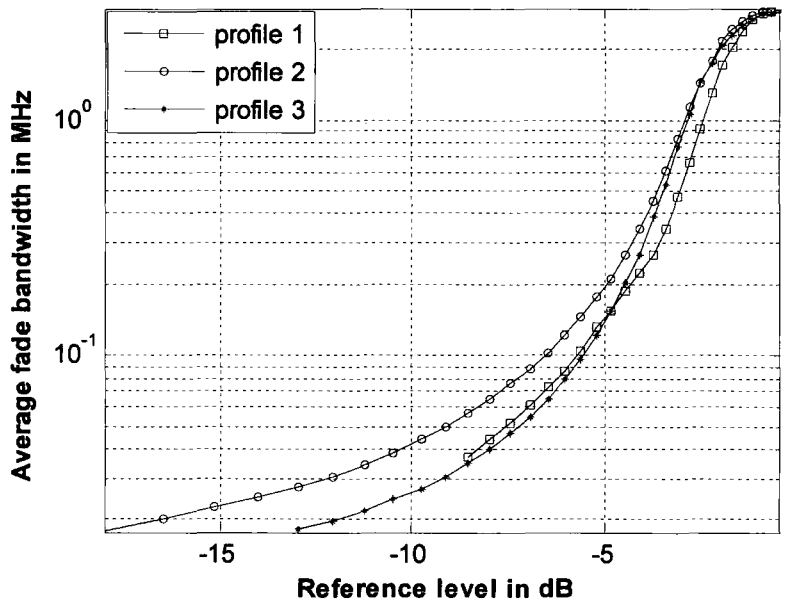

(a) 2.5 GHz band

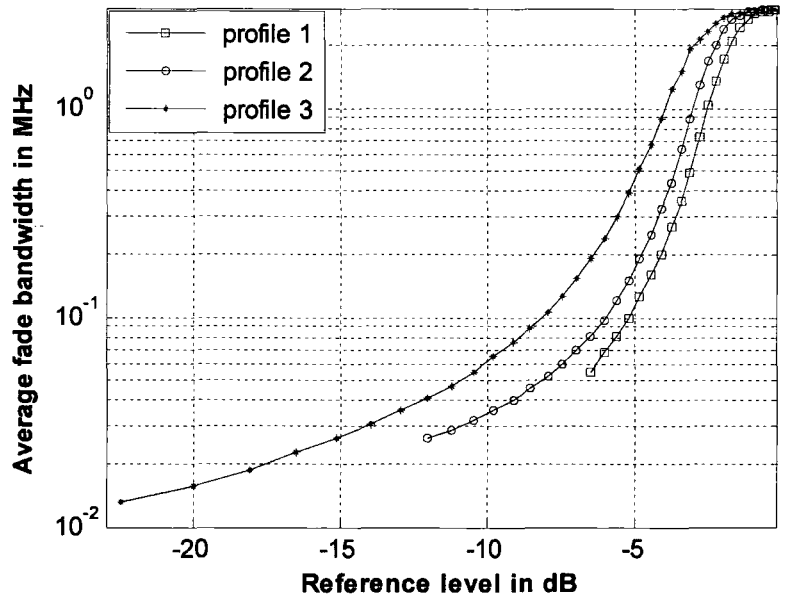

(b) 3.5 GHz band

Figure 6.26 Comparison of average fade bandwidth for three profiles of 2.5 GHz band (a) and 3.5 GHz band (b)

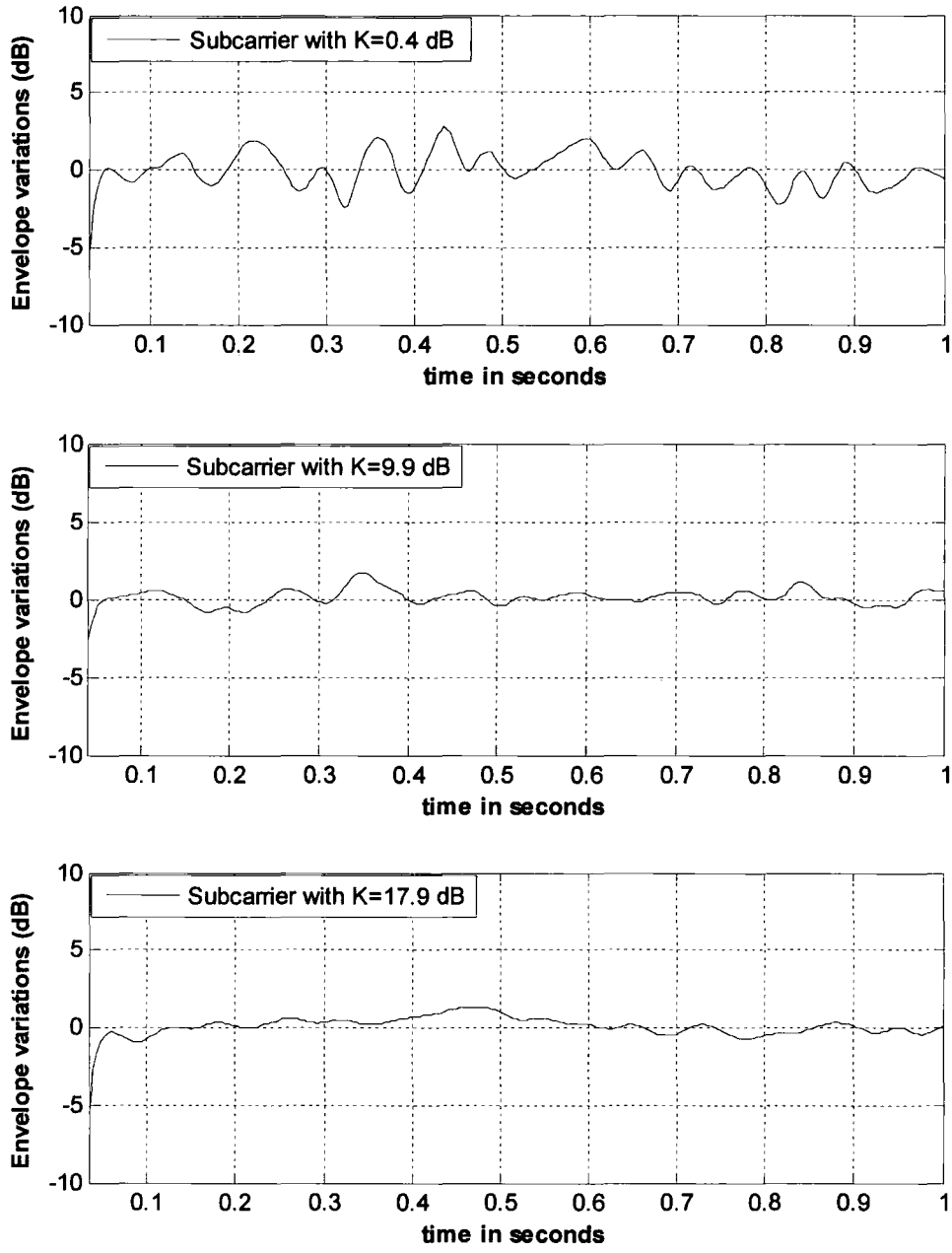

Figure 6.27 Envelope variations about rms values of subcarriers with different values of K factor

6.3.1.2 Simulation Results and Analysis for Rate 3/4 Coded OFDM System

Simulations have also been carried out to obtain BER results of rate 3/4 coded system for channel profiles 2 and 3 of 2.5 GHz band. Figures 6.28 and 6.29 present the simulation results for 256 OFDM system employing QPSK and 16-QAM constellation mapping respectively.

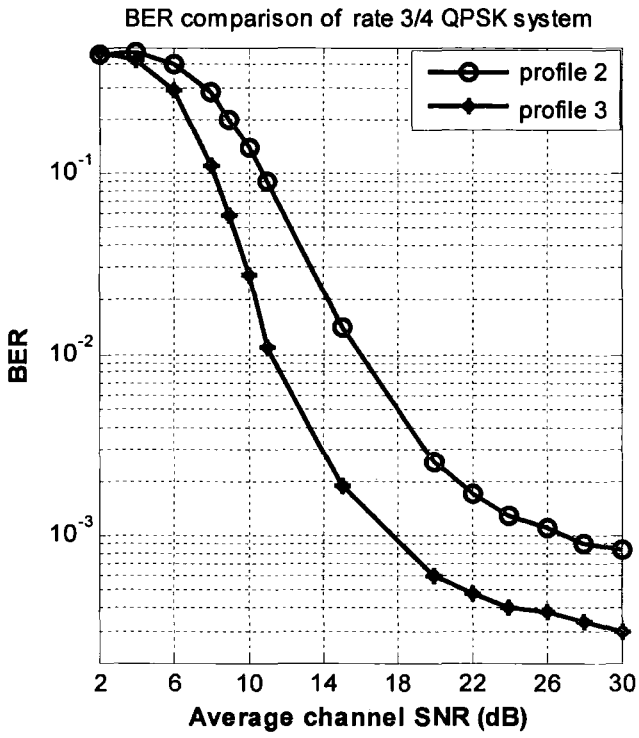

Figure 6.28 BER performance of rate 3/4 coded 256 OFDM IEEE 802.16-2004 WirelessMAN employing QPSK and measured channel profiles 2 & 3 for 2.5 GHz band depicted in Figures 6.8-6.9

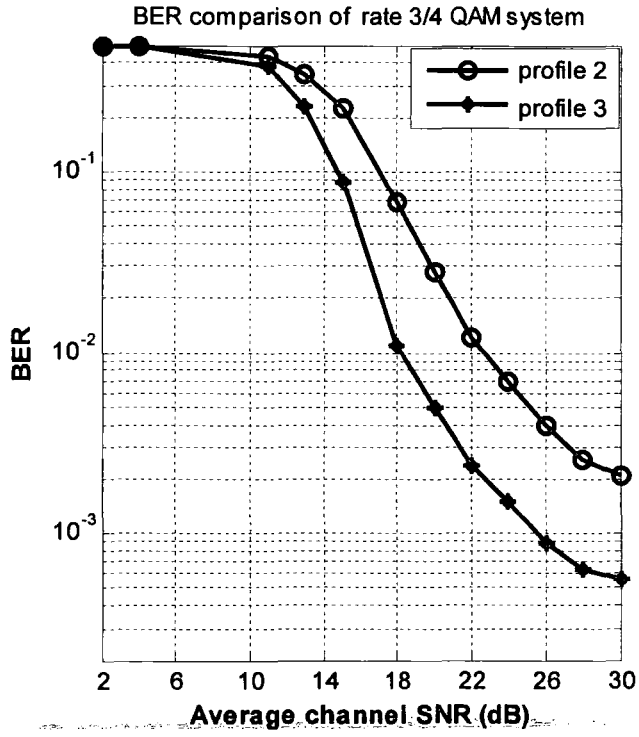

Figure 6.29 BER performance of rate 3/4 coded 256 OFDM IEEE 802.16-2004 WirelessMAN employing 16-QAM in a measured channel profile 2 & 3 for 2.5 GHz band depicted in Figures 6.8-6.9.

As shown before that profile 2 is more frequency selective as compared to profile 3, therefore, the system yielded better performance in profile 3 than profile 2. In comparing BER curves for rate 3/4 system with those presented in Figures 6.17 and 6.18 for rate 1/2 system in the same channel profiles, it can be noticed that the performance of the OFDM system also depends upon the code rate of the forward error correction (FEC) scheme. Puncturing of coded bits on the one hand increases the transmission efficiency of the system but on the other hand degrades the error correcting capability of the decoder. Due to a high degree of frequency selective fading, the subcarriers lying in the frequency selective nulls region of the channel transfer function will have a lower signal to noise ratio (SNR). Consequently, when the decoder optimally weights extremely low SNR code bits at its input, it treats them as 'don't care' puncture bits. If too many punctures are observed in a particular interval, then the FEC is more likely to deliver errors. As the rate 3/4 system already has more punctured bits as compared to rate 1/2 system, deep nulls in the transfer function have a higher impact on rate 3/4 systems as compared to rate 1/2. As evident from the simulation results depicted in Figures 6.17- 6.20, the system's performance for rate 1/2 system improves with an increase in signal to noise ratio, whereas in case of rate 3/4 coded system the BER improves up to a certain limit. No significant improvement in BER can be observed beyond this limit.

The channel profiles that have been presented so far in Figures 6.7 to 6.12 for the 2.5 GHz and 3.5 GHz bands exhibit RMS delay spread ranging from 0.22 μs to 3.4 μs. In order to further study the effect of frequency selective fading on rate 3/4 coded system, another measured profile at 2.5 GHz has been selected to be used in the third phase of the simulations. Fig 6.30 shows some of the impulse responses (4 out of 249) and their corresponding transfer functions. This profile has a RMS delay spread of 4.4 μs. As seen from the distribution of multi-path components in the profile, there are high levels peaks around an excess delay of about 15 μs. These peaks are only 8 to 10 dB down as compared to the main peak. This profile results in severe frequency selective fading which can be observed from Figure 6.30. It can also be noticed that its transfer function is more erratic as compared to those used in previous simulations and the spacing between the dips of frequency selective pattern are inconsistent and varying across the OFDM symbol bandwidth.

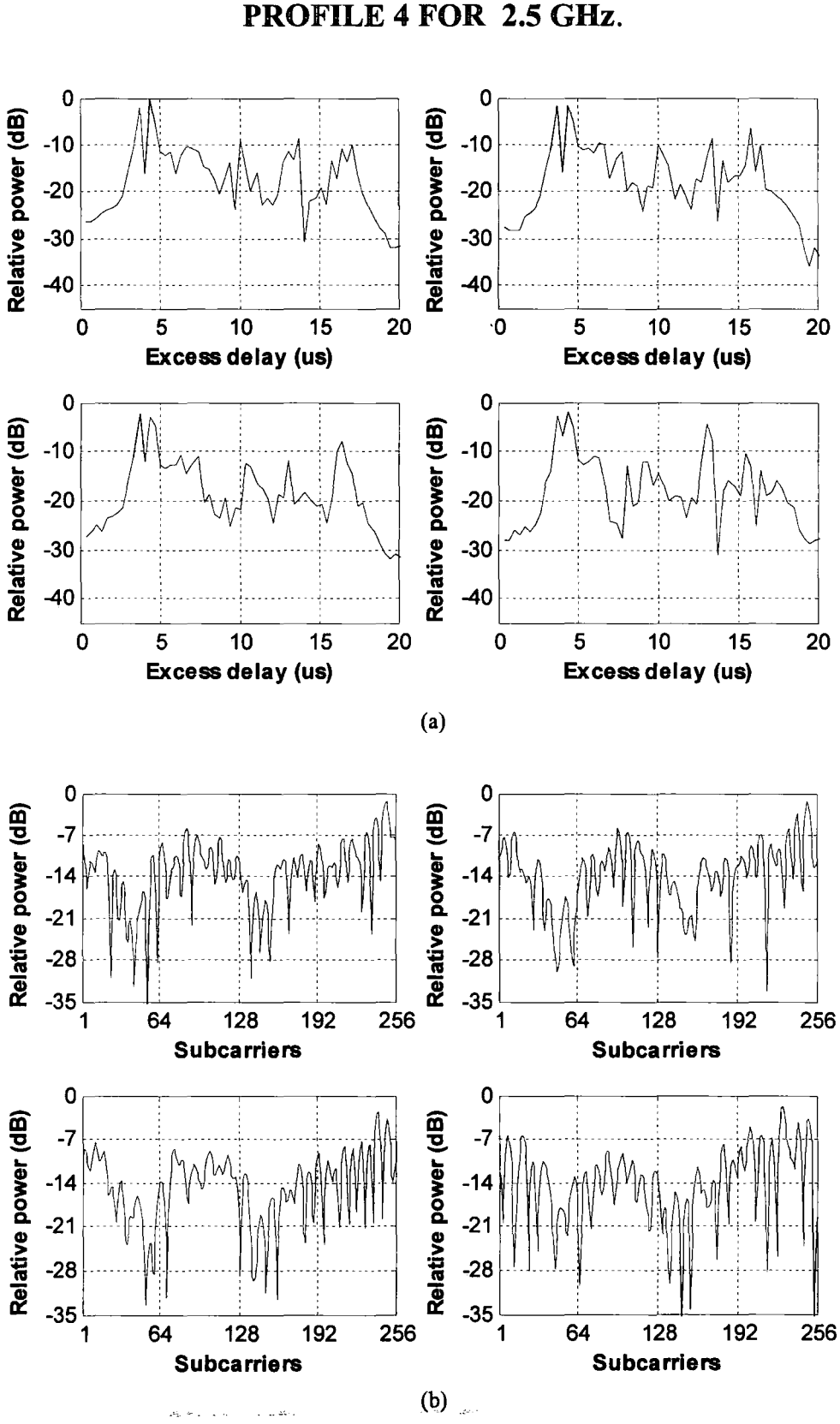

Figure 6.30 (a) Examples of channel impulse responses, (b) their corresponding channel transfer functions.

The K factor plot, depicted in Figure 6.31, further testifies the presence of variations in the fading depth across the whole subcarriers bandwidth. However, as evident from the Doppler power spectrum presented in Figure 6.32, this profile exhibits very slow variations in time which shows a maximum 2 Hz Doppler shift.

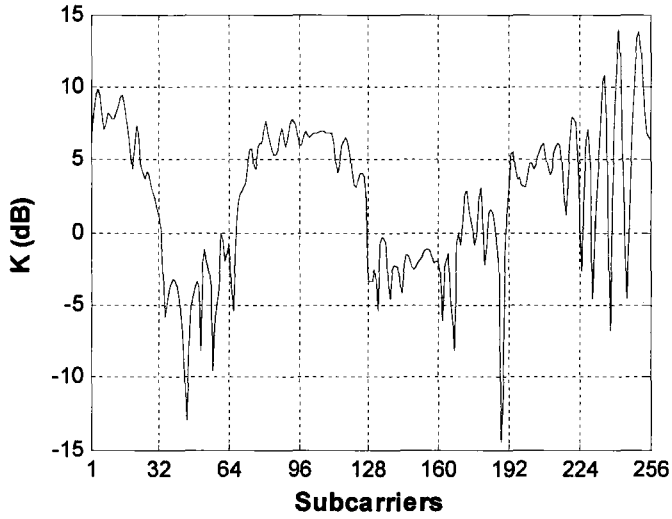

Figure 6.31 K-factor versus subcarriers for channel profiles 4 of 2.5 GHz band.

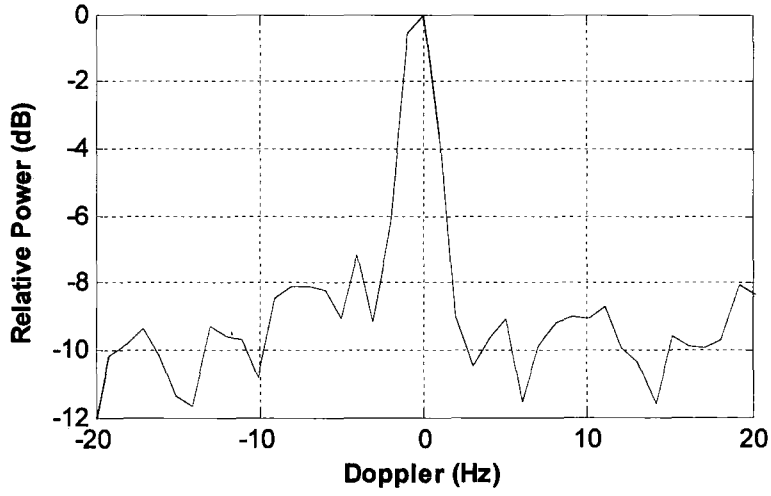

Figure 6.32 Average Doppler power spectrum of profile 4 for 2.5 GHz

Figures 6.33 and 6.34 present the comparison between the BER performance results for rate 1/2 and 3/4 coded OFDM systems employing QPSK and 16-QAM constellation mapping respectively.

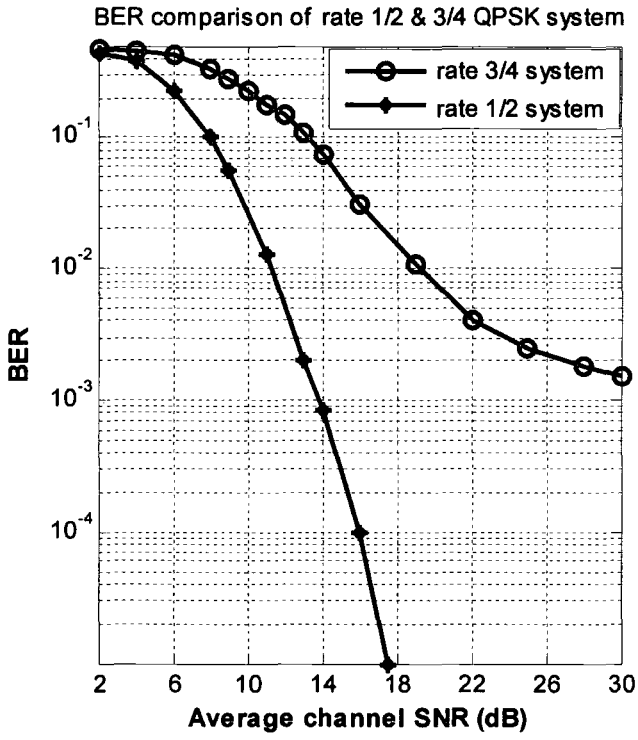

Figure 6.33 BER comparisons between rate 1/2 and 3/4 coded system employing QPSK in a measured channel profile 4 for 2.5 GHz band depicted in Figure 6.30.

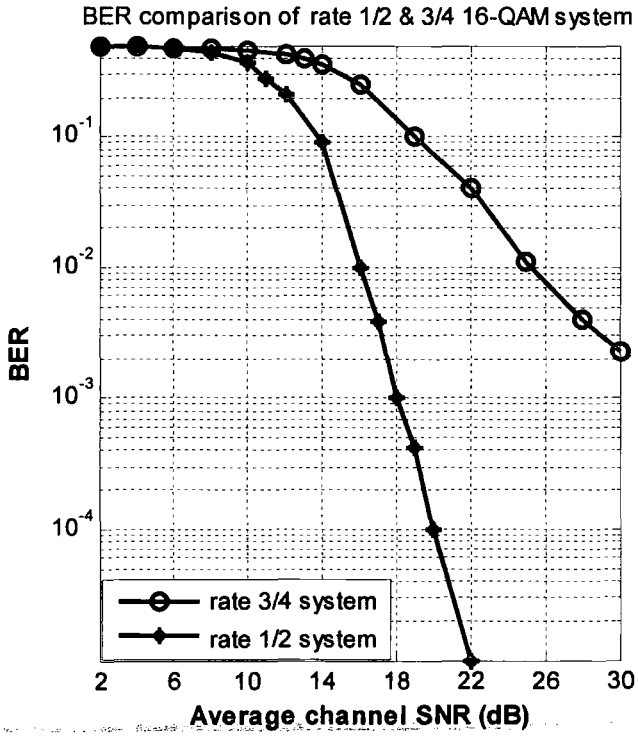

Figure 6.34 BER comparisons between rate 1/2 and 3/4 coded system employing 16-QAM in a measured channel profile 4 for 2.5 GHz band depicted in Figure 6.30.

It can be observed that the rate 1/2 coded system performed better than rate 3/4 coded system. It can further be noticed that the slope of the BER curve for rate 3/4 system decreases for values of SNR ratio greater than 22 dB for QPSK and 30 dB for 16-QAM. No significant improvements in BER are evident beyond these values.

6.4 SUMMARY AND CONCLUSIONS

Bit error rate (BER) performance of 256 OFDM based physical (PHY) layer of IEEE802.16-2004 Wireless Broadband Access (WBA) system was studied using measured channel transfer functions for 2.5 GHz and 3.5 GHz band. Frequency domain channel simulator was employed to obtain BER results of rate 1/2 and rate 3/4 coded OFDM system employing QPSK and 16-QAM constellation mapping. A Variety of measured channel transfer functions, which differ in terms of frequency selective fading, were used in the simulations. Their corresponding impulse responses yielded an average RMS delay spread ranging between 0.8 μs to 4.6μs. The channel data employed in this work for simulations were measured between the 7^{th} and 10^{th} of December 2004 in Martlesham, UK. The sounder employed 10 MHz bandwidth to measure the channel at a sweep repetition frequency (SRF) of 250 Hz. Measured data were processed to extract transfer function for 249 consecutive sweeps. This work has employed processed data that was made available in the form of a matrix containing complex time frequency functions. The transfer function for each sweep comprised 512 points for 2.5 GHz and 3.5 GHz band. The 512 points for both bands are separated by 11.6 kHz. The 249×512 points matrix contained time variant transfer functions for the duration of approximately one second. IEEE 802.16-2004 WirelessMAN is a variable bandwidth system. The channel bandwidth can be integer multiples of 1.25 MHz, 1.5 MHz, and 1.75 MHz with maximum of 20 MHz. This work has used the first 256 points out of 512 to construct a channel with 3 MHz bandwidth. These transfer functions were first converted into impulse responses by inverse FFT operation. These impulse responses were zero padded and then again transformed to transfer functions to be used in the fast convolution based channel implementation. All processing was carried out prior to the start of simulation. During the simulation phase, these transfer functions moved from the MATLAB work space sweep by sweep and entered into the

channel (based on FFT convolution) where they were point wise multiplied by the spectrum of an OFDM signals.

From the BER results presented in Figures 6.17-6.20 for profiles p1-p3 of both bands, it can be concluded that the performance of WBA system over a frequency selective channel mainly depended upon the frequency domain fading and the channel coding rate. Small channel variations in time do not impact the BER performance of WBA system as it is meant for stationary sites. The measured average Doppler power spectrum for 2.5 GHz and 3.5 GHz revealed a maximum Doppler of 2 Hz. The BER performance decreased with an increase in variations in the channel transfer functions. More erratic transfer functions yielded poor performance results. The series of deep fades lowered the individual signal to noise of the subcarriers and in turn degraded the average BER performance. The BER results presented for profiles 1-4 showed that the system performed worst in profile 4 as its transfer function was more erratic as compared to the rest of the profiles and the spacing between the dips of frequency selective pattern were inconsistent and varying across the OFDM symbol bandwidth. The BER performance in profile 1 is the best among the four profiles. The channel transfer functions for profile 1 are relatively smooth and do not contain deep fades. In order to present an overall picture of fading on each subcarrier, K factor of each subcarrier was calculated and plotted. For smooth transfer functions, the subcarriers had high K-factor and their envelopes exhibited a good fit with Rice distribution. On the other hand, most of the subcarriers of erratic transfer functions obeyed Rayleigh distribution and had low K-factor. Moreover, large variations in the values of K-factor across the whole transmission bandwidth were observed for more frequency selective transfer functions. The Kolmogrov-Simirnov (K-S) goodness-of-fit test was employed to determine the best-fit distribution for the amplitudes of OFDM subcarriers.

Due to the presence of large variations in the channel transfer function, the coding rate also limits the attainable bit error rate. This is because the puncturing weakens the capability of forward error correcting coding in the presence of a series of deep fades in the channel transfer function. From the performance results presented in Figures 6.33 and 6.34 for rate 1/2 and 3/4 coded system respectively in profile 4 of 2.5 GHz, it is apparent that rate 1/2 coded system performed better than rate 3/4 coded system. It can be observed that the slope of the BER curve for rate 3/4 system decreases

for values of SNR ratio greater than 22 dB. No significant improvement in BER was noticed beyond this value.

Frequency domain level crossings and average bandwidth of the fades are the second order statistics and can be employed to quantify the severity of frequency selective fading across the bandwidth of OFDM symbol.

6.5 BIBLIOGRAPHY

1. V. Fung, T.S. Rappaport, " Bit error simulation of $\pi/4$ DQPSK mobile radio communications using two-ray and measurement based impulse response model, " IEEE Journ. on Selected Areas in Communications, vol. 11, no.3, April 1993, pp. 393-405.
2. T.S. Rappaport, "Simulation of bit error performance of FSK, BPSK, and $\pi/4$ DQPSK in flat fading indoor radio channels using a measurement based channel model, "IEEE Trans. on Vehicular Technology, vol. 40, no. 4, Nov 1991, pp. 731-740.
3. IEEE 802.16-REVD/D5-2004, "Draft IEEE standards for local and metropolitan area networks-part 16: Air interface for fixed broadband wireless access system," May 2004.
4. L. Hanzo, W. Webb and T. Keller, Single and Multi-carrier Quadrature Amplitude Modulation, West Sussex, England: IEEE Press, John Wiley & Sons, Ltd, 2000.
5. H. Harada and R.J. Prasad, Simulation and Software Radio, London: Artech House, 2002.
6. R.V. Nee and R. Prasad, OFDM for Wireless Multimedia Communications, Boston: Artech House, 2000.
7. Ziemer and Tranter, Principles of communications: System modulation and noise, Boston: Houghton Mifflin company, 1990.
8. G.C. Clark and J.B. Cain, Error Correction Coding for Digital Communications, New York: Plenum Press, 1988.
9. J.G. Proakis, Digital Communications, New York: McGraw-Hill, 1993.

10. A.J. Viterbi, "Convolution codes and their performance in communication systems," IEEE Trans. on Communications Technology, vol. COM-19, no.5, Oct 1971, pp.751-772.
11. R. Steele, Mobile Radio Communications. London, England: Pentech Press Limited, 1992
12. J. Chuang, "The effects of time delay spread on portable radio communications channels with digital modulation," IEEE Jour. on Selected Areas in Communications, vol. SAC-5, no. 5, June 1987, pp. 879-889.
13. C.I. Justin, "The effects of delay spread on 2-PSK, 4-PSK, 8-PSK and 16-QAM in portable radio environment", IEEE Trans. on Vehicular Technology, vol. 38, no. 2, May. 1989, pp. 43-45.
14. Y. Li, "Pilot-symbol-aided channel estimation for OFDM in wireless systems," IEEE Trans. Vehicular Technology, vol. 49, no. 4, Jul. 2000.
15. S. Coleri, M. Ergen, A. Puri, and A. Bahal, "Channel estimation techniques based on pilot arrangement in OFDM systems," IEEE Trans. on Broadcasting, vol. 48, no.3, sep 2002.
16. L.J. Cimini, "Analysis and simulation of digital mobile channel using orthogonal frequency division multiplexing," IEEE Trans. Communications, vol.33, no.7, July 1985, pp. 665-675.
17. IEEE 802.16a-03/01, "Channel models for fixed wireless applications," IEEE 802.16, June 2003.
18. K. Witrisal, Y.H. Kim and R.J. Prasad, "A new method to measure parameters of frequency-selective radio channels using power measurements," IEEE Trans. on Communications, vol. COM-49, no. 10, Oct. 2001, pp. 1788-1800.
19. S.J. Yang, Y.C. Lei, and T.D. Chiueh, "Design and simulation of baseband transceiver for IEEE 802.16a OFDM-Mode subscriber station," IEEE Asia-Pacific Conference on Circuits and Systems, Dec 6-9, 2004.

CHAPTER 7

CONCLUSIONS AND FURTHER WORK

7.1 CONCLUSIONS

Testing of a communication system using channel simulator instead of field trials is cost effective, less time consuming and produces more conclusive results. The advancements in digital signal processing techniques have enabled the implementation of channel simulators in the digital domain. Digital implementation is flexible, accurate, and more economical. A Combination of hardware and software tools permits the user to select various simulation parameters through user friendly graphical interface.

Channel simulators for single carrier and multicarrier OFDM systems based on time variant transfer functions of the channel have been designed and implemented using DSP techniques in SIMULINK. For a single carrier system, the simulator was based on the Bello's transfer function channel model. The DQPSK modulation scheme of the U.S. Digital Cellular Standard IS-54 with two-ray power delay profile was used to model the channel in the frequency domain. The implementation was validated by comparing the BER simulation results against the tapped delay line results. For multicarrier OFDM system, the simulator was based on the physical (PHY) layer standards for IEEE 802.16-2004 Wireless Metropolitan Area Network (WirelessMAN) and employed measured channel transfer functions at 2.5 GHz and 3.5 GHz bands in simulations. The channel model was implemented in the frequency domain by FFT convolution. The designed system was first validated by studying its BER performance over an additive white Gaussian noise (AWGN) channel and comparing BER simulation results with the theoretical results and other published results. The close match between them validated the SIMULINK implementation of 256 carriers OFDM system.

Transfer function modelling approach has many advantages over impulse response modelling. These include: independence of fading statistics over the bandwidth, fulfilment of central limit theorem for all frequencies and instants with respect to all domains, and consistent extension from narrowband to wideband.

However, its main advantage arises for ultra wideband systems, where the number of taps in the time domain becomes very large as the bandwidth permits the resolution of more components, therefore limiting the applicability of the central limit theorem.

The design of the transfer function channel simulator was optimized by determining the actual number of branches needed to achieve a very close approximation of the channel. Simulation of a two ray power delay profile with equal power was performed by varying the number of branches between 3 to 10 times the B/B_c, where B_c is the coherence bandwidth of the channel at correlation coefficient of 0.5. Each branch was modelled as FIR bandpass filter and a complex multiplier. The simulation results showed that $10B/B_c$ branches gave close agreement with the tapped delay line model. This number was π times higher than $10B\tau_{max}$, previously speculated by Bello. As the maximum excess delay (τ_{max}) is not necessarily the best indicator for gauging the performance of a given system in a channel since different channels with the same value of τ_{max} can yield very different profiles of signal intensity over the delay span. Therefore, it seems more appropriate to link and define the total number of branches (N) in the frequency domain channel model in relation with the coherence bandwidth (B_c) of the channel. Although, there is no fixed definition of coherence bandwidth since it is always defined with reference to arbitrary correlation coefficient, the widely employed value of 0.5 can be used to relate the number of branches with the coherence bandwidth.

The concept of transfer function modelling can be applied to OFDM systems. Due to the cyclic prefix, a channel can be represented as a bank of multipliers where each OFDM carrier is multiplied by its corresponding transfer function. Therefore, it is equally possible to implement the channel in the frequency domain by carrying out point wise multiplication of the spectrum of the OFDM signal with the transfer function of the channel. This point wise multiplication can be implemented by employing FFT convolution between the OFDM time domain sequence and the channel impulse response. FFT convolution is faster than linear convolution. Moreover, the linear convolution of two finite duration sequences can also be performed by multiplying DFT's and taking the inverse if the sequences are first zero padded to sufficient lengths.

Therefore, the circular convolution of two zero padded sequences yields the same results as of those produced by regular convolution.

Frequency domain channel simulator for IEEE 802.16-2004 Wireless Broadband Access (WBA) system was employed to study the bit error rate performance of rate 1/2 and rate 3/4 coded OFDM system employing QPSK and 16-QAM constellation mapping under a variety of measured channel transfer functions at 2.5 and 3.5 GHz band. These transfer functions differ from one another in terms of frequency selective fading. The performance of WBA system over a frequency selective channel mainly depended upon the frequency domain fading and the channel coding rate. Small channel variations in time do not impact the BER performance of WBA system as it is meant for stationary sites. The measured average Doppler power spectrums for 2.5 GHz and 3.5 GHz bands revealed a maximum Doppler of 2 Hz. The BER performance decreased with increase in variations in the channel transfer functions. More erratic transfer functions yielded poor performance results. The series of deep fades lowered the individual signal to noise of the subcarriers. These variations across the OFDM symbol bandwidth lessen the effectiveness of the interpolation algorithm which delivers the channel estimates for preamble pilots located at even numbered positions.

Due to the presence of large variations in the channel transfer function, the coding rate also limits the attainable bit error rate. Puncturing weakens the capability of forward error correction (FEC) codes in the presence of a series of deep fades in the channel transfer function. From the performance results presented for rate 1/2 and 3/4 coded systems, it is apparent that rate 1/2 coded system performed better than rate 3/4 coded system.

The degree of frequency selective fading can also be determined by measuring the frequency domain level crossings and average bandwidth of fades within the OFDM symbol bandwidth with respect to a specified level. The number of crossings at low level increase with an increase in frequency selective fading. It was observed that channel transfer functions with deep fades (in frequency) exhibited values of average bandwidth of fades even at low reference level. Therefore, it can be concluded that level crossings and average bandwidth of fades in the frequency domains are the manifestations of frequency selective fading and can be used to quantify channel transfer functions.

It was further noticed that the depth of fading on each OFDM subcarrier was different. Different subcarriers had different K factors and hence exhibited different statistical distributions depending upon the value of K. Subcarriers with low K values followed Rayleigh distributions. Large variations in K factors were also revealed across the OFDM symbol bandwidth. This implies that K factor plot for OFDM subcarriers can be used to visualise the frequency selective fading.

In the dimension of time, each subcarrier exhibited small variations with respect to the rms value of the envelope due to small Doppler. These variations were mainly confined within 2 to 3 dB from the rms value. With 2 Hz Doppler, the maximum level crossing rate of 2 can be expected. Therefore, the impact of time domain level crossing rate and average fade duration are insignificant on the performance of IEEE 802.16-2004 OFDM system.

7.2 FURTHER WORK

The architecture proposed in this work for transfer function mobile channel simulator can be implemented using suitable Digital Signal Processor (DSP) to permit real time simulation of ultra wideband systems. These days, high speed DSP chips are available in the markets which are capable of implementing the various blocks such as, FIR Filters, random process generators and multipliers. For statistical simulations, the gain functions for each branch of the transfer function model can be generated either by Jakes sums of sinusoids method or filtered Gaussian method. A number of implementations have already employed DSP chips such as, TMS320C6701, TMS320C31, and TMS32050A to generate random processes using both methods. For measurements based simulations, the measured transfer functions can be stored in the RAM prior to simulations. During the simulation phase, these can be retrieved and interpolated to match the sampling rate of the signal.

The existing architecture has employed FIR filters to slice the input signal bandwidth. These were designed using frequency sampling method. Each FIR filter produced the desired results with 160 taps. Further work can be carried out to apply other techniques to reduce the filter order. This will lessen the processing burden on DSP for real time simulation.

In the current design, one random process was generated separately for each branch and then the required amount of correlation was established. However, it is also possible to derive multiple random processes with the required correlation from one process by introducing delays. The amount of delay will control the correlation among them.

In respect of OFDM simulator, its channel estimation and equalisation block can be modified to implement upcoming IEEE 802.16e OFDM system meant for providing wireless broadband services to mobile users. In the case of IEEE 802.16-2004 system, the channel variations are very small and preamble-aided LS channel estimation technique can provide reasonably good estimates. However, in the case of mobile users, the fast channel variations have to be catered for. In that case, the preamble can be employed to carry out initial channel estimation and 8 pilots can be used to track subsequent variations in the channel transfer functions. Moreover, due to a high degree of frequency selective fading, Linear Minimum Mean Square Estimation (LMMSE) technique will have to be employed. However, it is proposed to retain lowpass interpolation method to estimate the channel at unknown values because it outperforms other interpolation techniques. Moreover, the existing SIMULINK design is flexible and can be easily modified to facilitate future implementations of OFDM systems.

EUROPEAN COOPERATION
IN THE FIELD OF SCIENTIFIC
AND TECHNICAL RESEARCH

EURO-COST

SOURCE: School of Engineering,
University of Durham,
UK

COST 273 TD(05) 011
Bologna, Italy
2005/Jan/19-21

Mobile Channel Simulator using Transfer Function Model

Khawar Khokhar & Sana Salous
Centre for Communication Systems
School of Engineering
University of Durham
Durham DH1 3LE
UK
Phone: + 44-191 334 2532
Fax: + 44-191 334 2407
Email: sana.salous@dur.ac.uk

Mobile Channel Simulator using Transfer Function Model

Khawar Khokhar & S. Salous

University of Durham, Durham, UK
sana.salous@durham.ac.uk

Abstract: *A mobile channel simulator is employed to replicate the effects of multi-path propagation using hardware or software in order to evaluate and quantify the performance of mobile communication systems. The process of development of a mobile communication system requires that the system is tested time and again under a variety of propagation conditions, which can possibly exist. Testing a system in the field is not only expensive but also time consuming. Moreover, due to the stochastic nature of mobile channels, these varieties of conditions may not be found at the time of field-testing. Hence a number of field trials are needed for complete evaluation of system performance. However, channel simulators enable the assessment of system performance under controlled propagation environments in a laboratory. The work presented here pertains to the simulation of frequency selective mobile fading channels by employing the time variant transfer function. The simulator was designed in SIMULINK® using DSP techniques and validated by comparing simulated and published BER results for DQPSK modulation schemes in a two-ray channel environment.*

1. Introduction

A channel is considered as an element that transforms the input into the output. It is, therefore, analogous to a linear filter. The mobile radio channel can be described in terms of a two-port filter with randomly time varying transmission characteristics. The input and output of a channel can be described either in time or frequency domain. Therefore, the relationship between the input and the output can be explained in a number of ways using different time-frequency input-output relationships. This leads to four system functions, input delay spread function $h(t,\tau)$, output Doppler spread function $H(f,v)$, time variant transfer function $T(f,t)$, and delay-Doppler spread functions $S(\tau,v)$ [1]. These functions are called Bello's system functions [2].

Since the time variant behaviour of the mobile communication channel can be explained and modelled either in the time or frequency domain using Bello's four system functions, the mobile channel simulator can also be constructed on the basis of any one of these four system functions. A literature research revealed that the channel simulators that have been built so far are based on the impulse response modelling approach that is based upon the Bello's input delay spread function. This function models the channel in the time domain. The impulse response approach employs the time variant Finite Impulse Response (FIR) transversal filter, called a tapped delay line filter, to model and build a mobile channel simulator.

However, a mobile channel simulator can also be designed in the frequency domain by employing the time variant transfer function $T(f,t)$ of the channel. Modelling the communications channel using the time variant transfer function $T(f,t)$ has been envisaged by several researchers as an alternative and a more suitable technique as compared to impulse response modelling [3]. This is of course equally applicable for statistical as well as deterministic modelling. The time variant transfer function modelling approach has many advantages as compared to the impulse response modelling approach especially in the context of ultra wideband systems [3]. This can consistently be extended from narrowband to wideband and in general narrowband modelling techniques can readily be employed. In impulse response modelling, however, the various parameters associated with the fading statistics of the time variant mobile channel are bandwidth dependent. These parameters are valid only for the specific bandwidth used in measurements. Hence, it is not possible to establish a standard impulse response model that can be rightly employed for all bandwidths. The reasons behind this bandwidth dependency are based upon the fact that the increase in bandwidth will result in the resolution of more

constituent components of the fading signal. As bandwidth increases, the number of resolved components increase, thereby affecting the statistical parameters of the fading signal and making it a function of bandwidth. In case of an ultra wideband channel, a situation may arise where the number of unresolved components may not be enough to fulfil the criteria for the central limit theorem on which the impulse response modelling approach is based. In the case of time-variant transfer function modelling, however, the question of non-fulfilment of the central limit theorem does not arise for the reason that there is a superposition of the maximum number of available multi-path components for all frequencies and instants. Also, the time variant transfer function is the only system function among the four Bello functions for which there is a superposition of all multi-path components with respect to all domains. In case of all other system functions, there is a resolution of multi-path components with respect to at least one domain [3, 4]

2. Transfer Function Channel model

The channel transfer function models the power in the received signal as a function of frequency and describes the attenuation of frequencies in the transmission channel [5]. The transfer function of a channel is obtained by taking the Fourier transform of the input delay spread (impulse response) with respect to the delay variable τ and inverse Fourier transform of the output Doppler spread function with respect to the Doppler shift variable, ν [1]. A channel model based on the time variant transfer function was developed by Bello [2]. A block diagram of the model is shown in Fig.1 [3].

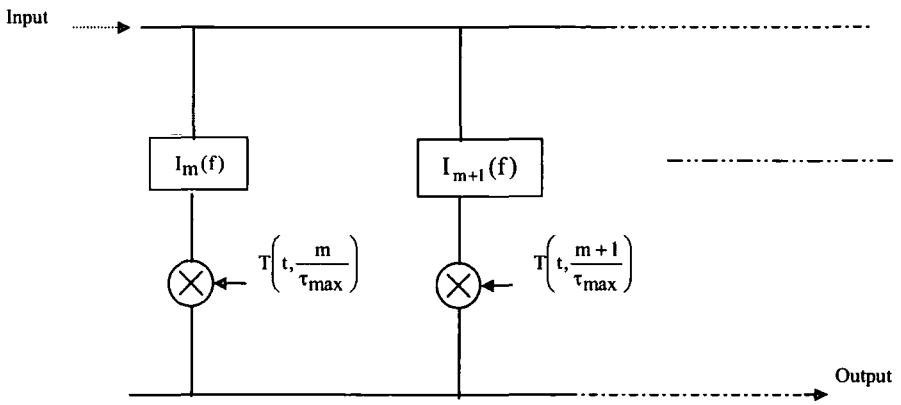

Fig 1. Channel model for time variant transfer function.

The output y(t) of the channel can be expressed as [2]

$$Y(t)=\sum_m T\left(\frac{m}{\tau_{max}},t\right)\int X(f)e^{-j2\pi\tau_0\left(f-\frac{m}{\tau_{max}}\right)}\text{sinc}\left[\tau_{max}\left(f-\frac{m}{\tau_{max}}\right)\right]df \quad (1)$$

Where X(f) is the input spectrum, τ_{max} is the maximum delay spread of the channel , τ_0 is equal to $\tau_{max}/2$, and m refers to the branch number. This equation reveals that the output of the channel is a summation of weighted outputs of a number of elementary parallel channels. Each parallel channel can be treated as a filter which filters the input and then multiplies its output by a gain function $T(m/\tau_{max},t)$. The transfer function of such a filter is denoted by $I_m(f)$ and is expressed as [3].

$$I_m(f) = e^{-j2\pi\tau_0\left(f-\frac{m}{\tau_{max}}\right)}\text{sinc}\left[\tau_{max}\left(f-\frac{m}{\tau_{max}}\right)\right] \quad (2)$$

Due to the randomly time variant nature of the channel, these gain functions are modelled as random processes. The width of each branch, i.e. the range of frequencies which each branch passes, is determined by the reciprocal of the maximum delay spread τ_{max} [3]. The number of branches is equal to the product of signal bandwidth and the maximum delay spread, $B\tau_{max}$. These are the minimum number of branches needed to cover the whole bandwidth of the input signal. When the width of each branch is taken as the reciprocal of the maximum delay τ_{max}, then each branch will be uncorrelated in frequency with respect to its adjacent branches. In [2], it has been stated that $10B\tau_{max}$ branches are to be employed to achieve very close approximation to the channel output. This implies that instead of employing one filter to simulate the coherence bandwidth of the channel, more filters/branches are needed to model coherence bandwidth of the channel. In this case, each branch will not be uncorrelated with respect to its adjoining branches; rather it will bear correlation depending upon the frequency separation between these branches. This correlation can be calculated from the spaced-frequency correlation function of the channel. Accordingly, more random processes are needed to be generated and the right amount of correlation has to be induced between these processes.

3. Simulation of Mobile Channel Based on Transfer Function Model.

Simulation of the transfer function model of a mobile propagation channel necessitates that the time variant transfer function is characterized in the context of frequency and time dimension. In the dimension of frequency, it exhibits the frequency selective fading and in the dimension of time, it represents the temporal variations of fading. Because the time variant impulse response is modelled as a complex-valued, zero-mean Gaussian random process in the time domain and the time variant transfer function is obtained by taking the Fourier transform of the time variant impulse response in the delay domain, this infers that T(f,t) possesses similar statistics and is also modelled as Gaussian random variable for any selection of time or frequency. In other words it is a random process in both time and frequency [6]. In the case of a static channel, it becomes a function of frequency and is thus modelled as a Gaussian process in frequency. The movement of the mobile results in Doppler and so this becomes a function of time as well as frequency. In that case, it is modelled as a Gaussian process both in time and frequency.

The autocorrelation function of the time variant transfer function T(f,t), called spaced-time, spaced-frequency correlation function, can be employed to determine the properties of T(f,t) in both dimensions i.e., time and frequency. The T(f,t) is sliced into a number of pieces. Each piece corresponds to one branch of the channel model shown in Fig.1. Each piece is modelled as a random process. At any instant in time, the combination of all these slices in the dimension of frequency will form a random process in frequency and is viewed as the transfer function of the channel at that instant. If any one of the slices is viewed in the dimension of time, it will also be a random process in time with correlation of its adjacent values determined by the space-time correlation function. Hence, the combination of all adjacent slices will yield the time variant transfer function, which can be viewed as a two dimension complex Gaussian process. The correlation of adjacent values of the time variant transfer function in the time and frequency is completely specified by the spaced-time, spaced-frequency correlation function [3].

4. Design of Channel Simulator using SIMULINK®.

The mobile channel Simulator has been designed in Simulink® by employing Digital Signal Processing Techniques. A block diagram of the simulator is shown in Fig.2. In order to implement the transfer function model of the channel, the applied complex signal is required to be sliced into a number of pieces. This slicing can be achieved by passing the complex signal through a bank of band pass filters. Each filters its own slice and thus attenuates the remaining portion of the signal. Each band pass filter has been implemented as an FIR filter, whose bandwidth and centre frequency is programmable. This implementation has used the frequency sampling method to calculate the filter coefficients. Before the start of the simulation, these filter coefficients are calculated and loaded into the workspace. The output of each filter is then multiplied by the random process as stated earlier. The summation of all the filter outputs gives the channel output.

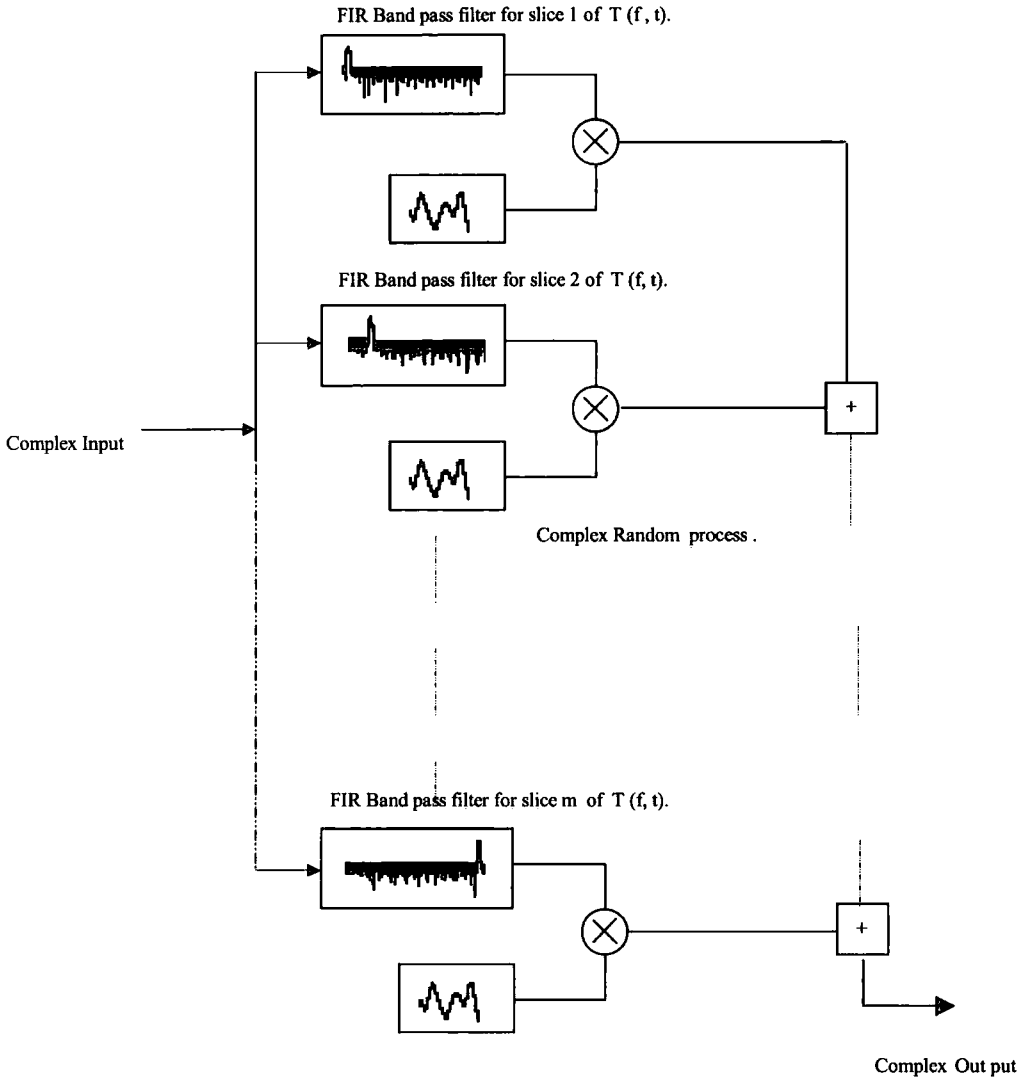

Fig 2. Block diagram of simulator.

4.1 Generation of Random Processes.

Each branch of the model consisting of the filter and a complex multiplier, needs its own complex random process. Therefore, the total number of random processes required are equal to the number of pieces into which the input signal is sliced. These random processes are characterised by their means and autocorrelation functions. The autocorrelation function determines the correlation between the fading values spaced in time. This explains the rapidity with which the fading takes place. The rate of fading can be viewed as Doppler shift in the frequency domain. Since, the power spectral density and autocorrelation function form the Fourier transform pair, the correlation properties can be induced into the random processes by passing the white random process through the filter which can transform the power spectral density into the desired shape. The white random process contains frequency components that have the same amount of energy and so the spectrum is flat. The PSD at the output of the filter is determined by the squared amplitude response of the filter's transfer function. The transfer function of the filter is obtained from the Doppler power spectrum. Many channel simulators [7,8] have employed the classical Doppler spectrum given in equation 3 to simulate the mobile propagation channel. The classical Doppler spectrum is usually called the U-shape spectrum because of its shape and is defined by the relationship defined in [9]. This has been derived assuming that the transmitted signal is un-modulated, the scattering environment is dense, and the receive antenna is

vertical with uniform azimuth gain and uniform distribution of the angle of arrival (0 to 2π). This relationship is valid for frequency range $\pm f_d$ about the carrier frequency.

$$S_{xx} = \frac{1}{\pi f_d \sqrt{1-\left(\frac{f}{f_d}\right)^2}} \tag{3}$$

In this Simulator, the built-in Rayleigh fading generators have been designed to generate independent coloured random processes. As discussed in sections 2 and 3, simulators will require correlated random processes, therefore, a degree of correlation is required to be established between these random processes. This has been achieved by mapping a pair of uncorrelated Gaussian random processes, X and Y, to a pair of random processes, X and Z, having a specified correlation level ρ. The relationship among X, Y, Z and ρ is based upon the following mathematical equation [10].

$$Z = \rho X + Y\sqrt{1-\rho^2} \tag{4}$$

The above equation was used to design a SIMULINK® block to establish a specified degree of correlation between two random processes.

5. Simulation Results.

Idealised power delay profiles are usually employed to evaluate the BER performance of channels [6]. There are two kinds of commonly used power delay profiles, two-ray profile and exponential profile. This work has employed two-ray power delay profile to simulate the mobile channel. In a two-ray power delay profile, BER is usually studied and expressed as a function of τ/T, where τ is the delay between the two rays and T is the symbol period. The value of τ/T can be varied by either changing the value of τ and keeping the symbol duration constant or keeping τ constant and varying the symbol duration. In this work, a fixed data rate of 24300 symbols/second was assumed and the value of τ was varied to obtain different values of τ/T. The main reason for using this data rate was to validate the simulation results with the published results [11]. In [11], the data rate of 24300 symbols/second was used for simulating outdoor Rayleigh fading channels. Moreover, this data rate has been specified in the U.S. Digital Cellular Standard IS-54.

The amplitude of the two rays was assumed equal while the delay between the two rays was varied to obtain different values of rms delay spreads. Table.1 shows the different values of τ, τ/T, rms delay spreads and coherence bandwidth employed in the simulation. These values of rms delay spread were used to obtain the coherence bandwidth employed in the simulation of the channel. The simulator's performance has been evaluated by simulating frequency selective Rayleigh fading channel and comparing the measured and published results of BER employing a DQPSK modulation scheme [11]. The DQPSK modulator accepts a binary data at the rate of 48600 bits/s and produces 24300 complex symbols per second at its output. The bandwidth of this complex baseband signal is 12.15 kHz i.e., one half of symbol rate [12]. The BER was measured by keeping the bandwidth of the input signal constant and varying the value of τ/T ranging from 0.1 to 1. This corresponds to varying the delay between two rays ranging from 4.11 μs to 41.15 μs and the coherence bandwidth of the channel from 8.10 to 81.10 kHz as shown in Table.1. The simulation was carried out for values of τ/T only between 0.1 to 1 since the BER stays constant at its ceiling of about 0.25 for values of τ/T greater than 1 [11]. The value of E_b/N_o was assumed to be 100 dB and was kept constant throughout the simulation. In the simulation, a Doppler frequency of 40 Hz was assumed. As shown in [11], the BER is not a strong function of Doppler. This simulator employs five branches to model the coherence bandwidth of the channel. The total number of branches needed depends upon the input signal bandwidth and the coherence bandwidth of the channel and can be calculated as $5B/B_c$, where

B is the signal bandwidth and B_c is the coherence bandwidth of the channel. As stated in section 2, the branches employed, the more accurate the channel output is. In [2], it has been stated that $10B\tau_{max}$ branches can give very close approximation to the channel output. However, the simulation results presented in Table.1 reveals that $5B/B_c$ branches are adequate to simulate the channel for the values of τ/T ranging from 0.2 to 1. However, when τ/T approaches 0.1, the coherence bandwidth of the channel becomes 81.10 kHz and if this coherence bandwidth is modelled by employing five branches then the bandwidth of each branch becomes 16.22 kHz which is greater than the input signal bandwidth i.e. 12.15 kHz and the number of branches come out to be 0.70. In this case, five branches can still be employed but the bandwidth of each branch will now be one fifth of the input signal bandwidth and correlation between any two branches is defined by the spaced-frequency correlation function of the two-ray channel model.

S.NO.	Time Delay between the two rays in μs (τ)	Time delay between the two rays/ Symbol duration in μs (τ/T)	τ_{rms} in μs	Coherence BW B_c in kHz
1.	4.11	0.1	2.05	81.10
2.	8.23	0.2	4.11	40.55
3.	12.34	0.3	6.17	27.00
4.	16.46	0.4	8.23	20.25
5.	20.57	0.5	10.28	16.21
6.	24.69	0.6	12.34	13.50
7.	28.80	0.7	14.40	11.57
8.	32.92	0.8	16.46	10.12
9.	37.03	0.9	18.51	9.00
10.	41.15	1	20.57	8.10.

Table 1. BER comparison of DQPSK for two-ray PDF at the data rate of 24300 symbols/second.

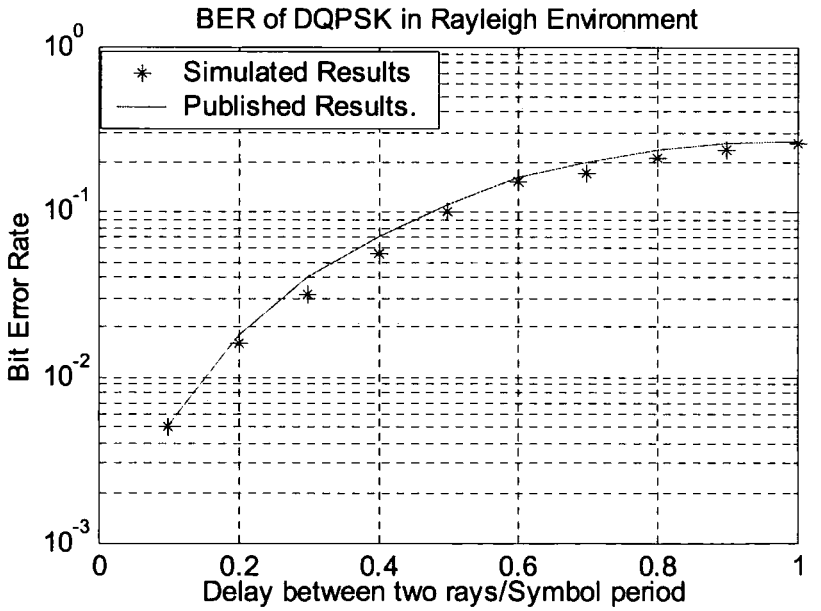

Fig 3. BER versus normalized delay between two-rays in a wideband Rayleigh fading environment.

S.NO.	Time Delay between the two rays in μs (τ)	τ/T in μs	BER (Tap delay line Model)	BER (Transfer function Model)
1.	4.11	0.1	0.005	0.005
2.	8.23	0.2	0.02	0.016
3.	12.34	0.3	0.05	0.04
4.	16.46	0.4	0.085	0.055
5.	20.57	0.5	0.131	0.10
6.	24.69	0.6	0.173	0.15
7.	28.80	0.7	0.22	0.17
8.	32.92	0.8	0.26	0.21
9.	37.03	0.9	0.29	0.24
10.	41.15	1	0.30	0.26

Table 2. BER comparison between the tap delay line model and the transfer function model for DQPSK using two-ray PDF at the data rate of 24300 symbols/second.

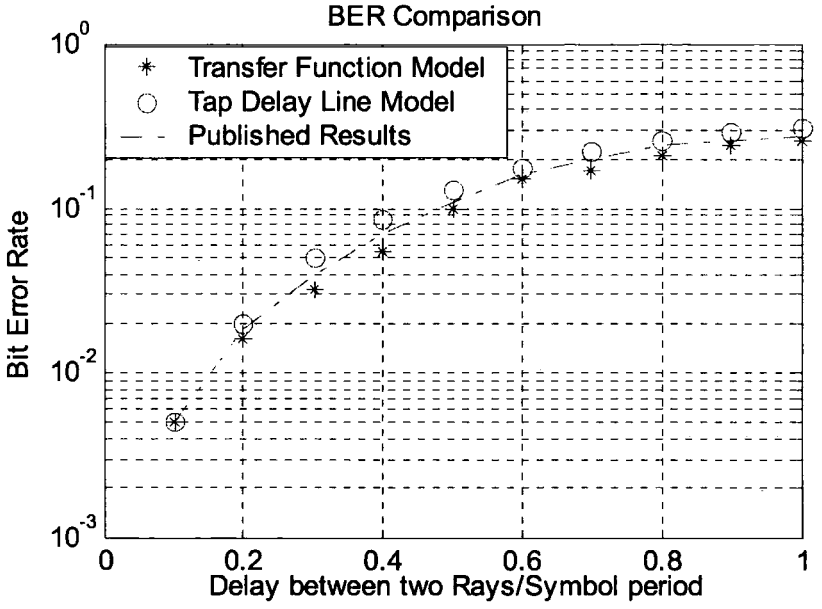

Fig 4. BER comparison for transfer function model, tap delay line model and published results.

Referring to the results presented in Table.1, when τ/T is 1, the coherence bandwidth of the channel is 8.10 kHz and the number of branches needed in the simulator for 12.15 kHz input signal are 8. When the value of τ/T decreases, the coherence bandwidth of the channel and the number of the branches needed in the model for a given bandwidth also decrease. The simulation and published results for BER as a function of τ/T are presented in Fig.3 which shows complete agreement with the published results.

These results have also been compared with the results obtained by using tap delay line model under the same channel parameters. Table.2 and Fig.4 present comparisons between these results and clearly show a close match between them.

6. Conclusions

A mobile channel simulator has been designed in Simulink® by employing the time variant transfer function of the channel. Simulation was carried out by assuming a two-ray power delay profile and the BER performance of a DQPSK scheme was studied in a Rayleigh environment. The BER results were compared with the published results and also with those obtained using a taped

delay line model under identical channel parameters. These results agree closely with each other and therefore demonstrate that the mobile channel can also be simulated based on the time variant transfer function of the channel. Current and future research is concerned with the application of the frequency transfer function method to OFDM systems.

Acknowledgements

The authors would like to extend their thanks to Mr Razavi for his discussions during the course of this work.

References

[1] Parsons J. D., The Mobile Radio Propagation Channel: John Wiley & Sons Ltd., ISBN 0 471 98857 X, 2000.

[2] Bello P. A., "Characterization of random time-variant linear channels," IEEE Trans. on Communication Systems, vol.CS-11, pp. 360-393, Dec. 1963.

[3] Ralf Kattenback, "Transfer function modelling and its application to Ultra-Wideband channels," COST 273 TD (02) 136, Lisbon, Purtugal, Sep. 19-20, 2002.

[4] Ralf Kattenback, "Statistical modelling of small scale fading in directional radio channel," IEEE Journal on Selected Areas in Communications, vol. 20, April. 2002

[5] Simon Saunder, Antenna and Propagation for Wireless Communication Systems: John Wiley & Sons Ltd.

[6] James K. Caver, Mobile Channel Characteristics: Kluwer Academic Publisher, ISBN 0 –7923-7926-8.

[7] Gaston A. Arrendondo,William H. Chriss and Edward H. Walker, "A multi-path fading simulator for Mobile Radio," IEEE Transaction on vehicular technology, vol. 22, Nov. 1973.

[8] Peter J. Cullen, Paul C Fannin, and Anthony Garvey, "Real-Time Simulation of Randomly Time-Variant Linear Systems: The mobile Radio Channel,"IEEE Transaction on Instrumentation and Measurement , vol. 43, Aug.1994.

[9] R.H Clark, "A statistical theory of mobile radio reception," Bell SysTec.J., vol. 47, pp. 957-1000, Jul-Aug. 1968,

[10] William H. Tranter, K.Sam. Shanmugan, T.S.Rapport & Kurt L. Kosbar, Principles of Communication System Simulation with Wireless Applocations: Prentice Hall Communications Engineering and Technologies Series, ISBN 0-13-494790-8.

[11] Victor Fung, Theodore S. Rapport, "Bit error simulation of $\pi/4$ DQPSK mobile radio communications using two-ray and measurement based impulse response model," IEEE Journal on Selected Area in Communications, vol.11, April.1993.

[12] Wayne Tomasi, Advanced Electronic Communications Systems: Prentice Hall, Inc, New Jersey, ISBN 0-13-011214-3.